# Investigating the Contribution of The Unfolded Protein Response to Prostate Cancer Bone Metastasis




Zeynep Kaya

A thesis submitted in fulfilment of the requirements for the degree of Doctor of Philosophy

Kellogg College

Nuffield Department of Surgical Sciences
University of Oxford

Michaelmas 2021

# Declaration

I declare that all the work presented in this thesis is the result of my own work unless otherwise stated and does not constitute part of any other thesis. The work herein described was carried out while I was a DPhil student of the Nuffield Department of Surgical Sciences working at the Botnar Research Centre, under the supervision of Professor Claire Edwards, Dr Srinivasa Rao, Professor Ian Mills, Professor John Christianson. I declare that I have not taken any credit that belongs to others.

Zeynep Kaya

5 November 2021

# Abstract

The majority of deaths from prostate cancer (PCa) arise following metastasis, particularly to the skeleton. ER stress and the unfolded protein response (UPR) promote primary PCa, however, the contribution of the UPR to PCa bone metastasis remains unknown. The aim of this work was to determine the role of the UPR in PCa bone metastasis, focusing on the osteogenic potential of PCa cells, epithelial to mesenchymal transition (EMT) and migration, and PCa-induced bone disease. Using paired androgen refractory cancer of the prostate (ARCaP) cell lines ARCaPE and ARCaPM which differ in their epithelial (E) and mesenchymal (M) characteristics, I found that components of IRE1 and ATF6 ER stress pathways are higher in ARCaPE cells than in ARCaPM and decreased upon osteogenic differentiation of ARCaPM cells. Inhibition of the IRE1 or PERK pathway increased alkaline phosphatase (ALP) activity in ARCaPM cells. Inhibition of specific arms of the UPR produced a varied response in EMT markers with no effect on migration of ARCaPM cells. Increasing ER stress using tunicamycin significantly reduced the migration of ARCaPM cells. The bone disease associated with PCa bone metastases is driven by alterations in a complex signalling network, including the RANKL/OPG pathway and Wnt signalling. ER stress, induced by tunicamycin, decreased RANKL and DKK1 expression and increased OPG expression in ARCaPM cells. This response of bone-related factors to ER stress was blocked by PERK inhibition. Taken together, my research demonstrates that the UPR has multiple effects in bone metastatic PCa cells, including a reduction in migration and in osteolytic factors following UPR activation, suggesting a novel mechanism by which the UPR may modulate PCa-induced bone disease.

To my family.

# Acknowledgements

First and foremost, I want to thank Cancer Research UK and Dulverton Trust for funding me and my studies throughout my studies, and for always supporting me.

The road to my DPhil was bumpy and "winding", I had to change my first research group. Looking back, I cannot think of how my DPhil would come to an end if I hadn't changed my lab, and still I have no regrets for doing that. I owe special thanks to Jane Johnson. Without your support, this would not have been possible. Besides, I am grateful to Professor Robert Gilbert, director of the graduate school, for supporting my change of program.

I was lucky and thankful to have landed in Professor Claire Edward's Lab after two years of coming to Oxford. I will always be thankful for her continuous support, her guidance in my research, and her time in going through all my assignments and presentations with me. You always helped me find my way. I can never thank you enough for being so understanding as I was navigating through my situation.

I would like to express my gratitude to my supervisor Dr Srinivasa Rao Rao, a talented advisor and a wise mentor, for his endless patience, and for always being there for advice or guidance, whether it be work-related or me just dropping by his office for some reason. Rao has been a model with his honesty, humbleness, and fairness; also a hope for me to still believe that being a nice person and a good scientist at the same time is possible.

My sincere thanks must also go to my supervisors Professor Ian Mills and Professor John Christianson for their time and valuable comments towards improving my work. In particular, to Professor Ian Mills for listening to my concerns when I first approached him, for making this opportunity possible, and for being both critical and constructive. To Professor John Christianson for his help and guidance throughout my project and for opening a window for learning everything there is to know about ER and the UPR.

I would like to give special thanks to my viva examiners Prof Ester Hammond and Prof Neil Cross for their time in reading my thesis and insightful comments on it.

Additionally, I am very grateful to Professor Valentine Macauley for supporting me and putting me in contact with Professor Ian Mills and Professor Claire Edwards. Professor Valentine was always there since the first day I came to Oxford, interviewed me during applications for the DPhil program, and guided me when I was trying to change my group. I will always remember her as an important part of my DPhil, one of the best parts indeed, for which I will always be deeply honoured.

I would like to thank everyone in the Edwards group who has helped in some capacity over the years. To Dr Emma Morris for all the help around the lab and great company at the bench. One thing that I will always remember from most of our conversations is this quote: "It is nice to be important, but more important to be nice". My thanks also go out to Professor James Edwards for his advices in the group meetings.

Some people brightened my days with their generous and heartfelt smiles, like Professor Stephanie Dakin, and I owe special thanks to her!

Many thanks go to fellow DPhil students and friends I met at the Botnar Research Centre, Rand Alkaissy, Sarah Salmon, Hajar Almoajil, and Giorgia Gaeta with whom we built a friendship through troubleshooting experiments and never-ending western blots.

NDS administrative staff Eleanor Wilson and Jo Snoeck who assisted me with the paperwork when required and the administrative staffs in the Botnar, Isuara Thomas, Nicholas Gee, Alan Bateman, Dave Banfield, Fryad Karim, Osman Aslam and Sonja Pawelczyk are all memorable for their prompt support. Thanks also to Silvia Barrientos, student funding administrator, for making things easier and for your kind approach in all the times we communicated.

I have not forgotten the support from Dr Shonagh Munro, Dr Heidi Olzscha, Alice Poppy Roworth and Dr Simon Carr; and I would like to thank them too.

Special thanks go to my friend and colleague Haroon Qureshi for his continuous support and wise advices. To Erdinç Sezgin, Dönem Avcı, Metin Aksu, Ceren Yalaz and Anne Nierobisch for sharing their experience when I was trying to change groups. To Burcu Gülen, Merve Turgut, Ece Akgül and Christina Revenco for sharing in one way or another this road with me; and to Oumou Traore, for her company, for being there every time I needed her, and for appreciating Turkish coffee as much as I do.

Enzacığım, my wise, logical, smart, elegant friend. I am so lucky to have met a person like you and to have been in places around Oxford with you. I am glad that I can keep the memories we shared in a form you created.

My dear friend Naile, just before I came to Oxford in 2016, I remember talking with you about the years we thought we would most likely change the most would be spent apart. I would like to thank both of you and me for still making room for each other in our lives despite everything that has changed and for not giving up on accommodating each other no matter what. Distance has taught me that a lot can change, that most people can move away, but our friendship has taught me that some things can still stay the same.

I am wholeheartedly grateful for my beautiful family. To my parents Lütfiye Kaya and Mehmet Kaya for your endless love and support, for everything you have done that helped me get to this day, and for raising me the way you did. Everything I am is because of you two. Thank you separately for every day you waited for my calls when I said I would call after I finish in the lab, no matter how late it was, despite the different time zones.

To my sister Gamze, my first and forever friend since the day I was born, thank you for being by my side through every good and bad. You have always inspired me with your hard work. To my brother Halil İbrahim, for always encouraging me to pursue my dreams and never give up. It is so empowering to know that you are always by my side. At the end of every difficulty I overcame, and after every achievement along the way, I always had a ticket to come and celebrate that with you. You are always my light at the end of the tunnel.

# Table of Contents

Abstract ..... v
Acknowledgements ..... ix
Table of Contents ..... xiii
List of Tables ..... xvii
List of Figures ..... xix
Abbreviations ..... xxiii

1 Introduction ..... 1

1.1 Prostate cancer ..... 1

1.1.1 Management of prostate cancer ..... 2
1.1.2 Progression into metastatic stage ..... 7

1.2 Prostate cancer bone metastasis ..... 12

1.2.1 Biological processes involved in prostate cancer metastasis ..... 14

1.2.1.1. Loss of cell adhesion ..... 14
1.2.1.2. Local invasion ..... 16
1.2.1.3. Invasion and intravasation ..... 18
1.2.1.4. Homing to bone ..... 21

1.3 Pathophysiology of Bone Metastasis ..... 23

1.3.1 Osteoblasts ..... 23

1.3.1.1. Runx2 ..... 25
1.3.1.2. ATF4 ..... 25
1.3.1.3. Alkaline phosphatase ..... 25
1.3.1.4. Collagen 1 ..... 26

1.3.2 Osteoclasts ..... 27
1.3.3 Bone remodelling ..... 27
1.3.4 Osteoblast-associated factors ..... 28

1.3.4.1. Endothelin-1 ..... 28
1.3.4.2. Wnt signalling ..... 29
1.3.4.3. Bone morphogenic proteins ..... 31
1.3.4.4. Insulin-like growth factors ..... 32

1.3.5 Osteoclast-associated factors ..... 33

1.3.5.1. RANK/RANKL/OPG axis ..... 33
1.3.5.2. Parathyroid hormone-related protein ..... 34
1.3.5.3. Transforming growth factor β ..... 35

1.3.6 The vicious cycle of bone metastases ..... 37
1.3.7 Treatment of PCa bone metastases ..... 38

1.3.7.1. Bisphosphonates....38
1.3.7.2. Denosumab....39
1.3.7.3. Use of radiopharmaceuticals....39
1.3.8 Models of prostate cancer EMT....40
1.3.8.1. Human prostate cancer ARCaP EMT model....41
1.3.8.2. Mouse prostate cancer DVL3 cell line model....42
1.4 The Endoplasmic Reticulum (ER)....43
1.4.1 The Unfolded Protein Response (UPR)....44
1.4.1.1. Different arms of the UPR....46
1.4.1.2. Integrated stress response (ISR)....49
1.4.1.3. Crosstalk between the arms of the UPR....51
1.4.2 ER-associated degradation (ERAD)....52
1.4.2.1. Substrate recognition....54
1.4.2.2. Retrotranslocation to the cytosol....55
1.4.2.3. Ubiquitination....57
1.4.2.4. Proteasomal degradation....58
1.4.2.5. Hrd1 complex....60
1.4.3 ER stress signalling in cancer....62
1.4.4 ER stress and prostate cancer....64
1.4.4.1. Targeting the ER stress response in prostate cancer....66
1.4.5 The UPR in bone development....69
1.5 Overall Hypothesis and Objectives....72
2 Materials and Methods....75
2.1 Materials....75
2.1.1 Chemicals and reagents....76
2.1.2 Primers....76
2.1.3 Antibodies....77
2.2 Methods....77
2.2.1 Bacterial growth....77
2.2.1.1. Culture conditions of E. coli....77
2.2.1.2. Antibiotics used for bacterial cultures....77
2.2.1.3. Production and storage of bacterial glycerol stocks....77
2.2.2 Cell Culture....77
2.2.2.1. Culture conditions....77
2.2.2.2. Cell viability assay (Alamar Blue)....79
2.2.2.3. SYTOX Green staining for cell death....79
2.2.2.4. Osteogenic differentiation....80
2.2.2.5. Alizarine Red S staining for mineral crystals....80
2.2.2.6. Real-time imaging for mineralisation via IncuCyte S3....81
2.2.2.7. Alkaline Phosphatase (ALP) activity assays....81

2.2.2.8. Secreted RANKL Enzyme-Linked Immunosorbent Assay (ELISA) ..... 83
2.2.2.9. Transwell migration assay ..... 83
2.2.2.10. Scratch assay ..... 83
2.2.3 Production of lentiviruses ..... 84
2.2.4 Viral transduction ..... 84
2.2.5 Cell imaging ..... 85
2.2.6 Molecular biology ..... 85
2.2.6.1. Protein characterisation ..... 85
2.2.6.2. RNA isolation ..... 87
2.2.6.3. Quantification of RNA concentration ..... 87
2.2.6.4. cDNA synthesis ..... 87
2.2.6.5. Real-time quantitative Reverse Transcription Polymerase Chain Reaction (qRT-PCR) ..... 87
2.2.6.6. XBP1 splicing assay ..... 88
2.2.6.7. RNA-Seq ..... 90
3 The effect of the UPR in prostate cancer osteomimicry ..... 93
3.1 Introduction ..... 93
3.2 Hypothesis and Objectives ..... 95
3.3 Results ..... 96
3.3.1 Optimising conditions for the study of the UPR & mineralisation ..... 96
3.3.2 The effect of osteogenic differentiation on the UPR ..... 103
3.3.3 The UPR expression in mesenchymal PCa cells ..... 106
3.3.4 Effect of the UPR inhibitors ..... 111
3.4 Discussion ..... 126
4 The effect of the UPR on PCa-derived osteoclast/osteoblast activating factors ..... 133
4.1 Introduction ..... 133
4.2 Hypothesis and Objectives ..... 134
4.3 Results ..... 135
4.3.1 Difference in basal expression of bone-related factors ..... 135
4.3.2 Effect of tunicamycin & inhibitors on osteoclastic gene expression ..... 136
4.3.2.1. Effect of tunicamycin & inhibitors on Wnt signalling pathway ..... 142
4.4 Discussion ..... 146
5 The effect of the UPR on EMT and migration in bone metastatic PCa ..... 153
5.1 Introduction ..... 153
5.2 Hypothesis and Objectives ..... 155
5.3 Results ..... 156
5.3.1 Differences in basal EMT markers in ARCaPE vs ARCaPM and DVL3 vs DVL3-SCM 156
5.3.2 Impact of the UPR on EMT & migration ..... 159

5.3.3 Effect of hypoxia on migration ..... 171
5.4 Discussion ..... 182
6 The effect of ALPL on the UPR ..... 191
6.1 Introduction ..... 191
6.2 Hypothesis and Objectives ..... 192
6.3 Results ..... 193
6.3.1 ALPL knockdown results in change in morphology of ARCaPM cells ..... 193
6.3.2 Effect of ALPL knockdown on the UPR ..... 195
6.3.3 RNA-Seq ..... 196
6.4 Discussion ..... 202
7 Overall Discussion and Limitations ..... 207
8 Appendix ..... 217
8.1 Materials ..... 218
8.1.1 Primers used for human cell line samples ..... 218
8.1.2 Primers used for mouse cell line samples ..... 220
8.1.3 The antibodies used in this study ..... 222
8.1.4 Antibiotics ..... 224
8.1.5 Target sequences for shRNAs and siRNAs ..... 224
8.1.6 Sequences of the capture oligos, adaptor and the indexes used in RNA-seq ..... 225
8.2 Supplementary Data ..... 226
8.2.1 Dkk1 amplification plot in DVL3 and DVL3-SCM cells ..... 226
8.2.2 Melt curves from qRT-PCR of SPARC in ARCaPM and ARCaPE ..... 227
8.2.3 RNA-seq results ..... 228
8.2.4 Gene ontology enrichment analysis of most significantly overrepresented genes ..... 232
References ..... 235

# List of Tables

*Table 1.1 Summary of proteins in ERAD* ..... 59

*Table 2.1 Thermocycling conditions for Taq DNA polymerase for XBP1 cDNAs* ..... 89

*Table 2.2 Thermocycling conditions for Q5 DNA polymerase for library amplification and indexing* ..... 91

*Table 8.1 Compounds used to induce UPR* ..... 217

*Table 8.2 Inhibitors of the UPR* ..... 217

*Table 8.3 Primers of EMT markers in human cell line* ..... 218

*Table 8.4 Primers of the unfolded protein response in human cell lines* ..... 218

*Table 8.5 Primers of osteogenic differentiation markers in human cell lines* ..... 219

*Table 8.6 Primers of housekeeping genes in human cell lines* ..... 219

*Table 8.7 Primers for XBP1 splicing assay in human cell lines* ..... 219

*Table 8.8 Primers of EMT markers in mouse cell lines* ..... 220

*Table 8.9 Primers of the unfolded protein response in mouse cell lines* ..... 220

*Table 8.10 Primers of osteogenic differentiation markers in mouse cell lines* ..... 221

*Table 8.11 Primers of housekeeping genes in mouse cell lines* ..... 221

*Table 8.12 TaqMan primer list* ..... 221

*Table 8.13 Primers for XBP1 splicing assay in mouse cell lines* ..... 221

*Table 8.14 Antibodies used for detection of the UPR* ..... 222

*Table 8.15 Antibodies for EMT markers* ..... 223

*Table 8.16 Detection reagents* ..... 223

*Table 8.17 Concentration of commonly used antibiotics in bacterial cultures* ..... 224

*Table 8.18 Vectors used for lentiviral packaging* ..... 224

*Table 8.19 siRNAs used in this study* ..... 224

*Table 8.20 RNA-Seq index list* ..... 225

*Table 8.21 List of most significantly differed genes with* $P_{adjusted} \leq 0.05$ ..... 230

*Table 8.22 The top 30 of the most overrepresented pathways* ..... 232

*Table 8.23 The most overrepresented pathways excluding RPLs* ..... 233

# List of Figures

*Figure 1.1 Natural history of prostate cancer* ..... 3
*Figure 1.2 Cellular progression of prostate cancer* ..... 9
*Figure 1.3 Schematic representation of osteoblast differentiation* ..... 24
*Figure 1.4 The vicious cycle of bone metastasis* ..... 37
*Figure 1.5 UPR signalling (ATF6, IRE1, PERK)* ..... 45
*Figure 1.6 eIF2 kinases and the integrated stress response* ..... 50
*Figure 1.7 Key steps of the mammalian ERAD system* ..... 53
*Figure 1.8 Unfolded protein response and cancer* ..... 63
*Figure 1.9 Chemical structures and mechanisms of action of the compounds used in this study* 73
*Figure 3.1 Bone marker gene expression differs between ARCaPE and ARCaPM cells* ..... 97
*Figure 3.2 ARCaPM cells deposit mineral crystals 15 days after growing in osteogenic medium* ..... 98
*Figure 3.3 Osteogenic differentiation of ARCaPM cells over time* ..... 99
*Figure 3.4 Bone marker gene expression does not change between control and differentiation medium in ARCaPM cells* ..... 101
*Figure 3.5 Treatment with β-glycerophosphate is sufficient for elevated ALP activity and mineral deposition in ARCaPM cells* ..... 103
*Figure 3.6 Markers of different arms of the UPR decrease upon differentiation* ..... 104
*Figure 3.7 mRNA transcript levels of the UPR components in ARCaPM cells during osteogenic differentiation* ..... 105
*Figure 3.8 EMT protein and gene expression between ARCaPE and ARCaPM cells* ..... 107
*Figure 3.9 Markers of different arms of the UPR are reduced in ARCaPM cells* ..... 108
*Figure 3.10 The UPR gene expression between ARCaPE and ARCaPM cells* ..... 109
*Figure 3.11 The UPR gene expression between DVL3 and DVL3-SCM cells* ..... 110
*Figure 3.12 Osteogenic marker gene expression between DVL3 and DVL3-SCM cells* ..... 111
*Figure 3.13 Effect of different concentrations of tunicamycin on the relative protein expression of UPR related genes in ARCaPM cells* ..... 113
*Figure 3.14 Baseline levels of the UPR related proteins and confirmation of inhibitor function* ..... 115

*Figure 3.15 Effect of ER stress inducers and the UPR inhibitors on viability of ARCaPM cells* ..... 116
*Figure 3.16 Mineral deposition and ALP activity in response different inhibitors of the UPR after 15 days* ..... 117
*Figure 3.17 Inhibiting IRE1 or PERK pathway results in changes in alkaline phosphatase activity levels in ARCaPM cells in control and differentiation medium* ..... 119
*Figure 3.18 ALP activity in ARCaPE cells in response to the UPR inhibitors* ..... 120
*Figure 3.19 ALP activity in ARCaPE cells in response to 5 µM UPR inhibitors* ..... 121
*Figure 3.20 Expression levels of the UPR, EMT and osteogenic markers on ARCaPE with inhibitors of the UPR for 72 h* ..... 122
*Figure 3.21 Inhibiting different arms of the UPR does not impact ALP activity in DVL3-SCM cells* ..... 123
*Figure 3.22 The levels mRNA transcripts of EMT and osteogenic markers in DVL3-SCM cells measured by qRT-PCR* ..... 125
*Figure 4.1 Expression levels of bone-related factors differs between ARCaPE and ARCaPM cells* ..... 135
*Figure 4.2 Expression levels of bone-related factors differs between DVL3 and DVL3-SCM cells* ..... 136
*Figure 4.3 Confirming inhibitor activity in ARCaPM cells at 4 h* ..... 138
*Figure 4.4 ALP activity in ARCaPM cells in response to 5 µM UPR inhibitors* ..... 139
*Figure 4.5 Effect of the UPR on RANKL and OPG expression in ARCaPM and DVL3-SCM cells* ..... 140
*Figure 4.6 Effect of the UPR on PTHRP expression in ARCaPM & DVL3-SCM* ..... 141
*Figure 4.7 Effect of the UPR on DKK1 in ARCaPM* ..... 143
*Figure 4.8 Effect of the UPR on CTNNB1 in ARCaPM* ..... 145
*Figure 5.1 EMT marker gene expression differs between DVL3 and DVL3-SCM cells* ..... 157
*Figure 5.2 Transwell migration of ARCaPM cells is enhanced compared to ARCaPE cells* ... 158
*Figure 5.3 Effect of tunicamycin as stress inducer on the migration of the human prostate cell ARCaPM* ..... 159
*Figure 5.4 Effect of the UPR inhibitors on ARCaPM migration* ..... 161
*Figure 5.5 Effect of tunicamycin and the UPR inhibitors on ARCaPM migration* ..... 163
*Figure 5.6 Effect of tunicamycin/thapsigargin ± UPR inhibitors on cell viability* ..... 164
*Figure 5.7 Effect of tunicamycin and the UPR inhibitors on the UPR components* ..... 166

*Figure 5.8 Effect of thapsigargin and the UPR inhibitors on the UPR components ..... 167*
*Figure 5.9 Effect of tunicamycin & thapsigargin on EMT markers ..... 168*
*Figure 5.10 Effect of the UPR inhibitors on ARCaPM migration ..... 170*
*Figure 5.11 Effect of 0.4% hypoxia as stress inducer on the migration of ARCaPM cells ..... 172*
*Figure 5.12 Effect of hypoxia and the UPR inhibitors on the UPR components ..... 174*
*Figure 5.13 Effect of hypoxia and the UPR inhibitors on EMT markers ..... 176*
*Figure 5.14 Effect of the UPR inhibitors on ARCaPM migration under hypoxia ..... 177*
*Figure 5.15 Early hypoxia induced wound healing in ARCaPM cells ..... 178*
*Figure 5.16 Cell death in ARCaPM after 12 h in hypoxia ..... 179*
*Figure 5.17 Prolonged hypoxia results in increased cell death in ARCaPM cells ..... 180*
*Figure 5.18 Prolonged hypoxia delayed wound healing in ARCaPM cells ..... 181*
*Figure 6.1 ALPL knockdown results in epithelial like morphology in ARCaPM cells ..... 194*
*Figure 6.2 Markers of different arms of the UPR in response to ALPL knockdown in ARCaPM cells ..... 195*
*Figure 6.3 ALPL knockdown with siRNA results in epithelial like morphology in ARCaPM cells ..... 197*
*Figure 6.4 mRNA profiling of ALPL knockdown ARCaPM cells ..... 199*
*Figure 6.5 Volcano plot of the most differentially expressed genes ..... 200*
*Figure 6.6 Normalised mRNA counts for ALPL and markers of the UPR ..... 201*
*Figure 8.1 Amplification plot of Dkk1 and Gapdh in DVL3 and DVL3 SCM cells ..... 226*
*Figure 8.2 Melt curves from qRT-PCR of SPARC ..... 227*
*Figure 8.3 Distance matrix of samples ..... 228*
*Figure 8.4 Principal component analysis of samples in RNA-seq ..... 229*

# Abbreviations

| | |
|---|---|
| aa | Amino acid |
| ALP | Alkaline phosphatase |
| ANOVA | Analysis of variance |
| AR | Androgen receptor |
| ARCaP | Androgen refractory cancer of the prostate |
| ATF4 | Activating Transcription Factor |
| ATF6 | Activating transcription factor 6 |
| ATP | Adenosine triphosphate |
| Bcl-2 | B-cell lymphoma 2 |
| BiP | Binding immunoglobulin protein |
| BMP | Bone morphogenetic protein |
| BMS | Bone marrow stromal |
| BPH | Benign prostate hyperplasia |
| CDH1 | E-Cadherin |
| CDH2 | N-Cadherin |
| cDNA | Complementary DNA (deoxyribonucleic acid) |
| CHOP | Transcription factor C/EBP homologous protein |
| CM | Conditioned media |
| CNX | Calnexin |
| CREB | cAMP-responsive element-binding |
| CRPC | Castration-resistant prostate cancer |
| CRT | Calreticulin |
| DERLIN | Degradation in ER protein 1 |
| DHT | Dihydrotestosterone |
| DKK1 | Dickkopf-1 WNT signalling pathway inhibitor-1 |
| DUB | Deubiquitinating enzyme |
| ECM | Extracellular matrix |
| EDEM | ER degradation-enhancing $\alpha$-mannosidase-like protein |
| EGFR | Epidermal growth factor receptor |
| eIF2$\alpha$ | Eukaryotic translation initiation factor-2 |
| ELISA | Enzyme-linked immunosorbent assay |
| EMT | Epithelial mesenchymal transition |
| ER | Endoplasmic reticulum |
| ERAD | ER-associated degradation |
| ERdj | ER-resident DNAJ |
| ERFAD | ER flavoprotein associated with degradation |
| ERN1 | Endoplasmic reticulum to nucleus 1 |
| ERN2 | Endoplasmic reticulum to nucleus 2 |
| ERQC | ER quality control compartment |
| ERSE | ER-stress element |

| | |
|---|---|
| ET-1 | Endothelin-1 |
| ETA | Endothelin-1 receptor subtype A |
| ETAR | Endothelin-A receptor |
| FAM8A1 | Family with sequence similarity 8 member A1 |
| FDR | False discover rate |
| FGF | Fibroblast growth factor |
| GADD34 | Growth arrest and DNA damage-inducible 34 |
| GAPDH | Glyceraldehyde 3-phosphate dehydrogenase |
| GP78 | Glycoprotein 78 |
| GRP78 | 78 kDa glucose-regulated protein |
| GRP94 | 94 kDa glucose-regulated protein |
| GSK3$\beta$ | Glycogen synthase kinase 3$\beta$ |
| HBME | Human bone marrow endothelium |
| HERP | Homocysteine-responsive ER-resident ubiquitin-like domain protein |
| HIF1$\alpha$ | Hypoxia-inducible factor 1-alpha |
| Hrd1 | HMG-coA reductase degradation protein 1 |
| HSP | Heat shock protein |
| IGF | Insulin-like growth factor |
| IGFBP | IGF-binding protein |
| IGF-IR | IGF I receptor |
| IL-6 | Interleukin-6 |
| IRE1 | Inositol requiring enzyme 1 |
| JNK | C-Jun N-terminal kinase |
| MAPK | Mitogen-activated protein kinase |
| mCRPC | Metastatic castrate resistant PCa |
| M-CSF | Macrophage-colony stimulating factors |
| MET | Mesenchymal to epithelial transition |
| miRNA | MicroRNA |
| MMP | Matrix metalloproteinase |
| NF-$\kappa$B | Nuclear factor kappa-light-chain-enhancer of activated B cells |
| NKx3.1 | Homeobox protein NKx3.1 |
| Npl4/NPLOC4 | Nuclear protein localisation protein 4 homolog |
| OCN | Osteocalcin |
| OPG | Osteoprotegerin |
| OS-9 | Osteosarcoma 9 |
| PCa | Prostate cancer |
| PDI | Protein disulphide isomerase |
| PERK | PKR-like ER kinase |
| PI3K | Phosphatidylinositol 3-kinase |
| PIA | Proliferative inflammatory atrophy |
| PIN | Prostatic intraepithelial neoplasia |
| PP1C | Protein phosphatase 1C |
| PSA | Prostate specific antigen |
| PTEN | Phosphatase and tensin homologue |

| | |
|---|---|
| PTH | Parathyroid hormone |
| PTHrP | Parathyroid hormone-related peptide |
| RANK | Receptor activator of nuclear factor-kappa B |
| RANKL | Receptor activator of nuclear factor-kappa B ligand |
| RIDD | Regulated IRE1-dependent decay |
| RING | Really interesting new gene |
| RP | Radical prostatectomy |
| RUNX2 | Runt-related transcription factor 2 |
| S1P | Site-1 protease |
| S2P | Site-2 protease |
| SCID | Severe combined immunodeficient |
| SDF-1 | Stromal-derived factor-1 |
| SEL1L | Suppressor of lin-12-like protein 1 |
| shRNA | Short hairpin RNA |
| siRNA | Small interfering RNA |
| SNAI1 | Snail |
| SNAI2 | Slug |
| SRP | Signal recognition particle |
| STAT3 | Signal transducer and activator of transcription 3 |
| TGFBR1 | Type I TGF-β receptor |
| TGF-β | Transforming growth factor-beta |
| TIMP | Tissue inhibitor of metalloproteinases |
| TRAF2 | TNFR-associated factor 2 |
| TRAMP | TRansgenic Adenocarcinoma Mouse Prostate |
| TRAP | Tartrate-resistant acid phosphatase |
| Ub | Ubiquitin |
| UBAC2 | Ubiquitin-associated domain-containing protein 2 |
| UBXD8 | Ub-like (UBX)-domain-containing 8 |
| UDP | Uridine diphosphate |
| UFD1 | Ubiquitin fusion degradation protein 1 |
| uPA | Urokinase-type plasminogen activator |
| uPAR | uPA receptor |
| UPR | Unfolded protein response |
| UPRE | UPR element |
| UPS | Ubiquitin–proteasome system |
| VCP | Valosin-containing protein |
| VEGF-A | Vascular endothelial growth factor-A |
| VEGFR2 | Vascular endothelial growth factor receptor 2 |
| VIMP | VCP-interacting membrane protein |
| Wnt | Wingless |
| XBP1 | X-box binding protein 1 |
| XTP3-B | Transactivated protein B |
| YOD1 | Ubiquitin thioesterase OTU1 |
| ZEB1 | Zinc finger E-box binding homeobox |

# 1

# Introduction

## 1.1 Prostate cancer

Prostate cancer (PCa) is the second most common cancer in adults in the UK and the most common cancer in men in the UK. It accounts for nearly 50,000 new cases in a year in the UK [1]. The number of newly diagnosed prostate cancer cases has been increasing over the past decades as more people are getting tested, and also due to the increase in the population age. Even so, the survival rate of prostate cancer is also increasing owing to the advances in prostate cancer screening, making early detection possible [2].

Prostate cancer usually does not show any symptoms in the early stages. PSA (prostate-specific antigen) test might help early detection in the early stages of the disease. Autopsy studies indicated that nearly one-third of the men over the

age of 50 displayed evidence of prostate cancer in histology [3]. Yet, due to the asymptomatic nature of PCa at early stages, the majority of the cases remain undetected [4].

The choice of the course of treatment for a newly diagnosed man is not straightforward as the disease progression is hard to predict and the test used for the detection plays an important role in this decision. For example, based on biopsy, a patient can be diagnosed with local PCa although the tumour may have already spread beyond the prostate, which will not be revealed until the surgery. Watchful waiting can be an option to follow up PCa in some men, if they do not have any symptoms [5].

### 1.1.1 Management of prostate cancer

Among newly diagnosed cases, nearly one-fifth of the cases remain asymptomatic, and the mortality rate is less than 5% [6]. The tumour in these patients is well-differentiated, localised and the chance of progressing to the metastatic stage remains low. Hence, the approach for these patients may be active surveillance, where cancer remains untreated until it starts growing [7]. This process involves routine monitoring of the disease via physical examinations, PSA testing and prostate biopsies in order to detect any progression early [8].

Figure 1.1 summarises the typical progression of prostate cancer when it is not treated. At the beginning of the PCa, the cancer is localised and fully contained within the boundaries of the prostate and is defined as local in terms of the disease burden. The treatment options at this stage include ablation of the tumour by surgery or radiotherapy, aiming for complete removal of the cancer cells. The surgical removal of the prostate (radical prostatectomy) is the treatment modality

as long as prostate cancer remains locally confined to the prostate gland. Complications of radical prostatectomy are related to urinary and sexual function.

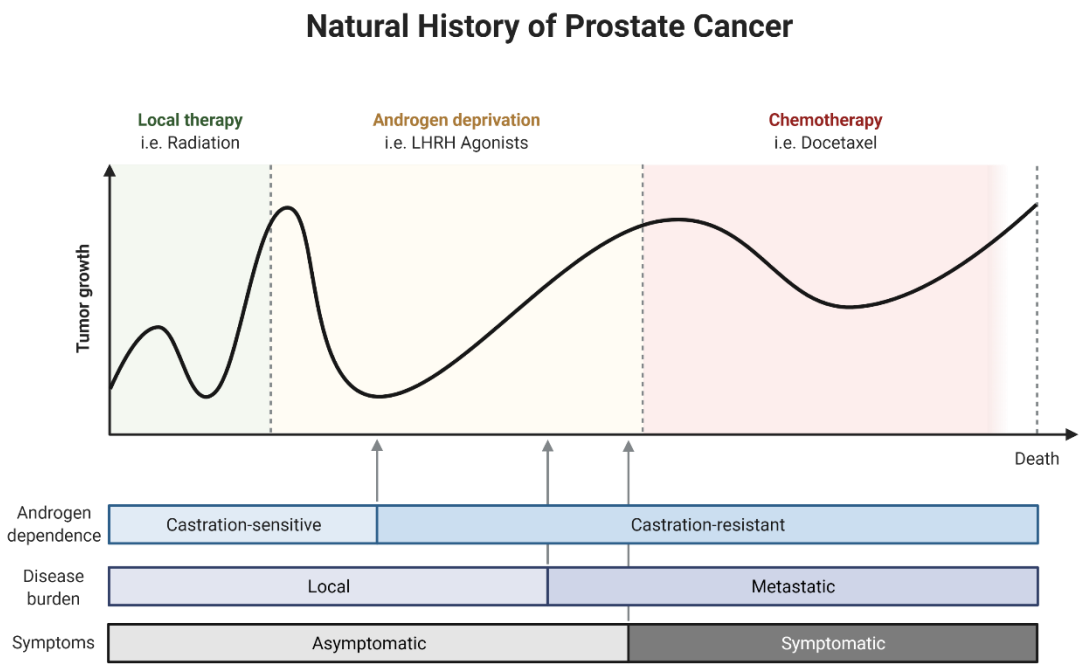



Figure 1.1 Natural history of prostate cancer

The natural history of prostate cancer tumour growth plotted against time until death. Retrieved from BioRender.com [9].

The second option for men with localised prostate cancer is radiotherapy, which can be divided into two categories: external beam radiotherapy and brachytherapy [1]. In external beam radiotherapy high energy X-rays are directed to the tumour externally. Brachytherapy (also known as seed implant radiotherapy) involves surgical insertion of rice-sized radioactive seeds next to the prostate tumour, aiming to kill the nearby tumour cells. The ProtecT trial conducted by Freddie C. Hamdy *et al.* compared the effectiveness of surgery, radiotherapy and watchful waiting in prostate cancer patients with localised tumour; no significant difference in prostate cancer specific mortality was detected among the different groups at 10 years [10]. Although radical prostatectomy and

radiotherapy are curative in most patients, approximately one-third of the cases will experience recurrence with an increase in PSA levels. The tumour in these patients is hormone-sensitive, and androgen deprivation therapy, whether continuous or intermittent, is used to treat the relapsed but hormone-sensitive prostate cancer. Decreasing the level of testosterone to castration levels helps to prevent the growth of prostate cancer cells and decreases the elevated PSA levels.

The majority of prostate cancers respond to reduced hormone levels by decreasing in size or slowing down the growth at the early stages of the disease. After this initial response, prostate cancer will progress to an androgen-independent stage where they no longer respond to hormone therapy. At this stage, prostate cancer cells adapt to very low levels of testosterone in the body, resulting in gradual progress into castration-resistant prostate cancer (CRPC). Most patients progress into this castration-resistant stage despite the initial response to lowering testosterone levels. Several mechanisms have been proposed to explain the progress to CRPC, however, most of the mechanisms involve persistent androgen receptor signalling under androgen deprived conditions. Examples of the mechanisms through which prostate cancer cells become hypersensitive to low levels of androgen include amplification of the androgen receptor (AR) or gain of function mutations resulting in AR signalling even in low levels of androgens; constitutively active splice variants, intratumoral synthesis of testosterone, increased activity of AR coactivators, and epigenetic alterations [11–24].

In addition to the mechanisms that directly involve the AR, CRPC can also be driven by alternative pathways that contribute ligand-independent AR signalling in the absence of androgens. An example of this is interleukin-6 (IL-6) signalling, the expression of which has been reported in prostate cancer cell lines LNCaP, DU-145, and PC3; as well as in prostate cancer specimens [25–27]. Studies in

LNCaP cells revealed that IL-6 activated MAPK- and STAT3-mediated transcription of AR, and overexpression of IL-6 induced mRNA transcription of PSA in the absence of androgen [28–31]. IL-6 was also elevated in metastatic prostate cancer patients and the level of expression correlated with tumour burden [32, 33]. Other pathways that contribute to persistent AR signalling independent of androgens include insulin-like growth factor (IGF) and Src [34].

The treatments of CRPC include anti-androgen therapies, chemotherapy, and immunotherapy. The current chemotherapies used for the treatment of CRPC include docetaxel and cabazitaxel, while the antiandrogens used are abiraterone acetate and enzalutamide. Sipuleucel-T is the first immunotherapy agent used for hormone-resistant prostate cancer, which works by autologous injection of antigen-presenting cells of the patients following *ex vivo* isolation and activation by Sipuleucel-T [35].

With advances in screening of patients and next-generation sequencing of the cancer genome, several new drugs became available for the treatment of PCa [36]. Examples of these are Olaparib and Rucaparib that inhibit the poly(adenosine diphosphate–ribose) polymerase (PARP) in patients with loss-of-function mutations in DNA repair genes [37–40]. The phase 2 trial of Talazoparib, another PARP inhibitor, was recently reported for its use in metastatic CRPC [41]. In addition to the above-mentioned treatments, radiopharmaceuticals have been integrated into the CRPC treatment. Radium-223 dichloride (Ra-223) is in use for the treatment of bone metastases of the PCa [42, 43]. Areas where there is active bone growth and healing absorb Radium-223 thanks to its chemical similarity to calcium.

Following the first line of therapy, the tumour burden decreases, and PSA levels decline, but eventually, PCa progresses to metastasise and spread from the

prostate to distant organs. At this stage, secondary hormonal therapies that interfere with androgen signalling are used for PCa that have spread outside the gland. Ultimately, PCa is not responsive to any chemotherapy approach, and the disease is considered to be incurable.

The underlying causes of prostate cancer progression can be attributed to both intracellular mechanisms related to the tumour itself, or the extracellular tumour microenvironment. It is therefore imperative to understand disease pathogenesis in order to develop potentially curative treatments for advanced prostate cancer.

Although surgical, radiation and chemotherapeutic approaches have been remarkably successful in managing localised prostate cancer, metastatic prostate cancer remains fundamentally difficult to treat. It is for this reason that prostate cancer ranks second among the male cancers that lead to fatality. The concept of treatment strategies has largely remained to target the tumour itself so far, however, prostate cancer-related death is mostly due to metastasis, highlighting the importance of understanding the mechanisms behind this progression.

### 1.1.2 Progression into metastatic stage

The prostate gland is a walnut-sized gland that generates essential seminal fluid components. It is made up of three zones: the central zone (CZ), the periurethral transition (TZ), and the peripheral zones (PZ), as well as an anterior fibromuscular stroma, and it is positioned beneath the bladder [44–46]. The ductal tube from the seminal vesicle to where it enters the descending urethra is contained in the central zone. The peripheral zone, which is located at the back of the gland, is where the most majority of prostatic intraepithelial neoplasia (PIN) and cancer (60–75 percent) originates [47–49]. The transitional zone surrounds the transitional urethra and is located right underneath the bladder. This area of the prostate is affected by benign prostate hyperplasia (BPH).

Prostate transformation is a multistep process that involves the development of proliferative inflammatory atrophy (PIA), then, PIN that give rise to localised invasive lesions which subsequently transform into advanced metastatic prostate cancer.

Metastasis, one of the six original hallmarks of cancer, is the process by which the tumour cells spread to distant sites and establish secondary tumours by invading the local tissue through entering the bloodstream or lymphatic system [50]. The locally growing tumour can transform into a more systemic and life-threatening disease with invasion and metastasis.

Inflammation has been proposed to play a role in cancer progression in different tissues and is considered as an enabling characteristic of cancer [51]. Inflammation of the prostate causes PIA that consists of regenerating atrophy in response to cellular damage [52]. Proteins of most of the known tumour suppressors genes of prostate cancer including phosphatase and tensin homologue (*PTEN*), *NKX3.1* and p27 encoding *CDKN1B* are downregulated at this stage of

the progression [52, 53]. Inflammation recruits immune cells that secrete chemokines and cytokines that have the potential to transform cells in the areas of PIA [54]. Inflammatory cells also release a range of toxic compounds including reactive oxygen species and nitric oxide to wash out the infectious organisms by interacting with their genome to cause damage [55]. $H_2O_2$ and nitric oxide (NO) released by inflammatory cells can also interact with the DNA of prostate cells during tissue damage and regeneration [56, 57]. This interaction can cause DNA damage creating stable genomic mutation, yet, areas of PIA have been shown not to have genetic defects [58]. Immunohistochemistry of the regions of prostate atrophy showed high levels of GSTP1 expression, possibly in response to oxidative stress, providing protection from immune cell activity [52]. Later, hypermethylation of CpG islands around the *GSTP1* promoter region results in transcriptional repression of the *GSTP1* [59]. Morphological studies indicated transition between PIA areas, either inflammatory or non-inflammatory, with high grade prostatic intraepithelial neoplasia, and also with adenocarcinoma, indicating a stepwise progression to malignancy [52, 60].

The normal prostate epithelium consists of basal cells (40%) and luminal cells (60%); and is surrounded by a basement membrane. Luminal cells of prostate epithelium express high levels of AR and maintain homeostasis of the prostate. Prostatic intraepithelial neoplasia (PIN) is premalignant lesions that are considered to be precursors to prostate cancer [61]. They are characterised by expansion of luminal cells and reduction of basal cells with an intact basement membrane. The luminal cells in PIN display enlarged nuclei and nucleoli and have elevated cell cycle marker expression [62].

The progression from normal prostate to PIN is characterised by chromosomal loss in region 8p21 which contains the gene *NKX3.1* encoding for prostate-specific,

androgen-regulated homeobox gene in 20% of the PIN lesions [63]. NKX3.1 play role in prostate differentiation and gene alterations of it has been reported to be the earliest among genetic alterations during prostate carcinogenesis [64]. Similarly, silencing of *GSTP1* by promoter hypermethylation occurs early in the progression into malignancy and is observed >70% of cases of PIN, while it is silenced in >90% of PCa [59, 65].

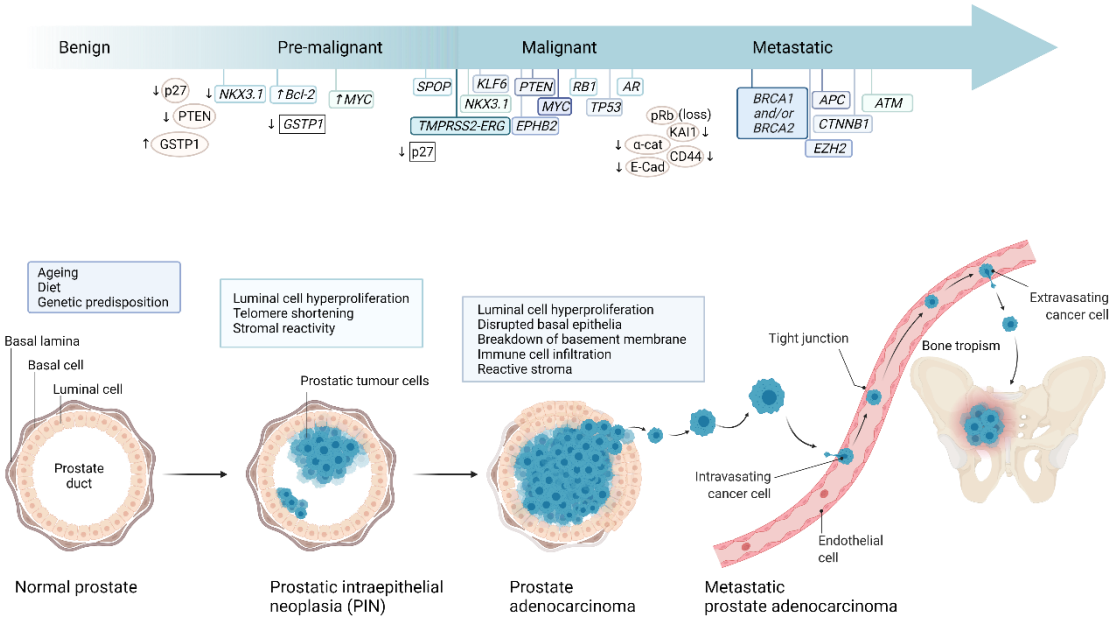



Figure 1.2 Cellular progression of prostate cancer

Schematic representation of cellular progression from normal prostate to metastatic prostate adenocarcinoma [66–68]. The luminal cells of the prostate are shown in orange and the transformed cells are shown in blue. Common mutations of PCa are shown in square boxes. Proteins are shown in rounded boxes. Alterations in the gene expressions are shown as framed text. Downregulation is denoted with an arrow pointing down and upregulation is denoted with an arrow pointing up.

Adapted by permission from Springer Nature: Nature Reviews Disease Primers (Ref. [67], Figure 4), copyright 2021.
Created with BioRender.com.

Progression from PIN to carcinoma is accompanied by destruction of basal cells which therefore involve loss of basal cell markers p63, and cytokeratin 5 and 14 [69–71]. Enlarged nucleus and nucleoli define the cellular characteristics during this transition [72]. The basement membrane surrounding both luminal and basal

cells is destroyed, leading to the local invasion of the tumour, marked by loss of basement membrane proteins laminin 5 and collagen VII [73].

Different stages of malignant transformations harbour different molecular alterations. More than 50% of the primary tumours have inactivated transcription factor KLF6 [74]. The negative regulator of PI3K lipid phosphatase PTEN is lost in 10-15% of the primary tumours, and cell cycle regulator RB protein is lost in 19%. Tyrosine kinase receptor EPHB2 is inactivated in 12%, the oncogene c-myc is amplified in nearly 10% of the primary PCa tumours. Cyclin-dependent kinase inhibitor p27 is downregulated during PCa progression and is associated with poor prognosis [75]. DNA at 12p12-13 which is near p27 encoding *CDKN1B* is lost in almost 50% of distant metastases of prostate cancers [76].

Metastasis of prostate cancer starts when the malignant cells in the prostate acquire migratory properties and detach from the primary tumour in the prostate.

The tumour progresses from a well-differentiated state to moderately differentiated, then to a poorly differentiated state, via the loss of epithelial organisation. Tissue organisation in the prostate epithelium is mediated by cell-to-cell adhesion proteins, including E-Cadherin, $\alpha$-catenin, CD44, metastasis suppressor KAI1 and laminin receptor $\beta$4-integrin, and decreased cell adhesion proteins results in epithelial disorganisation [68, 77–81].

The migration of tumour cells through the lymphatic and circulatory systems to distant organs is the next key step of prostate cancer metastasis. While localised tumours can be cured, advanced metastatic cancer is almost always fatal. The development of metastatic foci of prostate cancer cells in the lymph nodes and bones morphologically characterises this stage in cancer progression. Several genetic changes are associated with metastatic transformation. Deletions at

chromosome 10q which contain *PTEN* and somatic mutations of the *PTEN* allele are observed in more than 12-17% of localised primary PCa, and this increased to 30-43% in metastatic PCa, indicating a role for *PTEN* in PCa metastasis [82].

The polycomb group protein enhancer of zeste homolog 2 (EZH2) has been reported to be overexpressed in hormone-refractory metastatic prostate cancer indicating a role in prostate cancer progression [83]. Studies in different cancer cell lines proposed a potential role for EZH2 in regulating metastases and identified EZH2 to control matrix-metalloproteinases (MMPs) [84].

Fluorescence *in situ* hybridisation with a region-specific probe for c-myc in matched prostatic intraepithelial neoplasia, localised PCa and lymph node metastases radical prostatectomy specimens revealed that substantial c-myc amplification was increased from 0% in PIN, to 8% in carcinoma and to 21% in metastatic specimens. Gain of chromosome 8 (containing c-myc at q24.21) was the most frequent aberration in PIN and carcinoma, which correlated with the Gleason score [85].

Hepsin is a transmembrane serine phosphatase that is overexpressed in nearly 90% of localised prostate cancers [86–88]. *In vivo* studies in probasin promoter-driven hepsin transgenic mice indicated that hepsin has a role in the disintegration of the basement membrane, whether direct or indirect; and overexpression of it impaired epithelial-stromal adhesion, suggesting a role in promoting PCa progression and metastasis [68, 89]. Later studies indicated that hepsin inhibition suppressed prostate cancer bone metastases in mouse models [90].

Overall, prostate tumours harbour different mutations at different stages during progression, and identifications of the genomic alterations is essential for adjustment of the treatment.

## 1.2 Prostate cancer bone metastasis

"When a plant goes to seed, its seeds are carried in all directions; but they can only live and grow if they fall on congenial soil."

Stephen Paget – 1889

The "seed and soil" hypothesis, as it was first proposed by Dr. Stephen Paget in 1889, explains cancer metastasis based on the plant seeds and the soil they can grow: tumour cells (seeds) can only colonise organs (soil) that provides them with ideal growth conditions.

Although prostate cancer can metastasise to different parts of the body including lungs, liver, and brain; it is known for its high potential for skeletal metastasis. More than 80% of the metastatic prostate cancer patients undergoing docetaxel treatment had bone metastases [91, 92]. Among the patients who died from prostate cancer metastases, bone was reported to be the most common metastasis site and the frequency of bone metastasis was 90.1% among 556 patients [93]. Despite its frequency, therapies for bone metastatic prostate cancer are only palliative, and thus, understanding the mechanism of prostate cancer bone metastasis is essential for the discovery of new therapeutics [94].

The dynamic change of a cell from one state to another is referred to as cellular plasticity and involves molecular and phenotypic alterations in the cells [95]. Initially used to describe the broad reprogramming capacity in the stem cells, cellular plasticity acts as a driving factor behind many cancers, including PCa [96, 97]. It is modulated by a number of complicated mechanisms including transcriptional regulation and epigenetic changes [98, 99]. The genes involved in embryonic development are commonly suppressed or reactivated during cell malignancy which allow tumour cells to evade normal growth restrictions,

allowing them to flourish and survive while avoiding therapeutic treatment and immune surveillance [100]. Similarly, in PCa, cellular plasticity helps tumour cells acquire resistance to targeted treatments in a variety of ways, including increased stemness, and trans differentiation between different cell lineages [101, 102].

Despite the fact that the epithelial-mesenchymal transition (EMT) is a fundamental event in embryonic development, it also plays a critical role in cancer progression. The transformation of an epithelial cell into a mesenchymal phenotype, which is characterised by decreased cell-cell adhesion and enhanced migratory characteristics, provides invasive and metastatic behaviour in preclinical models and is considered as one of the main contributors to PCa progression [103]. However, EMT is a spectrum rather than a binary differentiation of epithelial and mesenchymal states, and many tumour cells are characterised by a hybrid phenotype, with epithelial and mesenchymal cells mixed together (hybrid state), helping tumour cells to spread to secondary locations [104].

Although EMT facilitates the early spread of tumour cells, mesenchymal-epithelial transition (MET) is necessary for efficient seeding and colonisation of circulating tumour cells in distant metastatic sites. This dynamic switching between different phenotypical states could possibly regulate the spread of PCa cells into secondary sites, which could lead to the spread of metastatic disease. There is still a need for more evidence to confirm the role of EMT-MET axis in cellular reprogramming which might be used for different treatment strategies for monitoring prostate cancer.

### 1.2.1 Biological processes involved in prostate cancer metastasis

A tumour cell must overcome numerous barriers to achieve effective spread and metastatic development. Prostate cancer metastasis, like other neoplasms, involves a number of steps, including cell detachment from the primary tumour, local migration, invasion, intravasation, circulation, and extravasation of tumour cells, and finally angiogenesis and colonisation at the new location.

#### 1.2.1.1. Loss of cell adhesion

Tumour metastasis has been shown to be associated with the epithelial-mesenchymal transition (EMT), which promotes the loss of tight junctions between cancer cells, increases metastasis and invasion of cancer cells, and inhibits apoptosis.

EMT is characterised by the loss of epithelial markers (such as E-Cadherin) and increased expression of mesenchymal proteins including N-Cadherin and Vimentin which is a type III intermediate filament that promotes migration [105, 106]. Src, Ras, Wnt/-catenin, PI3K/Akt, MAPK, and TGF-β are other pathways that have been linked to EMT [107].

##### *1.2.1.1.1. E-Cadherin*

The classical cadherins are single-span transmembrane proteins made up of three parts: a hydrophobic transmembrane region, an extracellular area, and a C-terminal intracellular portion that is highly conserved [108]. Their intracellular domain contains binding sites that link them to their cytoplasmic partners catenins and actin cytoskeleton [109].

E-Cadherin is a calcium dependent cell adhesion molecule expressed in epithelial cells [110]. The extracellular region of E-Cadherin extends from the cell surface and binds to cadherins on neighbouring cells providing cell-to-cell contact. Loss

of E-Cadherin enables dissociation of cancer cells from the tumour mass and facilitate metastasis. Snail, Slug, and Twist are among transcription factors that inhibit E-Cadherin expression and promote EMT [111–113].

Secretory epithelial cells in normal prostate tissue express E-Cadherin [114]. The expression of E-Cadherin is decreased in PCa and is associated with poor prognosis [78].

#### *1.2.1.1.2. N-Cadherin*

Unlike E-Cadherin, which is expressed in epithelial cells, N-Cadherin is expressed in nerve tissue, and the levels are low in other normal cells. EMT transition involves increased N-Cadherin expression and a decrease in E-Cadherin, called cadherin switching. Several malignancies have elevated expression of N-Cadherin including prostate cancer [115]. N-Cadherin expression in cancer cells has been linked to carcinogenesis and metastasis. While E-Cadherin provides stable cell-to-cell adhesion, cells expressing N-Cadherin are more dynamic [116].

#### *1.2.1.1.3. β-catenin*

β-catenin is a multifunctional protein that functions as a signalling molecule as well as a structural component of the adherent junction complex. It binds the cytoplasmic portion of E-Cadherin to the cytoskeleton, as well as α-catenin in adherent junctions.

Because β-catenin is quickly ubiquitinated by GSK-3β phosphorylation and then destroyed by proteasome, its cytoplasmic abundance is low in normal cells. The Wnt pathway, on the other hand, inhibits β-catenin degradation by destroying the GSK-3β/β-catenin complex. As a result, β-catenin's phosphorylation is inhibited, resulting in the protein's accumulation.

Membranous β-catenin expression is abundant in the normal prostate, while nuclear β-catenin expression is low. However, the membranous expression in PIN is lower, indicating that the loss of adherent junctions occurs early in tumour formation [117]. Loss of adherent junctions early in tumour formation may be a primary cause of membranous β-catenin loss.

### 1.2.1.2. Local invasion

Aside from cell-cell adhesion, epithelial cells are also linked to the extracellular matrix (ECM). A metastatic cell's ability to move requires contact with the ECM. When a cell gains the capacity to spread, it interacts differently with the ECM. Integrins play a key role in epithelial cell adhesion to the ECM, where they form complexes known as focal adhesions.

#### *1.2.1.2.1. Integrins*

The interaction between the ECM and the cell determines the proliferation, survival, and migration of normal prostate epithelial cells [118]. Integrins attach to the components of the basement membrane and interstitial stroma, such as fibronectin, laminin, and collagens, to mediate interactions between cancer cells and the ECM during the early invasion of metastatic cells.

Integrins are glycoprotein heterodimers that traverse the cell membrane and bind to particular subsets of ECM ligands. They are made up of 24 glycoprotein heterodimers made up of combinations of 18 α and 8 β subunits. Distinct integrins can attach to different ligands, but different integrins can share the same ligand, highlighting the role of integrins in cell communication.

The most abundant integrins in normal prostate epithelial cells are α5β1, α6β1 and α6β4; however, αvβ3 and α3β1 integrins are also present [119]. PCa metastasis is linked to the changes in the expression of integrins and the molecules

that regulate the downstream signalling processes they mediate [120]. The invasiveness of prostate carcinoma cells is linked to reduced expression of α6 integrins in biopsy samples [121].

α6β4 integrin forms hemidesmosomes in normal prostate epithelial cells, connecting intermediate filaments to laminin-5 in the ECM [122]. In tumours, however, α6β4 integrin expression is reduced, weakening cell-cell adhesion, and promoting migration [123]. The primary ligand of α6β4 integrin, laminin-5, is similarly decreasing in expression as PC progresses indicating the importance of local ECM's composition for physiology.

#### *1.2.1.2.2. Focal adhesion kinase*

Integrin signalling is mediated by the interaction of integrins with focal adhesion kinase (FAK), a protein tyrosine kinase that is found at cell membrane focal adhesions [124]. Several tumour-progressing mechanisms, such as cell growth, adhesion-based differentiation, adhesion, motility, and apoptosis, are known to be regulated by integrin-dependent signalling [119].

Cell migration involves the formation of focal adhesions at the cell's leading edge, which serve as an anchor for the cell to drag itself over the ECM. The focal adhesions are then disintegrated at the cell's rear edge as it progresses and withdraws its rear edge. Inhibiting focal adhesion turnover increases the number and size of focal adhesions and inhibits cell migration [125].

Previous studies in PCa cell lines have linked elevated FAK levels to a higher risk of metastatic spread [126]. An immunohistochemistry examination of different prostate tissues revealed that FAK was primarily expressed in the basal epithelial cell layer and the level of expression was elevated in PIN lesions, predominantly in neoplastic cells compared to the normal cells in the surrounding tissue, while

FAK expression in BPH was similar to normal tissue. Higher grade and metastatic carcinomas also had higher FAK expression, indicating the importance of FAK in tumour progression [127].

### 1.2.1.3. Invasion and intravasation

The basement membrane and the interstitial connective tissue around the prostate constitutes a physical barrier for the neoplastic cells that they need to overcome. The next step in the metastatic cascade is partial degradation of the extracellular matrix followed by the escape of the tumour via the vasculature. While the basement membrane is mainly composed of type IV collagen, laminin and heparan sulphate proteoglycan, the main components of interstitial connective tissue are types I, II, III collagen fibres, proteoglycans, and glycoproteins [128]. Matrix metalloproteinases (MMPs) and other proteinases are the enzymes involved in the degradation of the ECM and basement membrane.

#### *1.2.1.3.1. Matrix metalloproteinase (MMPs)*

The matrix metalloproteinases are a family of zinc-binding endopeptidases, that degrade several components of the ECM including collagen, proteoglycans, and glycoproteins. MMPs are mainly produced as proenzymes and require activation by other MMPs via proteolytic cleavage. For example, MMP-2 is produced as the inactive pro-MMP-2 and is cleaved by MMP-14 to produce the active MMP-2, which in turn activates MMP-9.

Both MMP-2 and MMP-9 overexpression is linked to a higher Gleason score and invasive characteristics, and MMP-2 overexpression is correlated with a lower risk of disease-free survival [129–131]. MMP-9 has a key role in the initiation and progression of PCa bone metastases [132]. MMP-9 promotes PCa bone metastases by degrading ECM and basal membrane elements like type IV collagen,

fibronectin, and laminin [133]. Comparison of mRNA and protein levels in radical prostatectomies indicated MMP-9 protein levels in malignant prostate tissue to be substantially greater than the levels in normal prostate tissue [134].

MMPs are negatively regulated by tissue inhibitors of metalloproteinase (TIMPs) [135]. In malignant human prostate cancer tissues, loss of TIMP-1 was linked to MMP overexpression [136].

#### *1.2.1.3.2. Serine proteinases*

This family of proteinases include trypsin, thrombin, plasmin, cathepsin G, and urokinase-type plasminogen activator (uPA), all of which possess a serine residue at their active site.

##### *Urokinase-type plasminogen activator*

The most extensively studied member of this group is the urokinase-type plasminogen activator (uPA), a pro-enzyme, that is activated upon binding to uPA receptors (uPAR). Upon binding to uPAR, uPA catalyses the conversion of the inactive plasminogen to the active serine protease plasmin, which then cleaves laminin, fibronectin, fibrin, vitronectin, and collagen directly or indirectly [137]. Plasmin can activate latent proteinases, including MMPs, that can also digest a variety of ECM components [138].

Different studies have shown the impact of the uPA/uPAR complex on tumour invasion and metastasis of many types of cancers including prostate cancer [139–141]. *In vitro* studies indicated that elevated uPA secretion resulted in increased invasive phenotype due to increased ECM degradation in PC-3 and C4-2 cells that secrete more uPA than LNCaP cells [142]. This was later supported with *in vivo* studies by Dong *et al*.: injection of uPA-silenced PC-3 cells in bone xenografts resulted in reduced tumour burden and bone degradation compared to injection

of PC-3 cells with normal levels of uPA [143]. Furthermore, studies on clinical prostate cancer specimens have linked high levels of uPA and uPAR expression to higher tumour grades (Gleason score of 8 or above), enhanced invasion, and lymph node metastases [144]. These findings show that tumour-derived uPA expression plays a key role in prostate tumour bone development.

#### *1.2.1.3.3. Cysteine proteinases*

Cysteine proteinases have a cysteine residue in their active site and are most active at low pH. Cathepsin B, K, and L that can degrade different ECM components including collagen IV, fibronectin and laminin belong to this category of proteinases.

Several studies comparing prostate cancer tissue to BPH and normal prostate tissue identified elevated levels of cysteine proteinases in malignant tissues. For example, cathepsins B and S expression was elevated in PCa tissue compared to BPH and normal prostate tissue, and the expression level of cathepsin K was higher in PCa compared to normal prostate [145–148].

#### *1.2.1.3.4. Aspartyl proteinases*

Aspartyl proteinases include cathepsin D, whose serum level, when combined with the number of positive cores on a prostatic biopsy, has been shown to be a good predictor of extra-prostatic disease [149]. High levels of cathepsin D have been correlated with relapse and metastasis in metastatic breast cancer [150, 151].

### 1.2.1.4. Homing to bone

Bone is a nutritionally rich site with high blood flow around red marrow. Transforming growth factor, insulin-like growth factors I and II, fibroblast growth factors, platelet-derived growth factors, bone morphogenetic proteins, and calcium are just a few of the growth factors found in bone [152]. These growth factors, which are produced and activated during bone resorption, provide tumour cells with a good ground to thrive on. The bone microenvironment is also physiochemically distinct from that of any other organ in the body [153]. Low oxygen, acidic pH, and high phosphate concentrations in the bone matrix provide an ideal habitat for tumour development [154, 155]. The above-mentioned growth factors, as well as the chemical properties of the bone microenvironment, combine to promote the vicious cycle of bone metastasis [156].

After invading a distant organ, cancer cells enter a proliferative state, leading to the formation of secondary tumours. The primary tumour partly directs the organ choice for metastatic development by releasing substances that act systemically at distant secondary locations, altering the local environment and attracting host immune cells, promoting the colonisation of these sites [157]. The presence of the pre-metastatic niche suggests that metastasis to a certain organ is more of a foregone conclusion, with tumour cells leaving the main tumour with a predetermined destination.

Prostate tumour cells have a preference for binding to human bone marrow endothelial (HBME) cells over other endothelial cells [158, 159]. The processes by which tumour cells adhere to the bone are considered to be mediated by substances generated or expressed in both the bone and the tumour. Endothelial cells in the bone contain adhesion molecules such as P-selectin, which can interact with prostate cancer cell surface molecules such as the sialyl-Lewis$^X$ carbohydrate

in a low-affinity manner [160, 161]. Subsequently, the attachment of the PCa cells to the bone epithelium is mediated by integrins, but other factors are also involved [162]. For example, expression of integrin $\alpha v\beta 3$ in C4-2 cells promotes bone metastatic growth in a mouse xenograft model, while integrin $\alpha 2\beta 1$ expression in LNCaP cells helped attachment to the Collagen-1 in the bone after tibial injection, suggesting a role in the spread of the tumour in the bone [163, 164]. Another factor that has a role in the bone metastatic nature of PCa is Cadherin-11, also known as osteoblast-cadherin, which is expressed in bone metastatic PCa and mediates bone homing [165].

The factors in the bone microenvironment also act as chemoattractant for PCa cells that promote migration towards the bone [166]. One example of this is the chemokine stromal-derived factor-1 (SDF-1 or CXCL12) that attracts PCa cells for bone localisation [167]. Metastatic PCa cells express elevated levels of the SDF-1 receptor CXCR4 [168]. The role of SDF-1/CXCR4 in mediating the chemotaxis of PCa to bone is validated in human PCa cell lines LNCaP, C4-2B, and PC3: antibodies of SDF-1 inhibited migration of LNCaP, C4-2B, and PC-3 tumour cells, an antibody to CXCR4 blocked the invasion of C4-2B cells, and SDF-1 inhibitor T-140 blocked the invasion of PC-3 cells [169, 170]. Although CXCR4–SDF-1 axis has been shown to be important for bone metastases of other cancer types including breast, kidney, lung, and pancreas; the bone trophic nature of PCa is not limited to the CXCR4/SDF-1 axis [171].

After PCa cells reach the bone site, the vicious cycle starts: the factors released from the tumour result in osteolysis, and the factors released as a result of osteolytic destruction promote tumour growth.

## 1.3 Pathophysiology of Bone Metastasis

Bone is a dynamic tissue that continuously remodels itself with the balanced activity of bone making osteoblasts and bone-resorbing osteoclasts. The growth of tumours in bone depends on the lost balance between osteoblasts and osteoclasts.

Skeletal metastases are categorised as either osteoblastic (when bone production outnumbers bone resorption) or osteolytic (when bone resorption outnumbers bone formation). In most of the metastases, patients have both osteoblastic and osteolytic lesions, with some patients having mixed lesions containing both blastic and lytic components. For example, among the bone lesions of breast cancer, up to 15% are osteoblastic or mixed, while 80% of patients with metastatic disease have osteolytic lesions [172]. Although bone metastasis of prostate cancer is predominantly osteoblastic, the lesions may have elevated bone resorption [173].

Many of the mechanisms that govern bone cell development, also impact prostate cancer bone metastases. In order to understand PCa bone metastases, it is necessary to first consider normal bone biology. Osteoblasts, osteoclasts, mineralised bone matrix, and other cell types (bone lining cells and osteocytes) make up the bone microenvironment.

### 1.3.1 Osteoblasts

Osteoblasts are bone-forming cells that arise from mesenchymal stem cells, which also give rise to adipocytes, chondrocytes and muscle cells [174]. Osteoblasts synthesise the components of the bone matrix including calcium phosphate crystals, mainly hydroxyapatite, and various constituents of extracellular matrix, such as type 1 collagen and proteoglycans. Thus, they have a polarised shape and are positioned on the bone surface to ensure the mineral deposition is in the

direction of the bone matrix. Osteoblast differentiation from MSCs require transcription factors Runx2 and Osterix and involve the synthesis of bone morphogenetic proteins (BMPs) and members of the Wingless (Wnt) pathways.

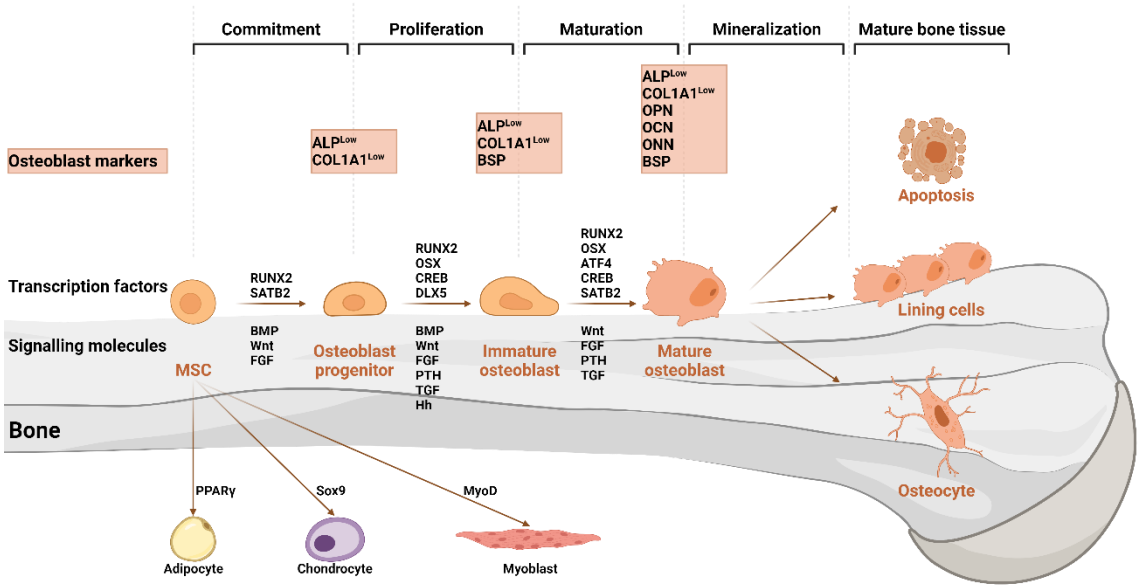



Figure 1.3 Schematic representation of osteoblast differentiation

The transcription factors and signalling molecules involved in the process are shown above or below the arrows indicating each step. The osteoblast markers are highlighted in orange boxes. MSC, mesenchymal stem cell. ALP, alkaline phosphatase. COL1A1, collagen type 1 alpha 1 chain. BSP, bone sialoprotein. OPN, osteopontin. OCN, osteocalcin. ONN, osteonectin. RUNX2, runt-related transcription factor 2. SATB2, special AT-rich sequence-binding protein 2. OSX, osterix. CREB, cAMP-responsive element-binding. DLX5, Distal-Less Homeobox 5. ATF4, activating transcription factor 4. BMP, bone morphogenetic protein. FGF, fibroblast growth factor. PTH, parathyroid hormone. TGF, transforming growth factor. Hh, hedgehog. $PPAR_{\gamma}$, Peroxisome proliferator-activated receptor gamma. Sox2, SRY-Box Transcription Factor 2. MyoD, myoblast determination protein 1.

Modified from [175], created with BioRender.com.

#### 1.3.1.1. Runx2

Runt-related transcription factor (Runx) is a transcription factor family (Runx1, 2 and 3) that scaffold DNA binding proteins involved in transcription of haematopoiesis (Runx1), osteogenesis (Runx2) and neurogenesis (Runx3).

Runx2 is expressed as the master regulator in the progenitor of osteoblasts, MSCs, and in bone metastatic cancers [176]. Runx2 regulates transcription of genes involved in osteoblast differentiation, including alkaline phosphatase (ALP), bone matrix proteins, bone sialoprotein (BSP) II, osteopontin (OPN), fibronectin, and collagen I [175]. Runx2 also promotes the expression of Osterix (OSX), the other key transcription factor involved in osteoblast differentiation. Besides promoting osteoblast differentiation, Runx2 also support tumour induced osteoclastogenesis activating transcription of RANKL and suppressing that of osteoprotegerin (OPG) [177].

#### 1.3.1.2. ATF4

Activating transcription factor (ATF) 4 is a transcription factor in the cAMP-responsive element-binding (CREB) protein family, involved in osteoblast differentiation. It promotes osteoblastogenesis by interacting with RUNX2 for the transcription of osteocalcin (OCN) also by promoting β-catenin levels [178].

#### 1.3.1.3. Alkaline phosphatase

Alkaline phosphatases (ALP) are isoenzymes that catalyse the hydrolysis of organic phosphate esters into inorganic phosphate at high pH [179]. They are metalloenzymes that need zinc and magnesium as co-factors for enzymatic activity and are found on the cell membrane's outer layer. ALPs are classified into two main groups as tissue-specific ALPs and tissue-nonspecific ALPs [180].

Tissue-specific ALPs are only detected in tissues where they are expressed physiologically. Intestinal ALP (IALP, also known as IAP), placental ALP (PALP, also known as PLAP), and germinal tissue ALP (GCAP) are the tissue-specific alkaline phosphatases. Although ALPs are found in diverse bodily tissues and have distinct physiochemical characteristics, they are true isoenzymes since they catalyse the same reaction.

Tissue-nonspecific alkaline phosphatase (TNSALP; TNALP; TNAP), or liver/bone/kidney make up the majority of the proportion circulating in the blood and are thus of clinical importance [181]. Alkaline phosphatase (ALP) is a marker of early osteoblast differentiation that is expressed in the osteoblast precursors. A single gene encodes tissue nonspecific ALP, which is expressed in the liver, bones, and kidneys. The amino acid sequence of all tissue-nonspecific ALPs is the same, but the carbohydrate and lipid side chains differ; post-translational changes give their distinct physicochemical characteristics. The expression of alkaline phosphatase is regulated by RUNX2, MSX2 and SOX9. After translation, ALP undergoes N-linked and O-linked glycosylation in the endoplasmatic reticulum (ER) and Golgi apparatus [182].

Bone-specific alkaline phosphatase (bALP) is a nonspecific kind of ALP generated by osteoblasts during matrix maturation to hydrolyse inorganic pyrophosphate (PPi) and create phosphate (Pi), which is utilised in the production of calcium hydroxyapatite [183]. Thus, osteoblastic activity can be measured by ALP, a biochemical marker of bone formation.

#### 1.3.1.4. Collagen 1

The creation and deposition of type 1 collagen, the most common and significant extracellular matrix protein found in bone, is the first step in the formation of the bone matrix [184]. Collagen 1 is a bone structural protein that gives flexibility

and strength. Type 1 collagen also serves as a scaffold for bone formation and aids in the deposition of other matrix proteins like hydroxyapatite. 90% of the bone matrix contain collagenous proteins, which constitute the structure of osteoid produced by osteoblasts.

### 1.3.2 Osteoclasts

Osteoclasts are bone-resorbing cells that arise from the differentiation of monocyte-macrophage lineage cells. They arise from the monocyte fusion and have from about 2 to 12 nuclei per cell, and can be distinguished by intense tartrate-resistant acid phosphatase (TRAP) activity, and calcitonin and vitronectin receptors expression [184].

Osteoclast differentiation is triggered by the interaction of monocyte precursors with osteoblasts in the bone microenvironment, allowing the precursor cells to develop into osteoclasts. By attaching their surface integrins to a bone protein called vitronectin, terminally developed osteoclasts form a tight bond with the bone matrix.

Multiple infoldings of the osteoclast cell membrane produce a "ruffled border" between the osteoclast and the bone. Across the ruffled boundary, osteoclasts secrete acid and proteases, which dissolve the mineral of bone, degrade the organic matrix, and finally undergo apoptosis.

### 1.3.3 Bone remodelling

The normal bone environment is a nutritionally rich microenvironment due to the release of growth factors during bone remodelling. Normal bone remodelling is the process by which the old bones are replaced by newly formed stronger bone cells with the coordinated actions of bone-resorbing osteoclasts and bone-forming

osteoblasts. The process depends on calcium, vitamin D and phosphate [185]. When cancer metastasises to the bones, bone formation and bone resorption are imbalanced, resulting in osteolytic or osteoblastic lesions. Different types of cancer cells secrete different osteoblastic and osteolytic factors, the underlying mechanism is mostly context dependent.

### 1.3.4 Osteoblast-associated factors

The formation of osteoblastic lesions is triggered partly by tumour cells secreting osteoblastic factors, which include endothelin-1 (ET-1), BMP, and IGF [186].

#### 1.3.4.1. Endothelin-1

Endothelin-1 (ET-1) is a vasoconstrictor generated by the vascular endothelium and plays an important function in vascular homeostasis. It activates secondary messenger systems to mobilise calcium and induce protein kinase C via binding to ET receptor subtype A (ETA), which is connected to heterotrimer G proteins, and stimulates bone growth [187]. This process promotes phosphate transport and is necessary for the calcification of the bone matrix. ET-1 also stimulates osteoblast proliferation while inhibiting the development and mobility of osteoclasts [188–190].

ET-1 is a direct mitogen for osteoblast progenitors *in vitro* and *in vivo*, and is produced by tumour cells, including PCa cells in bone environment [191–193]. Nelson and Carducci were the first to link ET-1 to osteoblastic metastases in prostate cancer, implying that exogenous ET-1 promotes prostate cancer cell proliferation [194, 195]. When compared to males with early-stage prostate cancer, the level of serum ET-1 is higher in men with osteoblastic prostate cancer metastases [186].

Atrasentan is a highly specific and strong ET receptor antagonist that dramatically inhibits the development of osteoblastic responses to cancer in bone in a range of experimental systems. In an animal model of prostate cancer bone metastases, atrasentan dramatically reduced bone lesions but not lesions outside the skeleton, indicating the role of ET-1/ETAR signalling, and limiting this to bone metastasis [196].

Although phase 2 trial of atrasentan in CRPC patients revealed an increase (from 129 to 196 days) in the time to progression and delayed PSA progression; a phase 3 trial with metastatic PCa patients (mostly bone metastasis) indicated that atrasentan could not decrease the primary endpoint of time to progression [195, 197].

The effects of ET-1 are also mediated by activating osteoblast endothelin A receptor (ETAR) and subsequent reductions in secreted Dickkopf homolog 1, a Wnt signalling inhibitor; with a consequent increase in Wnt signalling, another pathway important for osteoblasts differentiation [198].

### 1.3.4.2. Wnt signalling

There are at least 19 glycoproteins in the Wnt family, which are divided into canonical and noncanonical signalling molecules depending on the downstream pathway triggered [199].

The canonical Wnt pathway is activated upon binding of Wnt protein to the frizzled and LRP5/6 transmembrane receptor complex, inactivating the enzyme glycogen synthase kinase 3β (GSK3β) by interacting with Axin, Frat-1, and Dvl proteins, inhibiting β-catenin phosphorylation. β-catenin, when is not phosphorylated, accumulates in the cytoplasm, and translocates to the nucleus, where it controls transcriptional expression of Wnt target genes by interacting

with the Tcf/Lef family of transcription factors. Inactive Wnt pathway releases GSK3β resulting in phosphorylation of β-catenin, followed by ubiquitination which targets it to proteasomal degradation [200, 201].

The Wnt pathway can be controlled by two inhibitor families: Dickkopf (DKKs) and secreted frizzled-related proteins (sFRP). DKKs binding induces internalisation, ubiquitination, and degradation of LRP5/6 by the proteasome. On the other hand, sFRP blocks the Wnt pathway by preventing Wnt-FRZ receptors interaction or by binding directly to FRZ [202]. Increased Wnt secretion, reduced inhibitor expression, or constitutive activation of β-catenin activate downstream target genes including c-Myc, c-Jun, and other genes involved in cancer growth and metastasis [203–205].

Wnt signalling induces the expression of Runx2 in osteoblasts and stimulates osteoblast development in the bone [206]. Wnt signalling also increases BMP-2 expression, causing non-osteogenic cells to transdifferentiate into osteoblasts [207]. MMP-14, a cancer cell invasion and metastasis enhancer, is also a direct target of the Wnt/β-catenin pathway [208].

PCa-derived Wnt promotes osteoblast differentiation and has autocrine effects on tumour growth in prostate cancer bone metastasis [204]. Advanced, metastatic, and hormone-refractory PCa were all linked to increased nuclear β-catenin expression [209]. The level of Wnt inhibitor DKK1 is higher in the early stages of PCa and falls as the disease progresses, resulting in Wnt pathway activation and osteoblast development [210]. Increasing Wnt signalling by inhibiting DKK1 increased osteoblastic activity in osteolytic PC3 cells. Reduced Wnt activity after overexpression of DKK1, however, changed a mixed osteolytic–osteoblastic phenotype of prostate C4-2B cells to an osteolytic phenotype [211].

All these findings suggest that dysregulation of the Wnt pathway is important in PCa bone metastases, and that an imbalance between components that promote and inhibit Wnt signalling may define the kind of bone lesion caused by PCa cells [210].

### 1.3.4.3. Bone morphogenic proteins

Bone morphogenic proteins (BMPs) are members of the TGF-β family and play a role in osteoblast differentiation both *in vitro* and *in vivo* [212–214]. BMP signalling activates the Type I kinase intracellular receptor, which phosphorylates SMAD, which then translocates to the nucleus and stimulates the production of bone-forming genes [215]. The effect of BMPs change depending on the type of BMP in cancer cells.

BMP-7 expression is elevated in osteoblastic bone lesions compared to the normal bone in clinical PCa tissues [216].

BMP-6 expression was first reported in prostate tissue samples from more than half of patients with clinically diagnosed metastatic prostate cancer, but not in non-metastatic or benign prostate tissue samples [217]. Additional research has validated the elevated expression of BMP-6 in metastatic prostate cancer cells [218, 219]. Anti-BMP-6 antibody injections in immunodeficient mice decreased osteoblast counts and tumour development of LuCaP 23.1 prostate cancer cells transplanted in human bone [220]. Expression of Noggin (a BMP antagonist) in LAPC-9 osteoblastic prostate cancer cells promoted osteolytic bone metastases in an intratibial xenograft mouse model, confirming BMPs' osteoblastic impact [221]. The formation of lesions caused by osteolytic PC3 cells was slowed by ectopic expression of Noggin through retroviral expression vector combined with injection of RANKL/RANK pathway inhibitor RANK-Fc [222].

BMP-2 from osteoblasts contribute to PCa cell migration by activating β1 and β3 integrins via activation of the Akt and ERK pathways, which in turn induce IKKα/β phosphorylation and NF-κB activation [223].

Given their essential function in normal bone homeostasis, it's uncertain if BMPs are a feasible target for therapeutic development against bone metastases.

### 1.3.4.4. Insulin-like growth factors

Insulin-like growth factor 1 (IGF-1) is the most abundant growth factor in the bone matrix and is released during the resorption of bone [152].

Both IGF-1 and IGF-2 work by binding to IGF receptors and are involved in bone growth as well as in the key stages of cancer metastasis such as cell proliferation, survival, invasion, and angiogenesis [125, 224]. IGFs stimulate osteoblasts to increase bone matrix apposition and inhibit collagen breakdown and elevated IGF levels in the blood have been linked to increased risk of breast, prostate, and colorectal cancer [225, 226].

Different studies suggested important roles for IGF signalling in driving bone metastases. However, it's uncertain whether bone-derived IGFs play a role in the development of bone metastases as the findings related to the role of IGF on bone metastases are variable.

IGF levels have been linked to prostate cancer progression in clinical studies, with high levels of IGF-1 being linked to a Gleason score ≥ 7 [227]. IGF-1 was elevated in bone metastasis biopsies from prostate cancer patients, and studies in PC-3 cells indicated that IGF-1 promotes cancer cell proliferation and chemotaxis [228, 229]. IGF1R inhibition reduced PCa cell invasion and inhibited MMP-2, a protease required for invasion [230]. In a prostate cancer xenograft model,

neutralising antibodies to human IGF1 or mouse or human IGF-2 slowed the progression of bone lesions [231].

Other research, on the other hand, implies that IGF-1 is not required to trigger the osteoblastic response in prostate cancer. An *in vitro* study in MC3T3 cells (osteoblast precursor cell line) investigating the effect of exogenous IGF-1 found no effect on osteoblast activity. Conditioned media from PC-3 cells induced osteoblast differentiation of MC3T3 cells, and blocking IGF-1 activity using antibody did not prevent this [232]. Overexpression of IGF-1 in PC-3 cells did not affect the osteolytic behaviour of the cells after intratibial injection.

### 1.3.5 Osteoclast-associated factors

Osteoclast differentiation and bone resorption can be triggered by cytokines and growth factors produced by metastatic cancer cells. The osteolytic factors RANKL, PTHrP, and TGF-β are among the most important osteolytic factors in prostate cancer, contributing to bone resorption and osteolytic bone metastases.

#### 1.3.5.1. RANK/RANKL/OPG axis

Receptor activator of NF-kappa B ligand (RANKL) is a TNF superfamily cytokine that works by binding to receptor activator of the nuclear factor-κB (RANK) on the surface of osteoclast precursors, triggering trimerisation and activation of the receptor [233].

TGF-β-inducible kinase TAK1 interacts with TNF receptor-associated factor 6 (TRAF6) via binding adapter protein TAB2, and activates mitogen-activated protein kinase (MAPK), resulting in activation of NF-κB and activator protein-1 (AP-1) [234]. Activated NF-κB and AP-1 by TAK1 then induces the transcription of genes required for osteoclast maturation [235].

Osteoprotegerin (OPG) is a soluble receptor containing only the extracellular RANK domain secreted by osteoblasts and acts as a decoy receptor for RANKL binding [236].

Tumour cells can use the RANK/RANKL/OPG axis to induce PCa–bone metastasis. PCa cells can induce osteoblasts to release soluble RANKL for direct activation of osteoclasts [237]. Bone resorption by mature osteoclasts results in the release of factors to boost PCa cell growth and survival, as the bone is rich in growth factors and cytokines [238].

The RANK/RANKL/OPG axis is disrupted as an approach to prevent metastatic tumour growth in the bone. Denosumab is a completely human monoclonal $IgG_2$ antibody against RANKL with a high affinity for human RANKL. It is used to prevent bone loss in prostate and breast cancer–bone metastases by reducing bone turnover and thereby cancer growth on the skeleton [239–241].

RANKL expression is upregulated in ARCaPM cells compared to epithelial ARCaPE in the ARCaP EMT model, implying that it plays a role in the EMT [242, 243]. In conclusion, RANKL/RANK/OPG system is a complex intercellular regulation mechanism involving cancer cells and the tumour microenvironment, and it is a promising therapeutic target for managing bone turnover in cancer–bone metastases.

### 1.3.5.2. Parathyroid hormone-related protein

Parathyroid hormone-related peptide (PTHrP) is the homolog of parathyroid hormone, and both are ligands for parathyroid hormone receptor. PTHrP increases the production of RANKL in osteoblasts and decreases the expression of OPG (a soluble decoy receptor that binds to RANKL), leading to the activation of osteoclasts, thereby promoting osteolytic metastasis [244, 245].

PTHrP expression in prostate cancer varies depending on the stage of the disease, with expression seen in 33% of benign prostate hyperplasia, 87% of well-differentiated tumours, and 100% of poorly differentiated and metastatic tumours [246]. Clinical specimens of prostate cancer indicated an elevated level of PTHrP in osteoblastic bone metastases [247]. PTHrP produced by prostate cancer cells can improve both osteoclastogenesis and osteoblastogenesis. While PTHrP secretion activates PTH receptor signalling to stimulate osteoclastogenesis via RANKL signalling, PTHrP produced by tumour cells may potentially contribute to skeletal development by promoting tumour cell proliferation, adhesion, and survival via autocrine or paracrine pathways [248, 249]. Overexpression of PTHrP promoted EMT in DU-145 cells via upregulation of mesenchymal markers Snail and Vimentin and downregulating E-Cadherin suggesting a role for PTHrP in metastatic PCa [250].

#### 1.3.5.3. Transforming growth factor β

Transforming growth factor-β (TGF-β) is a tumour suppressor expressed in normal epithelial cells. During tumour progression, however, many types of tumour cells including prostate epithelial cells become insensitive to TGF-β growth inhibition [251, 252].

TGF-β signalling is triggered after TGF-β ligand binding to Type II TGF-β receptor, which recruits and phosphorylates Type I TGF-β receptor, leading to the activation of SMAD and non-SMAD signalling pathways. TGF-β regulates cell proliferation and differentiation via phosphorylating SMAD proteins, which enter the nucleus and regulate TGF-responsive genes, or by inducing activation of SMAD-independent pathways, including PI3K, AKT and/or mitogen-activated protein kinase pathways.

In prostate cancer bone metastasis, TGF-β is activated by osteoclast-derived proteases or cancer-secreted PSA and uPA after cleavage of its precursor, promoting the production of PTHrP and IL-11, which controls bone growth and resorption [153, 253–256]. TGF-β1 secreted by osteoblasts has also been shown to stimulate chemotaxis of PC3 cells, indicating a role in maintaining the "soil" condition in the bone for metastasis of the "seed" PCa [257].

TGF-β signalling has also been linked to tumour metastasis through TGF-β-induced EMT [258, 259]. SMAD/TGF-β signalling stimulates the expression of several transcription factors, including ZEB1, ZEB2, and SNAI1 [260]. TGF-β stimulates Smad3 and Smad4 to assemble a Smad3/4 complex, which interacts with the CDH2 promoter area and upregulates N-Cadherin production by engaging directly with a particular Smad-binding motif [261]. Moreover, TGF-β signalling induce *SNAI2* expression that is known to inhibit *CDH1* expression, resulting in cadherin switch and EMT [262].

### 1.3.6 The vicious cycle of bone metastases

PCa bone metastasis is the driven interaction between invading tumour cells, osteoblasts, and osteoclasts, resulting in increased tumour growth and bone disease. However, the mechanism of action for bone metastasis development from prostate cancer is poorly understood.

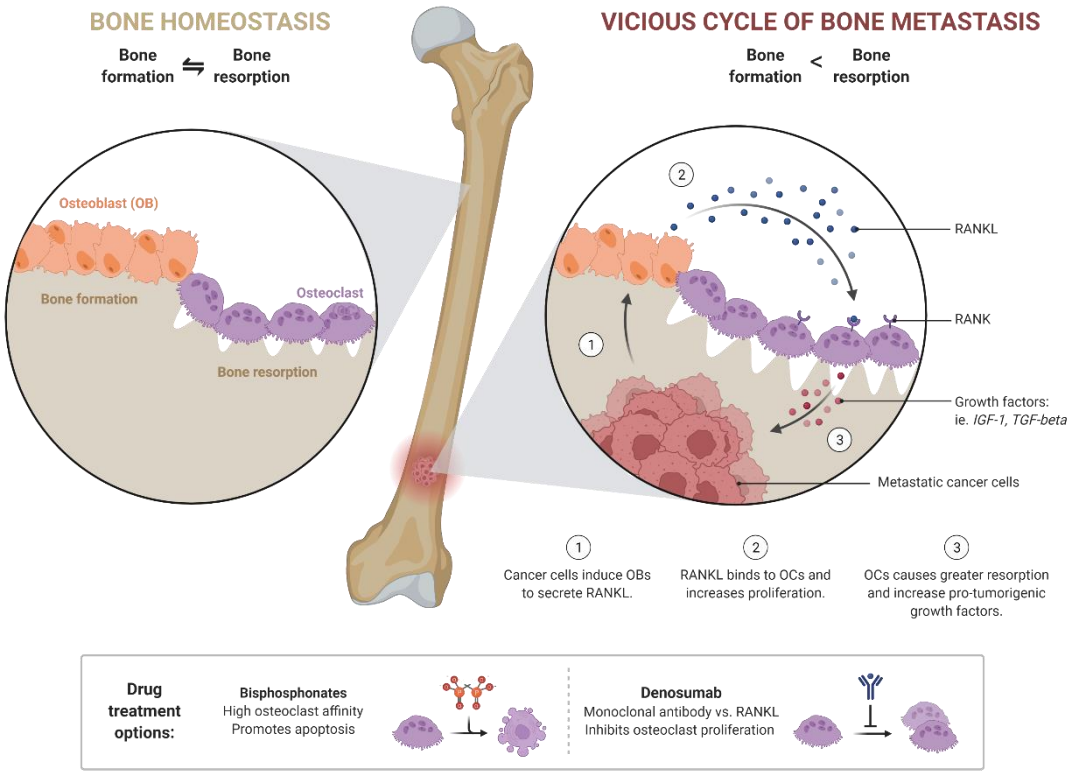



Figure 1.4 The vicious cycle of bone metastasis

Bone homeostasis balances bone formation by osteoblasts (OBs) and bone destruction by osteoclasts (OCs). Metastatic cancer cells induce RANKL secretion by osteoblasts, to bind RANK on osteoclasts, resulting in osteoclast differentiation. Increased osteoclast activity destroy bone, releasing growth factors from bone matrix to induce tumour growth. This vicious cycle between tumour cells and osteoclasts causes bone destruction and tumour growth. Different drugs can break this cycle either by promoting apoptosis (bisphosphonates) or by inhibiting osteoclast differentiation (denosumab, a monoclonal antibody for RANKL).

Reprinted from "Metastasis to Bone Disrupts Bone Homeostasis", by BioRender. Retrieved from Biorender.com [263].

PCa cells acquire an osteoblast-like phenotype, termed osteomimicry, in the bone niche by expressing factors involved in bone cell differentiation and maintenance, which triggers a vicious cycle of tumour growth, bone disturbance, and changes in the bone remodelling process. Tumour cells secrete bone-related soluble factors that activate osteoclasts and may shift normal osteoblasts toward a cancer-associated osteoblast (CAO) phenotype. For example, an increase in osteoclast activating factor PTHrP increases the expression of RANKL and other factors in the bone microenvironment and decreases the expression of OPG resulting in bone resorption [264]. Bone cells, on the other hand, secrete growth factors, such as TGF-β that help PCa cells survive in the bone microenvironment. However, the relevance of this pathway in PCa bone metastasis remains to be elucidated.

### 1.3.7 Treatment of PCa bone metastases

Metastatic PCa cells in the bone disrupt the normal mechanisms underlying bone health and strength, resulting in the complications of the disease, including bone pain and fractures. The treatment of bone metastases helps prevent and treat such complications.

#### 1.3.7.1. Bisphosphonates

Bisphosphonates are a group of drugs used in the treatment of osteoporosis. They inhibit osteoclast-mediated bone destruction and can recover the lost homeostasis between bone formation and resorption that is disturbed by prostate cancer bone metastasis. In addition to inhibiting osteoclast-mediated bone resorption, bisphosphonates have an immunomodulatory effect and can inhibit angiogenesis, induce apoptosis, inhibit cancer cell adhesion to bone stroma [265]. The chemical structure of the side chains determines the potency of bisphosphonates. Bisphosphonates are classified into three groups. First-generation bisphosphonates have the lowest potency among all bisphosphonates. Clodronate

and etidronate belong to this group. Nitrogen-containing bisphosphonates are second-generation molecules and have a better potency than first-generation bisphosphonates due to inhibiting mevalonate pathway enzymes. Pamidronate and alendronate are examples of this group. Third generation bisphosphonates have the best potency among all three groups. These molecules have additional modifications on their nitrogen-containing side chain. Examples of third-generation bisphosphonates are zoledronic acid, ibandronate, neridronate and risedronate. Although bisphosphonates are quickly removed from the bloodstream, their half-lives in bone are measured in years, with alendronate's half-life predicted to be 10 years [266].

#### 1.3.7.2. Denosumab

Denosumab is a monoclonal antibody that inhibits osteoclast function through inhibiting RANKL signalling by binding to and neutralizing RANKL. Denosumab delays the symptoms of the bone disease including fractures [267].

#### 1.3.7.3. Use of radiopharmaceuticals

Radioactive isotopes that can mimic the components of the ECM for bone targeting has been used for the treatment of bone metastases. One of the first approved example of the radioactive isotopes is Strontium-89, a beta particle–emitting that is used for the treatment of PCa bone metastasis via mimicking Ca-binding [268]. Another example is Samarium-153, a beta particle–emitting radionuclide that is used for helping pain in the patients with bone metastases via ethylenediamine tetra (methylene phosphonic acid) linkage targeting [269]. These radionuclides localise to areas of increased bone turnover and deliver local doses of radiation through the emission of beta particles [270]. Both Strontium-89 and Samarium-153 have been shown to help with bone pain in metastatic prostate cancer: however, they did not provide survival benefit when they were

used as single agents [271]. Radium-223 on the other hand, an alpha emitting radiopharmaceutical (mentioned in *Section 1.1.1*), has been shown to prolong overall survival in metastatic prostate cancer [272]. External beam radiation therapy is also used to treat painful bone metastases [273].

### 1.3.8 Models of prostate cancer EMT

EMT, like in many other solid cancer models, is implicated in the development and metastasis of PCa. EMT in prostate cancer has been studied using *in vitro* and *in vivo* models, which have revealed many processes implicated in EMT, including androgen deprivation and TGF-β signalling. Most studies of EMT in cancer use *in vitro* cell models, in which EMT is induced mainly through ectopic expression of transcription factors that induce EMT such as SNAI1 or through stimulation with growth factors like TGF-β [274]. In contrast to many other malignancies, cell lines produced from primary prostate tumours are in little abundance. DU145, PC-3, and LNCaP are the three most common PCa cell lines, however, they are all derived from metastatic PCa.

The development of transgenic and xenograft animal models and human prostate cancer cell lines have provided new insights into the molecular basis of PCa metastasis. For example, LuCaP 35 xenograft model, which is derived by implanting lymph nodes containing metastatic androgen-independent CaP into athymic mice mimic the PCa progression in men as these cells are androgen sensitive and produce PSA [275]. CWR22 model is derived from CaP and they cause rise in PSA levels in nude mice [276].

The osteoblastic function of CRPC has been studied in very few models. For example, the IGR-CaP1 xenograft model mimics the mixed osteolytic/blastic bone lesions that are observed in metastatic prostate cancer patients [277]. This

is useful for investigation of the mechanisms that lead to mixed bone lesions prostate cancer, one aspect that distinguishes PCa from other cancer types, which mostly form osteolytic lesions. However, ARCaP cell line model helps investigation of EMT in the concept of bone metastasis as ARCaP M and E cells differ in their ALP expression. Using the paired cells of human and mouse prostate cancer cells enables a functional comparison of epithelial and mesenchymal characteristics in bone metastatic potential setting.

#### 1.3.8.1. Human prostate cancer ARCaP EMT model

Androgen-repressed human prostate cancer cell line (ARCaP) is a human prostate cancer cell line derived from peritoneal seeding in a patient with prostate cancer bone metastasis. Despite the expression of wild type androgen receptor, ARCaP cells have low levels of PSA compared to LNCaP cells, and exhibit androgen repressed cell growth. mRNA and protein expression of androgen receptor and prostate-specific antigen is low, and androgen represses PSA expression [278].

ARCaPM and ARCaPE cells are derived by serial dilution of ARCaP cells and show mesenchymal and epithelial characteristics, respectively. ARCaPM cells have an increased growth rate and higher migratory capacity compared to ARCaPE cells [279]. ARCaP cells differ in their metastatic ability in mouse models: intracardiac injection of ARCaPM cells form bone and adrenal tumour whereas ARCaPE cells have a lower potential for metastasis. For this reason, ARCaP cells provide *in vitro* model very similar to the pathophysiology of advanced and fatal prostate cancer bone metastasis. Using paired cell lines allows the investigation of metastatic biomarkers and to explore therapeutics that could eradicate metastasis in cancer cells.

### 1.3.8.2. Mouse prostate cancer DVL3 cell line model

DVL3 is a novel cell line derived from tumour in the Dorsal, Ventral and Lateral prostate lobes of a trp53$^{-/-}$/Pten$^{-/-}$ Pb-Cre4 mouse [280]. As the cells are engrafted in syngeneic mice with complete immunocompetency, DVL3 presents an ideal model for developing and validating novel therapeutics, particularly immuno-modulators without ruling out the immune system in the engrafted mice. Tumours formed from DVL3 cells in immune-competent mice maintain the morphological, lineage, and immune characteristics of localised high-risk PCa. DVL3 cells express androgen receptor (AR) and have deletion of the most frequently observed mutations in PCa, representing an adenocarcinoma phenotype similar to tumours of PCa patients.

DVL3-SCM (referred to henceforth as SCM cells) cells are derived by continuous growth of DVL3 cells in a low mitogenic medium (Mills group, unpublished data). SCM cells have higher mesenchymal characteristics compared to DVL3 cells. Upon injection into mice, DVL3 cells form highly vascular, non-invasive tumour mass; whereas SCM cells, the mesenchymal derivative of DVL3 cells, form muscle-invasive, low vascular tumours (Mills group, unpublished data).

## 1.4 The Endoplasmic Reticulum (ER)

Proteins have many functions inside the cell. In order for protein molecules to fulfil their role and to gain functional activity, the proteins must fold into their three-dimensional structures defined for their functions. However, newly synthesised proteins in the cell have the risk of forming toxic species because of incorrect folding and assembly.

The cell has a complex system that uses molecular chaperone network mechanisms to ensure efficient folding and prevent aggregation of proteins. The endoplasmic reticulum (ER) is an important organelle found in eukaryotic cells and is involved in different cellular functions, including intracellular $Ca^{2+}$ homeostasis, calcium storage, and organelle biogenesis.

The ER contributes to the synthesis, folding and trafficking of protein as well as lipid synthesis and is responsible for maintaining a balance between the protein load of the cells and folding capacity in the cells. Most of the proteins are translocated into the ER where they can be modified (namely *N*-linked glycosylation) and folded into secondary and tertiary structures. While adequately folded proteins are sent to Golgi for further trafficking, misfolded proteins are exported to the outside of the ER for degradation, a process called ER-associated degradation (ERAD).

The disruption of the balance between the demand for new protein and ER protein folding capacity results in an increase and accumulation of unfolded or misfolded proteins in the cell leading to changes and disruption in organelle homeostasis, called endoplasmic reticulum stress [281].

### 1.4.1 The Unfolded Protein Response (UPR)

ER stress engages the unfolded protein response (UPR), which is an adaptive response from ER, mediated by three stress sensors. The fundamental role of the UPR is to reduce the burden on the ER caused by unfolded or misfolded proteins and restore organelle homeostasis. The initial response from the cells to cope with the stress is a transient response, where the cells aim to decrease the protein load entering the ER by decreasing the translation of new proteins [282]. The next step is to increase the capacity of the ER for correct folding of the proteins that have already been synthesised but are not yet modified to their terminal structure by increasing the transcription of UPR target genes encoding structural components of the ER, chaperones and enzymes that function in the ER for correct protein folding and ERAD factors to degrade misfolded proteins. The final step in this response is cell death and is only activated when the cell cannot withstand the stress but must respond to protect the organism.

The regulation of ER stress is mediated by three stress transducers: activating transcription factor 6 (ATF6), inositol-requiring enzyme 1 (IRE1), and PKR-like ER kinase (PERK). These stress transducers of ER have three domains: an N-terminal domain that resides in the ER lumen, a single-pass transmembrane domain that anchors them to the ER membrane, and a cytosolic domain that enables the signal transduction to the transcriptional or translational machinery [283]. When the cell is not stressed, each of these stress sensors is normally bound and held in an inactive state by BiP (immunoglobulin heavy chain binding protein), an ER chaperone that assist in nascent protein folding [284].

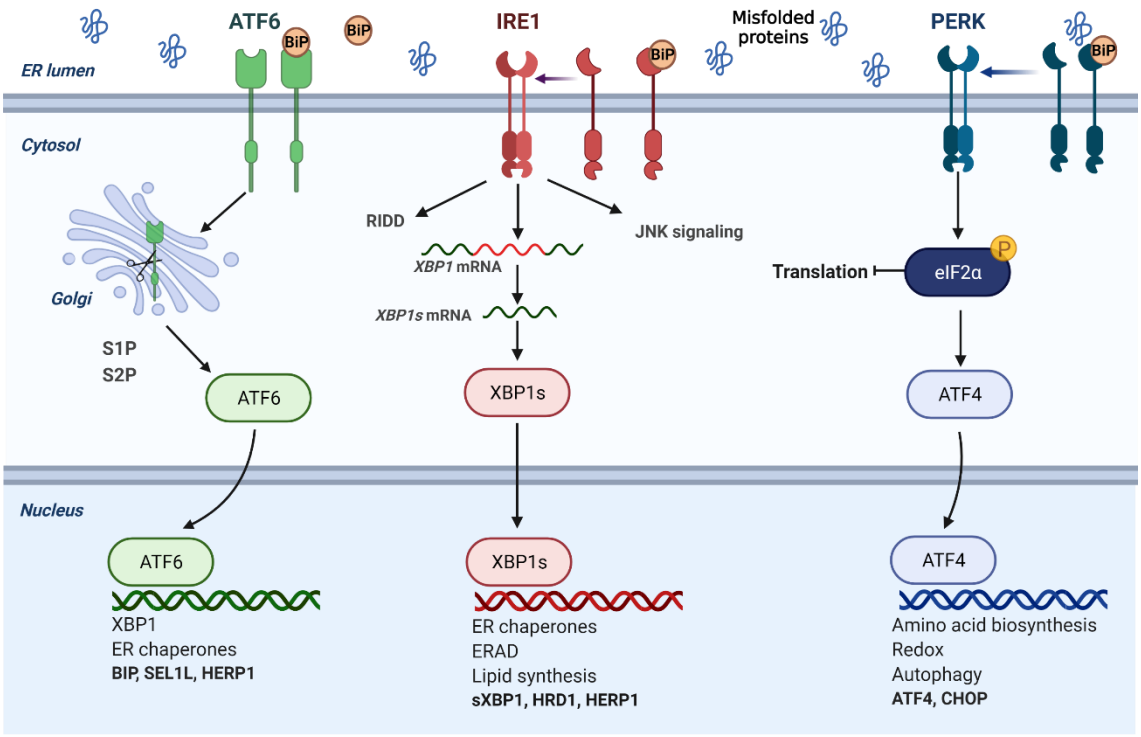



Figure 1.5 UPR signalling (ATF6, IRE1, PERK)

An imbalance between protein load and protein capacity in the ER results in the activation of the ER stress transducers activating UPR signalling. ATF6 (green) IRE1 (red, middle) and PERK (blue, right) are three transducers of ER stress.

The accumulation of unfolded and misfolded proteins in the ER lumen triggers binding by BiP (GRP78), releasing the ER stress sensors ATF6, IRE1 and PERK, resulting in activation of downstream signalling called UPR.

ATF6 translocates from ER to the Golgi apparatus where it is cleaved to its active form by site-1 and site-2 proteases (S1P/S2P). The cleaved fragments then migrate to the nucleus and bind to the ER stress response element that controls and activate the expression of UPR target genes including XBP1, BiP, and genes involved in ERAD, lipid biosynthesis and ER expansion.

IRE1 activation results in splicing of the 26-base intron from the mRNA precursor of X-box binding protein 1 (XBP1) generating a translational frameshift in XBP1 that encodes the transcription factor XBP1. XBP1 transcription factor upregulates the expression of ER chaperones and activates the ERAD program and phospholipid biosynthesis.

PERK activation phosphorylates eukaryotic translation initiation factor 2α (eIF2α), which attenuates the general translation but selectively induce the expression activating transcription factor 4 (ATF4), which then increases the pro-apoptotic CCAAT/enhancer-binding protein-homologous protein (CHOP) expression.

Created with BioRender.com using the template from Emma Madden, PhD Candidate, NUI Galway.

An increase in misfolded proteins in the ER lumen requires more binding by BiP to maintain their solubility, resulting in the release of ATF6, IRE1 and PERK from their inactive state to initiate the UPR. Activation of these arms is not only regulated by the chaperone BiP; they can also sense the unfolded and misfolded proteins by their ER-luminal domain [285, 286]. Each of these sensors recognises the elevated protein folding load and conveys this information to the cytosol where they regulate different signalling pathways in response to the UPR. While the UPR is primarily involved in stress adaption and cell survival; in the presence of irreversible ER stress, a switch to pro-apoptotic signalling events causes cells death.

### 1.4.1.1. Different arms of the UPR

#### *1.4.1.1.1. Activating transcription factor 6 (ATF6)*

ATF6 is one of the ER stress sensors located in the ER membrane [287]. ATF6 is activated upon binding to unfolded proteins in the ER lumen or by dissociation of BiP in response to its binding of unfolded proteins. Activation results in ATF6 translocation to the Golgi apparatus where it is cleaved to its active form by site-1 and site-2 proteases (S1P/S2P), releasing the *N*-terminal cytoplasmic domain that contains a bZIP motif for binding to the DNA [287]. Cleaved ATF6 acts as a transcription factor for the UPR related genes including ERAD components and ER chaperones, as well as XBP1.

#### *1.4.1.1.2. Inositol-requiring enzyme 1α (IRE1α)*

The mammalian genome has two IRE1 isoforms, IRE1α (encoded by *ERN1* gene) and IRE1β (encoded by *ERN2* gene), which are expressed differently depending on the cell type. Because the IRE1α is expressed ubiquitously by all cell types, most mammalian UPR research focuses on it; while IRE1β expression is limited to the gastrointestinal and respiratory tracts [288, 289]. Both IRE1α and IRE1β

are kinases/endonucleases that oligomerise in the ER membrane in response to ER stress; however, while IRE1α activates the transcription factor XBP1 via an unconventional splicing, IRE1β response to ER stress is partial translational attenuation [290].

IRE1α (hereinafter referred to simply as IRE1) is the most evolutionarily conserved among the three stress sensors and is found in animals, plants and the yeast *Saccharomyces cerevisiae* [291–293]. IRE1 is a type 1 ER-resident transmembrane protein consisting of a luminal domain and a cytoplasmic region containing a protein kinase domain. Elevated unfolded proteins cause IRE1 *trans*-autophosphorylation of kinase domains followed by oligomerisation, which can be achieved by binding to the IRE1 domain located in the ER lumen. Alternatively, IRE1 oligomerisation can be triggered as a result of dissociation from BiP. IRE1α activation by phosphorylation in response to stress activates its RNAse domain, which then splices the transcription factor X-box binding protein 1 (XBP1) mRNA [294, 295]. While the unspliced XBP1 encodes for XBP1u that inhibits the UPR; spliced XBP1 mRNA encodes a transcriptional activator of the UPR target genes to regulate the expression of genes related to protein folding, including chaperones and foldases to increase the folding capacity of the cells [296]. Compared to PERK, the IRE1 and ATF6 pathways are more pro-survival in terms of the response they induce following ER stress.

IRE1α degrades other target mRNAs through a process called regulated IRE1-dependent decay (RIDD) [297]. IRE1 reduces the level of protein flux into the ER by degrading the mRNAs located in the ER membrane through RIDD [298].

IRE1 also interacts with TRAF2 (TNFR-associated factor 2) and activates ASK1 (apoptosis signal-regulating kinase 1) to then activate JNK (c-Jun N-terminal kinase) pathway [299, 300]. Triggering the JNK pathway may also activate

apoptosis under irreversible ER stress conditions [301]. JNK pathway activation by IRE1 in response to ER stress can also trigger autophagy by regulating the Beclin1 activity through phosphorylation of BCL2 [302].

#### *1.4.1.1.3. Protein kinase RNA-like ER kinase (PERK)*

The third branch of the UPR is mediated by PERK (encoded by the *EIF2AK3* gene), which is an ER-resident transmembrane kinase that resembles IRE1 [284]. Similar to IRE1, PERK has a cytoplasmic kinase domain that can *trans*-autophosphorylate itself in response to ER stress. Phosphorylated PERK can then phosphorylate the $\alpha$ subunit of the eukaryotic translation initiation factor 2 (eIF2$\alpha$) at serine 51. Phosphorylated eIF2$\alpha$ attenuates general translation in the cells by delaying the ternary complex formation; thus, PERK helps to slow down the flow of protein entering the ER to reduce ER stress [303]. As eIF2$\alpha$ can also be phosphorylated by other eIF2 kinases (PKR, haem-regulated inhibitor kinase (HRI) and general control non-derepressible-2 (GCN2)) this pathway is also called the integrated stress response (ISR) [304].

eIF2$\alpha$ phosphorylation also selectively increases the translation of *ATF4* (Activating transcription factor 4) mRNA. *ATF4* has two upstream open reading frames (uORFs), uORF1 and uORF2 in its 5′ untranslated region (UTR). uORF1 is a positive-acting motif near the 5′ terminus of *ATF4* mRNA that enables ribosome scanning and reinitiation at downstream coding areas. uORF2 overlaps the main-ORF in a different reading frame. As a result, it is classified as an inhibitory element [305].

Under normal conditions, the eIF2-GTP-tRNA$_i^{met}$ ternary complex is readily formed and ribosomes translate the uORF1. As the smaller subunit of the ribosome remains attached to the mRNA, it continues scanning the downstream ORFs, and reassociates with the readily available ternary complex, thereby

reinitiating translation at the uORF2. As the sequence of uORF2 overlaps that of the main-ORF, initiation of the main-ORF is inhibited in response to termination at uORF2. In stressed cells, however, eIF2α phosphorylation reduces the eIF2-GTP-$tRNA_i^{met}$ ternary complex formation on the scanning ribosomes at the downstream of the uORF1, resulting in skipping of the uORF2 and reinitiation at the main-ORF instead [306]. This results in increased expression of *ATF4*, which regulates the expression of genes related to the UPR, including genes related to quality control, autophagy, and cell death. Besides this, ATF4 also drives the expression of CHOP (transcription factor C/EBP homologous protein) and GADD34 (growth arrest and DNA damage-inducible 34). CHOP is a transcription factor that regulates genes encoding components involved in proliferation, differentiation and expression, and it is involved in the ER stress-mediated apoptosis [307]. GADD34 encodes for a protein phosphatase PP1C that dephosphorylates EIF2α, and counteracts phosphorylation of the same protein by PERK, resulting in termination of the integrated stress response. GADD34 is important in balancing the response from PERK downstream signalling [308].

While PERK is involved in cell recovery and regulates proteins involved in ER homeostasis in response to acute ER stress, it can activate apoptosis via CHOP expression if the stress is continuous [309].

#### 1.4.1.2. Integrated stress response (ISR)

Eukaryotic cells respond to different stress sources by activating a common adaptive pathway called the integrated stress response (ISR) to rebuild the impaired homeostasis. As a result, different eIF2α kinases are activated depending on the source of the stress. UPR activates PERK, amino acid deprivation and UV-light induce GCN2 (general control non-derepressible-2 or EIF2AK4 (eIF2α

kinase 4)), viral infection activates PKR (RNA-dependent protein kinase) and low levels of haem activate HRI (haem-regulated inhibitor).

The phosphorylation of eIF2α by either of the kinases results in general translation attenuation, and selective ATF4 activation to restore the homeostasis in the cell. Depending on the type of stress experienced and thus the type of kinase activated, ISR controls gene expression for the best response in a cell-dependent manner [310].

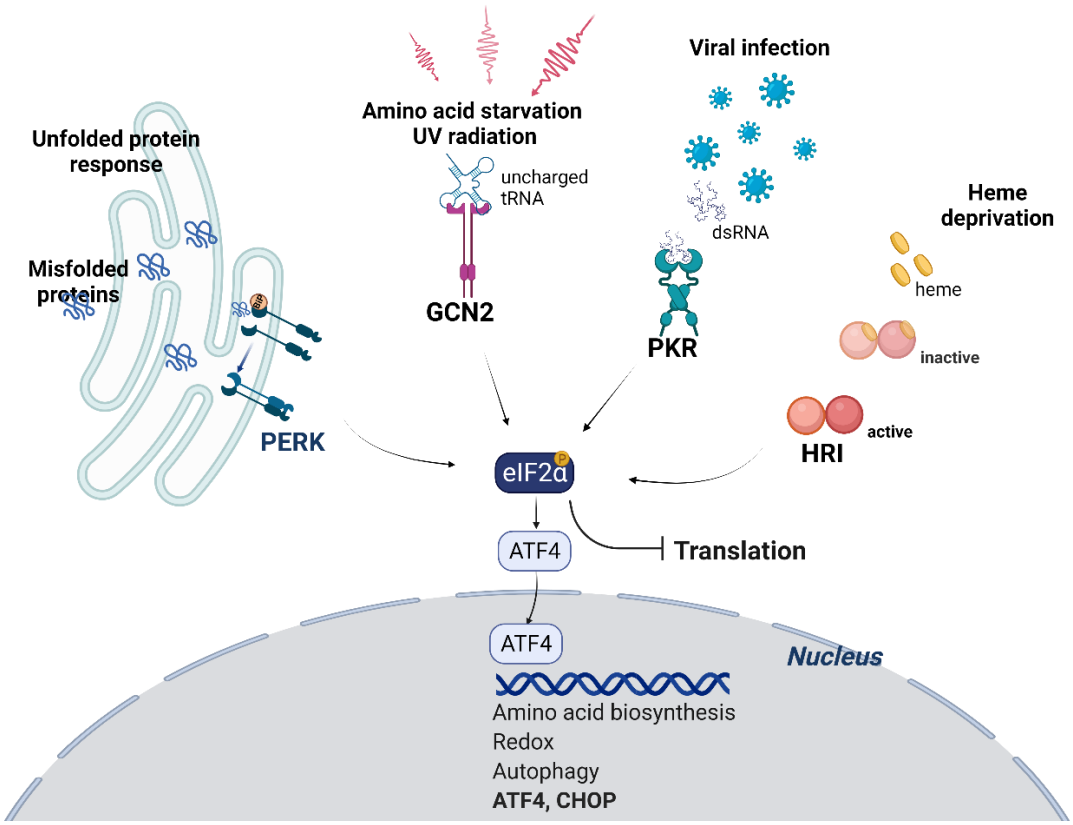



Figure 1.6 eIF2 kinases and the integrated stress response

Different conditions activate ISR protein kinases, PERK, GCN2, PKR and HRI (haem-regulated inhibitor), to regulate the levels of eIF2α phosphorylation, resulting in ATF4 dependent gene expression and general translation inhibition. PERK is activated in response to the unfolded protein response. GCN2 (general control non-depressible) is activated upon binding of uncharged tRNA in response to amino acid starvation. PKR (Protein kinase R) is activated by binding of dsRNA of the infecting virus. HRI is activated upon dissociation of heme from the HRI in response to heme deprivation.

Created with BioRender.com.

### 1.4.1.3. Crosstalk between the arms of the UPR

The cells respond to ER stress via three different signal transducers; however, these pathways communicate with each other. One example of this interaction is that while XBP1 transcription is induced by active ATF6 in response to ER stress, unspliced XBP1 controls the proteasomal degradation of the active ATF6 besides being a negative regulator of XBP1 [294, 311].

Although IRE1 and ATF6 affect the transcription or stability of each other, they may also act together in response to ER stress. A study investigating heterodimerisation of ATF6 and XBP1 found that ATF6-XBP1 heterodimer had a higher binding affinity for unfolded protein response element (UPRE) compared to homodimerisation of XBP1, indicating an essential role of ATF6 in UPRE-mediated transactivation and transcriptional induction of ERAD components [312]. This study concludes that the transcriptional induction of EDEM, HRD1, HERP, and cochaperones ERdj3 and p58IPK proteins depend on both ATF6 and XBP1.

There is also crosstalk between the PERK pathway and IRE1 and ATF6. It has been found that ATF6 synthesis and its trafficking between ER and Golgi is promoted by PERK [313].

ATF6, IRE1, and PERK work together to control the expression of a large number of partially overlapping target genes, resulting in a coordinated response. Each of the UPR transcription factor's target genes are influenced by the nature of the stimulus and the cell type that is impacted, potentially through interactions with other transcription factors. However, as each of the individual arms responds to stress differently, ranging from promoting cell death to adaptation to the experienced conditions, it can be challenging to discern the contribution from each to the final outcome.

A study found that persistent ER stress attenuates the response from IRE1 and ATF6, while PERK activity is maintained, resulting in decreased proliferation followed by cell death [314]. Contrary to persistent PERK signalling, maintaining IRE1 signalling under prolonged ER stress complements cell proliferation [315].

Overall, the outcome in response to ER stress is controlled by the interplay between each arm, and both the timing and the extent of activation of each arm determines the cell fate.

### 1.4.2 ER-associated degradation (ERAD)

Nearly one-third of all the proteins of a eukaryotic cell are synthesised on the ribosomes on ER membrane. Nascent proteins are translocated through the translocon into the ER for correct folding and to acquire the posttranslational modifications including *N*-linked glycosylation, and disulphide bonds needed for proper folding [316]. Folding of the proteins start during the translocation and continues with the activity of different ER-resident chaperones. However, the process is error-prone and genetic mutations of the protein and cellular stress may restrain proteins from reaching their native state. To prevent the toxic effect of aggregates of misfolded proteins and to maintain proteostasis in the ER, cells have acquired a quality control mechanism called ER-associated degradation (ERAD). This process is initiated upon activation of ATF6 and IRE1 pathway as part of the UPR and involves coordinated surveillance processes that eventually take aberrant proteins out of ER for degradation. For a better understanding of the contribution of the components, ERAD can be divided into four distinct but coupled modules: (1) the recognition of the misfolded proteins by chaperones, (2) retrotranslocation to the cytosol by Hrd1 complex, (3) ubiquitination by E3 ubiquitin ligases and (4) degradation by 26S cytoplasmic proteasome [317].

Although gp78 and HRD1 interact, each of these proteins form distinct complexes [318]. gp78 form complex with UbxD8 and UBAC2 and HRD1 form complex with SEL1L, HERP, Derlin and OS-9 [319].

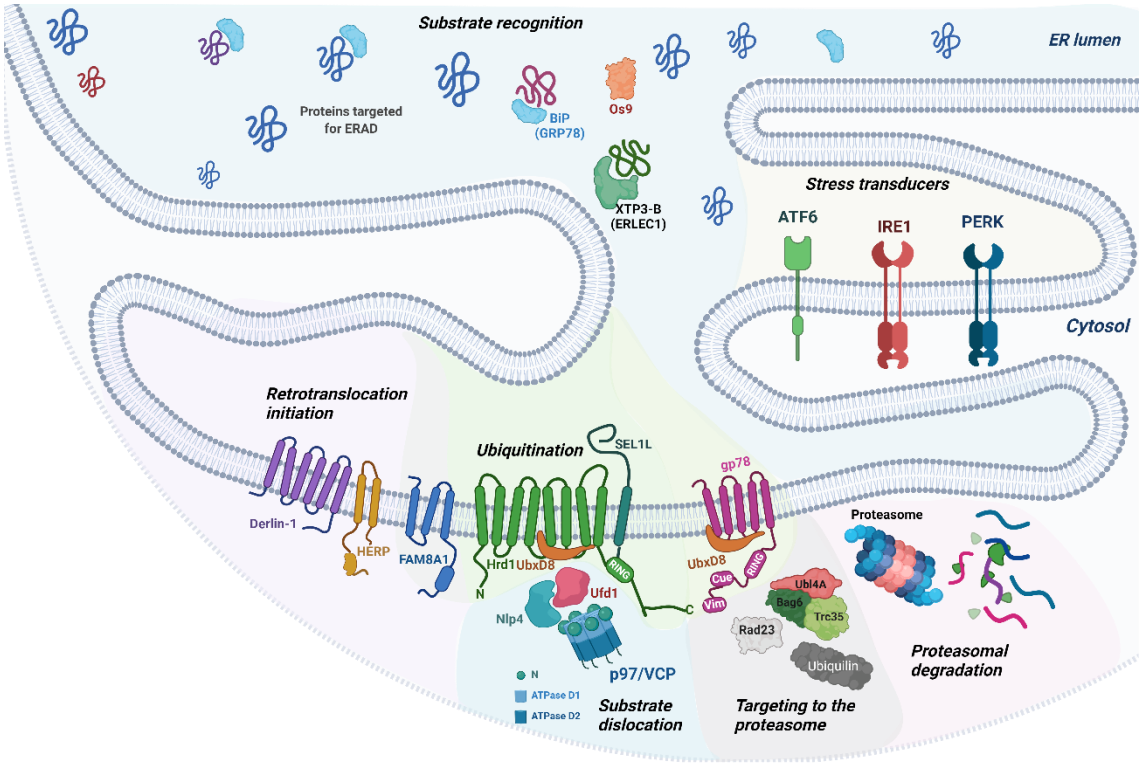



Figure 1.7 Key steps of the mammalian ERAD system

To facilitate retrotranslocation, proteins involved in ERAD are grouped into different modules. Within the ER lumen, molecular chaperones and lectins engage with misfolded and unfolded proteins which are targeted for ERAD (*Substrate recognition*). Proteins involved in substrate recognition bind to the membrane-embedded adaptors, which link substrate recognition to the dislocation machinery. Substrates are dislocated across the ER membrane, presumably through the channel of proteins (dislocons), in a process that is powered by the energy released by ATPase activity of VCP/p97 (*Retrotranslocation*). Substrates are polyubiquitinated by E3 ligases once they reach the cytosol (*Ubiquitination*), sending them to the cytosolic 26S proteasomes for degradation (*Degradation*).

Adapted by permission from Springer Nature: Nature Structural & Molecular Biology (Ref. [317], Figure 2), copyright 2014.

Created with BioRender.com.

### 1.4.2.1. Substrate recognition

The substrates for ERAD include the proteins that could not form their native structure due to genetic alterations resulting in alterations in the protein sequence, loss of ER homeostasis due to high protein demand and due to errors in protein translation. The transfer of the target proteins to the cytosol starts after recognition by ER chaperones and lectins.

#### *1.4.2.1.1. Recognition of glycosylated proteins*

Upon entry to the ER, proteins are co-translationally modified by the addition of $Glc_3Man_9GlcNAc_2$ (Glc: glucose, Man: mannose, GlcNAc: N-acetylglucosamine). Deglucosylation by glucosidases enables the recognition of these proteins by lectin-like chaperones calnexin (CNX) or calreticulin (CRT), which facilitate their folding. Further deglucosylation of the protein generates a glycoprotein with $Man_9GlcNAc_2$ residue, which enables further recognition by CNX/CRT, allowing the exit of the proteins from ER. The proteins that could not reach the final folding state are subject to reglucosylation by UDP-glucose/glycoprotein glucosyl transferase (UGGT), allowing their recognition by CNX/CRT for further attempts of folding. Proteins that failed correct folding escape CNX/CRT cycle and are diverted to ERAD for degradation. This diversion is achieved by the removal of the terminal mannose residues by mannosidases that generate substrate oligosaccharides with deglucosylated, demannosylated forms [320]. The important ER resident mannosidases are ERManI [321, 322], EDEM1 [323, 324] and EDEM3 [325, 326]. Following demannosylation, the proteins are recognised by mannose-specific lectins that direct them to ERAD. Two important lectins that recognise trimmed oligosaccharides are osteosarcoma 9 (OS-9) and transactivated protein B (XTP3-B)/Erlectin and they share a mannose-6-phosphate receptor homology (MRH) domains [327–329]. These two lectins are

proposed to be functionally redundant for stabilising ERAD substrates as knockdown of either had only mild effect while silencing both of them slowed degradation of ERAD substrates [330].

#### *1.4.2.1.2. Recognition of non-glycosylated proteins*

Oligosaccharides in the glycosylated proteins provide a common feature for misfolded glycoproteins. However, despite the lack of oligosaccharides in their mature form, non-glycosylated proteins are also targeted for ERAD. Both OS-9 and XTP3-B were shown to be involved in the degradation of non-glycosylated proteins [327, 328]. Presence of a cryptic glycosylation site that allows post-translational protein glycosylation has been shown to allow the proteins to enter canonical glycan-dependent ERAD [331]. Alternatively, BiP interaction with OS-9 and XTP3-B can enable the recognition of unfolded non-glycosylated proteins [328, 329]. Recognition of non-glycosylated proteins by OS-9 and XTP3-B can also be possible by the intrinsic polypeptide binding capacity of these lectins [326].

Overall, different protein interactions exist in the cells to allow recognition, in both glycan dependent and independent manner.

### 1.4.2.2. Retrotranslocation to the cytosol

The proteasome responsible for the degradation of misfolded proteins resides in the cytosol. Thus, the proteins in the ER lumen that are targeted for degradation must be transferred across the ER bilayer. As most of the ERAD substrates are hydrophobic, the process of translocation and degradation must be coupled to prevent aggregates of proteins in the aqueous environment. Although ERAD involves functionally distinct modules, different adaptors allow coupling of the substrates to different proteins of different stages. ATPase valosin-containing protein (VCP)/p97 is a homohexameric ATPase that drives substrate dislocation.

RNAi mediated knockdown, chemical inhibition, or expression of dominant-negative subunits of VCP/p97 indicated that the majority of the ERAD substrates are stabilised in response to decreased VCP/p97 activity [320]. VCP/p97 resides in the cytosol and it physically pulls the ERAD substrates out of the ER lumen after they are partially passed through ER membrane. Thus, VCP/p97 depends on other proteins that bring ERAD substrates in close proximity for pulling them to the cytosol and initiation of ubiquitination.

#### *1.4.2.2.1. SEL1L*

ERAD machinery is a complex of proteins embedded in the ER membrane and involve ubiquitin ligases as the central processing unit. Most of the ERAD substrates are soluble glycoproteins that reside inside ER lumen while some are integral membrane glycoproteins that have domains exposed to the lumen. Suppressor/Enhancer of Lin-12-like (SEL1L), a polytopic protein, is proposed to be a structural component of the protein complex that translocates the substrates to the cytosol and it scaffolds the luminal ERAD substrates to the membrane-embedded Hrd1 [332]. It binds to OS-9 and XTP3-B, to EDEM1 and EDEM3, and ERFAD-ERp90 [318, 327–329, 333–336]. SEL1L is also part of a complex that includes Derlin-1, Derlin-2, AUP1, UBxD8, VIMP, and HERP which then recruit other complexes in the downstream modules of the ERAD machinery for substrate dislocation [318, 328, 329, 335, 337–340]. Through interacting with proteins involved in different modules of ERAD, SEL1L serves as a network that coordinates ERAD substrate recruitment, dislocation, and ubiquitination.

#### *1.4.2.2.2. HERP*

HomoCys-responsive ER-resident protein (HERP) is a transmembrane protein that acts as a receptor for non-glycosylated BIP substrates [341]. This protein has been implicated to precipitate with Derlin-1, ubiquitylated proteins and the 26S

proteasome [342]. Its interaction with misfolded proteins and the components of ERAD machinery indicate a bridging role for HERP.

#### *1.4.2.2.3. Derlins*

Derlins are multiple membrane-spanning domain proteins that take part in the retrotranslocation channel and regulate the process. Derlins have been proposed to bind to ERAD substrates linking them to the other components of the machinery [343]. For example, Derlin-1 is suggested to take a role in releasing the substrate from the cytosolic face of the ER membrane after their transfer across the membrane [344]. Besides, Derlin-1 has been shown to be important in the US11-dependent degradation of MHC class one (major histocompatibility complex class I) through its interaction with p97 ATPase via VIMP (VCP-interacting membrane protein) [345, 346].

### 1.4.2.3. Ubiquitination

ERAD substrates are tagged with ubiquitin, a highly conserved small protein of 76 aa (amino acid) during their retranslocation from ER for proteasomal degradation in the cytosol. Ubiquitination is a coordinated series of molecular events that involve three classes of proteins, namely E1 ubiquitin-activating enzymes, E2 conjugating enzymes and E3 ubiquitin ligases [347–349]. First, ubiquitin is activated by the formation of a high energy E1-ubiquitin thioester bond between the C-terminal carboxyl of ubiquitin and the active site of the E1 enzyme, in a process that requires hydrolysis of ATP. Then the ubiquitin is transferred to the E2 by transesterification. Finally, E2 acts in coordination with E3 to transfer ubiquitin to the target substrate. Mammalian E3 ligases involved in ERAD contain cytosolic RING (really interesting new gene) domains [350]. Hrd1 is a well characterised E3 ligase in ERAD machinery and it mediates ubiquitin-dependent degradation of misfolded proteins [351, 352]. Lys48-linked

polyubiquitinated ERAD substrates are recognised by the p97 complex resulting in the transfer of the substrates to the cytosol [317].

#### 1.4.2.4. Proteasomal degradation

ERAD substrates tagged by the ubiquitin are extracted from ER and degraded by the cytosolic 26S proteasome. The energy required for pulling the substrates to the cytosol is provided by AAA-ATPase family member p97/VCP [353]. Besides recruiting ERAD substrates to the cytosol, p97/VCP links them to cytoplasmic cofactors required for processing. The binding partners of p97/VCP include E3 ligases Hrd1 and gp78, deubiquitination enzymes (DUBs) ataxin3 and YOD1 and other ERAD accessory factors such as UbxD2 and VIMP [354, 355]. p97/VCP directly binds to NGly1, a cytoplasmic deglycosylating enzyme, and recruits it to the ERAD machinery, where it removes the N-linked glycans from ERAD substrates [353]. Finally, the proteins are released from the membrane and transferred to the 26S proteasome by cytosolic chaperones. The journey of unfolded proteins ends at cytosol, with degradation by the proteasome.

Table 1.1 Summary of proteins in ERAD

*ER proteins*

| | Role | Location, Structure | Ref. |
|---|---|---|---|
| *XTP3-B* | Lectin, scaffolds with HRD1-SEL1L | ER lumen, mannose 6-phosphate receptor homology (MRH) domain | [329] |
| *OS-9* | Lectin, mannose-trimmed N-glycan recognition | ER lumen | [326] |

*ER membrane proteins*

| | Role | Location, Structure | | | Ref. |
|---|---|---|---|---|---|
| | | TM | N terminal | C terminal | |
| *Derlin-1* | Retrotranslocation of luminal ERAD substrates | 6 | Cytoplasmic | Cytoplasmic | [344] |
| *SEL1L* | Adaptor, links lumenal substrate recognition factors to HRD1 | 1 | ER lumen | Cytoplasmic | [338] |
| *HRD1 (SYVN1)* | Ubiquitin ligase | 8 | Cytoplasmic | Cytoplasmic, Ring domain | [356, 357] |
| *FAM8A1* | Cofactor, binds to HRD1 independent of SEL1L | 3 | Cytoplasmic | | [318] |
| *HERP (HERPUD1)* | Cofactor, substrate delivery from the ER membrane to cytoplasmic proteasomes | 2 | Cytoplasmic, interacts with Hrd1 | Cytoplasmic, interacts with Derlin-1 | [358] |
| *gp78 (AMFR, RNF45)* | Ubiquitin ligase | 5 | ER lumen | Cytoplasmic, Ring domain, Cue domain, | [319] |
| *UbXD8* | Accessory protein, Interacts with SEL1L | 1 | Cytoplasmic, UBA | Cytoplasmic, UAS-UBX | [319] |

*Cytosolic proteins*

| | Role | Structure | Ref. |
|---|---|---|---|
| *VCP/p97 (Cdc48)* | Binds the ubiquitinated substrate with the help of adaptor proteins and converts the energy from ATP hydrolysis to structurally remodel the target protein | Hexameric AAA (ATPases associated with diverse cellular activities); each monomer consists of a globular N domain and two ATPase domains D1 and D2 | [359] |
| *Ufd1* | Ubiquitin adapter, recruit substrates to the N-terminal side of the p97 | UT6 domain with SHP motifs for Cdc48 binding ubiquitin-binding UT3 domain | [360] |
| *Npl4* | Ubiquitin adapter | N-terminal UBX-like domain – zf-Npl4 - MPN domain-CTD | [361] |
| *Bag6* | Directs retrotranslocated ERAD substrates to the proteasome | | [362] |
| *Ubl4A* | Bag6 protection from proteosome activity | | [363] |

Adapted by permission from Springer Nature: Nature Structural & Molecular Biology (Ref. [317], Table 1), copyright 2014.

### 1.4.2.5. Hrd1 complex

The ERAD system is a distributed network centred on the E3 ubiquitin ligases, which collaborate with membrane-embedded translocation and cytoplasmic substrate recognition modules [318]. The Hrd1 ubiquitin ligase complex is the best-studied ubiquitin ligase complex involved in ERAD to date.

Synoviolin/Hrd1 (Hydroxymethylglutaryl reductase degradation protein 1) is an evolutionarily conserved E3 ligase involved in the degradation of misfolded proteins [364, 365]. It is a polytopic protein containing at least six transmembrane segments that span ER membrane and has a cytosolic RING domain. The polytopic structure provides Hrd1 coordination with different accessory proteins while the RING domain facilitates ubiquitination of ERAD substrates, directing them for degradation. Cryo-EM structure of Hrd1 suggests a channel-like organisation of five transmembrane domains that link the ER lumen to the cytosol, which could mediate the export of proteins across the ER membrane [357].

An integrative mapping strategy on the ERAD network demonstrated that different substrates rely on a different set of Hrd1-associated cofactors [318].

Hrd1 and its cofactor SEL1L constitute the basis of ERAD complex [337, 366]. SEL1L acts as a scaffold for Hrd1; upon interaction with OS-9 and XTP3-B, it brings ERAD substrates to Hrd1 allowing their ubiquitination [327–329]. Other factors that interact with Hrd1 via SEL1L scaffolding are EDEM1, the molecular chaperone BiP/Grp78, the reductase ERdj5, and the ER flavoprotein ERFAD. Besides acting as an adaptor for interaction factors of Hrd1, SEL1L has been shown to have a role in the stabilisation of Hrd1 [367].

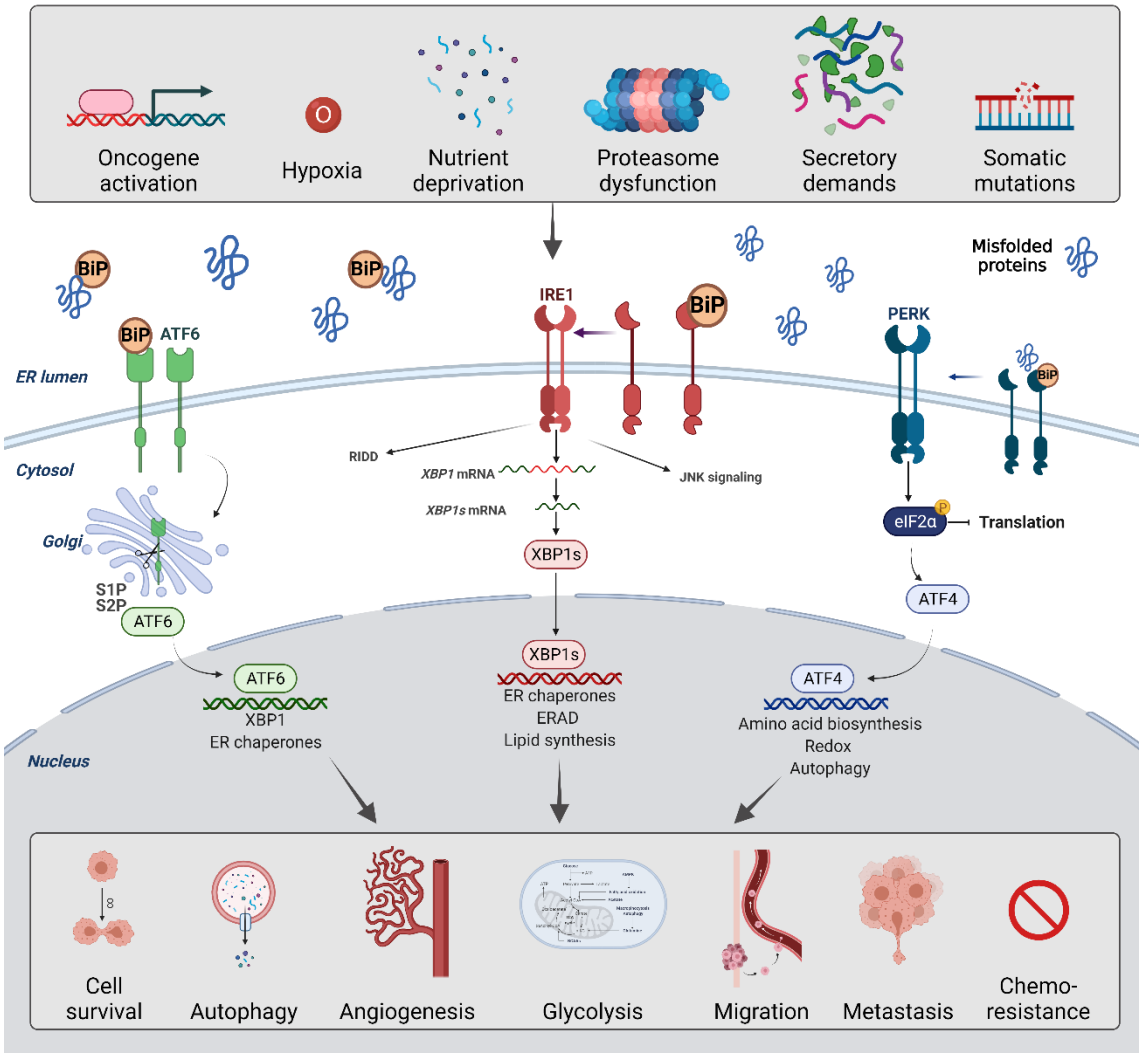
ER quality control compartment (ERQC) is where ERAD substrates accumulate before they are targeted for degradation in proteasomes [368]. Herp (HomoCys-responsive ER-resident protein), also known as HERPUD1, is a ubiquitin-like domain (UBL) containing protein localised in the ER membrane. ER stress induces HERP, which then brings ERAD machinery to the ERQC through interaction with Hrd1 in a UBL domain-dependent manner [342, 369, 370].

Recent studies have identified FAM8A1 (family with sequence similarity 8 member A1) as an interaction partner of HRD1 [318]. FAM8A1 was found to bind to the majority of Hrd1 in the cells, and the binding was independent of SEL1L [371], suggesting regulatory roles for the interacting factors on Hrd1 activity [318]. It promotes Herp-Hrd1 interaction, which is essential for ERAD [356].

### 1.4.3 ER stress signalling in cancer

Solid tumours experience a variety of microenvironmental stimuli and intracellular alterations that will limit their growth. The tumour microenvironment is highly hypoxic, deficient in glucose, and has low levels of nutrients due to abnormal vascularisation. Oncogene activation, increased protein synthesis and secretion and genetic mutations resulting in aberrant protein production all generate a burden for proliferation and constitute a barrier that malignant cells must overcome. Whether extrinsic or intrinsic, these adverse factors result in the accumulation of misfolded or unfolded proteins creating stress in the ER [372, 373]. To survive this stress and re-establish homeostasis in the ER, cancer cells respond by activating the UPR [373]. Studies have shown elevated levels of all three arms of the UPR in different cancer types including lung, breast, colon, oesophageal carcinomas, glioblastoma, stomach, prostate, pancreas, liver; as well as hematopoietic cancers (leukaemia, lymphoma, and myeloma) [372]. Activation of the UPR contributes to cell survival, invasion, angiogenesis, mitochondrial function but also can contribute to autophagy and cell death. The overall result of the UPR activation depends on tissue type as well as the type and chronicity of ER stress.

It is important to note that, although the main role of the UPR in cells is to support cell proliferation, persistent ER stress might lead to cell death. For this reason, studies investigating the role and contribution in the UPR should be tumour and stress condition specific.




## Figure 1.8 Unfolded protein response and cancer

Cancer cells experience different internal (oncogenic activation, proteasome dysfunction, secretory demands, somatic mutations) or external stresses (hypoxia, nutrient deprivation, acidosis) during transformation. The increased protein demand in response to the stress experienced disrupts the homeostasis in ER due to the accumulation of unfolded or misfolded proteins. BiP binding to unfolded proteins release the UPR stress transducers ATF6, IRE1 and PERK, and cancer cells initiate the unfolded protein response to increase the protein folding capacity to adapt to the conditions. The UPR provides an adaptive mechanism for cancer cells and contributes to different mechanisms including cell survival, autophagy, angiogenesis, glycolysis, migration and metastasis, and resistance to chemotherapeutics [374–376].

Adapted by permission from Elsevier: The American Journal of Pathology (Ref. [374], Figure 1), copyright 2020; The American Physiological Society: American Journal of Physiology-Cell Physiology (Ref. [375], Figure 1), copyright 2017; and Springer Nature: Nature Immunology (Ref. [376], Figure 1), copyright 2014.
Created with BioRender.com.

### 1.4.4 ER stress and prostate cancer

Previous studies have linked signal transducers of the unfolded protein response ATF6, IRE1 and PERK to different cancers [314, 377–379]. This section summarises the research related to the UPR in prostate cancer.

A study comparing tissues from PCa patients and BPH compared the expression of the UPR transducers ATF6, IRE1 and PERK using immunohistochemistry [380]. The levels of ATF6, IRE1 and PERK were elevated in PCa compared to BPH. The expression of these were strongly correlated with the patients' PSA levels and the Gleason score. Kaplan–Meier curve analysis indicated that patients with negative ATF6, IRE1 and PERK expression had longer survival times for cancer specific-death and longer survival times for PSA recurrence compared to those with positive expression.

As previously described, androgen receptor (AR) signalling is important in the development of the prostate and is one of the major signalling pathways in prostate cancer [381]. AR signalling directly regulates the UPR pathways in normal and prostate cancer cells. Androgen signalling induces the expression of ER stress response genes N-myc downstream-regulated gene 1 (NDRG1), protein disulphide isomerase-related protein (PDIR), homocysteine-responsive ER-resident ubiquitin-like domain member 1 protein (HERPUD1), and oxygen-regulated protein 150 (ORP150) [382].

AR signalling directly activates IRE1$\alpha$–XBP1s pathway and drive the expression of XBP1s target genes including RAMP4 and EDEM1 in LNCaP and VCaP PCa cells, as well as in human PCa tumours [383]. In line with the pro-survival role of AR in PCa, inhibiting AR-regulated IRE1 signalling via genetic manipulation decreases prostate cancer proliferation and increases apoptosis. One possible explanation to AR-regulated pro-survival role of the IRE1$\alpha$–XBP1s arm of the

UPR is due to its role in direct transcriptional regulation of c-MYC signalling [384]. Moreover, c-MYC has been shown to be positively correlated with AR expression and protein stability of both AR and AR-variants in PCa samples [385]. Previous studies indicate that the IRE1 pathway might have a role in the progression into castration resistance in prostate cancer.

Parallel with its role in sustaining cell proliferation, in AR sensitive cells, AR signalling downregulates PERK activation and eIF2$\alpha$ phosphorylation, which are involved in cell death [383]. In contrast to PERK activation and eIF2$\alpha$ phosphorylation, ATF4 protein levels are elevated in response to AR signalling both in AR sensitive, and castration-resistant PCa (CRPC) model 22Rv1 cells suggesting either post-transcriptional or post-translational modifications in androgen regulation for ATF4 activation [386]. Similarly, ATF4 expression is elevated in human PCa specimens compared to benign prostate and in CWR22R hormone-refractory tumours, suggesting a role for ATF4 in CRPC progression [387].

The prostate is a major secretory organ, and it depends on ER signalling. The high demand for ER activity is enhanced in the prostate tumours and thus, ER stress-causing agents affect the prostate tumours. Cancer targeting therapies have been shown to induce ER stress in PCa, indicating the importance of studying the UPR in the concept of treatment. For example, proteasome inhibitor bortezomib stimulates the UPR and activate the PERK arm and induce cell death in PCa cells [388]. Similarly, salicylanilide derivatives induce autophagy cell death by activating the PERK arm in CRPC cells PC3 and C4-2 [389]. Celastrol leads to autophagy and activates IRE1, PERK and BiP [390]. Triptolide induces autophagy in PCa cell lines by inducing ER stress [391]. The antitumour role of metformin involves upregulation of the PERK arm of the UPR in prostate cancer

cells [392]. S1P triggers ER stress in PC3 cells, as a result, increases XBP1 splicing, resulting in autophagy [393]. The above-summarised studies point out the importance of understanding PERK pathway regulation in the UPR in the concept of treatment of PCa.

### 1.4.4.1. Targeting the ER stress response in prostate cancer

Understanding the contribution of the UPR to cancer therapies is important. Due to its interaction with AR signalling and involvement in prostate secretion, the UPR has been investigated in the context of development of prostate cancer treatments.

#### *1.4.4.1.1. ATF6 inhibitors*

Compared to the studies involving the IRE1 or PERK pathway, the data related to the ATF6 pathway is limited as ATF6 inhibitor Ceapins have only recently been identified [394]. Ceapins inhibit the ATF6 branch by confining ATF6 on the ER membrane and inhibiting its translocation to the nucleus, required for the transcriptional activation [395]. Later studies revealed that Ceapins inhibits ATF6 translocation to the nucleus by inducing physical interaction with ABCD3 peroxisomal transporter [396].

By transcriptionally regulating the expression of ERAD components and ER chaperones, and hence increasing the folding capacity of the ER, ATF6 pathway might have pro-survival role in cancer and may promote tumour progression. Previous studies have assigned a role for ATF6 in tumorigenesis and chemotherapy resistance in different cancers including colorectal cancer and lymphomas; however, the studies investigating ATF6 in prostate cancer is limited. For example, elevated ATF6 levels were correlated with decreased disease-free survival in colon cancer patients [397]. Similarly, in patients with

Hodgkin lymphoma, higher levels of ATF6 was reported [398]. One study reported that activation of ATF6 resulted in survival against chemotherapy induced apoptosis in osteosarcoma cells while knockdown of ATF6 improved sensitivity of osteosarcoma cells to chemotherapies [399]. These studies suggest that inhibition of ATF6 pathway can potentially decrease the PCa proliferation.

#### *1.4.4.1.2. IRE1 inhibitors*

Several compounds targeting IRE1 have been studied in PCa. IRE1 inhibitors can be classified into two categories; those that act on the kinase domain and those that act on the endonuclease activity.

Consistent with the pro-survival role of IRE1 in prostate cancer, IRE1 inhibitor Toyocamycin slows cell growth *in vitro* and tumour growth LNCaP or VCaP xenografts in nude mice [383, 400]. Later studies agreed with the effect of toyocamycin in inducing apoptosis in PC-3 cells by interfering with mitochondrial function and increasing ROS production [401]. Similarly, IRE1$\alpha$ RNase inhibitor MKC8866 suppresses the growth of LNCaP, VCaP, 22Rv1 and C4-2B xenografts [384]. Inhibiting IRE1 RNase activity with MKC8866 synergistically enhances the effect of clinical PCa drugs including enzalutamide, abiraterone and cabazitaxel both *in vitro* and *in vivo* [384]. Decreased XBP1 splicing via overexpression of a mutated (K599A) kinase-deficient IRE1, also slows cell proliferation, supporting the pro-survival role of IRE1-XBP1 signalling [402].

Most of the studies related to IRE1 pathway inhibition investigate their effect in androgen-sensitive cells; however, in PCa, tumours progress to become unresponsive to androgen deprivation. Thus, investigation of the UPR in AR negative or androgen repressed cells is necessary to improve the treatment of castration-resistant prostate cancer.

#### *1.4.4.1.3. PERK inhibitors*

PERK pathway activation in response to ER stress results in translational attenuation which helps cells cope with the protein load exerted on the ER and contribute to cell survival, however, continuous ER stress results in PERK dependent CHOP mediated cell death.

The earliest compound that has been used to inhibit PERK activity is GSK2606414 which is a kinase domain inhibitor of PERK, identified by screening of already registered kinase inhibitors for PERK activity [403]. Then GSK2656157 was identified as an optimised analogue of GSK2606414 [404]. Both compounds have been shown to inhibit RIPK1 kinase activity besides inhibiting PERK activity [405]. However, GSK2656157 was later shown to fail to represent the physiological outcome of decreased PERK activity as it was acting independently of eIF2$\alpha$ phosphorylation [406].

GSK2606414 was used in PC3 and LNCaP cells to investigate the contribution of PERK to HIF1-$\alpha$ activity under hypoxic conditions [407]. The study found that new HIF1$\alpha$ protein synthesis was inhibited due to the interaction of PERK with the 5′ untranslated region in the HIF1$\alpha$ mRNA. Considering its potential to inhibit adaptation to the hypoxic conditions of the tumour, PERK activating compounds might establish the potential of treating hypoxic PCa, either confined to the primary site or in bone metastases.

Later on, a small molecule has been identified to reverse the effect of eIF2$\alpha$ phosphorylation by inducing the assembly of more active translation eIF2B and was called ISRIB for integrated stress response inhibitor [408]. Inhibiting p-eIF2$\alpha$ activity using ISRIB stimulates cytotoxicity in patient-derived prostate cancer xenografts [409].

Different studies have shown that the PERK pathway is activated in response to several known cancer-targeting therapies. Due to its role both in lowering the load on ER and in cell death, investigating the increase and decrease in PERK activity is crucial for understanding its role in the progression of prostate cancer.

### 1.4.5 The UPR in bone development

ECM proteins and calcium phosphate make up the majority of the skeletal system. Osteoblasts and chondrocytes must generate a substantial array of ECM, including collagens, non-collagenous proteins, proteoglycans, and glycoproteins, in order to build and preserve the skeletal system's integrity. About 70% of the bone volume is made up of hydroxyapatite, while the rest is made up of ECM proteins generated by osteoblasts. As a result, these cells must continually deal with the stress of excessive protein production while both transporting and secreting newly synthesised proteins efficiently.

Protein quality control in the ER maintains the skeletal system's integrity, and the UPR aids in homeostasis maintenance and ensures the secretion only properly folded proteins. Likewise, the UPR in the skeletal system functions as a key regulator of osteoblast and chondrocyte differentiation, as well as the formation of osteoclasts, in addition to its role as an adaptation mechanism against ER stress [410–413]. As a result, targeting the arms of the UPR might be used as a therapeutic target in bone malignancies.

The expression of RUNX2, followed by that of Osterix, determines a cell's progression into the osteoblast lineage (*Section 1.3.1.1*). Two putative XBP1 binding sites exist in the promoter region of the gene that encodes Osterix (*SP7*), which are highly conserved across species [414, 415]. Osterix is activated by XBP1s, which works as a transcription factor after IRE1 activation [412]. One

study correlated the PTH-dependent increase in osteoblast differentiation to ATF4-dependent up-regulation of Osterix [416].

ATF4, one of the downstream targets of the PERK arm of the UPR, plays a vital role in maintaining osteoblast activities in more mature osteoblasts. ATF4 has been implicated to have different roles both in osteoblast formation and also osteoclast differentiation. One study identified a critical role for ATF4 due to its interaction with RSK, which takes part in multiple stages of osteoblast differentiation including the timing of the onset of the differentiation, termination of the differentiation and also in expression of osteoblast specific genes [417].

Through its association with RUNX2, ATF4 regulates the transcription of osteoblastic genes, most notably the *BGLAP* (bone gamma-carboxyglutamate protein) gene, which encodes Osteocalcin [418, 419]. Through its expression in osteoblasts, ATF4 also governs osteoclast differentiation and, eventually, bone resorption [420]. ATF4 binds to the promoter of the RANKL and induces its expression and release by osteoblasts. RANKL binding to its receptor RANK on osteoclasts controls osteoclast lineage commitment and activity. ATF4 stimulates bone growth in this way. In osteoblasts, ATF4 also stimulates amino acid transport and type I collagen synthesis [421].

The membrane-bound transcription factor OASIS (encoded by *CREB3L1*) is structurally similar to ATF6. In addition to ATF4, COL1A1 transcription is also promoted by ATF6 [411].

Several studies have shown that the UPR can indirectly regulate osteoclastogenesis. Through signalling cascades regulated by NFκB and c-Fos, intracellular RANK signalling eventually stimulates the expression of NFATc1, the master transcriptional regulator of osteoclastogenesis [422]. IRE1-XBP1

pathway promotes osteoclastogenesis by increasing NFATc1 transcription in osteoclast precursors [413]. Multiple myeloma cells increase the expression of RANKL in bone marrow stromal cells in an XBP1s-dependent way, therefore mediating osteoclast development in multiple myeloma bone lesions [423].

The components of PERK pathway, however, have opposing effects on NFATc1 transcription. While ATF4 expression induces NFATc1 through transcriptional activation, stabilisation of eIF2$\alpha$ phosphorylation using phosphatase inhibitor (which increases ATF4 levels) has been shown to reduce NFATc1 expression, hence suppress osteoclast differentiation [424–426].

Comparison of gene expression between wild type and *Ern1*$^{-/-}$ mouse embryonic fibroblasts has shown that BMP2 induced *Pth1r* transcription was inhibited in the absence of IRE1a. Likewise, *Xbp1* knockdown inhibited osteoclast differentiation by suppressing PTH-induced *Rankl* production in primary osteoblasts. Two potential XBP1 binding sites in the promoter region of *Pth1r* have been identified in osteoblasts and the osteoblast-like cell line MC3T3-E1. This study denoted association of the IRE1$\alpha$-XBP1 pathway with osteoclast differentiation [427].

## 1.5 Overall Hypothesis and Objectives

For years, the concept of treatment strategies has remained targeting the tumour itself, but the majority of deaths from PCa arise following metastasis, particularly to the skeleton. The AR is one of the major drivers in prostate cancer, regulating genes and pathways in PCa, including the UPR. Although the IRE1-XBP1 arm of the UPR has been shown to play role in bone formation and bone resorption by regulating PTHrP, the role of the UPR in PCa bone metastasis is unknown.

The general hypotheses of this work are: 1) The UPR and potentially ERAD associated genes are involved in osteomimetic activity of prostate cancer cells, 2) The UPR inhibitors impact the expression of osteoblast and osteoclast activating factors, 3) ER stress impacts the EMT marker expression and migratory capacity in metastatic prostate cancer cells, and 4) Alkaline phosphatase is important in linking the UPR to the osteomimetic properties of metastatic prostate cancer cells.

The overall aim of this work is to investigate the key steps in the process of bone metastasis using in vitro model systems and determine the role of the UPR in this process, focusing on the effect of the UPR on the osteogenic potential of PCa cells, EMT and migration and on PCa bone disease related factors. Paired cell lines from human and mouse prostate cancer were used for the investigation of the role of UPR in PCa bone metastasis considering their epithelial and mesenchymal characteristics. The contribution of each arm of the UPR was studied using pharmacological inhibitors targeting each pathway, and different ER stress modulators were used for activation of the UPR.

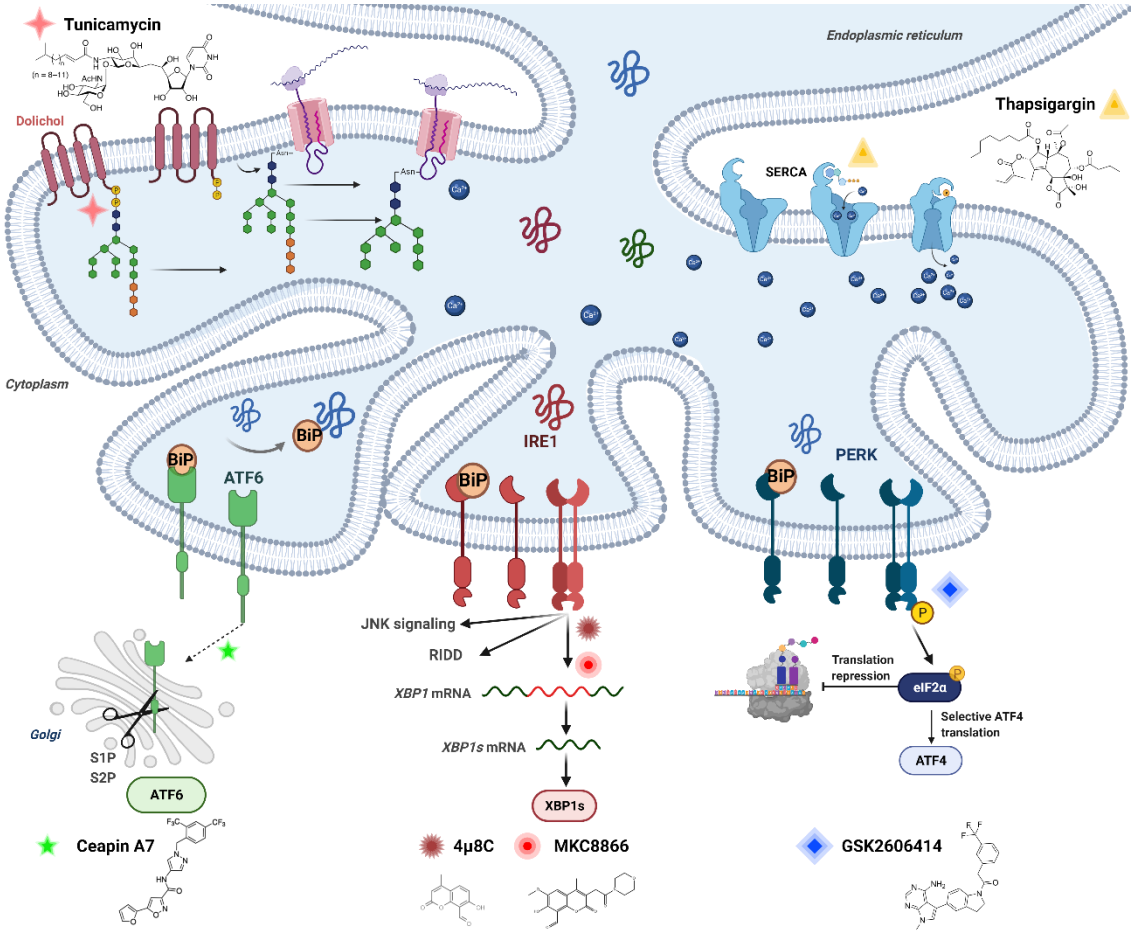



Figure 1.9 Chemical structures and mechanisms of action of the compounds used in this study

Tunicamycin (N-glycosylation inhibitor) and thapsigargin (Irreversible SERCA pump inhibitor) were used to induce ER stress; and Ceapin-A7 for ATF6 inhibition, GSK2606414 for PERK inhibition and 4μ8c or MKC8866 for IRE1 inhibition.

Created with BioRender.com.

# 2

# Materials and Methods

## 2.1 Materials

All chemicals were purchased from Sigma-Aldrich or Merck unless otherwise stated. Molecular biology reagents were obtained from Biorad, Promega, Invitrogen, Thermo Fisher Scientific, Zymo Research, Roche, and New England Biolab. Cell culture reagents were purchased from Gibco, Invitrogen, Labtech, or Sigma. Antibiotics were purchased from Bethyl, Santa Cruz Biotechnology, Protein Tech, Thermo scientific, Sigma, Abcam, Cell Signaling, Merck or Millipore.

### 2.1.1 Chemicals and reagents

ER stress was induced with tunicamycin or thapsigargin and UPR was inhibited using Ceapin-A7 for ATF6 pathway, 4μ8C and MKC8866 for IRE1 pathway and GSK2606414 for PERK pathway. The compounds are added to the treatment wells at indicated concentration by dilution from the stocks. The details of the chemicals are listed in Table 8.1 and Table 8.2.

Controls of each experiment were treated with the same final concentration (v/v) of the solvent (DMSO) as vehicle. If more than one compound was used, the final volume of the solvent in the control well was adjusted to the total volume of all compounds used.

### 2.1.2 Primers

Oligonucleotide primers used for qRT-PCR were purchased from (Invitrogen, Sigma-Aldrich or Eurofins Scientific).

The primers used to amplify the cDNA from human cell lines are listed in *Section 8.1.1*. The primers for EMT are listed in Table 8.3. The primers for the UPR are listed in Table 8.4. The primers for the osteogenic differentiation markers are listed in Table 8.5. The primers for housekeeping genes are listed in Table 8.6.

The primers used to amplify the cDNA from mouse cell lines are listed in *Section 8.1.2*. The primers for EMT are listed in Table 8.8. The primers for the UPR are listed in Table 8.9. The primers for the osteogenic differentiation markers are listed in Table 8.10. The primers for housekeeping genes are listed in Table 8.11.

### 2.1.3 Antibodies

The antibodies used in this study are listed in Table 8.14 and Table 8.15. The detection reagents used for detecting horseradish peroxidase (HRP)-labeled antibodies during Western blotting are listed in Table 8.16

## 2.2 Methods

### 2.2.1 Bacterial growth

#### 2.2.1.1. Culture conditions of E. coli

Liquid cultures of *E. coli* were grown from glycerol stocks in Luria Bertani (LB) Broth, Vegitone (Sigma-Aldrich, Cat. #28713) in sterile 500 ml Erlenmeyer flasks with baffled-base for large cultures (100 ml) at 37 °C with shaking (225 rpm) overnight. After plasmid transformation, *E. coli* strains were grown on solid media, on LB agar at 37 °C.

#### 2.2.1.2. Antibiotics used for bacterial cultures

The final concentrations of commonly used antibiotics are listed in Table 8.17.

#### 2.2.1.3. Production and storage of bacterial glycerol stocks

Bacterial stocks were prepared by mixing the bacterial cultures with 50% glycerol in a 1:1 ratio in a 2 ml cryo-vial. The glycerol stock tubes were kept at -80 °C for long term storage.

### 2.2.2 Cell Culture

#### 2.2.2.1. Culture conditions

ARCaPE and ARCaPM human prostate cancer cells lines were purchased from Novicure Inc, USA (Cat. #3423 and #3422 respectively). Both cells were grown

in MCaP medium (aka T-medium) supplemented with 5% (v/v) heat-inactivated fetal bovine serum (FBS) and 1% penicillin-streptomycin (Gibco, Cat. #15140122), unless otherwise indicated. The medium was replaced every 2–3 days and upon reaching 80% confluency the cells were subcultured with 0.25% trypsin.

22Rv1 human prostate cancer cells were maintained in RPMI 1640 medium with 10% FBS, vitamins, non-essential aminoacids, L-glutamine, sodium pyruvate and penicillin-streptomycin (complete RPMI medium) unless otherwise indicated.

DVL3 and DVL3-SCM cells were provided by Mills lab. DVL3 cells were cultured in RPMI (Lonza 1640) medium supplemented with 10% FBS and 100 nM DHT (added fresh to each flask) unless otherwise indicated. The cells were subcultured in 1/20 when they reached 80% confluency.

DVL3-SCM cells were grown in Keratinocyte Serum-Free Media (Gibco, Cat. #17005042) supplemented with 2 ng/ml leukaemia inhibitory factor (Life Technologies, Cat. #LIF1010), 2 ng/ml stem cell factor (Life Technologies, Cat. #78062.1), 1 ng/ml granulocyte-macrophage colony-stimulating factor (Life Technologies, Cat. #130-093-862) and 2 mM L-glutamine, unless otherwise indicated. The cells were split when they reached 80% confluency by washing with 1X PBS followed by trypsin. 2% FBS in PBS solution was used to neutralise trypsin and the cells were seeded into a new unused flask in every passage.

Human embryonic kidney HEK293T cells were cultured in DMEM supplemented with 10% FBS.

All the cells were cultured at 37 °C in a humidified incubator with 5% $CO_2$.

#### *2.2.2.1.1. MCaP medium*

MCaP medium (aka T-Medium) was prepared by mixing DMEM low glucose (Sigma-Aldrich, Cat. #D6046) with F-12K (3 g/L sodium bicarbonate, 5 ug/mL insulin, 13.6 pg/mL triiodothyronine, 5 ug/mL transferrin (Sigma-Aldrich, Cat. #T8158), 0.25 ug/mL biotin, 25 ug/mL adenine) in 4:1 ratio and then adding 5% FBS and 1% Pen Strep to the final medium.

#### *2.2.2.1.2. Hypoxic growth conditions*

Hypoxic conditions (0.4% $O_2$, 5% $CO_2$, balance $N_2$) were maintained using a MiniGalaxy incubator (RS Biotech, Irvine, UK).

### 2.2.2.2. Cell viability assay (Alamar Blue)

Alamar Blue assay was used to measure the cell viability. Cells were seeded in a 96-well plate (3000 cell/100 µl/well) and treatment was done as indicated in each experiment. On the day of assay, 20 µl of resazurin solution, prepared from resazurin sodium salt (Sigma-Aldrich, Cat. #R7017), at 1 mg/ml final concentration in 1X PBS, was added to each well (1:10 ratio with total growth medium) and the plate was left to incubation (~3 hr) at 37°C in a humidified incubator with 5% $CO_2$ until the colour change was visible. The fluorescence was measured by reading at 545 nm excitation and 585 nm emission wavelength using a fluorimeter (Fluostar). The background fluorescence was eliminated by subtracting the fluorescence values of blank wells from each treatment. Untreated cells were used as control group for normalisation calculations.

### 2.2.2.3. SYTOX Green staining for cell death

Cells were seeded in a 96 well plate as $3x10^5$ cells per well and left for 24 h for adhesion. Adherent cells were treated as indicated, SYTOX green was added to the wells in 1:8000 dilution (Invitrogen ™, S7020). SYTOX green incorporation

was visualised and analysed in the IncuCyte Live Cell Analysis System (Essen Bioscience) using the green fluorescent channel. The total number of dead cells was quantified by adjusting the threshold values to the control treatment and calculated with automated count.

### 2.2.2.4. Osteogenic differentiation

ARCaPM and ARCaPE cells were seeded in 12 well plates with 200,000 cell/well density in MCaP medium and left to grow to confluency before the start of osteogenic differentiation for 2–3 days. MCaP medium was changed to osteogenic differentiation medium (α-MEM (Gibco, Cat. #22561-021) containing 5% FBS, 1 nM Dexamethasone, 20 mM β-glycerophosphate, 50 mM ascorbic acid) to induce osteogenic properties. Control wells were kept in α-MEM containing 5% FBS and 1% antibiotics. Cells were cultured for the indicated days in the presence of osteogenic differentiation medium or control medium and the cells were not split till the end of the experiment. The medium for all different conditions was changed every two or three days.

### 2.2.2.5. Alizarine Red S staining for mineral crystals

Following osteogenic differentiation, mineral formation was seen under the microscope. To stain the mineral deposition, the cell medium was discarded, and the cells were fixed with 10% formalin for 10 mins. After fixation, the wells were washed twice with deionised water and 400 µl of Alizarin Red S solution (40 mM in water, pH 4.1-4.3) was added to the wells to completely cover the cell layer. The plates were left for incubation for 30 mins followed by washing with deionised water twice. The cells were imaged under an inverted microscope and the plate was scanned on a scanner (EPSON).

### 2.2.2.6. Real-time imaging for mineralisation via IncuCyte S3

The cells were seeded at 50,000 cell/cm$^2$ in cell culture multiwell plates and left to grow to confluency before the start of the experiment (For morphology experiments the cells were seeded less than recommended density in the multiwell plates). Osteogenic differentiation medium was prepared as previously described. The medium was changed to control and differentiation medium, and the cells were not split till the end of the experiment. The medium was changed every 2-3 days. Calcein green (calcium hydroxyapatite) was used for staining the calcium crystals. 10 mM Calcein solution (in 0.1 M of NaOH) was diluted 1:10 in dd$H_2O$ to prepare 1 mM working solution, which was then diluted 1:1000 to the final solution at 1 µM and added to the differentiation or control medium. Calcein was added to the medium on every medium change. The cells treated for osteogenic differentiation were kept at 37 °C in a humidified incubator with 5% $CO_2$ and monitored in the presence of Calcein Green in the IncuCyte S3 for the indicated time. The phase-contrast and fluorescent pictures were periodically obtained for the indicated time course.

### 2.2.2.7. Alkaline Phosphatase (ALP) activity assays

#### *2.2.2.7.1. Staining for ALP activity*

The cells were stained for ALP activity using naphthol AS-MX phosphate and fast blue RR salt-based Leukocyte Alkaline Phosphatase Kit (Sigma-Aldrich, Cat. #85L1). The content of 1 Fast Blue RR salt capsule was dissolved in 48 ml of deionised water. Naphthol AS-MX solution was mixed with Fast Blue RR solution in a 2:48 ratio. The cells were fixed in the tissue culture plate with 10% Formalin at room temperature for 10 min, then washed once with deionised water. A freshly prepared working solution was added to the plate and incubated at room

temperature for 30 min in dark, then washed once with deionised water. The cells were visualised under the microscope and scanned on a scanner (EPSON).

#### *2.2.2.7.2. Quantitative measurement of ALP activity*

The cells for ALP activity assay were collected in CelLytic buffer as previously described without phosphatase inhibitors. 4-Methyl Umbelliferyl Phosphate disodium salt (Sigma-Aldrich, Cat. # M8186) was used as the substrate to measure the ALP activity. 20X 4-MUP stock was prepared by dissolving 2.05 mg 4-Methyl Umbelliferyl Phosphate disodium salt in 2 ml Tris 50 mM (pH 8.0) and the working solution was freshly prepared on the day of the experiment by diluting 4-MUP stock in 1:20 with Tris as required.

10 µl total protein lysate from each sample was added to a 96-well plate in triplicates and the sample volume for each well was completed to 60 µl by adding 50 µl of Tris buffer. 100 µl of the 4-MUP working solution was added to each well in an order. The plate was incubated at 37 °C for 30 min in the dark, then the reaction was terminated by adding 100 µl of $Na_2CO_3$ to each well in the same order as 4-MUP. The fluorescence was measured by reading at 360 nm excitation and 450 nm emission, with 435 nm cut-off in wavelength using a fluorimeter. Alkaline phosphatase activity is proportional to the fluorescence reading. The activity/µg of protein was calculated by measuring the protein concentration using BCA assay.

### 2.2.2.8. Secreted RANKL Enzyme-Linked Immunosorbent Assay (ELISA)

Secreted RANKL levels in the conditioned media of ARCaPM cells treated with ER stress inducers and the UPR inhibitors were measured using the DuoSet Human RANKL ELISA Kit (mouse RANKL ELISA Kit for DVL3-SCM cells), as recommended by the manufacturer (R&D Systems, Minneapolis, MN). The concentration of the lowest standard of the assay was 78.1 pg/ml.

### 2.2.2.9. Transwell migration assay

Transwell assays were performed to analyse cell migration towards FBS. A total of 2.5 x $10^4$ cells were seeded in the top chamber of 24-well transwell plates of 8 µm pore size (353097, Falcon) and cultured in serum-free medium. Medium containing FBS was added to the bottom chamber and cultured in 5% $CO_2$ and 37 °C, unless otherwise indicated. After 48 hours, cells were fixed with 10% formaldehyde, permeabilised with 100% methanol and were stained with 1% Toluidine Blue. The cells inside the transwell that did not migrate were removed with a cotton swab. Each transwell was photographed from 5 fields of view (top, centre, bottom, left and right) using a Nikon eclipse TE300 microscope, using 4X objectives. Each experiment was performed in triplicate.

### 2.2.2.10. Scratch assay

The migration capacity of ARCaPE and ARCaPM cells were assessed using a scratch-wound assay. The cells were seeded into the inner 60 wells of the 96-well IncuCyte® ImageLock Plates in a cell density of 3 × $10^5$ cells per well and grown to confluency before the start of experiment. The outer wells are filled with 100 µL PBS to avoid evaporation effects of the adjacent wells. 96-pin IncuCyte® WoundMaker was used to simultaneously create wounds in all wells of the plate by gently removing the cells from the confluent monolayer. After washing the

wells with PBS to remove the detached cells, media containing the appropriate treatment was added to corresponding wells in a final volume of 200 µl and the plate was placed inside the IncuCyte. The plate was incubated in the IncuCyte® S3 Live-Cell Analysis System and wound closure was tracked for up to 48 h. Images of the scratched areas of each well were obtained at indicated time intervals. IncuCyte® S3 Software 2018C was used for data analysis.

### 2.2.3 Production of lentiviruses

The pLKO.1 lentiviral vector system (Sigma) was used to deliver shRNA. The details of the shRNAs used are listed in Table 8.18.

Lentiviruses were packaged using second generation packaging system in 293T cells. 293T cells ($3x10^6$) were seeded in a 10 cm plate and next day 10 µg of transfer vector (pLKO.1 backbone vector containing shRNA), 5 µg of packaging plasmid psPAX2 (Addgene Plasmid #12260), 5 µg of envelope expressing plasmid pMD2.G (Addgene Plasmid #12259) were transfected using 30 µl of Lipofectamine 2000 Transfection Reagent (Thermo Fisher, Cat. 11668030) in OptiMEM (Life Technologies, Cat. 31985062). Supernatants containing the viral particles were collected 48 and 72 h following transfection. Viral containing media was filtered with a 0.45 µm filter, concentrated 10X using Lenti-X Concentrator Solution (Clontech, Cat. 631232), and aliquoted and stored at -80°C.

### 2.2.4 Viral transduction

ARCaPM cells were seeded into 6 well plates (200,000 cells/well) and transduced with lentiviruses at a dilution of 1:20 in media containing 10 µg/ml of polybrene (Sigma, H9268). The cells were assayed 72 h after transduction.

### 2.2.5 Cell imaging

The cellular morphology after transduction was imaged by live cell imaging using the IncuCyte Imaging System (Essen BioScience, Hertfordshire, United Kingdom) with phase contrast microscopy, 10X objectives. At least 3 biological experiments were performed ($n \geq 3$).

### 2.2.6 Molecular biology

#### 2.2.6.1. Protein characterisation

##### *2.2.6.1.1. Cell lysis and quantification of the concentration*

The growth medium was removed from the cells to be assayed, the cells were washed once with 1X PBS, and the PBS was discarded. Cells were lysed using Mammalian Cell Lysis/Extraction Reagent CelLytic™ M (Sigma-Aldrich, Cat. #C2978). 25X Protease inhibitor cocktail (Roche, Cat. #11873580001) was added to the CelLytic M reagent and 150 µl of lysis buffer was used for cells in 1 well of 12-well plate. The required volume of CelLytic M reagent was added to the wells and the plate was incubated on a shaker for 15 min. The lysed cells were collected and centrifuged for 15 mins at maximum speed on a tabletop centrifuge to pellet the cellular debris, and the supernatant containing the protein was transferred to a new tube for storage at –80 °C. Protein concentration was determined using Pierce ™ bicinchonic acid (BCA) Protein Assay Kit (Pierce, Cat. #23227).

*2.2.6.1.2. Western Blot*

Protein samples were mixed with 4x Loading buffer (Invitrogen, Cat. #NP007) and 10x reducing buffer (Invitrogen, Cat. #NP009) and denatured for 10 mins at 95 °C. 20-30 µg total protein from each sample were loaded in a Mini-PROTEAN® TGX™ Gels (Bio-Rad) as calculated, 10 µl of Precision Plus Protein™ Kaleidoscope™ Prestained Protein Standards Ladder (Bio-Rad, Cat. #1610375) was added as the first sample. The gel was run at 120 V for at least 40 mins, then the proteins were transferred onto PVDF membrane (Biorad, Cat. #1704156) in a Trans-Blot Turbo Transfer System (Biorad). The membranes were blocked using 5% non-fat dry milk (Santa Cruz, Cat. #sc-2325) in TBS-Tween (prepared from 10X Tris Buffer Saline, and 0.1% Tween-20) at room temperature for 1 hr. The membrane was cut if more than one protein was to be probed, then the cut membranes were put into a 50-ml tube containing primary antibody in appropriate dilution and incubated in the cold room overnight on a slow rocker. The membranes were washed in TBS-T 5 times for 5 mins for each wash. The membranes were transferred to the horseradish peroxidase-conjugated secondary antibody and incubated at room temperature for 1 hr. The membranes were washed in TBS-T 5 times for 5 mins for each wash. The membranes were developed using ECL western blotting substrate (Novex© ECL, Cat. #WP20005). The signals were detected in Uvitec Alliance 4.7 chemiluminescence and fluorescence imaging system.

The antibody was stripped of the membrane for detection of the housekeeping gene (β-Actin) as the loading control. The membrane was washed with TBS-T and then treated with 10 ml Restore™ PLUS Western Blot Stripping Buffer (Thermo Scientific, Cat. #46430) at 37 °C on a rotator for 15 mins, then washed briefly with TBS. The stripped membrane was blocked with 5% non-fat dry milk and the same procedure was followed for the next antibody.

### 2.2.6.2. RNA isolation

TRIzol™ Reagent (Thermo Fisher, Cat. #15596018) was used following the manufacturer's instructions for cell lysis. Total RNA was isolated from cells using Direct-zol RNA Kits (Zymo Research) according to the manufacturer's instructions and eluted in 50 µl nuclease-free DEPC-treated water. DNase I treatment was done as part of the isolation process in the columns provided.

### 2.2.6.3. Quantification of RNA concentration

The relative yield of RNA was measured by spectrophotometric analysis at 260 nm ($A_{260}$) wavelength using the NP80 NanoPhotometer (Implen) full-spectrum UV-Vis spectrophotometer.

### 2.2.6.4. cDNA synthesis

1-2 µg of isolated RNA was added to 20 µl of Reverse Transcription Premix 2 (Primerdesign, PrecisionTM) in a final reaction volume of 30 µl for cDNA synthesis. The tubes containing the reaction mixture was incubated at 42°C for 20 minutes for reverse transcription, then 72 °C for 10 minutes for heat inactivation. The cDNA product was kept at -20°C.

### 2.2.6.5. Real-time quantitative Reverse Transcription Polymerase Chain Reaction (qRT-PCR)

Relative gene expressions in different RNA samples were detected by using Fast SYBR green master mix (Thermo Scientific, Cat. #4385617) in a final volume of 10 µl in a 384-well non-skirted PCR plate (Agilent). Microamp Optical adhesion film (Thermo scientific, 4311871) was used for sealing of the plates and the reaction mixture was briefly spun in a centrifuge for 1 min. Reactions were then amplified in ViiA 7 Real-Time PCR System (Life Technologies) and data acquisition was performed using the ViiA 7 Software (Life Technologies).

The Delta-Delta Ct method (the $2^{-\Delta\Delta CT}$ method) was used to calculate the level of relative fold gene expression in different samples [428]. First, $\Delta C_T$ is calculated by subtracting the cycle threshold ($C_T$) value of the housekeeping gene from the $C_T$ value of the gene of interest to normalise the gene of interest to the housekeeping gene:

$$\Delta C_T = C_T \text{ (gene of interest)} - C_T \text{ (housekeeping gene)}$$

Then, $\Delta\Delta C_T$ is calculated by subtracting the $\Delta C_T$ value of the control sample from the $\Delta C_T$ value of each sample to normalise to the control (or untreated) sample:

$$\Delta\Delta C_T = \Delta C_T \text{ (samples)} - \Delta C_T \text{ (control or untreated sample)}$$

Finally, 2 to the power of negative $\Delta\Delta C_T$ is calculated to find the fold gene expression:

$$Fold\ gene\ expression = 2^{-\Delta\Delta C_T}$$

## 2.2.6.6. XBP1 splicing assay

The splicing of XBP1 mRNA was measured as the indication of activation of the IRE1 arm of the UPR [294]. RNA isolation and cDNA synthesis were done as described in S*ections 2.2.6.2* and *2.2.6.4*

RNAs extracted after experiments were reverse transcribed into cDNA, which was then used to detect the difference in size caused by the removal of the intron from unspliced XBP1 mRNA via PCR. The 26 nt difference was visualised on a 3% w/v agarose gel.

### *2.2.6.6.1. Polymerase Chain Reaction (PCR) for XBP1 splicing*

Taq DNA polymerase containing BioMix™ ready-to-use 2x reaction mix (Bioline, Cat. #25006) was used for amplification of XBP1 cDNAs. PCR was done in a total volume of 50 µl using 5 µl 10 µM forward primer, 5 µl 10 µM reverse primer.

The primers used for samples from human and mouse samples are listed in Table 8.7 and Table 8.13, respectively. 2.5 µl cDNA from the cDNA synthesis reaction was used as the template for PCR. For each sample to be tested, an additional reaction was set for β-Actin as control. The PCR was run with the following conditions:

Table 2.1 Thermocycling conditions for Taq DNA polymerase for XBP1 cDNAs

| *Step* | *Temperature* | *Time* |
|---|---|---|
| *Initial Denaturation* | 94°C | 2 min |
| | 94°C | 1 min |
| *35 Cycles* | 59°C | 1 min |
| | 72°C | 30 sec |
| *Final Extension* | 72°C | 5 minutes |
| *Hold* | 4°C | ∞ |

Samples were spun down and loaded on a 3% agarose gel for detection of the bands.

#### *2.2.6.6.2. Agarose gel electrophoresis*

Agarose gels were prepared by melting 3% (w/v) agarose (Cleaver Scientific) in TAE (Tris-Acetate-EDTA) buffer, Ethidium bromide (0.5 µg/ml) was added for visualisation of DNA with UV light. PCR mix already contained red dye for visualisation and direct loading onto a gel. Low molecular weight DNA ladder (Thermo Fisher, Cat. #SM1193) was run together with the samples to determine the size of the DNA products. Electrophoresis was conducted under constant voltage. DNA was visualised with UV.

## 2.2.6.7. RNA-Seq

### *2.2.6.7.1. siRNA transfection for RNA-Seq*

The details of the siRNAs used in this study are listed in Table 8.19. The siRNA was dissolved in RNAase-free water to make a final concentration of 20 µM. siRNAs were transfected in ARCaPM cells using Lipofectamine RNAiMax (Life Technologies, Cat. 13778150) according to the manufacturer's protocol. ARCaPM cells seeded into 6 well plate (200,000/well) were reverse transfected by mixing diluted siRNA (75 pmol/well) in Opti-MEM with diluted Lipofectamine RNAiMax (9 µl/well) in Opti-MEM, incubated at room temperature for 5 minutes for the nucleic-acid complex formation, then addition to the target cells. The cells were incubated for a further 72 h and then harvested for protein and RNA analysis.

### *2.2.6.7.2. RNA library prep for Illumina*

Libraries were prepared according to a modified protocol from [429]. RNA was isolated using Direct-zol DNA/RNA Miniprep kit from Zymo Research, then was concentrated using Zymo RNA Clean and Concentrator -5 (Zymo Research, Cat. #R1013). ~1 µg of total RNA was fragmented in reverse transcription buffer and the poly(A) tails were captured with a poly-T20VN oligonucleotide (IDT) and the captured mRNA was reverse transcribed using SmartScribe Reverse Transcriptase (Takarabio, Cat. #639537). The RNA was removed by treating with RNase H and RNase A and cDNA was purified with AMpure XP beads. A 5' adapter was ligated to the purified cDNA with T4 RNA Ligase 1 (New England Biolabs, Cat. #M0204) at 22 °C for 12-16 h overnight, and the reaction was terminated by addition of 10 mM Tris HCl pH 8.0, 15 mM EDTA.

The ligated cDNAs were purified with AMpure XP beads and amplified by PCR using NEBNext i5 and i7 index primers with Q5 polymerase for 18 cycles (Table 2.2).

Table 2.2 Thermocycling conditions for Q5 DNA polymerase for library amplification and indexing

| *Step* | *Temperature* | *Time* |
|---|---|---|
| *Initial Denaturation* | 98°C | 2 min |
| *18 Cycles* | 98°C | 30 sec |
| | 65°C | 1 min 15 sec |
| *Final Extension* | 65°C | 5 minutes |
| *Hold* | 4°C | ∞ |

The sequence of capture oligos, adapter and the index primers are listed in *Section 8.1.6*.

#### *2.2.6.7.3. TapeStation*

Quality control of the library was performed with an Agilent 4150 TapeStation system using the High Sensitivity D1000 ScreenTape analysis kit (Agilent, Santa Clara, CA, USA).

#### *2.2.6.7.4. Qubit*

The DNA concentration was quantitated using a Qubit fluorometer (Invitrogen) with Qubit dsDNA HS Assay Kit (Invitrogen, Q32851) according to the manufacturer's instructions.

#### *2.2.6.7.5. Illumina sequencing*

A NextSeq 500/550 Mid Output Reagent Cartilage v2 kit (150 cycles) (15057940) was used for paired end sequencing. Libraries from six samples (3 for siCTRL, 3 for siALPL) were multiplexed in an equimolar pool and sequenced on an Illumina NextSeq-500. The index sequences are listed in Table 8.20.

#### *2.2.6.7.6. Data analysis*

The sequencing data were analysed by Dr. Srinivasa Rao. Briefly, raw sequencing data were demultiplexed using bcl2fastq (v2.20) [430], reads trimmed with BBDuk (v38.79) [431, 432]; aligned to the human genome (hg38) with STAR (v2.7.9a) [433] and differential expression analysis was performed with DESeq2 (v1.34.0) [434].

# 3

# The effect of the UPR in prostate cancer osteomimicry

## 3.1 Introduction

Prostate cancer, unlike most other cancers, primarily metastasises to the skeleton and induces osteoblastic responses. The preference of prostate cancer cells to metastasise to bone involves unique interactions between tumour cells, the bone marrow microenvironment, and bone cells.

In 1999, Koeneman et al. postulated that *"bone is a highly restricted and protective environment that prohibits the growth and survival of cancer cells. In order to thrive in the bone environment, cancer cells must acquire "bone cell-like" properties".*

The capacity of tumour cells (that preferentially metastasise to bone) to develop a bone cell phenotype, particularly osteoblast-like, is known as osteomimicry. By producing bone matrix proteins, the osteoblast marker alkaline phosphatase, and chemicals that regulate the osteoblast/osteoclast crosstalk, prostate cells try to mimic osteoblasts.

Cells of prostate cancer secrete several proteins that are highly specific to bone, such as osteocalcin (OC), osteopontin (OPN), bone sialoprotein (BSP) and osteonectin (ON). Previous studies have shown that prostate cancer cells can be induced to exhibit osteoblastic mineralisation. For example, bone homing metastatic human PCa cells from the LNCaP line, C4-2B, were observed to mineralise *in vitro* when supplied with required conditions [435]. This study identified bone-specific transcription factor Cbfa1 (also called Runx2), which was highly expressed in C4-2B cells compared to parental LNCaP cells, as an important factor required for mineral deposition.

In PCa, ALP has been shown to be a useful prognostic marker in predicting cancer outcome, independent of therapy [436]. During the progression of bone metastases, the level of bone-specific ALP in serum is clearly elevated [238, 437]. Previous work demonstrated that ALPL expression was elevated in metastatic PCa cells [438]. Decreasing ALPL expression promoted mesenchymal-to-epithelial transition in cells expressing ALPL and displaying mesenchymal phenotype. Likewise, ALPL expression was lower in epithelial derivative of ARCaP cells, identifying ALPL as a crucial factor required for both EMT and osteomimicry.

By unravelling the molecular mechanisms driving cancer cells' osteomimetic capabilities novel treatment targets may be identified, with the goal of improving and extending the lives of patients with bone metastases.

## 3.2 Hypothesis and Objectives

Cancer cells have increased metabolism and external stressors from their microenvironment and have increased UPR as a pro-survival mechanism. Studies have shown the relevance of the UPR both in prostate cancer and bone development (*Sections 1.4.4*and *1.4.5*), however, no previous study investigated the interplay between the UPR, prostate cancer and bone metastasis. For example, it is known that androgen receptor directly regulates IRE1 pathway; and another study has shown that activation of the IRE1-XBP1 arm of the UPR induces PTHrP dependent osteoclast and osteoblast activity in bone cells [384, 427]. However, the role of the UPR in PCa-bone microenvironment has not been studied.

In this chapter I hypothesised that 1) the baseline expression levels of the UPR proteins are different between non-metastatic and metastatic prostate cancer cells, 2) the expression of the UPR components change under osteogenic conditions, and 3) inhibiting different arms of the UPR affect osteogenic potential in metastatic prostate cancer cells. To investigate these hypotheses, this chapter aims to determine the role of the UPR in the osteomimetic potential of prostate cancer cells in paired EMT models of human and mouse PCa, using an *in vitro* mineralisation assay. The specific aims are as follows:

- To determine the timing for *in vitro* mineralisation in ARCaPM cells
- To compare the components of the UPR in ARCaPE and ARCaPM cells at baseline, and before and after osteogenic differentiation
- To assess the impact of the UPR inhibitors on osteogenic potential and to determine whether osteoblastic differentiation can be perturbed by targeting the UPR in ARCaPE and ARCaPM cell lines

## 3.3 Results

### 3.3.1 Optimising conditions for the study of the UPR & mineralisation

Among the isogenous ARCaPM and ARCaPE cells, the osteoblast specific marker alkaline phosphatase *ALPL* is elevated in bone metastatic human prostate cancer ARCaPM cells [438]. This is associated with EMT, reduced survival and mineralisation of the prostate cancer cells in osteogenic culture conditions. *In vivo*, intracardiac injection of ARCaPM cells results in bone metastases in SCID mice [242].

First, I compared the bone marker expression in ARCaPE and ARCaPM cells to validate the differences between the two cells lines that have been reported previously. The expression levels of *ALPL* were higher in ARCaPM cells, while the levels of *SPARC* and *RUNX2* were higher in ARCaPE cells. *COL1A1* mRNA expression was not different between the two cell lines (Figure 3.1).

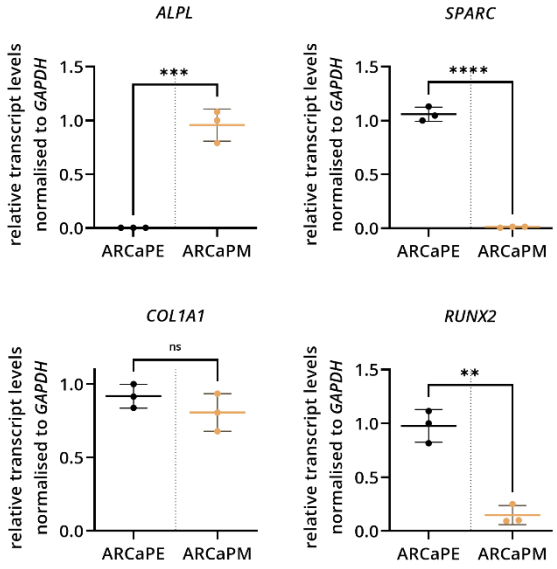



Figure 3.1 Bone marker gene expression differs between ARCaPE and ARCaPM cells

*ALPL* (A), *COL1A1* (B), *SPARC* (C) and *RUNX2* (D) gene expression in ARCaPE and ARCaPM cells were measured by SYBR Green real-time PCR and normalised to *GAPDH* expression. ARCaPE and ARCaPM cells were grown to confluency in MCaP growth medium. (Data summarises 3 independent experiments and shows the mean ± S. D.)
*Unpaired t-test, Alpha 0.05; ns P > 0.05, * P ≤ 0.05, ** P ≤ 0.01, *** P ≤ 0.001, **** P ≤ 0.0001)*

Next, I investigated the significance of osteoblastic potential in metastatic human prostate cancer cell lines using an *in vitro* mineralisation assay. Robust detection of Alizarine Red S staining indicated that only ARCaPM cells can form mineral crystals when grown in osteogenic differentiation medium. ARCaPE cells did not deposit mineral crystals and ALP activity did not increase (Figure 3.2-A).

Alkaline phosphatase activity is a key factor in osteogenic differentiation. To determine if the formation of mineral crystals was associated with an increase in ALP activity, a fluorescence-based assay was performed. The level of ALP activity was higher in ARCaPM cells compared to ARCaPE, and the level of ALP modestly increased by osteogenic differentiation only in ARCaPM cells, which is shown by ALP staining and ALP activity assay (Figure 3.2-B and C).

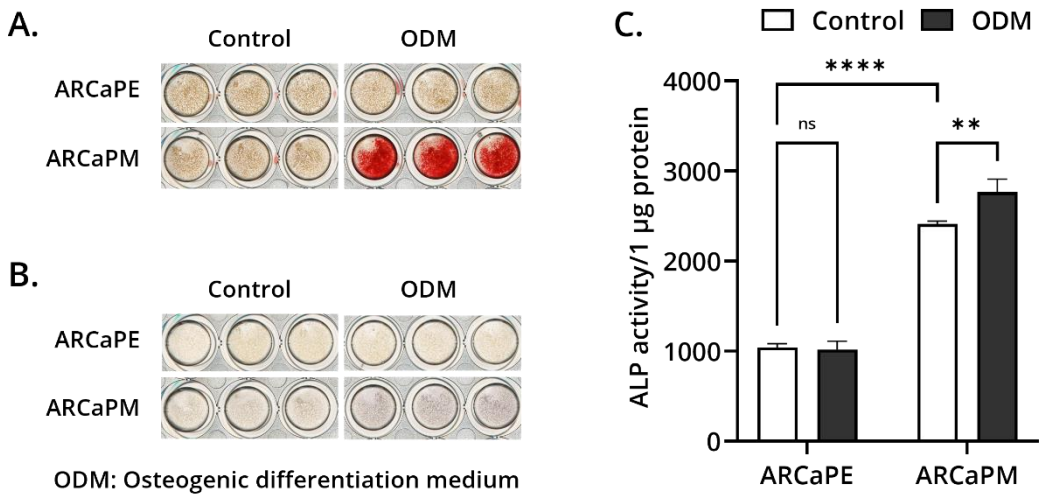



Figure 3.2 ARCaPM cells deposit mineral crystals 15 days after growing in osteogenic medium

ARCaPE and ARCaPM cells grown in control or osteogenic differentiation medium for 15 days were stained (red) for mineral deposition with Alizarin Red S. (A), for alkaline phosphatase activity with Leukocyte ALP staining kit (B). Images represent >3 independent experiments in triplicate. ALP activity in ARCaPE and ARCaPM cell lysates was measured using a fluorogenic ALP substrate and normalised with 1 µg protein concentrations (C). Data shows mean ± S. D.

*Two-way ANOVA with Tukey's multiple comparisons test, Alpha 0.05; ns $P > 0.05$, * $P \leq 0.05$, ** $P \leq 0.01$, *** $P \leq 0.001$, **** $P \leq 0.0001$*

Osteogenic differentiation is a sequence of molecular events that results in the formation of calcium deposits indicating mineralisation. To monitor the time required for mineral deposition, and dissect the progression with different molecular biology approaches, including the increase in ALP activity, ARCaPM cells were cultured in osteogenic differentiation media in a time course, and samples were collected at different intervals. ALP levels were higher in differentiation medium compared to control throughout the experiment (Figure 3.3). The difference between ALP activity in control and differentiation medium was lost on day 15 of differentiation. These data support a model where the increase in ALP occurs at an earlier time point. During this process, mineral deposition takes place after 9 days, after the increase in ALP levels as indicated with Leukocyte Alkaline Phosphatase staining, which happens 6 days after the

start of the experiment. This indicates that the increase in ALP activity occurs before the formation of mineral crystals.

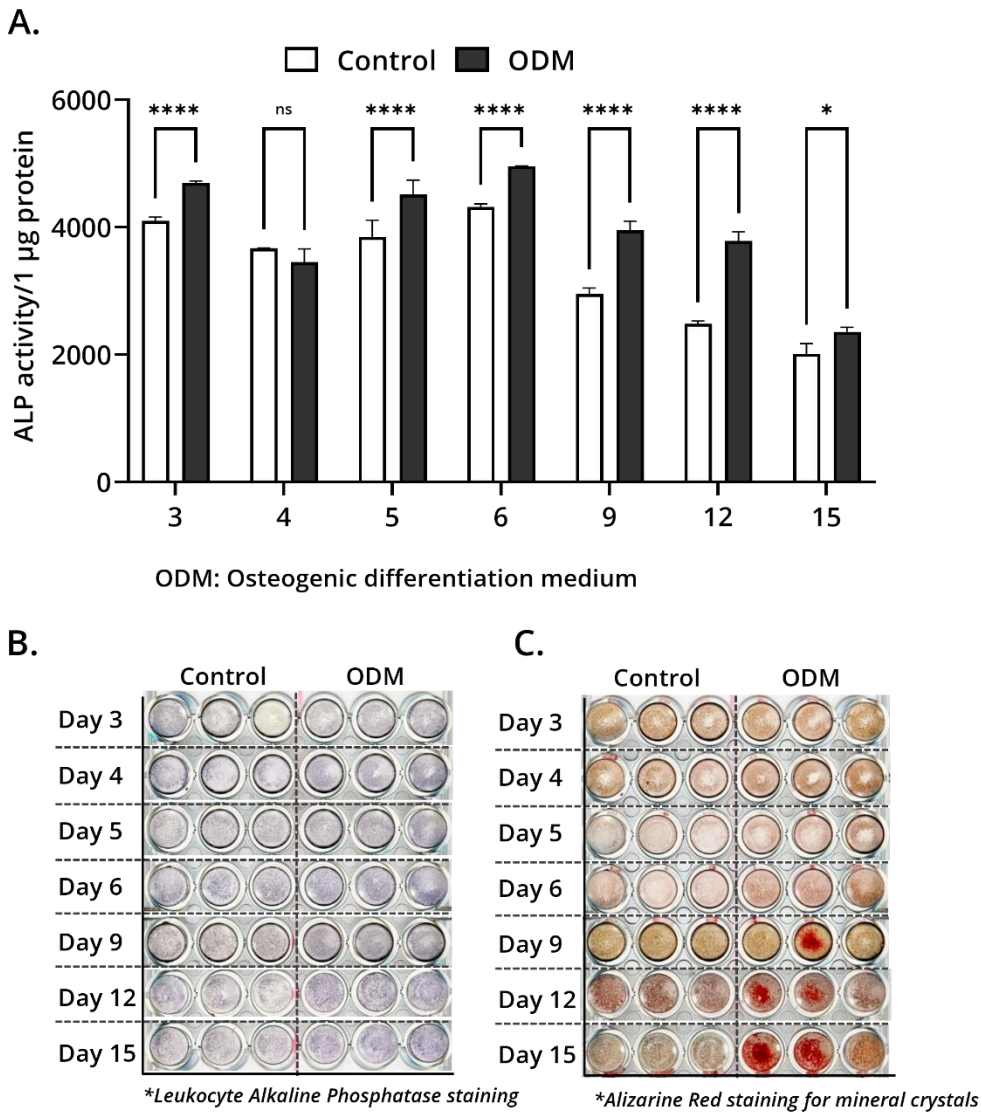



Figure 3.3 Osteogenic differentiation of ARCaPM cells over time

ARCaPM cells were grown in control or osteogenic medium for 15 days assayed at 3, 4, 5, 6, 9, 12 and 15$^{th}$ days. (A) ALP activity of ARCaPM cell lysates normalised to total protein concentrations. ODM indicate osteogenic differentiation medium. ARCaPM cells were stained for ALP activity using Leukocyte Alkaline Phosphatase kit after fixation with 10% Formalin for 10 mins (B) and stained (red) for mineral deposition with Alizarin Red S. (C) Images are representative of >3 independent experiments in triplicates. Data shows mean ± S. D.

*Two-way ANOVA, with Šídák's multiple comparisons test. Alpha 0.05; ns P > 0.05, * P ≤ 0.05, ** P ≤ 0.01, *** P ≤ 0.001, **** P ≤ 0.0001*

While mineralisation represents the phenotypic endpoint of osteoblast differentiation, understanding of the earlier genetic changes in response to osteogenic differentiation media is important to dissect the genes involved in mineral deposition.

To further optimise the parameters for assaying differentiation of ARCaPM cells, a panel of osteogenic markers was monitored in a time course assay and mRNA levels of the osteogenic markers were investigated during osteogenic differentiation (Figure 3.4). However, no significant trends were detected in the osteogenic markers *ALPL*, *COL1A1* and *RUNX2* compared to either control or differentiation treatment time course, indicating that mRNA levels of bone markers are not sensitive markers for osteogenic differentiation in ARCaPM cells.

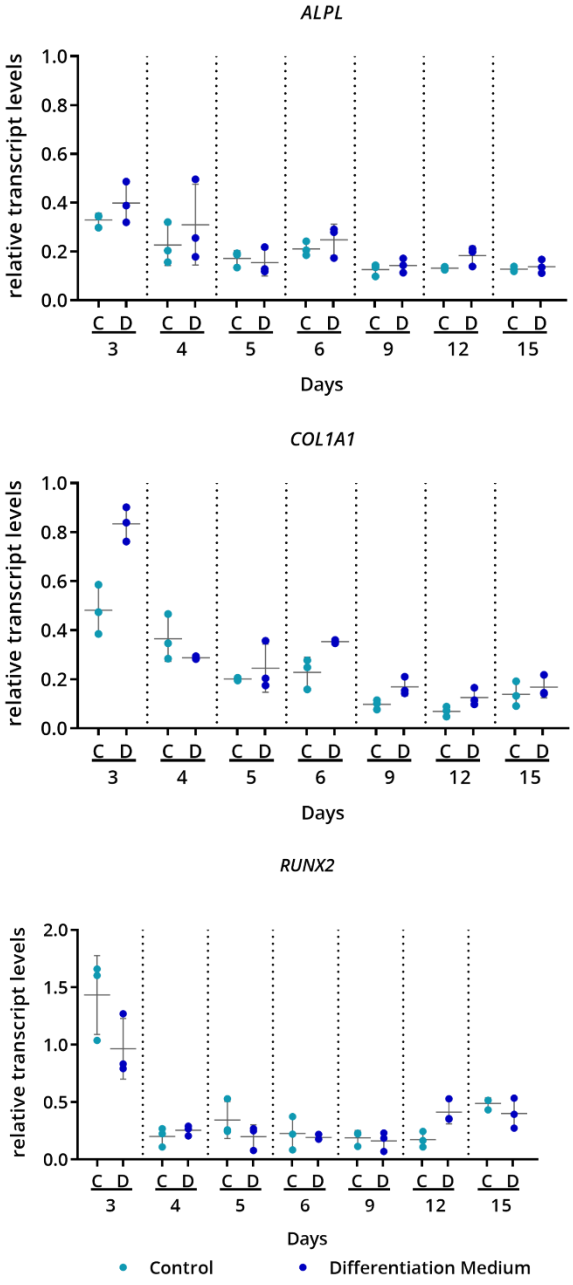



Figure 3.4 Bone marker gene expression does not change between control and differentiation medium in ARCaPM cells

ALPL, COL1A1 and RUNX2 gene expression in control and differentiation medium over a 15-day osteogenic differentiation of ARCaPM cells was measured by SYBR Green real-time PCR and normalised to GAPDH expression, then to the level of ARCaPM cells on day 0. (Data from 3 independent experiments and shows the mean ± S. D.)

*Two-way ANOVA, with Šídák's multiple comparisons test. Alpha 0.05; ns P > 0.05, * P ≤ 0.05, ** P ≤ 0.01, *** P ≤ 0.001, **** P ≤ 0.0001)*

The conventional method for inducing osteogenic differentiation in multipotent stem cells involves the treatment of a confluent monolayer of cells with a mixture of β-glycerophosphate (β-Gly), dexamethasone (Dex), and ascorbic acid (Asc) [439]. Dex, a synthetic glucocorticoid, induces upregulation of *FHL2* (a LIM-domain protein with 4.5 LIM domains) by binding to glucocorticoid response element in the *FHL2* promoter region, resulting in *RUNX2* activation by FHL2/β-catenin-mediated transcriptional activation. Dex also increases *RUNX2* activity by upregulating β-catenin-like molecule TAZ (transcriptional co-activator with PDZ-binding motif). Asc enhances COL1 production, which results in increased COL1/α2β1 integrin-mediated intracellular signalling. β-Gly is used as the phosphate in hydroxyapatite, and it also affects intracellular signalling molecules.

In order to investigate whether induction of RUNX2 and COL1A1 is required for increased ALP activity and mineral deposition, I eliminated the components of osteogenic differentiation medium Dex and L-Asc, and only added β-glycerophosphate as source of phosphate. Treatment of ARCaPM cells in α-mem medium supplemented with only β-glycerophosphate resulted in increased ALP activity after 10 days, and mineral deposition after 15 days (Figure 3.5).

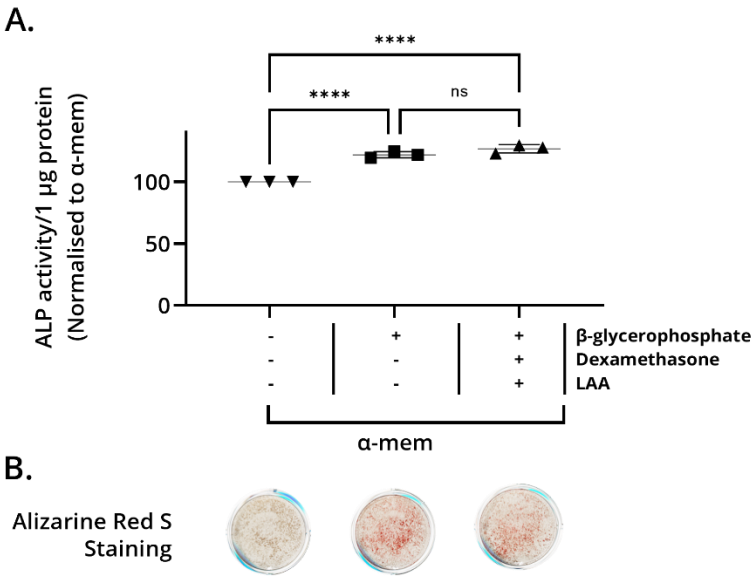



Figure 3.5 Treatment with β-glycerophosphate is sufficient for elevated ALP activity and mineral deposition in ARCaPM cells

ARCaPM cells grown in control medium, control medium containing only β-glycerophosphate or complete osteogenic differentiation medium were assayed 10 days after the start of the experiment for (A) ALP activity and stained (red) for mineral deposition with Alizarin Red S 15 days after the start of the experiment for (B). ALP activity was normalised to 1 µg of protein based on BCA protein assay kit. Data summarises 3 independent experiments and shows the mean ±S. D. *One-way ANOVA with Tukey's multiple comparisons test, Alpha 0.05: ns P > 0.05, * P ≤ 0.05, ** P ≤ 0.01, *** P ≤ 0.001, **** P ≤ 0.0001*

### 3.3.2 The effect of osteogenic differentiation on the UPR

To understand the contribution of the UPR to osteogenic potential and to assess the interplay between the UPR regulation and osteomimicry of ARCaPM cells, I monitored expression levels of components of different branches of the UPR. This was carried out before and after culture in osteogenic differentiation medium. Samples were collected at different time points during differentiation and the levels of the UPR components and targets were determined at both protein and RNA level. ATF4 and HERP1 protein levels decreased upon osteogenic differentiation after 5 days and change in the levels were consistent throughout this experiment from day 5 onwards (highlighted with dashed-blue line), indicating a role for the IRE1 and PERK arms of the UPR during osteomimicry

of ARCaPM cells (Figure 3.6). This is consistent with changes in the UPR during the osteogenic differentiation of prostate cancer cells.

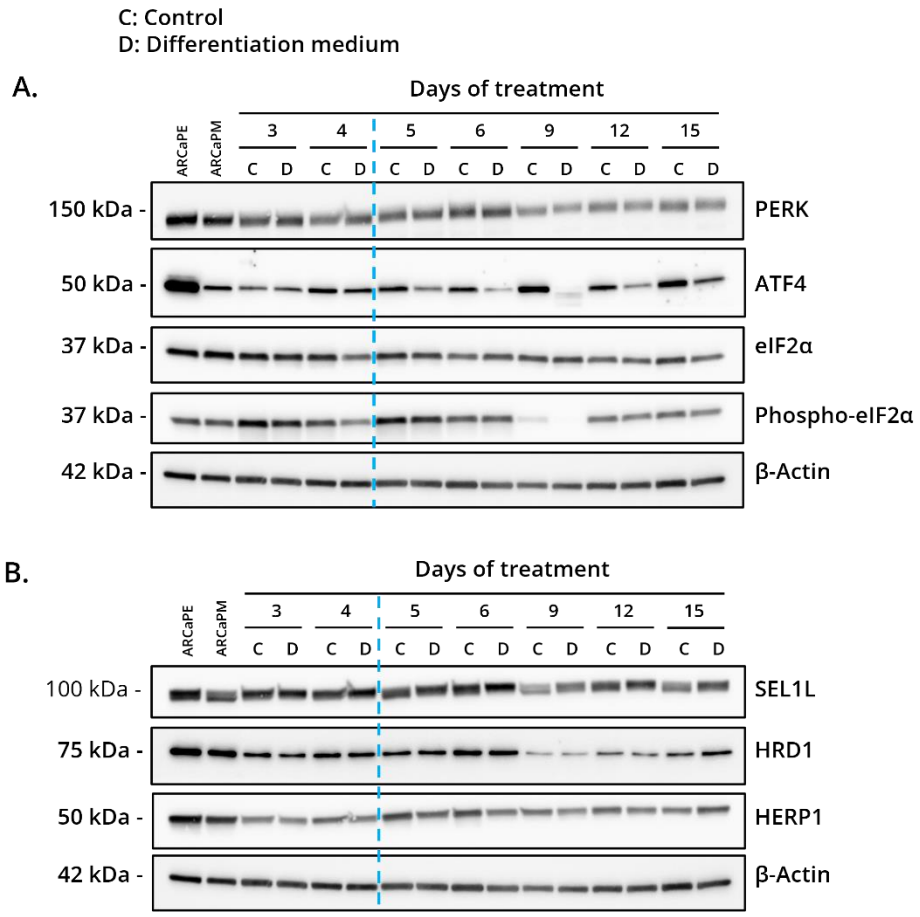



Figure 3.6 Markers of different arms of the UPR decrease upon differentiation

ARCaPM cells that were grown in control medium or osteogenic differentiation medium for up to 15 days. The medium was changed every other day and protein samples were collected from corresponding wells. ARCaPM cells grown in MCaP medium was used as control for basal levels of the UPR proteins. Cell were collected for immunoblotting using anti-PERK, anti-ATF4, anti-eIF2α, anti-Phospho-eIF2α, anti-SEL1L, anti-HRD1, anti-HERP1 and anti-β-Actin antibodies. Whole cell lysates from ARCaPE cells were used for comparison. Membranes were probed with the indicated antibodies and β-Actin was used as loading control. The blue line marks the day after the changes in ATF4 and HERP1 start.

To further compare the expression levels of the UPR target genes under control and differentiation conditions, I performed qRT-PCR on ARCaPM cells during osteogenic differentiation. *HRD1* levels were reduced after 3 days in

differentiation media, but the decrease was not significant. As a general trend, mRNA transcript levels of *SEL1L*, *HRD1*, *FAM8A1* and *HERP1* decreased after 4 days, however, no significant change was observed between control and differentiation medium at different time points (Figure 3.7).

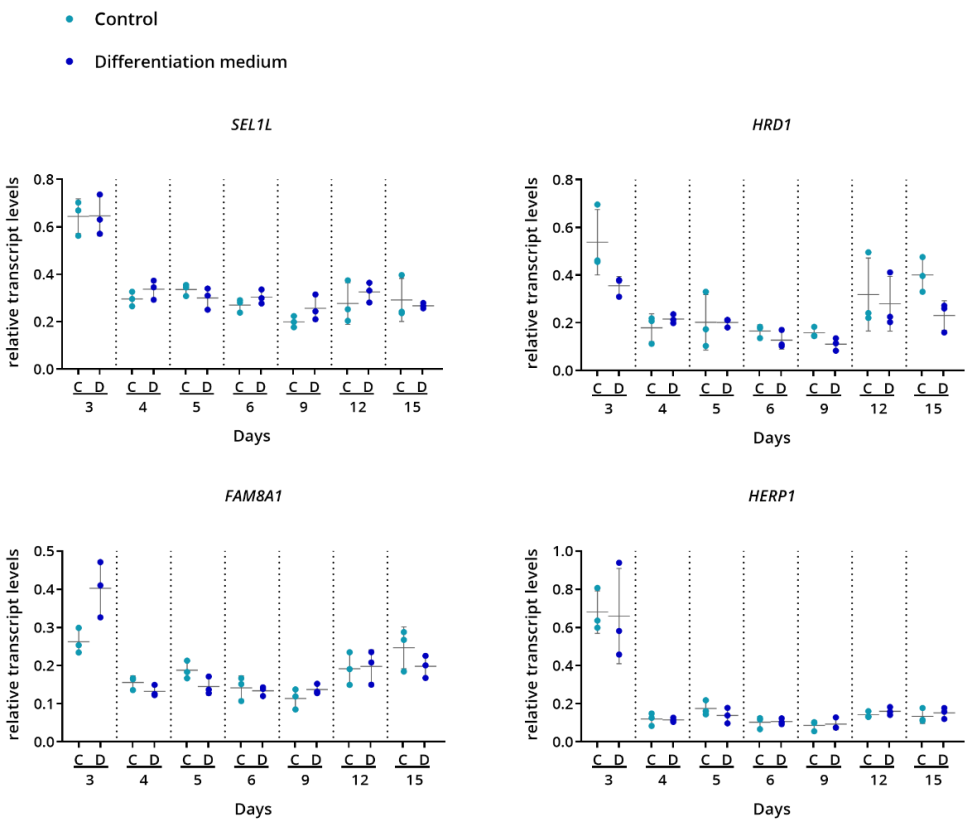



Figure 3.7 mRNA transcript levels of the UPR components in ARCaPM cells during osteogenic differentiation

mRNA expressions of the UPR components and in ARCaPM cells during osteogenic differentiation detected by qRT-PCR. The quantified individual RNA expression levels were normalised to *GAPDH* and fold change of each mRNA transcript in ARCaPM cells was relative to that of ARCaPM cells which were grown in MCaP medium. Three independent measurements per sample were performed and each dot represent one biological replicate under different conditions and days. The horizontal bar is the mean of three biological replicates which were normalised to ARCaPM cells in MCAP medium. (Data from 3 independent experiments and shows the mean ± S. D. )

*One way ANOVA with Šídák's multiple comparison, Alpha 0.05; ns P > 0.05, * P ≤ 0.05, ** P ≤ 0.01, *** P ≤ 0.001, **** P ≤ 0.0001*

### 3.3.3 The UPR expression in mesenchymal PCa cells

Prostate cancer cells differ in their epithelial and mesenchymal properties, with mesenchymal cells typically regarded as more metastatic. ARCaPE and ARCaPM cells represent paired epithelial and mesenchymal prostate cancer cells, which I have confirmed have differential expression of bone markers and different capacities for osteogenic differentiation.

To confirm the reported EMT-related differences between ARCaPE and ARCaPM cells, I performed western blot for the protein levels of EMT markers and RT-PCR for mRNA expression levels. Initial studies confirmed the differences in epithelial and mesenchymal gene and protein expression between ARCaPE and M cells (Figure 3.8). Both protein and mRNA levels of epithelial marker *CDH1* (E-Cadherin) were reduced in ARCaPM while mesenchymal marker *CDH2* (N-Cadherin) were elevated in ARCaPM. The mesenchymal marker Vimentin was elevated in ARCaPM at protein level, while the transcription level was similar between ARCaPM and ARCaPE cells.

ZO-1 is a junctional adaptor protein that has been reported to positively regulate cell migration [440]. Immunoblotting showed that levels of tight junction protein ZO-1 and Claudin levels were decreased in ARCaPM cells.

The master transcription factors *SNAI1* (Snail) and *SNAI2* (Slug) that play important roles in EMT were elevated in transcription level in ARCaPE cells. The mRNA transcription level of *VIM* and *ZEB1* was similar in ARCaPE and ARCaPM cells.

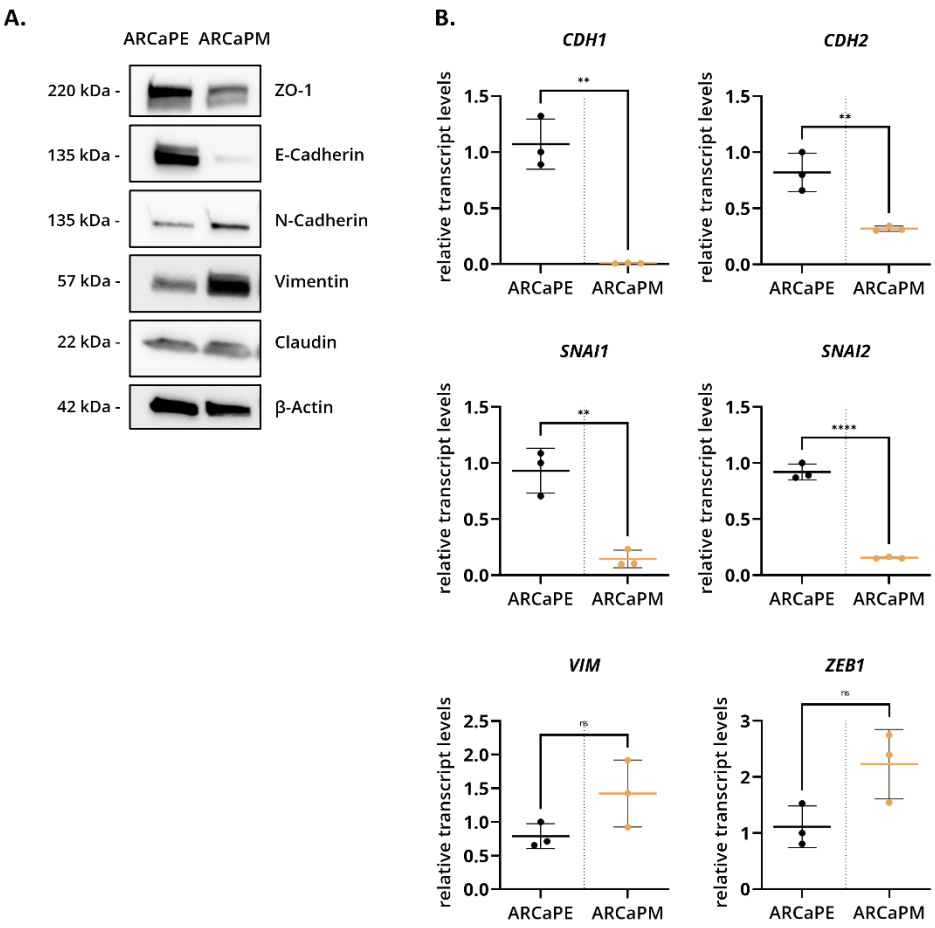



Figure 3.8 EMT protein and gene expression between ARCaPE and ARCaPM cells

(A) Immunoblotting of lysates from ARCaPE and ARCaPM cells. Cell lysates were analysed using anti-ZO-1, anti-E-Cadherin, anti-N-Cadherin, anti-Vimentin, anti-Claudin, and anti-β-Actin antibodies. β-Actin was used as loading control. (B) *CDH1*, *CDH2*, *SNAI1*, *SNAI2*, *VIM* and *ZEB1* gene expression in ARCaPE and ARCaPM cells were measured by SYBR Green real-time PCR and normalised with *GAPDH* expression. (Data summarises 3 independent experiments and shows the mean ± S. D.)

*Unpaired t-test, Alpha 0.05; ns P > 0.05, * P ≤ 0.05, ** P ≤ 0.01, *** P ≤ 0.001, **** P ≤ 0.0001)*

Next, I compared the levels of the UPR related protein expression in these cell lines to begin to investigate the interdependency of the UPR and EMT. PERK, ATF4, SEL1L, HERP1, FAM8A1 levels were reduced in ARCaPM cells, indicating a general decrease in the UPR in ARCaPM cells as compared to ARCaPE (Figure 3.9).

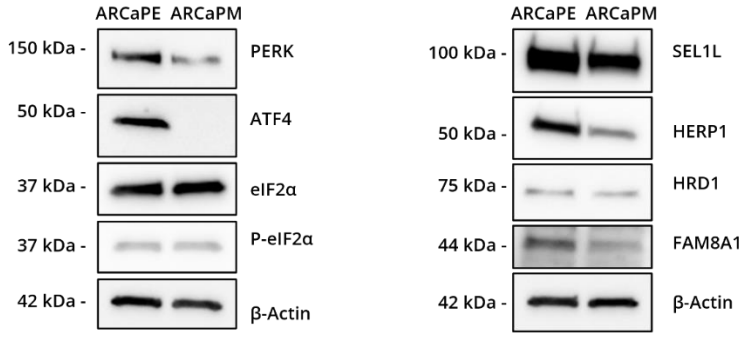



Figure 3.9 Markers of different arms of the UPR are reduced in ARCaPM cells

ARCaPE and ARCaPM cells were grown to confluency in MCaP growth medium. Cell lysates were analysed by immunoblotting using anti-PERK, anti-ATF4, anti-eIF2α, anti-Phospho-eIF2α, anti-SEL1L, anti-HRD1, anti-HERP1, anti-FAM8A1 and anti-β-Actin antibodies. β-Actin was used as loading control.

Comparison of mRNA expression levels of components of the UPR in ARCaPM and ARCaPE cells at basal levels show that *HERP1*, which was downregulated in response to osteogenic differentiation, was lower in ARCaPM cells compared to ARCaPE cells, suggesting that *HERP1* might be related to the process of osteogenic differentiation in terms of metastatic capacity of prostate cancer cells (Figure 3.10). In contrast to the decreased protein levels in ARCaPM, the mRNA expression level of *ATF4* was slightly elevated in ARCaPM cells, indicating that this mRNA is not being translated in ARCaPM cells.

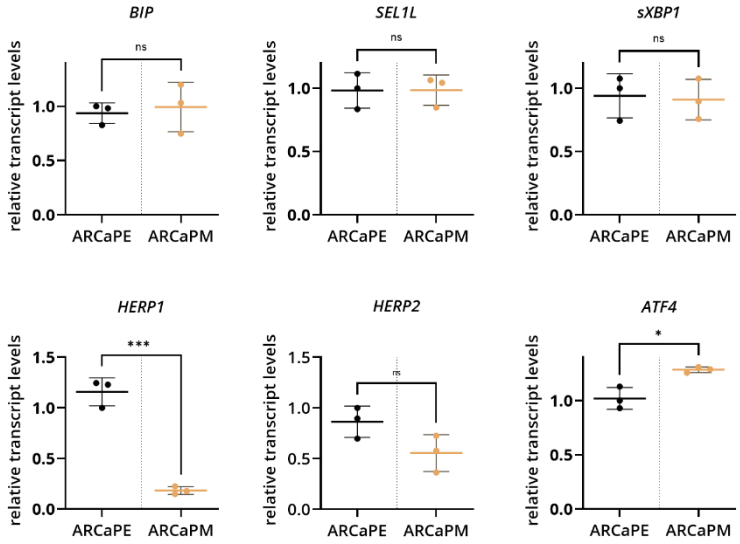



Figure 3.10 The UPR gene expression between ARCaPE and ARCaPM cells

*BIP*, *SEL1L*, *HERP1*, *HERP2*, *sXBP1* and *ATF4* gene expression in ARCaPE and ARCaPM cells were measured by SYBR Green real-time PCR and normalised with *GAPDH* expression. ARCaPE and ARCaPM cells were grown to confluency in MCaP growth medium. (Data summarises 3 independent experiments and shows the mean ± S. D.)

*Unpaired t-test, Alpha 0.05; ns P > 0.05, * P ≤ 0.05, ** P ≤ 0.01, *** P ≤ 0.001, **** P ≤ 0.0001)*

DVL3 is a novel cell line derived from mouse prostate cancer that has PTEN and p53 deletion [280]. DVL3-SCM cells were derived by continuous growth of DVL3 cells in low mitogenic medium (Mills Lab, unpublished data). Allografts of these cells result in completely different tumours. Upon injection into mice, DVL3 cells form highly vascular, non-invasive tumour mass, whereas DVL3-SCM cells form muscle invasive, low vascular tumour in mice. Engraftment into immunocompetent mice followed 6-8 weeks lag period in DVL3 cells until the formation of tumour, whereas in DVL3-SCM cells the lag phase was shortened and the time took takes to terminal mass was halved compared to DVL3 (Mills Lab, unpublished data). DVL3-SCM cells have higher mesenchymal characteristics compared to DVL3 cells. DVL3-SCM cells have elevated levels of Slug and Snail, which are master regulators of EMT, and these cells can form

colonies on soft agar in much higher efficiency compared to DVL3 cells (Mills Lab, unpublished data). DVL3-SCM tumour histology indicated bone deposition within the tumour. Overall, the osteoblastic potential of DVL3-SCM cells reflect more mesenchymal characteristics.

Next, I investigated the role of the UPR in paired mouse prostate cancer cells DVL3 and DVL3-SCM cells. Using the paired cells of human and mouse prostate cancer cells allows comparison of the contribution of epithelial and mesenchymal characteristics to the UPR in context of their ability for bone metastasis. The mRNA transcript levels of components of the UPR were elevated in mesenchymal DVL3-SCM cells compared to the epithelial DVL3 cells (Figure 3.11).

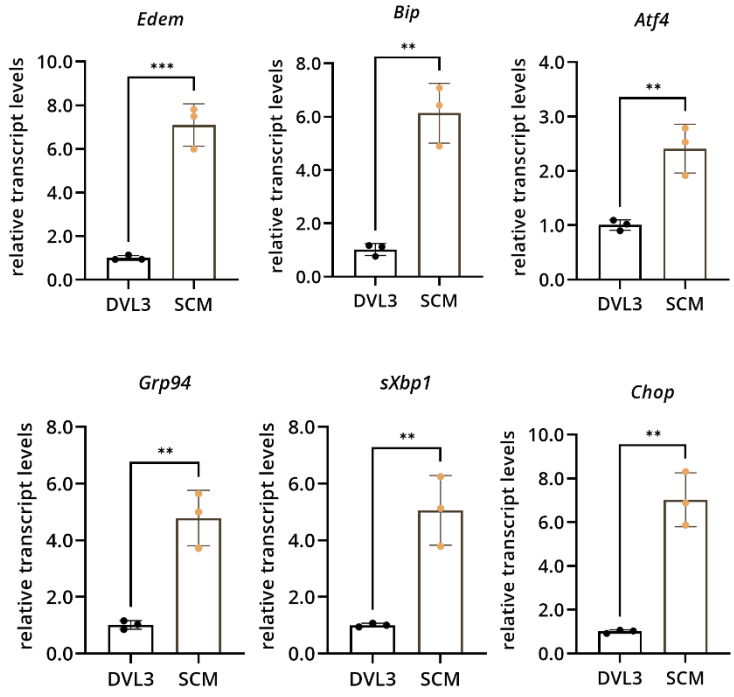



Figure 3.11 The UPR gene expression between DVL3 and DVL3-SCM cells

*Edem*, *Bip*, *Atf4*, *Grp94*, *sXbp1* and *Chop* gene expression in DVL3 and DVL3-SCM cells were measured by SYBR Green real-time PCR and normalised with Gapdh expression. DVL3 and DVL3-SCM cells were grown to confluency in RPMI or Keratinocyte growth medium, respectively. (Data summarises 3 independent experiments and shows the mean ±S. D.)
*Unpaired t-test, Alpha 0.05; ns P > 0.05, * P ≤ 0.05, ** P ≤ 0.01, *** P ≤ 0.001, **** P ≤ 0.0001)*

Comparison of the osteogenic marker gene expression in mouse prostate cancer cell pair showed that *Runx2, Alpl, Col1a1* were also significantly higher in mesenchymal mouse prostate cancer cells, suggesting an association between EMT, UPR and osteomimicry in these paired prostate cancer cells (Figure 3.12).

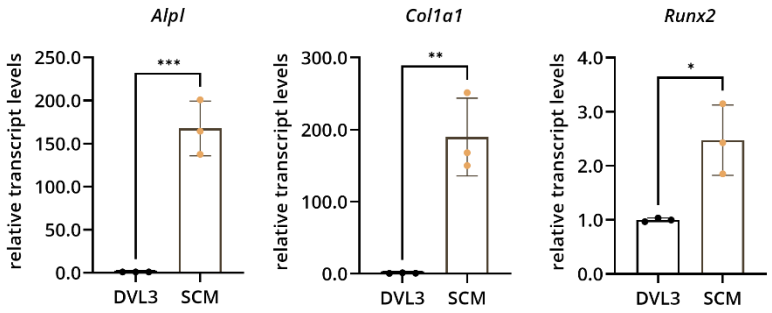



Figure 3.12 Osteogenic marker gene expression between DVL3 and DVL3-SCM cells

*Alpl*, *Col1a1*, and *Runx2* gene expression in DVL3 and DVL3-SCM cells were measured by SYBR Green real-time PCR and normalised with *Gapdh* expression. DVL3 and DVL3-SCM cells were grown to confluency in RPMI or Keratinocyte growth medium, respectively. (Data summarises 3 independent experiments and shows the mean ± S. D.)
*Unpaired t-test, Alpha 0.05; ns P > 0.05, * P ≤ 0.05, ** P ≤ 0.01, *** P ≤ 0.001, **** P ≤ 0.0001)*

### 3.3.4 Effect of the UPR inhibitors

As the level of the UPR related proteins changed during osteogenic differentiation, I investigated whether the inhibition of these pathways would contribute to or inhibit osteogenic potential I have seen in ARCaPM cells. For this purpose, first I used the UPR inhibitors and confirmed the mechanism of action for the inhibitor of each arm of the UPR. Then I used these inhibitors in control and differentiation medium to investigate their effect on osteomimicry.

Tunicamycin (Tm) is an antibiotic that inhibits N-linked glycosylation and is used to induce ER stress in cells [441]. It activates all of the ER stress branches by resulting in misfolded nonglycosylated protein accumulation. In order to

validate the activity of the UPR inhibitors, first I treated cells with tunicamycin, to establish that each arm of the UPR responded to ER stress.

Following treatment with Tm, a lower molecular weight band for SEL1L appeared, corresponding to its non-glycosylated form, and validating the activity of the compound. The levels of HRD1 and HERP1 increased in response to Tm and the increase was concentration dependent (Figure 3.13-A).

Activation of the IRE1 arm of the UPR in these cells after treatment was assessed by comparing XBP1 splicing using RT-PCR. XBP1 splicing was not observed when cells were not stressed, however, XBP1 splicing increased after treatment with Tm and the level of splicing correspondingly increased with increasing concentrations (the lower band in the agarose gel corresponds to sXBP1, Figure 3.13-B). Culturing ARCaPM cells in MCaP or $\alpha$-mem medium did not alter the baseline UPR level, and the response to tunicamycin was not affected by change in the media.

Treatment of cells with tunicamycin resulted in PERK phosphorylation, as can be observed by the presence of a higher molecular weight band in PERK western blots. PERK downstream ATF4 and CHOP were elevated and eIF2$\alpha$ phosphorylation levels were increased with increasing ER stress (Figure 3.13-C).

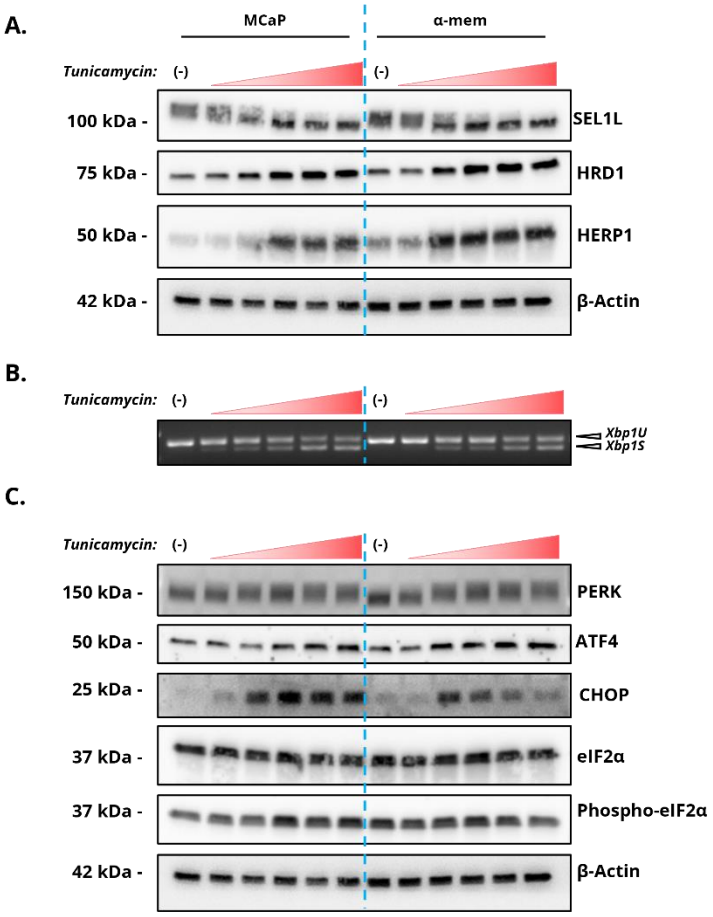



Figure 3.13 Effect of different concentrations of tunicamycin on the relative protein expression of UPR related genes in ARCaPM cells

ARCaPM cells in MCaP or α-mem medium were treated with increasing concentrations of N-glycosylation inhibitor tunicamycin (30, 100, 300, 1000, 3000 ng/ml) to induce ER stress. The cells were collected 24 h after treatment and western blot was done to monitor the relative protein expression of ERAD components (A), and PERK pathway components (C) in response to stress induction. Cell lysates were analysed by immunoblotting using anti-SEL1L, anti-HRD1, anti-HERP1, anti-PERK, anti-ATF4, anti-CHOP, anti-eIF2α, anti-P-eIF2α, and anti-β-Actin antibodies. β-Actin was used as loading control. XBP1 splicing assay for detection of IRE1 pathway activation (B). Blue line separates the MCaP medium and α-mem medium.

Next, I used UPR inhibitors and validated the mechanism of action for the inhibitor of each arm of UPR. Ceapin-A7 inhibits transport of ATF6 to the Golgi where it is cleaved to its active form to regulate the UPR related gene expression in response to ER stress. SEL1L is expressed constitutively and ATF6 can only inhibit the UPR induced SEL1L. More non-glycosylated SEL1L would be made under Tm-treated conditions, which Ceapin-A7 should prevent. The level of non-

glycosylated SEL1L in response to tunicamycin treatment decreased in the presence of ATF6 inhibitor Ceapin-A7 due to decreased ATF6 activity. The Tm induced elevated protein levels of both HRD1 and HERP1 decreased when ATF6 pathway was inhibited with Ceapin-A7 (Figure 3.14-A). When the cleaved form of ATF6 activates the XBP1 promoter, transcription of UPR-responsive genes is triggered [442]. As a result, ATF6 and IRE1 signalling converge to activate XBP1 transcription and mRNA splicing, respectively. ATF6 promotes XBP1 transcription, resulting in more substrate for IRE1-mediated splicing, which results in more active XBP1 and creates a positive feedback loop for UPR activation [442]. Hence, IRE1 inhibition results in similar response to ATF6 inhibition.

IRE1 activity can be inhibited by inhibitors that can either interfere with the catalytic core of the RNase domain or bind to the ATP-binding pocket of the kinase domain. IRE1 inhibitor 4μ8C inhibits phosphorylation of IRE1 by forming a stable imine bond at the lysine residue (K907) in the catalytic core of the endonuclease domain and thus inhibits splicing of XBP1 mRNA and IRE1-mediated mRNA degradation [443]. Tunicamycin mediated ER stress resulted in increased XBP1 splicing, and the increase in sXBP1 levels decreased when IRE1 phosphorylation was inhibited with 4μ8C. HRD1 protein level increase in response to tunicamycin was inhibited in the presence of IRE1 inhibitor. Similar response was observed with IRE1α RNase inhibitor MKC8866 (Figure 3.14-A and B).

GSK2606414 inhibits PERK phosphorylation and also eIF2α phosphorylation. GSK2606414 inhibited Tm induced PERK phosphorylation and subsequent increase in ATF4, CHOP, and eIF2α phosphorylation (Figure 3.14-C). HERP1 increase in response to Tm treatment was mitigated by PERK pathway inhibition.

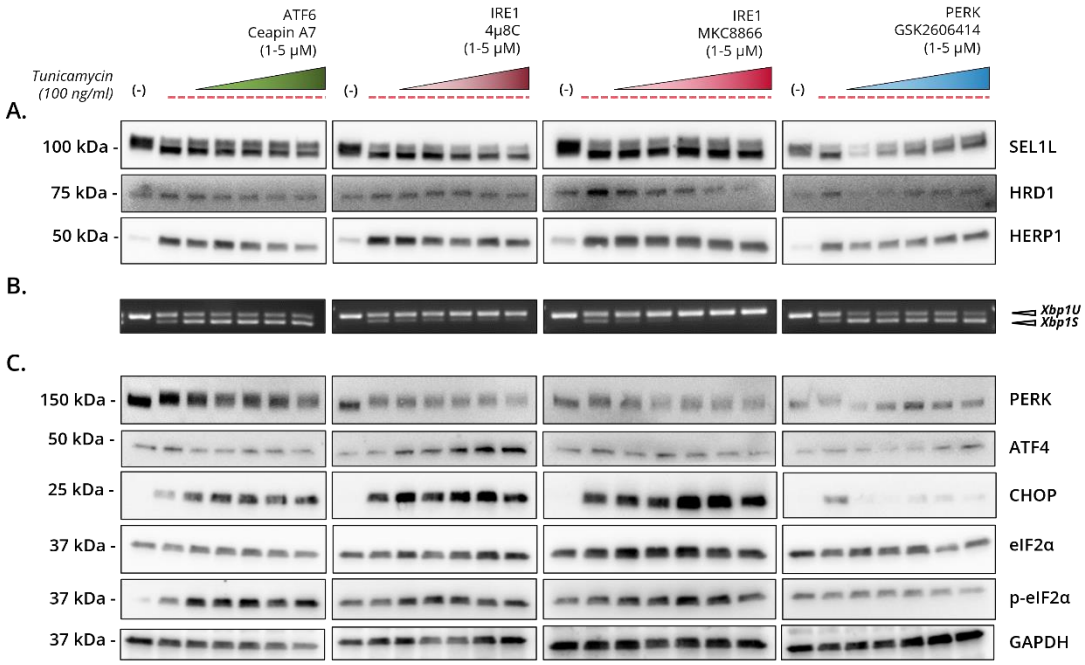



Figure 3.14 Baseline levels of the UPR related proteins and confirmation of inhibitor function

ARCaPM cells in MCaP medium were treated with indicated inhibitors at 1, 2, 3, 4 and 5 μM concentrations in the presence or absence of tunicamycin at 100 ng/ml concentration. The lysates were collected 24 h after treatment and western blot was done to monitor the levels of ATF6 (A), IRE1 (B) and PERK pathway components (C) in response to stress induction. Cell lysates were analysed by immunoblotting using anti-PERK, anti-ATF4, anti-CHOP, anti-eIF2α, anti-P-eIF2α, anti-SEL1L, anti-HRD1, anti-HERP1 and anti-β-Actin antibodies.

As osteogenic differentiation requires long term culturing, I next investigated the effect of the UPR inhibition on this process. In order to determine whether the UPR inhibitors impact cell viability and thus create an indirect effect on the process of differentiation, Alamar Blue staining was performed for measuring cell viability (Figure 3.15-A). The UPR inhibitors had no effect on cell viability after 72 hours when the cells were not stressed. However, the viability decreased when the cells were stressed with tunicamycin. Inhibiting the PERK arm with GSK2606414 further decreased the viability of the cells when added together with tunicamycin. Then, I decreased the concentration of tunicamycin to a level sufficient to induce stress but also a concentration that minimises cell death. I also included thapsigargin as an alternative compound to induce ER stress. Using

low levels of ER stressors minimised the effect on cell viability, however even with these lower amounts, inhibiting the PERK arm with GSK2606414 in the presence of tunicamycin or thapsigargin decreased cell viability (Figure 3.15-B).

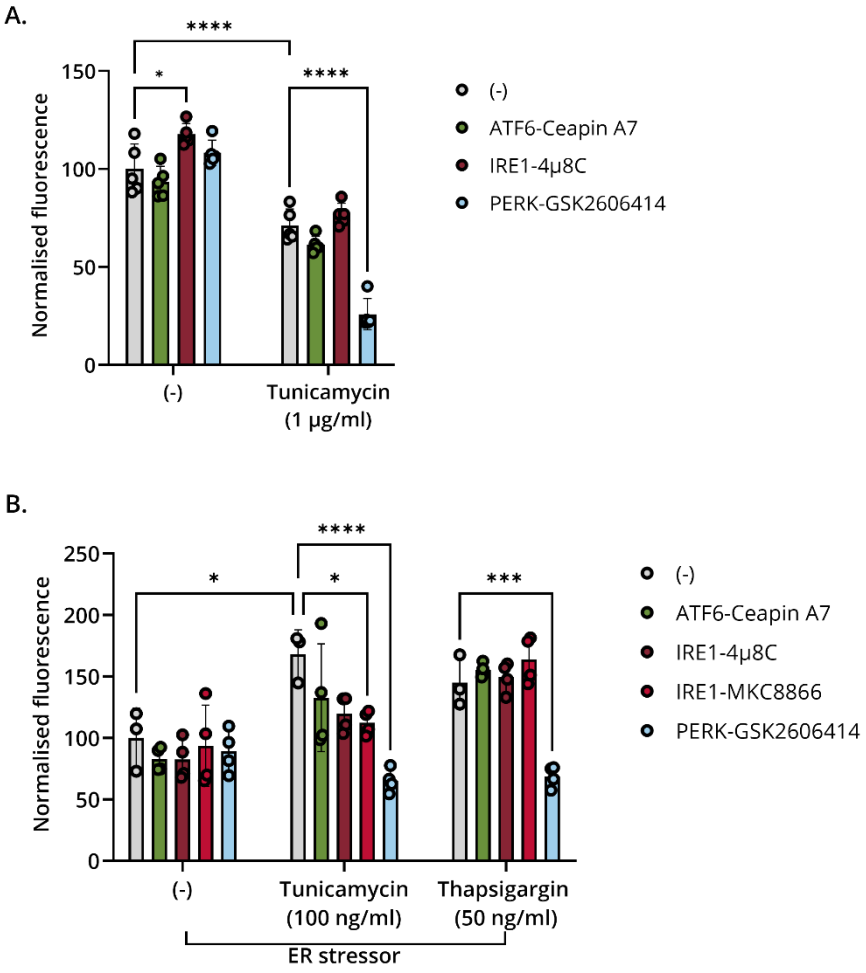



Figure 3.15 Effect of ER stress inducers and the UPR inhibitors on viability of ARCaPM cells

ARCaPM cells seeded into a 96 well plate in MCaP medium were treated with indicated inhibitors at 1 µM concentration in the presence or absence of ER stressors. (A) Effect of tunicamycin at 1 µg/ml concentration, (B) Effect of tunicamycin and thapsigargin at lower doses (tunicamycin at 100 ng/ml concentration; thapsigargin at 50 ng/ml concentration). DMSO was used as vehicle control to tunicamycin treatment at same dilution. 72 h after the treatment Alamar Blue was added and the plate was then read using a fluorimeter. The absorbance was normalised to ARCaPM cells in MCaP medium with DMSO. Data shows mean ± S. D.

*Two-way ANOVA with Tukey's multiple comparison test, Alpha 0.05; ns P > 0.05, * P ≤ 0.05, ** P ≤ 0.01, *** P ≤ 0.001, **** P ≤ 0.0001*

To investigate the effect of the UPR blockade on mineralisation of prostate cancer cells when the cells are cultured in osteogenic differentiation, a single time point experimental setup was used, and the effects on mineralisation and alkaline phosphatase was assayed 15 days after culturing. The UPR inhibitors did not inhibit the formation of mineral crystals in ARCaPM cells, as the cells still deposited mineral crystals after 15 days in osteogenic differentiation medium in the presence of each inhibitor (Figure 3.16). The level of ALP activity was modestly higher in differentiation medium but was not significant. This is consistent with the earlier findings: the difference between the level of ALP activity in control and differentiation media weakens at later timepoints in the course of osteomimicry (Figure 3.3).

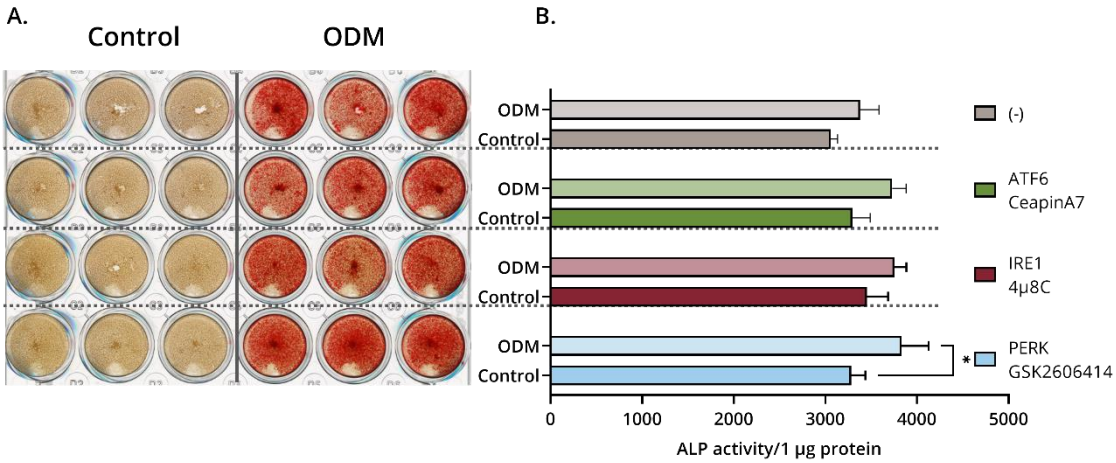



Figure 3.16 Mineral deposition and ALP activity in response different inhibitors of the UPR after 15 days

ARCaPM cells treated with indicated inhibitors at 1 μM concentration and cells grown in control or osteogenic medium for 15 days. The cells were stained (red) for mineral deposition with Alizarin Red S. (A), ALP activity in ARCaPE and ARCaPM cell lysates was measured using a fluorogenic ALP substrate and normalised with 1 μg protein concentrations (B). Data shows mean ± S. D. *Two-way ANOVA with Tukey's multiple comparison test, Alpha 0.05; ns P > 0.05, * P ≤ 0.05, ** P ≤ 0.01, *** P ≤ 0.001, **** P ≤ 0.0001*

Therefore, I investigated the effect of inhibiting the arms of the UPR on alkaline phosphatase activity levels at earlier time points in response to culturing in osteogenic differentiation medium. IRE1 and PERK inhibition increased the level of alkaline phosphatase activity in the control medium after 3 days, but this was not observed in differentiation medium (Figure 3.17). ATF6 inhibition decreased the ALP activity in the control medium during the course of the treatment except the 7$^{th}$ day. Three independent experiments indicated that IRE1 or PERK inhibitor in control medium increased the ALP activity in ARCaPM cells, but the inhibition of those pathways did not further increase the ALP activity in differentiation medium compared to inhibitor controls.

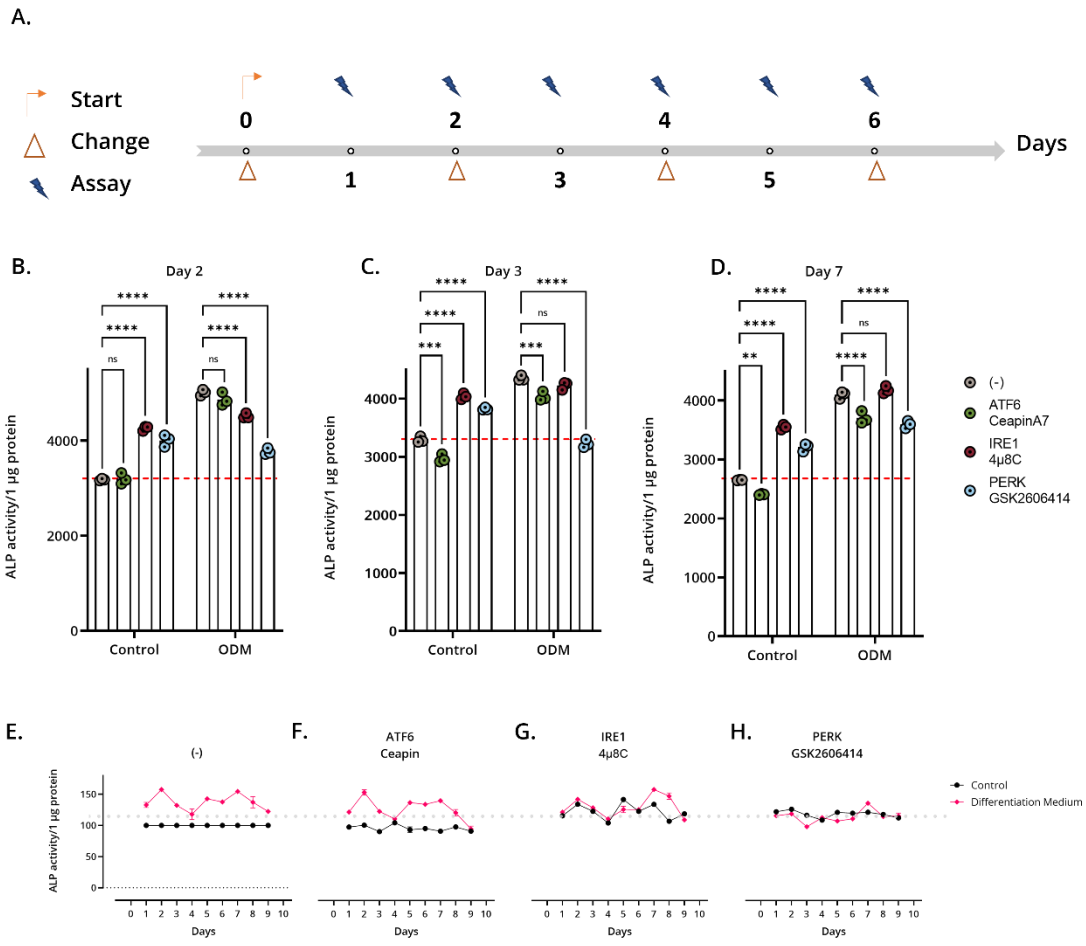



Figure 3.17 Inhibiting IRE1 or PERK pathway results in changes in alkaline phosphatase activity levels in ARCaPM cells in control and differentiation medium

(A) The schematic representation of time course experiment showing the medium changes and assay times throughout the experiment. (B-D) ALP activity of ARCaPM cells normalised to total protein concentrations under different conditions for 7 days. Each compound was added to control or differentiation medium (ODM) at 1 µM final concentration. (E-H) ALP activity in each measurement on each day of the experiment on (A) were normalised to the ALP activity of ARCaPM cells in control medium of that day and shown as line graph for each inhibitor. Error bars show standard deviation for 3 measurements.

*Two-way ANOVA with Dunnett's multiple comparisons test, Alpha 0.05; ns P > 0.05, * P ≤ 0.05, ** P ≤ 0.01, *** P ≤ 0.001, **** P ≤ 0.0001*

Next, with an identical experimental setting I investigated the inhibitor effect on ALP activity levels in ARCaPE cells and compared the response to ARCaPM cells. ARCaPE cells were cultured in control or differentiation medium for 7 days with inhibitors of different arms of the UPR at 1 µM concentration. ALP activity

was measured on day 2, day 3 and day 7. The level of ALP activity did not change in ARCaPE cells with either the UPR inhibition or differentiation media (Figure 3.18).

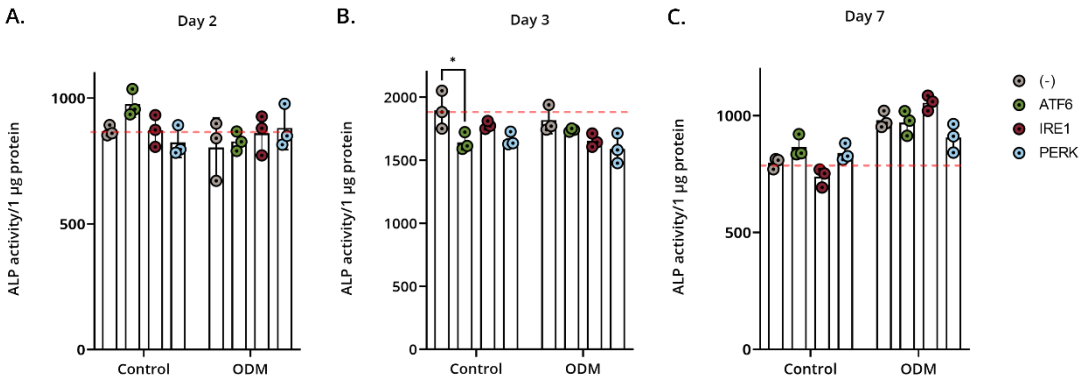



Figure 3.18 ALP activity in ARCaPE cells in response to the UPR inhibitors

*ALP activity in 1 µg protein of ARCaPE cells under different conditions for 2, 3 and 7 days. Each compound was added to control or osteogenic differentiation medium (ODM) at 1 µM final concentration. Error bars show standard deviation for 3 measurements.*

*Two-way ANOVA with Tukey's multiple comparison test, Alpha 0.05; ns P > 0.05, * P ≤ 0.05, ** P ≤ 0.01, *** P ≤ 0.001, **** P ≤ 0.0001*

To determine whether increasing concentration of the UPR inhibitors would impact ALP activity of ARCaPE cells, the cells were treated for 24 h, to minimise any deleterious effects of inhibitors on cell viability. Inhibition of the PERK pathway with 5 µM GSK2606414 slightly increased ALP activity in ARCaPE cells (Figure 3.19). Perturbation of other pathways did not have any effect on ALP activity.

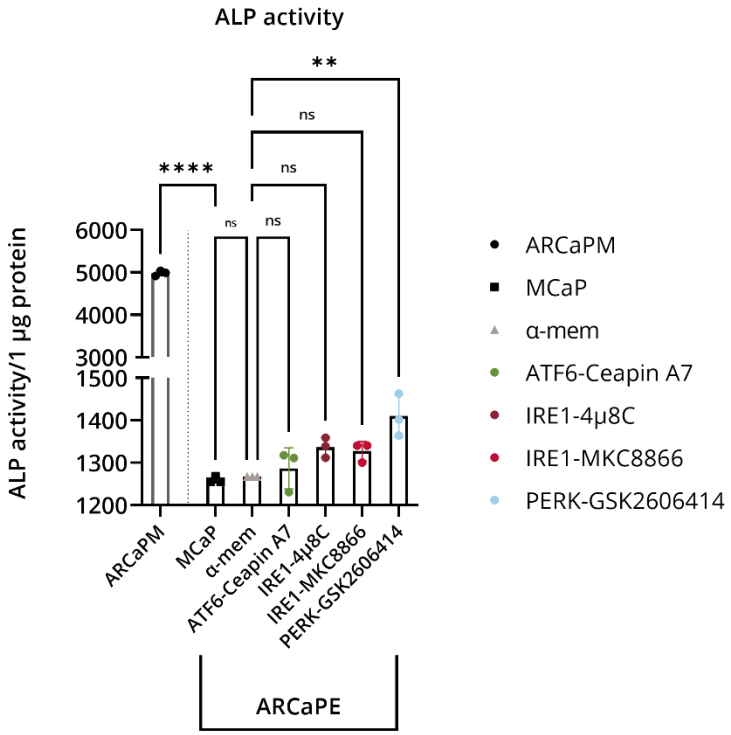



Figure 3.19 ALP activity in ARCaPE cells in response to 5 µM UPR inhibitors

ALP activity in 1 µg protein of ARCaPE cells under different conditions for 24 h. Each compound was added to control medium at 5 µM final concentration. Error bars show standard deviation for 3 measurements.

*One-way ANOVA with Tukey's multiple comparison test, Alpha 0.05; ns P > 0.05, * P ≤ 0.05, ** P ≤ 0.01, *** P ≤ 0.001, **** P ≤ 0.0001*

qRT-PCR of the markers of UPR, EMT and osteogenic differentiation did not show any effect of inhibitors on the RNA levels of these markers in ARCaPE cells (Figure 3.20).

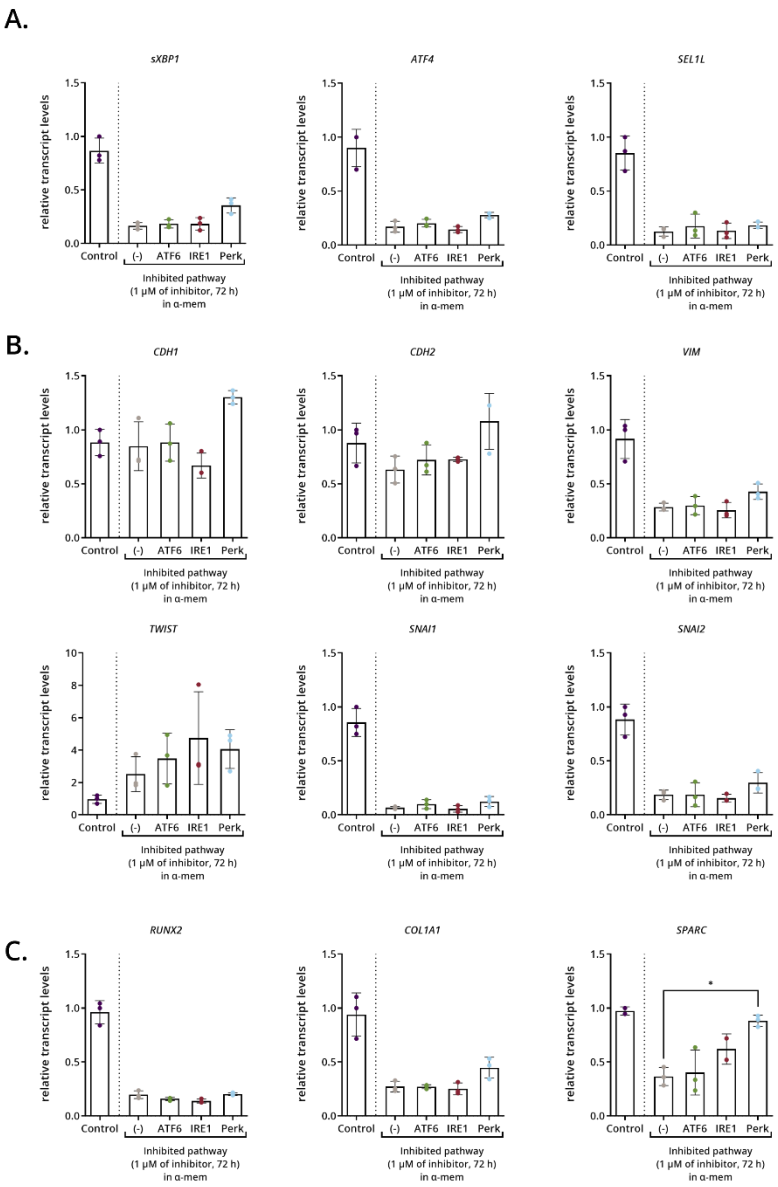



Figure 3.20 Expression levels of the UPR, EMT and osteogenic markers on ARCaPE with inhibitors of the UPR for 72 h

Cells were seeded on a 12 well plate with 200,000cell/ml density. Ceapin-A7, 4µ8C, and GSK2606414 were used to inhibit ATF6, IRE1 and PERK pathways, respectively. Inhibitor of each pathway was added to α-mem medium at 1 µM final concentration in three technical replicates and the cells were collected 72 h after treatment. RNA isolation, cDNA synthesis, and qRT-PCR was done as described previously. GAPDH was used as internal control and fold change of each mRNA transcript in treated samples was relative to that of ARCaPE cells which were grown in MCaP medium. The bars show the mean ± S. D of three replicate treatments, each one represented with a dot, which was performed in triplicates in qRT-PCR plate.

*Two-way ANOVA with Dunnett's multiple comparisons test, Alpha 0.05; ns P > 0.05, * P ≤ 0.05, ** P ≤ 0.01, *** P ≤ 0.001, **** P ≤ 0.0001*

Then I investigated the interplay between the UPR, EMT, and osteogenic potential in paired mouse prostate cancer cell lines DVL3 and DVL3-SCM cells. To monitor if the inhibition of different arms of the UPR would alter the ALP activity levels in DVL3-SCM cells, DVL3-SCM cells were treated with inhibitors targeting different arms of the UPR at 1 µM concentration for 2, 3 and 7 days. The ALP activity did not change in response to the inhibition of the arms of the UPR in keratinocyte medium after 2 or 3 days (Figure 3.21).

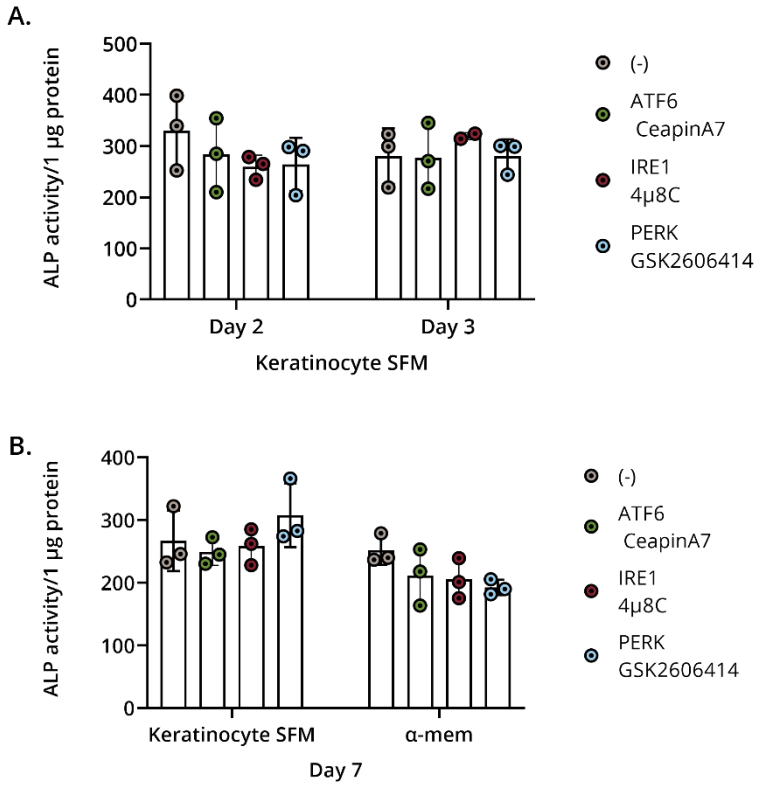



Figure 3.21 Inhibiting different arms of the UPR does not impact ALP activity in DVL3-SCM cells

DVL3-SCM cells were treated with 1 µM of inhibitors of the ATF6, IRE1 and PERK arms of the UPR for 2, 3 and 7 days and ALP activity was measured using a fluorescence-based assay using fluorogenic ALP substrate. ALP activity was normalised to 1 µg of protein based on BCA protein assay Data shows mean ± S. D.

*Two-way ANOVA with Tukey's multiple comparison test, Alpha 0.05; ns P > 0.05, * P ≤ 0.05, ** P ≤ 0.01, *** P ≤ 0.001, **** P ≤ 0.0001*

DVL3-SCM cells are cultured in serum free medium, and a switch to FBS containing medium affects their morphology due to stress. Attempts to investigate the osteogenic potential in mouse PCa cells failed as DVL3-SCM cells do not grow in FBS containing medium, which is the basis of differentiation medium.

Previous findings indicated that inhibition of the UPR affects EMT related gene expression in ARCaPM cells. To monitor the change in morphology in DVL3 cells in response to medium switch, and to investigate whether inhibition of different arms of the UPR would stop the change in morphology, the cells were monitored with the live cell imaging *IncuCyte* microscope with 12 h intervals over a 1-week time period. The UPR inhibitors did not have any effect on morphology upon change to FBS-containing $\alpha$-mem medium. Longer incubation (7 days) in keratinocyte medium or $\alpha$-mem medium did not have any effect on ALP activity (Figure 3.22).

I also checked the levels of EMT and osteogenic marker expression in mouse prostate cancer SCM cells in response to inhibitor treatment, but there was no significant effect.

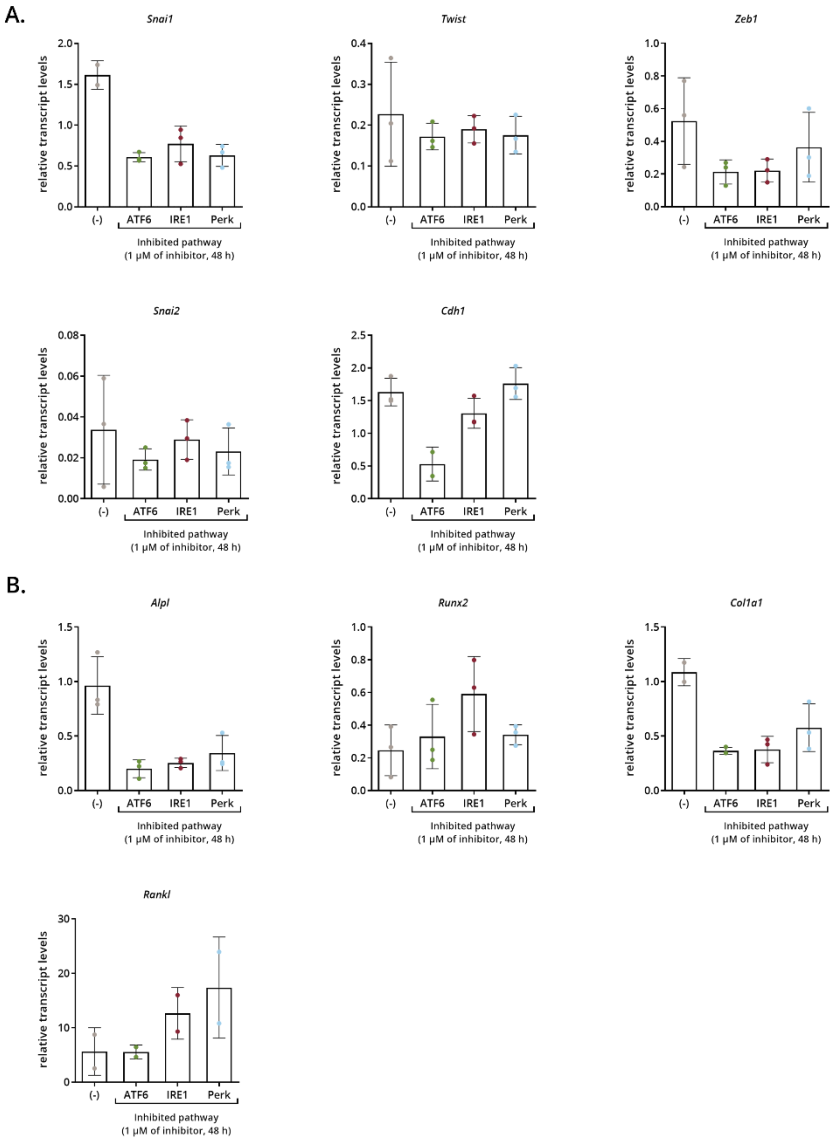



Figure 3.22 The levels mRNA transcripts of EMT and osteogenic markers in DVL3-SCM cells measured by qRT-PCR

(A) EMT marker and (B) osteogenic marker expression in DVL3-SCM cells. Ceapin-A7, 4µ8C, and GSK2606414 were used to inhibit ATF6, IRE1 and PERK pathways, respectively. Inhibitor of each pathway was added to Keratinocyte medium at 1 µM final concentration in three replicates and the cells were collected 48 h after treatment. *Gapdh* was used as internal control and fold change of each mRNA transcript in treated samples was relative to that of DVL3-SCM cells which were grown in Keratinocyte medium. The bars show the mean of three replicate treatments, each one represented with a dot, which was performed in triplicates in qRT-PCR plate. Error bars show standard deviation.

*Two-way ANOVA with Tukey's multiple comparison test, Alpha 0.05; ns P > 0.05, * P ≤ 0.05, ** P ≤ 0.01, *** P ≤ 0.001, **** P ≤ 0.0001*

## 3.4 Discussion

The work of this chapter has shown that the baseline expression level of the UPR proteins PERK, ATF4, SEL1L, HERP1 and FAM8A1 are elevated in ARCaPE cells compared to ARCaPM cells; the level of the UPR components ATF4 and HERP1 proteins decrease under osteogenic conditions and inhibiting IRE1 arm or PERK arm of the UPR increase the osteogenic potential in ARCaPM.

Among the paired ARCaPM and ARCaPE cells, ARCaPM cells, the metastatic derivative of ARCaP cells have increased alkaline phosphatase (ALP) activity. Comparison of baseline gene expression levels revealed that ARCaPM and ARCaPE cells express different osteogenic markers (Figure 3.1). Although the level of *ALPL* was higher in ARCaPM, *RUNX2*, and *SPARC* was lower in ARCaPM. *RUNX2* is one of the main regulators of osteogenic differentiation that regulates transcription bone-related factors in osteoblasts, including osteocalcin, osteopontin, collagen type I, and osteoprotegerin. One study has shown a correlation between increased motility and invasiveness, and *RUNX2*-mediated gene expression in metastatic PCa cells. In this study, overexpression of *RUNX2* in non-metastatic LNCaP cells promoted the expression of metastatic markers *MMP-2*, *MMP-9*, *MMP-13* [444].

During osteoblast differentiation, *RUNX2* expression is very low in uncommitted mesenchymal cells, but becomes more prominent in preosteoblasts, reaches its maximum level in immature osteoblasts, and decreases in mature osteoblasts, indicating a temporal regulation of gene expression [175]. Low levels of *RUNX2* and elevated levels of *ALPL* in ARCaPM cells compared to ARCaPE cells suggest transcriptional repression of *RUNX2* levels after induction of key osteoblast markers. A negative regulation by *RUNX2* downstream elements might control the levels of *RUNX2* transcription levels after their expression. Alternatively,

elevated ATF4 (an important cofactor of *RUNX2*) levels might account for the elevated *RUNX2* in ARCaPE cells.

Secreted protein acidic and rich in cysteines like 1 (SPARCL1), is a member of SPARC family, that resembles closely to SPARC/osteonectin [445]. The SPARC family of proteins consist of matricellular proteins that are secreted to the extracellular matrix, with anti-adhesive and anti-tumorigenic functions. Previously SPARCL1 has been shown to suppress the metastatic potential of PC3 cells *in vitro* and *in vivo* [446]. Likewise, low levels of *SPARC* expression could be due to suppression by factors that contribute to mesenchymal characteristics of ARCaPM cells.

Although the expression level of two master regulators of osteogenic differentiation were higher in ARCaPE cells, only ARCaPM cells deposited minerals in osteogenic medium (Figure 3.2-A), suggesting that SPARC and RUNX2 were not essential for osteomimicry in PCa cells, and the presence of alkaline phosphatase was indispensable for mineralisation(Figure 3.2-B and C). This, combined with the observation that β-glycerophosphate is sufficient for mineralisation (Figure 3.5), suggests that this is not osteogenic differentiation. Mineral deposition by ARCaPM cells does not necessarily indicate a differentiation towards osteoblast lineage.

Time-course differentiation of ARCaPM cells revealed that mineral deposition takes place after 9 days (Figure 3.3-C), following the increase in ALP levels which happens earlier in the process, i.e., 6 days (Figure 3.3-B), following an earlier increase in ALP activity that takes place after 3 days in osteogenic differentiation medium (Figure 3.3-A). Osteomimicry of prostate cancer cells is a sequence of events, where different processes take place at different times; thus, choosing

markers for the correct assessment of osteomimicry of prostate cancer cells is important.

The first evidence for changes in the UPR during the osteogenic differentiation of prostate cancer cells was a decrease in the protein levels of ATF4, phosphorylated eIF2$\alpha$ and HERP1; and an increase in the SEL1L levels in differentiation medium compared to control (Figure 3.6). This suggests activation of the ATF6 arm of the UPR, alongside decreased activity from the PERK arm. Gene expression did not change at RNA level (Figure 3.7), indicating that the changes in the UPR were happening at translational and/or post-translational levels.

A comparison of mRNA expression level of components of the UPR in ARCaPM and ARCaPE cells at basal levels show that *HERP1*, which was downregulated in response to osteogenic differentiation, was lower in ARCaPM cells compared to ARCaPE cells (Figure 3.10), suggesting that *HERP1* might be related to the process of osteogenesis. Decrease in HERP1 protein level further support the involvement of ER stress response in prostate cancer bone metastasis (Figure 3.6 and Figure 3.9). HERP1 acts as a scaffold protein that mediates compartmentalisation of the misfolded proteins and HRD1 (E3-ligase) at the ER-derived quality control compartment (ERQC) to initiate ERAD [369]. Thus, decreased HERP1 levels blocks Hrd1 complex assembly, hence reduction of ERAD substrates. Decreased HERP1 protein levels during osteogenic differentiation indicate that the process of the PCa cells mimicking the osteoblast cells might require inhibition of Hrd1 complex activity, and hence the retro-translocation and proteasomal degradation of ERAD substrates. This could be to maintain the unfolded proteins inside the ER lumen and increase the folding capacity inside the ER instead. As HRD1 is a E3 ubiquitin ligase, it catalyses the ubiquitination of proteins and targets them for proteasomal degradation [447]. Although this was previously described in the context of ERAD of misfolded proteins, HRD1

ubiquitination can also serve as post-transcriptional regulator. Decreased HERP1 protein levels, hence decreased HRD1 activity (due to halting of the complex assembly) might be to prevent proteasomal degradation of important factors involved in osteomimicry of PCa cells. Osteogenic differentiation involves downregulation of the UPR components that are high at basal levels in ARCaPE cells. *HERPUD1* gene expression was shown to increase in response to androgen treatment in LNCaP cells. Comparison of normal and tumour cells of 20 prostate cancer patients indicated a negative correlation between *HERPUD1* expression and the malignant status of the prostate [382].

Although the level of *ATF4* mRNA transcript was slightly elevated in ARCaPM compared to ARCaPE cells, the ATF4 protein was lower compared to ARCaPE cells (Figure 3.10). While baseline mRNA expression of *ATF4* is different between ARCaP cells, the mRNA level of such a protein that is known to be regulated at protein level, is not as important in understanding the differences in the UPR among ARCaPM and ARCaPE cells. This is because ATF4 protein levels selectively increase as a result of eIF2$\alpha$ phosphorylation which attenuate the ternary complex formation and hence favour the translation of the ORF that encode ATF4 instead of the translation of uORF2, which is located in the 5' UTR of the *ATF4* (Explained in *Section 1.4.1.1.3*). As the ATF4 mRNA is not translated in nonstressed cells, elevated ATF4 protein levels in ARCaPE indicate a more active PERK pathway compared to ARCaPM. Besides, lower level of ATF4 in ARCaPM cells may also indicate control of ATF4 protein levels at translational and/or post-translational levels. A previous study indicated that ATF4 was degraded by proteasomal degradation in non-osteoblastic cells [421].

Inhibiting IRE1 or PERK pathway increases ALP activity only in control medium in ARCaPM cells (Figure 3.17), suggesting that the levels of alkaline phosphate

activity are kept at a certain level by a control mechanism related to the IRE1 and PERK pathways; and that IRE1 and PERK inhibition might be releasing that control for alkaline phosphate activity, hence the levels cannot increase any further in osteogenic differentiation medium. If the UPR is upstream of ALP, this gives an opportunity for targeting the mineralisation in osteomimetic PCa cells.

Although both PERK and IRE1 inhibition increased ALP activity, my data suggests that PERK might do it through the conventional pathway, the SPARC-RUNX2 and ALPL axis. PERK inhibition induced a moderate *SPARC* expression in ARCaPM cells, although there was no increase in the mRNA transcript levels of *RUNX2* after 2 days, suggesting a regulation through the conventional osteogenic differentiation pathway. An active PERK pathway might have a role in inhibiting the expression of master regulators of osteogenic differentiation, i.e., RUNX2 and SPARC. ARCaPM cells do not express *SPARC* at baseline levels (Figure 3.1), and the induced expression is indirectly indicated by the similarity of melt curve to *SPARC* expressing ARCaPE cells (Supplementary Figure 8.2). On the other hand, IRE1 inhibition did not have any effect on mRNA levels of osteogenic genes, although ALP activity increased; suggesting an alternative mechanism for increased ALP activity in IRE1 inhibited condition.

The baseline levels of the UPR were different between ARCaPM and ARCaPE cells (Figure 3.9). The baseline UPR activity in ARCaPE may be dominated by a different arm of the pathway compared to ARCaPM cells, and so an inhibitor of that arm may make these cells more mesenchymal or increase their potential for osteoblast-like phenotype. However, inhibiting different arms of the UPR did not activate ARCaPE cells for osteoblast like phenotype (Figure 3.18, Figure 3.19 and Figure 3.20). One possible explanation for the interplay between EMT, UPR

and bone metastatic potential could be that the UPR is downstream of EMT, and perturbation of the UPR is not sufficient to promote osteomimicry.

Comparison of baseline osteogenic markers revealed that *Runx2, Alpl, Col1a1* were higher in mesenchymal mouse prostate cancer cells DVL3-SCMs (Figure 3.12). While the baseline levels of the UPR were elevated in epithelial cells in the paired *human* prostate cancer model, the mRNA expression levels of the UPR related genes were elevated in mesenchymal cells in the paired *mouse* prostate cancer model. While species-specific differences cannot be excluded, this indicates the involvement of another regulatory mechanism in the interplay between EMT, UPR and bone metastatic potential in the PCa cells.

First, ARCaP cells display AR repressed phenotype, and the growth is suppressed in response to DHT (dihydrotestosterone) and a synthetic androgen R1881 [278]. Thus, the ARCaP pair of PCa cells represent advanced prostate cancer. Mouse prostate cancer DVL3 cells on the other hand, express androgen receptor and are responsive to AR antagonists and represent high-risk localised disease. As human PCa pair cells and mouse PCa pair cells differ in their AR biology, the different interdependence between EMT, UPR and osteoblastic potential may be attributed to AR signalling. Second, ARCaP cells represent PTEN-wild type phenotype whereas DVL3 cells were generated from PTEN-/- mouse. Third, the elevated levels of the UPR components in DVL3-SCM cells compared to parental DVL3 cells may be attributed to the culturing conditions. The normal growth medium of DVL3-SCM cells contain several growth factors including recombinant epidermal growth factor (rEGF), leukaemia inhibitory factor (LIF), stem cell factor (SCF), granulocyte-macrophage colony-stimulating factor (GM-CSF) which can affect EMT, the UPR, and the potency of the cells, hence the differentiation. For example, EGF treatment together with TGF-β induced mesenchymal characteristics in ARCaPE cells [242].

Osteoblastic potential of ARCaP cells or DVL3 cells were monitored by expression and activity levels of alkaline phosphatase in response to UPR inhibitors. Future experiments might involve assessment of the effect of UPR inhibitors on other markers of osteoblast differentiation. This will help to understand whether mineralisation of ARCaPM cells is only because ALP activity levels are higher, and hence the cells are capable of mineral deposition as long as they are provided with a source of phosphate, or if these cells can truly differentiate into osteoblasts. In addition, investigation of the levels of PTHrP, RANKL, and/or OPG, which are secreted factors involved in regulation of osteoblast/osteoclast differentiation can provide more targetable factors for regulating the type of bone metastasis in PCa. Further investigation of the impact of UPR inhibitors on these factors -in case above mentioned secreted factors change in differentiation medium- may allow tuning of these markers using UPR inhibitors in PCa.

In summary, this chapter demonstrated the involvement of the UPR in alkaline phosphatase activities in ARCaPM cells. Comparison of epithelial ARCaPE and mesenchymal ARCaPM cells revealed that baseline protein levels of components of the UPR was elevated in ARCaPE cells, and inhibition of IRE1 and PERK pathways induced increased ALP activity levels in ARCaPM cells. Culturing ARCaPM cells in osteogenic differentiation medium resulted in decrease in several UPR related genes, including ATF4 and HERP1. Although the protein levels of these genes differed both between epithelial and mesenchymal cells and in response to culturing in osteoblast differentiation medium, the mRNA transcript levels did not change in neither of the condition, suggesting a translational and/or post-translational regulations. The specific aim of this section was to uncover the involvement of the UPR in bone metastatic potential of PCa cells. The results shown here indicated that UPR was involved in osteomimicry of ARCaP cells, mainly through the IRE1 and PERK arms.

# 4

# The effect of the UPR on PCa-derived osteoclast/osteoblast activating factors

## 4.1 Introduction

The bone disease associated with prostate cancer bone metastases is driven by changes in a complex network of signalling pathways, including the RANKL/OPG. Osteoclasts are mediators of bone resorption, and they maintain homeostatic balance of the bone by continuous remodelling of the microenvironment in response to various stimuli. Under normal physiological conditions, osteoblastic cells regulate osteoclast activity by maintaining a fine balance between osteoprotegerin (OPG), a decoy receptor for RANK, and

receptor activator of nuclear factor-κB ligand (RANKL) expression. Relatively higher level of RANKL is related to more osteolytic phenotype and higher levels of OPG compared to RANKL is associated with more osteoblastic phenotype. Parathyroid hormone-related protein (PTHrP) promotes osteoclastogenesis by inhibiting the expression of osteoprotegerin (OPG), and by enhancing the production of RANK ligand (RANKL) by osteoblasts.

Previous work has shown that RANKL is dysregulated in osteolytic metastasis in breast cancer by the secretion of PTHrP [245]. Increased bone resorption releases growth factors from the bone matrix, such as TGF-β, which signal back to the tumour cells to enhance PTHrP production and further drive tumour growth in the bone marrow, putting the cells in a vicious cycle of tumour growth. Another work has also shown that elevated UPR signalling following tunicamycin treatment increased RANKL expression in bone cells and the increase was inhibited when the PERK or IRE1 arms of the UPR were inhibited [448].

## 4.2 Hypothesis and Objectives

In this chapter I hypothesised that the elevated UPR impact the expression of osteoblast and osteoclast activating factors. For this purpose, this chapter investigates the effect of the UPR and inhibiting the arms of the UPR on genes regulating RANK signalling in prostate cancer cells. The aims of this chapter are:

- To compare the baseline expression levels of bone-related factors in paired prostate cancer cell lines
- To assess the impact of ER stress on the expression levels of bone-related factors and to investigate the impact of different arms of the UPR on this
- To study the effect of ER stress on the Wnt signalling pathway

# 4.3 Results

## 4.3.1 Difference in basal expression of bone-related factors

To begin, to determine the role of the UPR in PCa-derived bone-related factors, I first investigated the expression of bone-related factors in human prostate cancer cells. The mRNA levels of *PTHRP*, *RANKL* and *OPG* were higher in ARCaPM cells compared to epithelial ARCaPE cells at basal levels (Figure 4.1). Comparison of *RANKL*/*OPG* ratio between ARCaPM and ARCaPE cells revealed that ARCaPM cells have higher *RANKL*/*OPG* ratio, indicating a more osteolytic phenotype in mesenchymal cells.

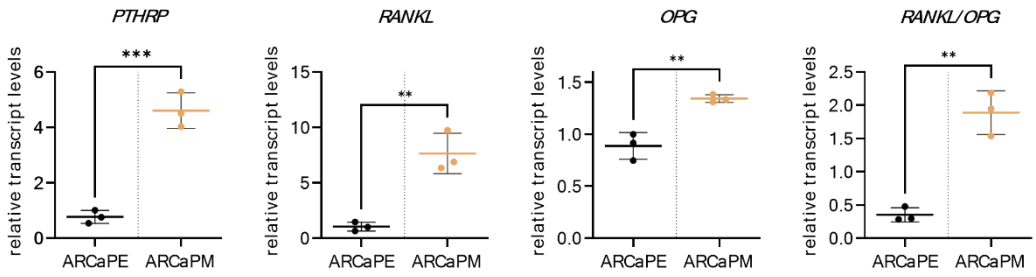



Figure 4.1 Expression levels of bone-related factors differs between ARCaPE and ARCaPM cells

ARCaPE and ARCaPM cells were grown to confluency in MCaP growth medium. *PTHRP*, *RANKL*, and *OPG* gene expression were measured by SYBR Green real-time PCR. *GAPDH* was used as housekeeping control gene and relative transcript level of ARCaPM was normalised to ARCaPE. *RANKL*/*OPG* ratio was calculated from *RANKL* and *OPG* expression data. Data summarises 3 independent experiments and shows the mean ± S. D.

*Unpaired t-test, Alpha 0.05: ns P > 0.05, * P ≤ 0.05, ** P ≤ 0.01, *** P ≤ 0.001, **** P ≤ 0.0001*

In a similar setting, mouse mesenchymal prostate cancer cell line SCM cells had a lower *Rankl*/*Opg* ratio compared to parental epithelial DVL3 cells, indicating a more osteoblastic phenotype (Figure 4.2).

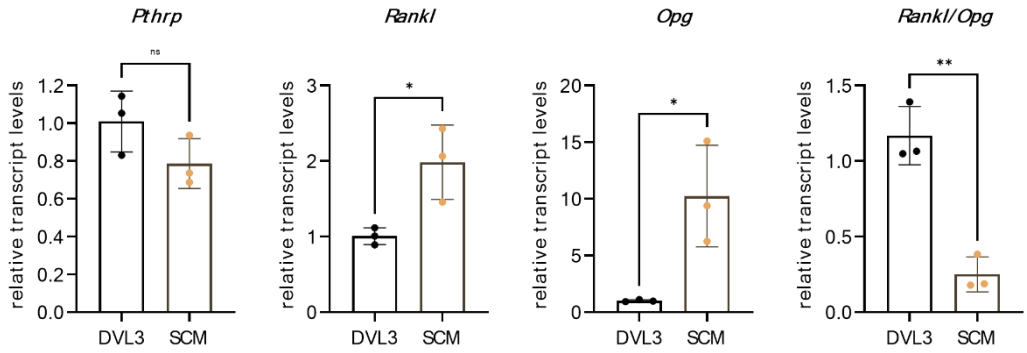



Figure 4.2 Expression levels of bone-related factors differs between DVL3 and DVL3-SCM cells

DVL3 and DVL3-SCM cells were grown to confluency in RPMI or Keratinocyte Serum-free growth medium, respectively. *Pthrp*, *Rankl*, and *Opg* gene expression were measured by SYBR Green real-time PCR. *Gapdh* was used as housekeeping control gene and relative transcript level of ARCaPM was normalised to DVL3 cells. *Rankl*/*Opg* ratio was calculated from *Rankl* and *Opg* expression data. Data shows the mean ± S. D.
*Unpaired t-test, Alpha 0.05; ns P > 0.05, * P ≤ 0.05, ** P ≤ 0.01, *** P ≤ 0.001, **** P ≤ 0.0001)*

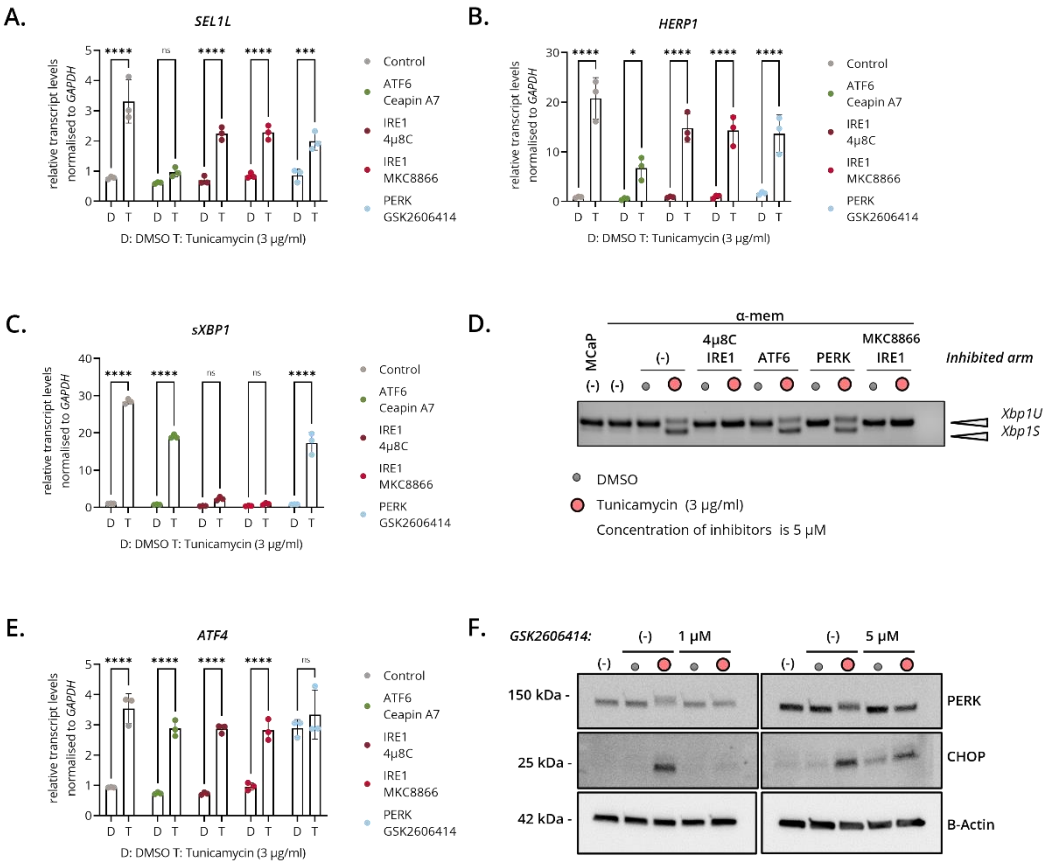
### 4.3.2 Effect of tunicamycin & inhibitors on osteoclastic gene expression

To investigate the contribution of the UPR to this regulation, I examined the bone disease related gene expression in human prostate cancer cells after limited treatment (4 h) with the UPR inhibitors and ER stressors. ARCaPM cells were stimulated with tunicamycin (3 µg/ml) and the ATF6, IRE1 or PERK pathways were inhibited by Ceapin-A7, 4µ8C or MKC8866, GSK2606414, respectively.

The tunicamycin concentration was selected to induce ER stress after 4 h while the doses of the inhibitor treatments were adjusted for each of the UPR arm (Figure 4.3). Cells were harvested 4 h after the start of the treatment, in TRIzol reagent for RNA or cell lysis buffer for protein analysis. mRNA transcript levels of *SEL1L* and *HERP1* was used to reflect ATF6 pathway response; spliced *XBP1*

mRNA level and *XBP1* splicing assay was used to reflect the IRE1 pathway response; and *ATF4* mRNA level and PERK and CHOP protein levels were used to measure PERK pathway response. SYBR Green real-time PCR was used to measure the mRNA levels.

*SEL1L* and *HERP1* mRNA levels increased with tunicamycin treatment, and the increase in the levels was prevented by co-administration of the ATF6 inhibitor Ceapin-A7 (Figure 4.3-A and B). Spliced *XBP1* increased with tunicamycin and was mitigated by both IRE1 inhibitors 4μ8C or MKC8866 (Figure 4.3-C). Tunicamycin treatment (3 μg/ml for 4 h) resulted in partial splicing of *XBP1,* which was inhibited by both 4μ8C and MKC8866 (Figure 4.3-D). ATF4 expression increased with tunicamycin treatment (Figure 4.3-E), which was prevented by a PERK inhibitor; however, the level of ATF4 mRNA in the presence of PERK inhibitor alone was elevated compared to the control. Immunoblotting for PERK pathway components indicated elevated PERK phosphorylation and CHOP expression in response to tunicamycin treatment (Figure 4.3-F). PERK phosphorylation inhibitor GSK2606414 inhibited the increase in PERK phosphorylation in response to tunicamycin treatment at 1 μM or 5 μM concentration. 5 μM GSK2606414 resulted in a modest increase in CHOP expression when the cells did not experience ER stress.




## Figure 4.3 Confirming inhibitor activity in ARCaPM cells at 4 h

ARCaPM cells seeded at 200,000 cell/ml in well plates were grown to 80% confluency in MCaP medium. The cells were treated with 5 µM of the inhibitors for ATF6, IRE1 and PERK pathway; tunicamycin (3 µg/ml) was used to induce ER stress and DMSO was used as vehicle control to tunicamycin treatment for 4 h.

(A) SEL1L, (B) HERP1, (C) sXBP1, and (E) ATF4 gene expression were measured by SYBR Green real-time PCR. *GAPDH* was used as internal control and gene expression in all the treatments was normalised to the transcript level of ARCaPM in MCaP medium Data shows the mean ±S. D.

(D) *XBP1* splicing in ARCaPM in response to the UPR inhibitors and tunicamycin. Unspliced and spliced *XBP1* RNA levels were measured by PCR of the cDNA synthesised from the reverse transcription of the RNA isolated from each treatment after 4 h. M indicate cells in MCaP medium and used as control.

(F) Immunoblot for ER stress markers PERK and CHOP for GSK2606414 treatment. D: DMSO T: Tunicamycin (3 µg/ml). Concentration of inhibitor is indicated above the lanes as 1 µM or 5 µM.

*Two-way ANOVA with Šidák's multiple comparisons test, Alpha 0.05; ns $P > 0.05$, * $P \leq 0.05$, ** $P \leq 0.01$, *** $P \leq 0.001$, **** $P \leq 0.0001$*

My previous results have shown increased ALP levels after the inhibition of the PERK or IRE1 arms of the UPR in ARCaPM cells (Figure 3.17). In contrast, limited exposure to the ER stress inducer tunicamycin resulted in a modest decrease in ALP activity levels (Figure 4.4).

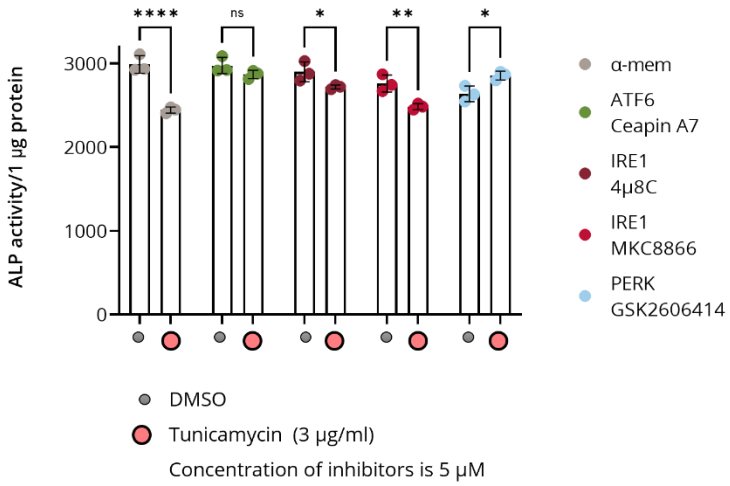


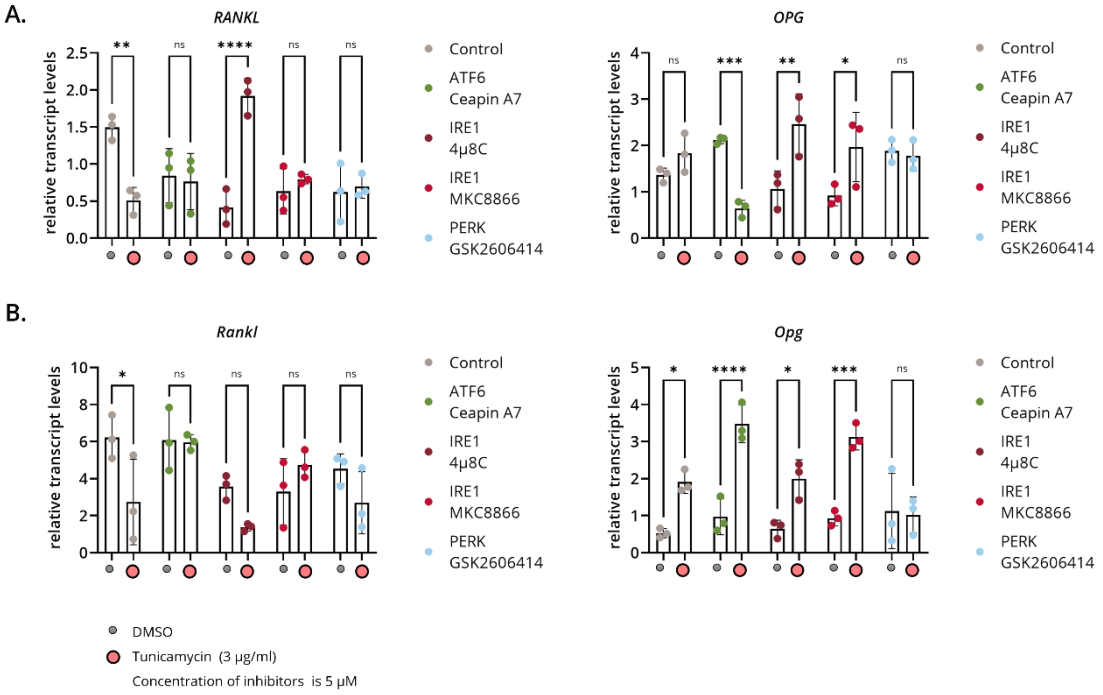

Figure 4.4 ALP activity in ARCaPM cells in response to 5 µM UPR inhibitors

ALP activity in 1 µg protein of ARCaPM cells under different conditions for 24 h. Each compound was added to control medium at 5 µM final concentration. Error bars show standard deviation for 3 measurements.

*Two-way ANOVA with Šidák's multiple comparisons test, Alpha 0.05; ns P > 0.05, * P ≤ 0.05, ** P ≤ 0.01, *** P ≤ 0.001, **** P ≤ 0.0001*

Previous work indicated that increased UPR by tunicamycin increased RANKL expression in primary osteoblastic cells [448]. However, the impact of elevated UPR on RANKL expression has not been studied on cancer cells that have osteogenic potential *in vitro*. Next, I investigated the effect of tunicamycin treatment on RANKL expression in prostate cancer cells and found that in human prostate cancer cell line ARCaPM, tunicamycin decreased RANKL, which is blocked by PERK and ATF6 (Figure 4.5-A).

A similar response was observed in mouse prostate cancer cell line DVL3-SCM: in response to tunicamycin treatment *Rankl* mRNA levels decreased, and *Opg* levels increased, with both ER stress-induced changes blocked by PERK inhibition (Figure 4.5-B).




## Figure 4.5 Effect of the UPR on RANKL and OPG expression in ARCaPM and DVL3-SCM cells

ARCaPM or DVL3-SCM cells seeded at 200,000 cell/ml in well plates were grown to 80% confluency in MCaP medium or Keratinocyte-SFM. ARCaPM cells were treated in α-mem medium and DVL3-SCM cells were treated in their own medium with 5 μM of the inhibitors for ATF6, IRE1 and PERK pathway; tunicamycin (3 μg/ml) was used to induce ER stress response and DMSO was used as vehicle control to tunicamycin treatment for 4 h.

(A) *RANKL* and *OPG* mRNA expression in ARCaPM cells and (B) *Rankl* and *Opg* mRNA expression in DVL3-SCM cells measured by SYBR Green real-time PCR. *GAPDH* was used as internal control. Gene expression in ARCaPM treatments was normalised to the transcript level of ARCaPM in MCaP medium. Gene expression in DVL3-SCM treatments was normalised to the transcript level of the cells in Keratinocyte-SFM medium, without compounds. Data shows the mean ± S. D.

*Two-way ANOVA with Šidák's multiple comparisons test, Alpha 0.05; ns $P > 0.05$, * $P \leq 0.05$, ** $P \leq 0.01$, *** $P \leq 0.001$, **** $P \leq 0.0001$.*

Tunicamycin induced ER stress did not induce *PTHRP* expression in ARCaPM cells except for when IRE1 pathway was inhibited with MKC8866; however, tunicamycin suppressed *Pthrp* levels in DVL3-SCM cells, and PERK inhibition blocked this effect (Figure 4.6).

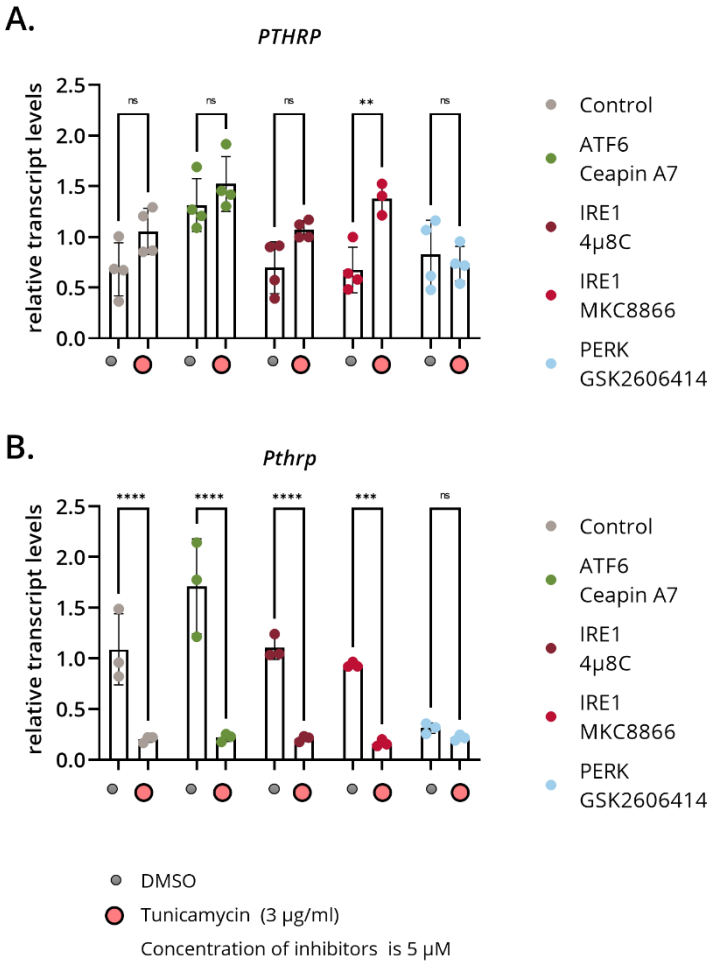



Figure 4.6 Effect of the UPR on PTHRP expression in ARCaPM & DVL3-SCM

(A) *PTHRP* mRNA expression in ARCaPM cells and (B) *Pthrp* mRNA expression in DVL3-SCM cells measured by SYBR Green real-time PCR. *GAPDH* was used as internal control. Gene expression in ARCaPM treatments was normalised to the transcript level of ARCaPM in MCaP medium. Gene expression in DVL3-SCM treatments was normalised to the transcript level of the cells in Keratinocyte-SFM medium, without compounds. Data shows the mean ±S. D.
*Two-way ANOVA with Šidák's multiple comparisons test, Alpha 0.05; ns P > 0.05, * P ≤ 0.05, ** P ≤ 0.01, *** P ≤ 0.001, **** P ≤ 0.0001*

Inhibition of the other arms of the UPR also have an effect on tunicamycin response; however, since the response to PERK inhibition in both human and mouse prostate cancer cells was most consistent, I focused on PERK regulation.

#### 4.3.2.1. Effect of tunicamycin & inhibitors on Wnt signalling pathway

While in the metastasis of most cancer types including breast cancer, bone metastases are more osteolytic, in prostate cancer bone metastases there is also an osteoblastic component. Osteoblast activation and maturation in prostate cancer is stimulated by the Wnt pathway. The inhibitor of Wnt signalling, dickkopf-1 (DKK1) is an important regulator that is suggested to play a role in both osteoblastic and osteolytic metastases by controlling the switch between osteolytic and osteoblastic activity. DKK1 can promote osteolysis, particularly during the early stages of cancer development, and the expression of DKK1 has been shown to decline in advanced bone metastases. DKK1 has been proposed as one of the switches that transitions PCa bone metastasis activity from osteolytic to osteoblastic. Thus, I investigated the effect of the UPR on DKK1 and assessed whether the effect on RANKL/OPG signalling is regulated by DKK1 in prostate cancer cells.

*DKK1* was increased in response to tunicamycin induced ER stress compared to DMSO control (Figure 4.7-A). Inhibition of ATF6 pathway by Ceapin-A7 or inhibition of IRE1 pathway by either 4μ8C or MKC8866 did not affect the tunicamycin induced increase in DKK1 mRNA. The increase in *DKK1* was inhibited when PERK pathway was blocked. This trend was similar to the levels of *OPG* (blastic component) in response to tunicamycin treatment and PERK inhibition, suggesting that the UPR could modulate prostate cancer bone disease, with ER stress reducing osteolysis, mediated by PERK pathway.

Baseline expression of *DKK1* was lower in human metastatic prostate cancer ARCaPM cells compared to epithelial ARCaPE cells (Figure 4.7-B). Mouse prostate cancer cells DVL3 and DVL3-SCM cells did not express *Dkk1* (Supplementary Figure 8.1).

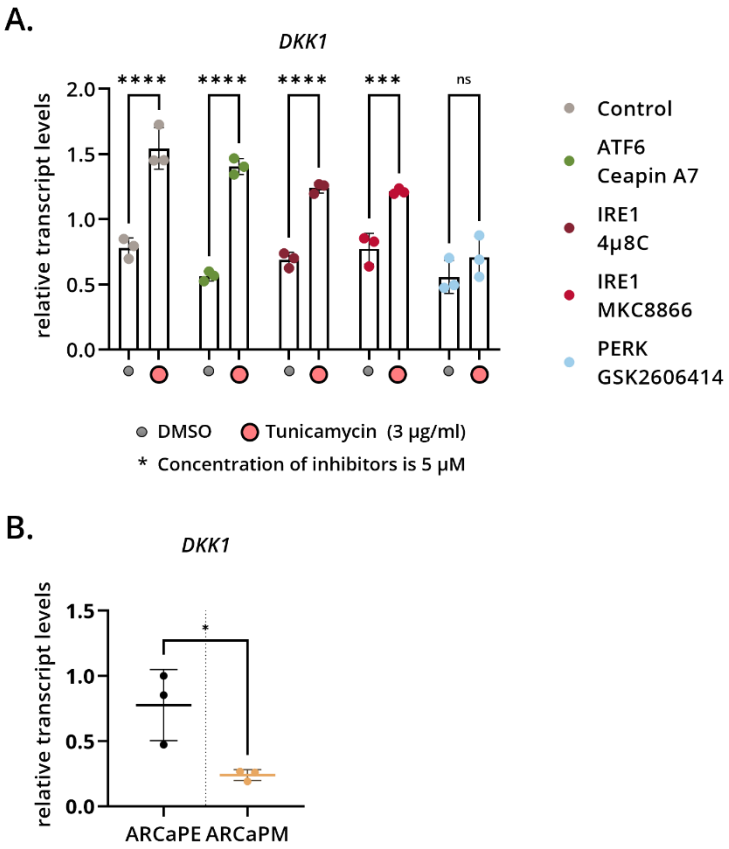



Figure 4.7 Effect of the UPR on DKK1 in ARCaPM

(A) ARCaPM cells were treated with 5 μM of the inhibitors for ATF6, IRE1 and PERK pathway (final concentration of each compound was 5 μM). Tunicamycin (3 μg/ml) was used to induce ER stress and DMSO was used as vehicle control to tunicamycin treatment for 4 h. Control indicate ARCaPM cells in α-mem medium. (B) Baseline expression of *DKK1* in ARCaPE and ARCaPM cells. *DKK1* gene expression was measured by SYBR Green real-time PCR. *GAPDH* was used as internal control and gene expression in all the treatments was normalised to the transcript level of ARCaPM in MCaP medium Data shows the mean ±S. D.

*(A) Two-way ANOVA with Šidák's multiple comparisons test, (B) Unpaired t-test, Alpha 0.05; ns P > 0.05, * P ≤ 0.05, ** P ≤ 0.01, *** P ≤ 0.001, **** P ≤ 0.0001.*

DKK1 acts as inhibitor of β-Catenin-dependent Wnt signalling. If the Wnt pathway is active, β-Catenin would be stabilised as a result of Wnt ligand binding to the receptor and consequently due to the disruption of destruction complex (AXIN, GSK3β, CK1, APC). In order to check whether the changes in *DKK1* level affect Wnt pathway, I tried to investigate Wnt pathway by different approaches. First, I looked at β-Catenin abundance at protein levels, but I did not detect any bands in western blots. I also tried investigating the involvement of Wnt signalling using Wnt reporter TOP-dGFP (Addgene plasmid #14715); however, treatment with Wnt ligand Wnt3A or LiCl did not activate the Wnt reporter in ARCaPM cells [451].

β-Catenin is a protein that is phosphorylated, ubiquitinylated and degraded. Hence, the mRNA level of such a protein that is known to be regulated at protein level, is not important in understanding the effect of DKK1 on it. mRNA levels of *CTNNB1* following ER stress (with tunicamycin or thapsigargin) did not change in the presence or absence of PERK inhibitor in ARCaPM cells (Figure 4.8).

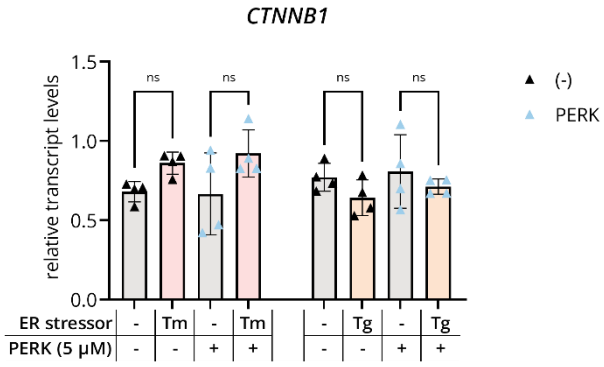



Figure 4.8 Effect of the UPR on *CTNNB1* in ARCaPM

ARCaPM cells were treated with 5 µM of the inhibitors for ATF6, IRE1 and PERK pathway (final concentration of each compound was 5 µM). Tunicamycin (3 µg/ml) or thapsigargin (1 µg/ml) was used to induce ER stress and DMSO was used as vehicle control for 4 h.

*CTNNB1* gene expression was measured by SYBR Green real-time PCR. GAPDH was used as internal control and gene expression in all the treatments was normalised to the transcript level of ARCaPM in MCaP medium Data shows the mean ± S. D.

*One-way ANOVA, with Tukey's multiple comparisons test. Alpha 0.05; ns P > 0.05, * P ≤ 0.05, ** P ≤ 0.01, *** P ≤ 0.001, **** P ≤ 0.0001.*

## 4.4 Discussion

The work of this chapter has shown that the bone-disease related factor expression was different between metastatic and non-metastatic prostate cancer cells; elevated UPR decreased RANKL and DKK1 expression and increased OPG expression in ARCaPM cells, and the response to the UPR was blocked PERK inhibition.

A complex network of signalling pathways, including RANKL/OPG, contributes to the bone disease associated with prostate cancer bone metastases. Previous studies have demonstrated a correlation between RANKL expression and the epithelial to mesenchymal transition in human prostate cancer cells. The induction of EMT in ARCaP cells resulted in increased expression of functional RANKL [242]. The UPR has been shown to regulate RANKL expression in osteoblasts in previous work, however, the interplay between RANKL and the UPR has not been studied in prostate cancer skeletal metastasis.

The baseline comparison of bone-related factors in ARCaPM and ARCaPE cells revealed elevated levels of RANKL and *RANKL*/*OPG* ratio in ARCaPM cells (Figure 4.1), indicating an osteolytic phenotype in mesenchymal cells. However, mouse mesenchymal prostate cancer cell line DVL3-SCM cells had a lower *Rankl*/*Opg* ratio compared to parental epithelial DVL3 cells (Figure 4.2), indicating a more osteoblastic phenotype in the epithelial parental cells. ARCaPM cells have a mixed osteolytic/osteoblastic phenotype *in vivo* whereas bone metastatic potential of the DVL3 and DVL3 SCM cells has not been studied *in vivo* [279].

The baseline RANKL/OPG ratio differed between human and mouse PCa cells (Figure 4.1 and Figure 4.2). Human PCa showed more osteolytic expression

pattern in mesenchymal cells whereas the trend was the opposite in mouse PCa cells. This could represent the role of AR regulated transcription in PCa: a more osteolytic phenotype in advanced PCa versus a more osteoblastic phenotype in high risk, localised PCa.

One observation regarding the concentration of PERK inhibitor was that 5 µM GSK2606414 induced a slight increase in CHOP expression when the cells did not experience ER stress (Figure 4.3-F). When high dosages of the inhibitor are used to suppress PERK phosphorylation, eIF2$\alpha$ phosphorylation is constrained, leading to decreased cellular protection and increased cellular stress, which results in increased CHOP levels [449]. As a result, the integrated stress response (ISR), which is an innate protective pathway is weakened. The other eIF2$\alpha$ kinases then in return compensate the reduced eIF2$\alpha$ phosphorylation, which lead to activation of pathways that are activated under different types of stimuli, including viral infection. This emphasises the need of dosage adjustment in achieving the ideal conditions to represent the elevated UPR in cancer, for studying PERK pathway response.

Tunicamycin is widely used in studies related to ER as it causes accumulation of unfolded or misfolded proteins and can induce UPR in a short time. However, there are limiting effects of using it in the studies investigating the UPR. First, the effect of these compounds is not solely on ER stress. Second, both tunicamycin and thapsigargin activate all three arms of the UPR. Third, due to its toxicity, tunicamycin does not allow studying prolonged ER stress. Some studies have used low concentrations of tunicamycin (50 ng/ml) to overcome this limitation; still, the stress caused by tunicamycin is not the ideal representation of physiological stress, moreover, triggering stress in the cells that proliferate under normal growth conditions create an acute stress, even the levels are low [450]. This can be limiting

for studies that involve longer culturing under certain conditions (as in the case of differentiation experiments) or prolonged treatment. For example, chondrogenic differentiation of human mesenchymal stem cells might take 2-3 weeks [451]. In this case, investigation of the influence of ER stress on this process by using tunicamycin as ER stress inducer would be limiting due to toxicity. Thus, different approaches are needed for mimicking ER stress in *in vitro* studies.

A study investigating the influence of IRE1 on PTHrP signalling in chondrocyte differentiation has shown that PTHrP level was elevated following IRE1 overexpression, however, this effect was significant only after 3 days [452]. IRE1 knockdown reduced the PTHrP mRNA expression, but the effect was significant on day 5. As in this study, overexpression, or knockdown of the components of the different arms of the UPR can provide a less toxic approach for the studies that require elevated ER stress and can allow investigation of each arm separately. Yet, using tunicamycin at high enough concentrations that will induce the changes in the components of the UPR in a short time might only allow investigation of the immediate effect of ER stress induction.

Treatment with tunicamycin resulted in decreased alkaline phosphatase activity levels after 4 h (Figure 4.4). Human TNAPs have been shown to be N-glycosylated [453]. Inhibiting N-glycosylation by tunicamycin can account for decreased ALP activity levels.

My investigation of the effect of tunicamycin treatment on *RANKL* expression in prostate cancer cells revealed that in the human prostate cancer cell line ARCaPM, tunicamycin decreases *RANKL* and increases *OPG*, which is blocked by PERK and ATF6 (Figure 4.5-A); and a similar response was seen in the mouse prostate cancer cell line DVL3-SCM: in response to tunicamycin treatment, *Pthrp*

and *Rankl* mRNA levels decrease, and *Opg* levels increase, and this effect is blocked by PERK inhibition (Figure 4.5-B and Figure 4.6-B). Even when ER stress responses varied, blockade of the response to tunicamycin by PERK was consistent throughout experiments.

It has been previously shown that IRE1-XBP1 branch promote PTHrP signalling and promote osteoclastogenesis [427]. Hence, IRE1 activation in elevated ER stress might account for regulation of osteoblastic and osteolytic components in bone disease. The effect of PERK inhibition might be due to compensation by IRE1 pathway activation.

Activation of each arm of the UPR, or overexpression of components of IRE1 or XBP1s could provide an alternative approach over the use of tunicamycin for the investigation of influence of ER stress in regulating the osteoclast/osteoblast activating factors.

Dickkopf-1 (DKK1), a Wnt signalling inhibitor, is a key regulator in both osteoblastic and osteolytic metastasis, regulating the transition between osteolytic and osteoblastic activity. Similar to OPG, the Wnt signalling inhibitor *DKK1* was increased in response to tunicamycin treatment and the increase in *DKK1* was inhibited when PERK pathway was inhibited (Figure 4.7-A). In addition, basal level expression of *DKK1* was lower in human metastatic prostate cancer ARCaPM cells compared to epithelial ARCaPE cells (Figure 4.7-B). This might indicate that inducing ER stress potentially decreases osteolysis, in a PERK pathway dependent manner. This study proposes an important role for the UPR in regulation of prostate cancer bone disease, possibly acting as a switch that changes PCa osteolytic to osteoblastic bone metastatic activity.

*Dkk1* expression was not detected in mouse prostate cancer cells DVL3 and DVL3-SCM (Supplementary Figure 8.1), suggesting another mechanism that control the switch from osteoblastic and osteolytic activity. Unpublished data from Mills group showed that *Ror2*, which is inhibited by *Dkk1*, was highly expressed in DVL3-SCM cells; consistent with decreased expression of *Dkk1* in these cells.

DKK1 expression in human umbilical vein endothelial cells (HUVECs) activated eIF2$\alpha$ and induced apoptosis, however, the effect of elevated ER stress on DKK1 levels has not been studied, and this needs further investigation [454].

mRNA level of *CTNNB1* gene (that encodes $\beta$-Catenin) was not affected by neither of the ER stress inducer (Figure 4.8). As the mRNA level of $\beta$-Catenin is hardly contributing to the activity of the $\beta$-Catenin which is tightly regulated at protein level. The experiments related to $\beta$-Catenin-dependent Wnt pathway failed to clarify the involvement of UPR in regulating RANKL and OPG levels. While this may reflect a need to optimise experimental conditions, it may also suggest a role for non-canonical Wnt signalling pathways. Further investigation of $\beta$-Catenin-dependent Wnt signalling is needed to understand if the RANKL and OPG levels are regulated by this pathway and also investigate whether the changes in the DKK1 level contribute to this pathway. Optimization of blotting conditions for $\beta$-Catenin stabilization and reporter assays for the transcriptional activity of $\beta$-Catenin is essential.

Further studies are required to investigate the outcome of elevated UPR in prostate cancer cell models as well as the involvement of PERK pathway in PCa driven osteolysis. The potential of PCa cells to regulate osteolysis depend on the secreted RANKL levels, while my study focused on the transcription level of RANKL and other bone related factors. Further investigation involves *in vitro*

experiments that includes the collection of conditioned media from ARCaPM cells treated with ER inducers and PERK inhibitor GSK2606414 or other inhibitors targeting PERK pathway and monitoring the levels of RANKL secretion. Conditioned media of ARCaPM and DVL3-SCM cells after 4 h of treatment were tested for the secreted RANKL levels, but no RANKL secretion was detected in neither of the cell type. The protein levels of RANKL, OPG, DKK1 and PTHrP need to be investigated in cell lysates and conditioned media after prolonged ER stress induction to allow the secretion of the proteins. Depending on the secreted protein, conditioned media can be used to test whether osteoblast or osteoclast precursors can differentiate to the mature osteoblast or osteoclasts. Then, this can represent the vicious cycle of bone metastasis *in vitro*.

One important limitation of my studies is that all of the treatments were done in tissue culture plates, when ARCaPM cells were cultured in isolation, whereas PCa bone metastases involve interaction between bone and PCa cells. Co-culturing PCa and bone cells will help to better understand if PERK pathway (or the other arms of the UPR) affects the interaction between these cells. Three-dimensional co-culture models can even allow investigation of these interactions in bone-like microenvironments. Later, if the hypotheses are further validated *in vitro*, *in vivo* models can be used. GSK2606414 is already shown to inhibit PERK phosphorylation *in vivo* [455], and can be used in *in vivo* metastasis models. These experiments will allow inhibition of PERK pathway in physiological ER stress and help to understand whether PERK inhibition can control the switch between osteoblastic and osteolytic metastases. In addition to this, compounds that are known to induce PERK activity (CCT020312, or MK-28) can be used to check the reversing effect of PERK activation [456, 457].

In conclusion, activation of the UPR decreases *RANKL*, *RANKL*: *OPG*, and increases *DKK1*, and the changes are blocked by the UPR inhibitors, especially PERK inhibitor. While further studies are required to identify how the UPR regulates expression of these factors, my studies suggest a previously unrecognised role for the UPR in the bone disease associated with prostate cancer bone metastases.

# 5

# The effect of the UPR on EMT and migration in bone metastatic PCa

## 5.1 Introduction

Bone alkaline phosphatase (ALP) has been proposed for use with PSA as a marker for bone metastatic disease progression [458]. As tumour derived ALPL, a key component of prostate cancer bone metastasis, regulates EMT and migration in ARCaP cells, this chapter investigates the effect of the UPR on EMT and migration in bone metastatic prostate cancer cells.

The metastatic capacity of cancer cells is often linked to epithelial to mesenchymal transition (EMT) [459]. The mechanisms regulating EMT in prostate cancer cells are complex and involve various pathways. Several studies investigated the involvement of different pathways in EMT regulation in ARCaP

cell lines. Extracellular Hsp90 (eHsp90) promotes cell motility and invasion in cancer cells and metastasis by activating EMT. Metastatic ARCaPM cells have an elevated eHsp90 mRNA level compared to epithelial ARCaPE cells [460]. MDA-9/Syntenin increases the levels of invasion-associated proteins via transcriptional regulation of STAT3 activation following to direct interacted with IGF-1R, resulting in invasion in prostate cancer. Prostate cancer had elevated *MDA-9/Syntenin* mRNA compared to the normal prostate [461]. Similarly, higher expression of MDA-9/Syntenin protein expression is elevated in mesenchymal ARCaPM cells compared to the epithelial ARCaPE cells[462]. MDA-9/Syntenin contains two PDZ (named after 3 proteins postsynaptic density-95 (PSD-95), discs-large, zona occludens 1 (ZO-1) in which the domain was initially observed) domains. PDZ interactions was shown to destabilise tight junctions and increase invasion of PC cells. SPARCL1 expression is lower in ARCaPM compared to ARCaPE, overexpression of it decreases metastatic potential *in vitro* and *in vivo* [446]. RANKL is elevated in advanced prostate cancer and metastatic prostate cancer cell models. Silencing RANKL by shRNA results in decreased metastatic potential and induces E-Cadherin expression, decreases mesenchymal marker expression in ARCaPM cells [242]. Monoamine oxidase A (MAOA) is a mitochondria-bound enzyme that has been shown to be elevated in poorly differentiated human prostate cancer. MAOA induces invasion of metastasis by inducing EMT and enhancing hypoxia mediator HIF1$\alpha$, contributing to aggressive PCa progression [463].

## 5.2 Hypothesis and Objectives

As the baseline expression levels of UPR components differ between ARCaPM and ARCaPE cells, I hypothesised that inducing ER stress impacts the epithelial and mesenchymal marker protein expression and migratory capacity of prostate cancer cells. To investigate these hypotheses and understand the contribution of the UPR to molecular mechanisms of EMT in prostate cancer, I investigated migration in ARCaP cells using transwell and wound healing assays in the presence of inhibitors of the UPR and induction of ER stress. The chapter specific aim of this section is to investigate the impact of the UPR inhibitors on EMT in ARCaPM and ARCaPE cell lines.

# 5.3 Results

## 5.3.1 Differences in basal EMT markers in ARCaPE vs ARCaPM and DVL3 vs DVL3-SCM

ARCaPM cells have an elongated spindle-shape, showing mesenchymal morphology, whereas ARCaPE cells grow in cobblestone like clusters, showing their epithelial phenotype. In *Section 3.3.3*, I have confirmed the previously reported differences between ARCaPM and ARCaPE at protein and RNA levels (Figure 3.8). The epithelial marker *CDH1* was higher in epithelial ARCaPE cells at protein and RNA levels at the basal levels compared to ARCaPM cells, and the protein level of mesenchymal marker *CDH2* (N-Cadherin) was lower in ARCaPE cells although the mRNA transcript level was higher. The protein levels of tight junction protein ZO-1 and Claudin levels were lower in ARCaPM cells; and the master transcription factors *SNAI1* (Snail) and *SNAI2* (Slug) were elevated in transcription level in ARCaPE cells.

Then I quantified EMT-related gene expression in mouse prostate cell lines to validate the reported profile. Comparing the expression level of EMT markers showed that epithelial marker E-Cadherin (*Cdh1*) was elevated in epithelial DVL3 cells and the mesenchymal markers *Twist, Snail, Slug* and *Zeb1* were elevated in SCM cells which are a mesenchymal derivative of DVL3 cells (Figure 5.1). The mRNA expression signature of EMT markers in epithelial (ARCaPE for human, DVL3 for mouse) and mesenchymal (ARCaPM for human, and DVL3-SCM for mouse) cells were consistent with their phenotypes.

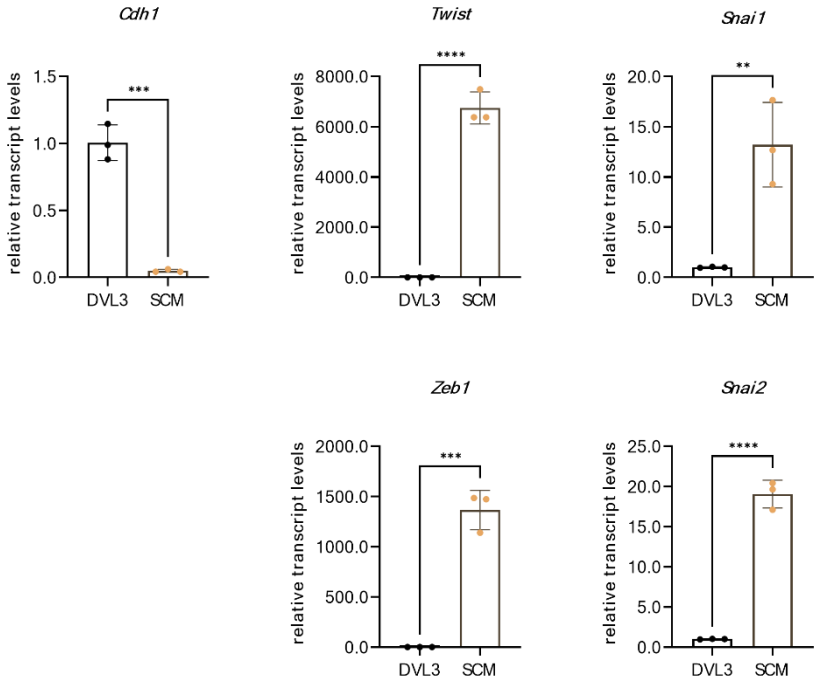



Figure 5.1 EMT marker gene expression differs between DVL3 and DVL3-SCM cells

DVL3 and DVL3-SCM cells were grown to confluency in RPMI or Keratinocyte SFM growth medium, respectively. *Cdh1*, *Twist*, *Zeb1*, *Snai1*, and *Snai2* gene expression in DVL3 and DVL3-SCM cells were measured by SYBR Green real-time PCR and normalised with GAPDH expression. (Data summarises 3 independent experiments and shows the mean ± S. D.
*Unpaired t-test, Alpha 0.05; ns P > 0.05, * P ≤ 0.05, ** P ≤ 0.01, *** P ≤ 0.001, **** P ≤ 0.0001)*

Migration is an important factor contributing to prostate cancer metastasis. The role of the UPR in migration and bone metastasis has not been well-studied. To investigate the role of the UPR in the process of prostate cancer migration, I used two distinct *in vitro* approaches. First, I investigated the migration capacity of ARCaP cells using a transwell migration assay. This assay requires the cells to actively pass through an 8 µm porous membrane towards a chemoattractant. ARCaPE and ARCaPM cells were serum-deprived in the upper compartment of Boyden chamber, normal growth medium was added to the lower compartment as attractant. ARCaPM cells had a greater capability for migration compared to ARCaPE cells (Figure 5.2). This supports previous reports of the metastatic ability of ARCaPM cells [279].

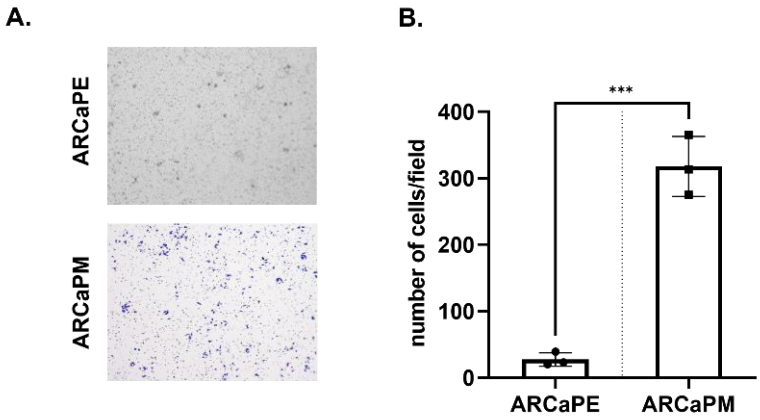



Figure 5.2 Transwell migration of ARCaPM cells is enhanced compared to ARCaPE cells

Cells previously cultured in MCaP medium to confluency were seeded in the migration insert in 0.5% FBS containing α-mem medium and let to migrate towards 5% FBS containing α-mem medium. After 48 hours, cells that migrated through the 8 µm porous membrane were fixed, stained, and counted from five fields using a light microscope. Representative images cells are shown on the left side (A). Data summarises 3 independent experiments and shows the mean ± S. D (B).

*Unpaired t-test, Alpha 0.05; ns P > 0.05, * P ≤ 0.05, ** P ≤ 0.01, *** P ≤ 0.001, **** P ≤ 0.0001)*

### 5.3.2 Impact of the UPR on EMT & migration

Next, I used this assay to investigate the role of elevated ER stress by different stressors on the migration capacity of ARCaPM cells.

To investigate prostate cancer cell migration in response to elevated ER stress by tunicamycin, I treated ARCaPM cells with a low dose of tunicamycin so that the cytotoxic effect of tunicamycin I previously observed would not impact any effect on migration. Tunicamycin significantly impaired cell migration in ARCaPM cells after 24 h (Figure 5.3).

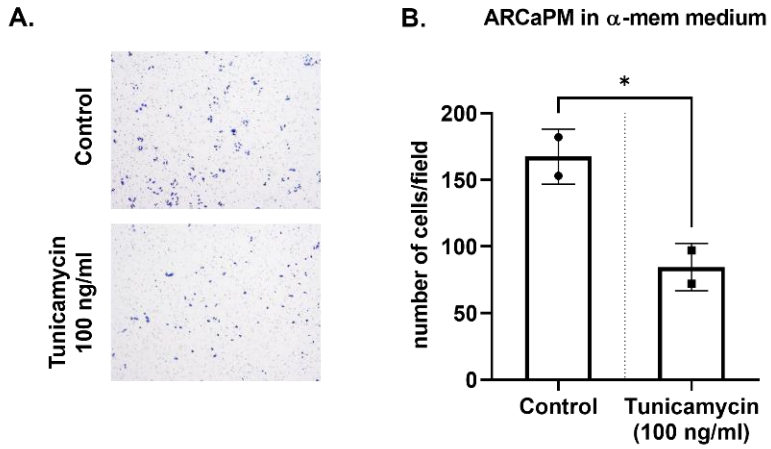



Figure 5.3 Effect of tunicamycin as stress inducer on the migration of the human prostate cell ARCaPM

ARCaPM cells previously cultured MCaP medium to confluency and seeded in in the migration insert in 0.5% FBS containing α-mem medium (with or without 100 ng/ml tunicamycin). After 48 hours, cells that migrated through the 8 µm porous membrane were fixed, stained, and counted from five fields using a light microscope. Representative images of untreated and tunicamycin-treated cells are shown on the left side (A). Data summarises 2 independent experiments and shows the mean ± S. D (B).

*Unpaired t-test, Alpha 0.05; ns P > 0.05, * P ≤ 0.05, ** P ≤ 0.01, *** P ≤ 0.001, **** P ≤ 0.0001)*

Next, I investigated whether inhibition of different arms of the UPR would restore the impaired cell migration in ARCaPM cells. First, I investigated the impact of using inhibitors for three transducers of the UPR (ATF6, IRE1, and PERK) when the cells were not stressed by tunicamycin. Tunicamycin stress decreased migration of ARCaPM cells after 48 h; however, inhibiting the arms of the UPR did not change the migration capacity of the cells when the cells were not stressed (Figure 5.4). The inhibitors of the UPR did not affect the viability of the cells; however, 100 ng/ml tunicamycin decreased the viability after 48 hours, raising the possibility that a loss of viability may contribute to the reduction in migration.

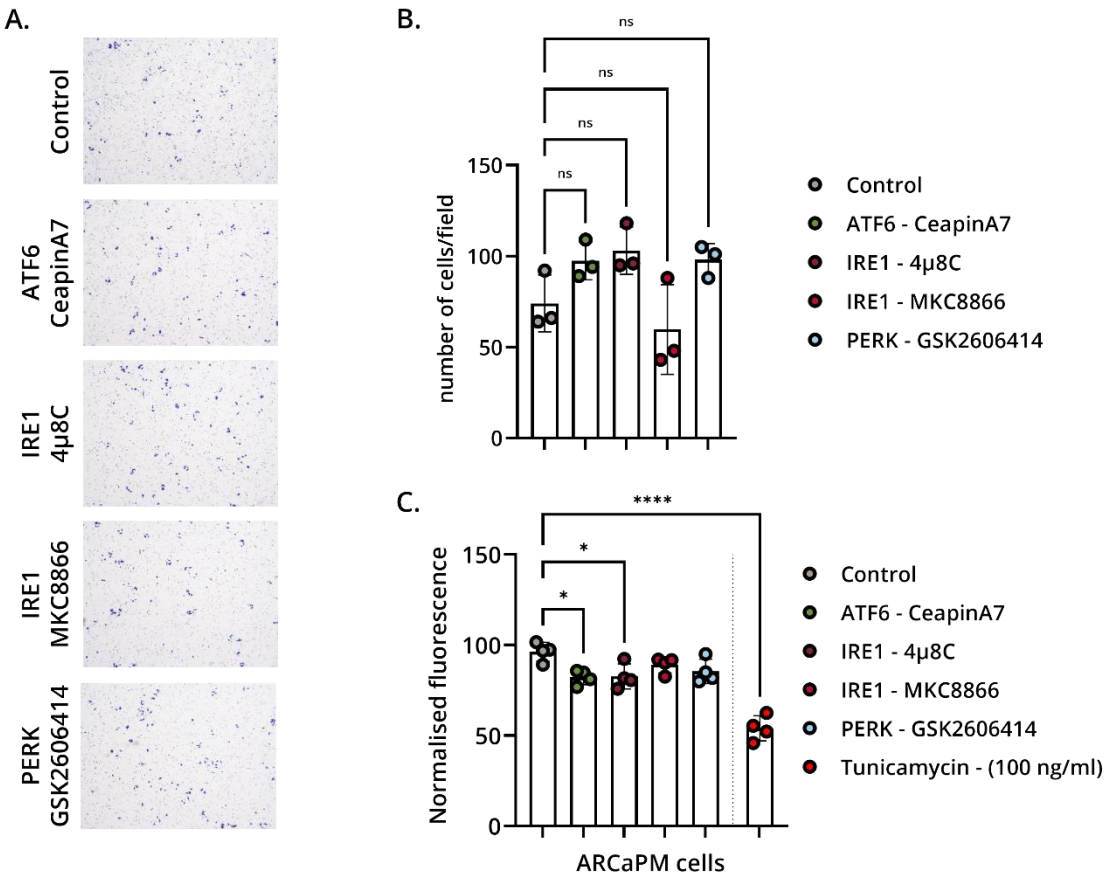



Figure 5.4 Effect of the UPR inhibitors on ARCaPM migration

ARCaPM cells were seeded in the migration insert in 0.5% FBS containing α-mem medium. The cells were treated with inhibitors of the UPR at 1 μM concentration or with tunicamycin at 100 ng/ml. After 48 hours, cells were fixed, stained and inside of the insert was wiped to clear the cells that did not migrated through the 8 μm porous membrane. The migrated cells were counted from five fields of three replicates using a light microscope at 4X objectives. Number of migrated cells (B), Alamar Blue staining for cell viability of ARCaPM cells treated with same concentrations of the compounds and duration in a 96-well plate (C). Data summarises 3 independent experiments and shows the mean ± S. D.

*One way ANOVA with Dunnett's multiple comparison, Alpha 0.05; ns P > 0.05, * P ≤ 0.05, ** P ≤ 0.01, *** P ≤ 0.001, **** P ≤ 0.0001)*

Next, I investigated if inhibition of different arms of the UPR would attenuate the effect of tunicamycin on ARCaPM migration. ARCaPM cells pre-treated with different inhibitors for 12 h, were exposed to tunicamycin for a further 24 h. Tunicamycin significantly reduced the number of viable cells in the transwells (Figure 5.5-A). The number of migrated cells in tunicamycin treated condition was significantly lower compared to non-treated cells after normalisation to cell viability (Figure 5.5-B and C). Pre-treatment with the UPR inhibitors did not rescue the decrease in cell migration in response to tunicamycin.

I also used another approach to measure cell proliferation and cell death. I assessed the effect of tunicamycin and thapsigargin in the presence of the UPR inhibitors on the viability of ARCaPM cells using Alamar Blue viability assay, which measures cell metabolism and measured cell death using SYTOX green. Inhibiting different arms of the UPR did not influence cell viability or the number of dead cells when the cells were not stressed (Figure 5.6). Inducing ER stress by either tunicamycin or thapsigargin increased cell death in ARCaPM cells after 72 h. Inhibiting the PERK arm in the presence of tunicamycin or thapsigargin further decreased viability and increased cell death.

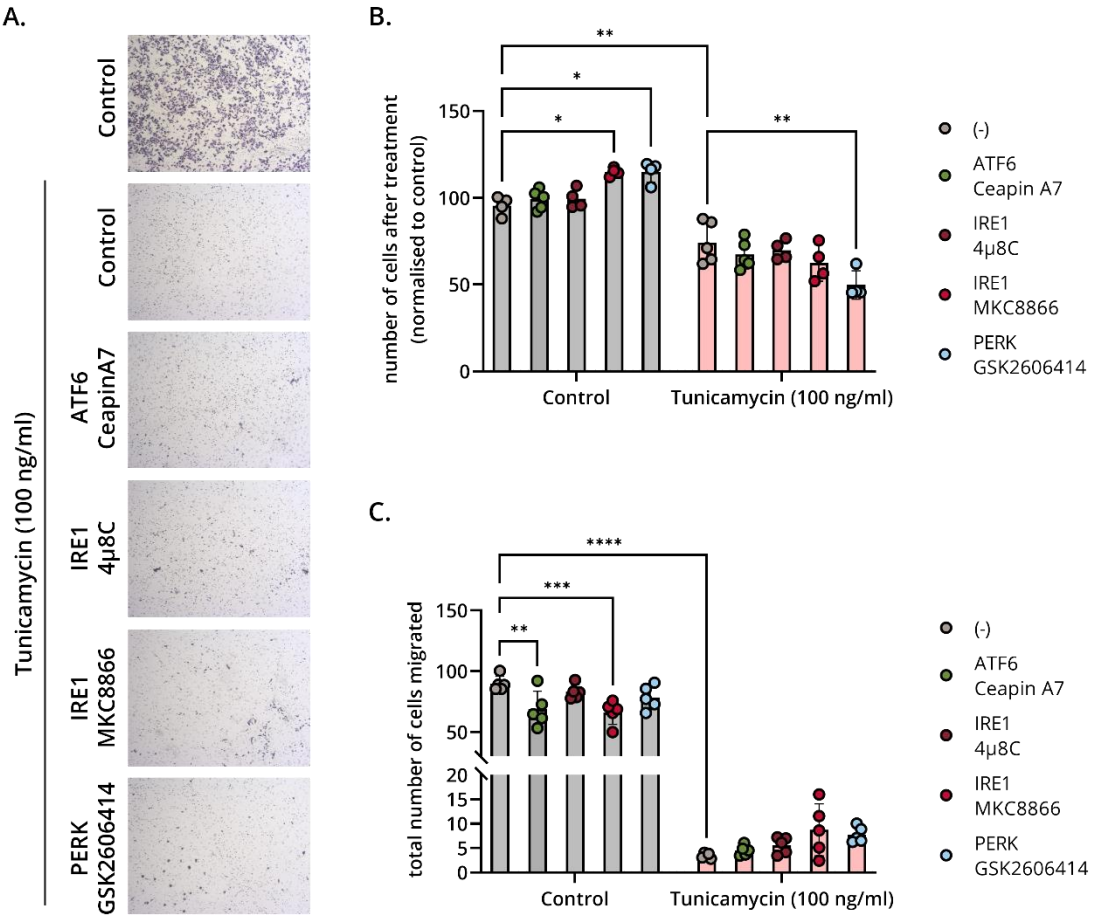



Figure 5.5 Effect of tunicamycin and the UPR inhibitors on ARCaPM migration

ARCaPM cells were seeded in the migration insert in 0.5% FBS containing α-mem medium. The cells were treated with inhibitors of the UPR at 1 μM concentration or with tunicamycin at 100 ng/ml. After 48 hours, cells were fixed, stained and inside of the insert was wiped to clear the cells that did not migrated through the 8 μm porous membrane. Number of cells after Toluidine blue staining normalised to control (B), number of migrated cells normalised to cell number after treatment (C). Data shows the mean ± S. D.

*One way ANOVA with Dunnett's multiple comparisons test, Alpha 0.05; ns P > 0.05, * P ≤ 0.05, ** P ≤ 0.01, *** P ≤ 0.001, **** P ≤ 0.0001)*

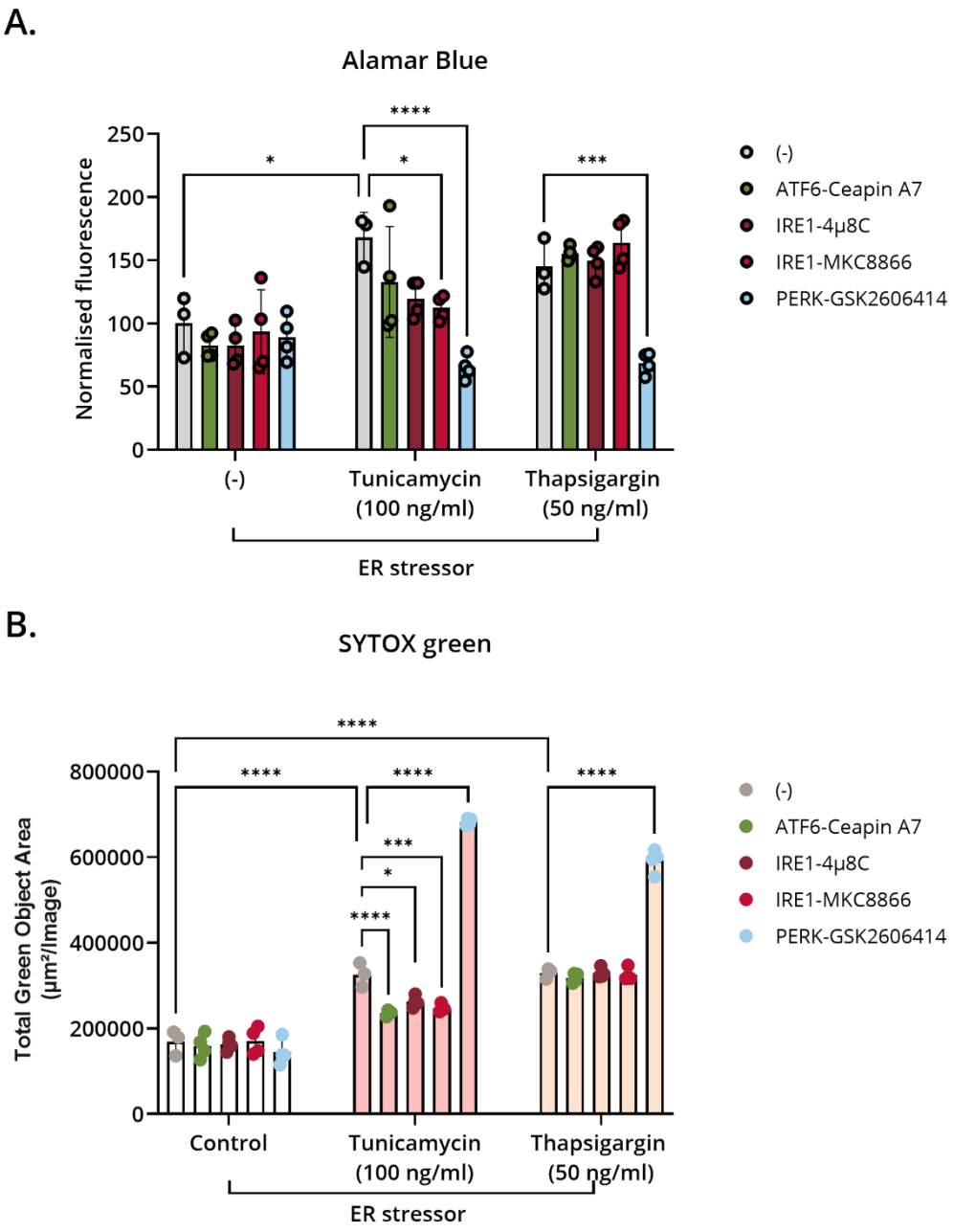



Figure 5.6 Effect of tunicamycin/thapsigargin ± UPR inhibitors on cell viability

ARCaPM cells seeded in 96-well plates were treated with inhibitors of the UPR only (1 μM concentration) or with tunicamycin (100 ng/ml) or thapsigargin (100 ng/ml). (A) Alamar Blue staining for cell viability based on metabolic activity normalised to non-treated ARCaPM after subtraction of background fluorescence. (B) Quantitative analysis toxicity measured by SYTOX green. Data shows the mean ± S. D.

*Two-way ANOVA with Tukey's multiple comparison with individual variances, Alpha 0.05; ns P > 0.05, * P ≤ 0.05, ** P ≤ 0.01, *** P ≤ 0.001, **** P ≤ 0.0001)*

To further investigate the involvement of the UPR in EMT, I again used Ceapin-A7 to inhibit ATF6 activity, and 4μ8C and MKC8866 to inhibit IRE1a activity, and GSK26406414 (GSK) to inhibit PERK activity, at concentrations previously shown to be effective (Figure 3.14). Western blotting of the UPR components was performed to confirm their ability to block both tunicamycin and thapsigargin ER stress responses. Ceapin-A7 suppressed basal levels of HRD1 and HERP1, and attenuated Tm or Tg induced increase of these UPR target genes. Tunicamycin treatment induced a low molecular weight band in the SEL1L blot which corresponds to non-glycosylated SEL1L as tunicamycin induces ER stress by inhibiting N-linked glycosylation. Thapsigargin on the other hand, increased SEL1L protein levels. The action of ATF6 inhibitor was validated with the decreased level of SEL1L (Figure 5.7-A). FAM8A1 levels decreased in response to ER stress, and IRE1 inhibition by either 4μ8C or MKC8866 restored the levels.

4μ8C and MKC8866 attenuated Tm or Tg induced increase in sXBP1 (Figure 5.7-B) and GSK26406414 attenuated Tm or Tg induced increase in PERK and eIF2$\alpha$ phosphorylation (Figure 5.7-C).

PERK, ATF4, eIF2$\alpha$, phosphor-eIF2$\alpha$ represent the PERK arm of the UPR. SEL1L, HRD1, and HERP1 represent the ATF6 arm of the UPR as in ARCaPM cells ATF6 inhibitor Ceapin-A7 inhibited the increase in these proteins in response to tunicamycin or thapsigargin induction. FAM8A1 represent the IRE1 arm of the UPR, the level of it was restored only in the presence of both IRE1 inhibitors in *Section 5.3.2*, Figure 5.7 and Figure 5.8. SEL1L, HRD1, HERP1 and FAM8A1 also represent the key components of the ERAD pathway.

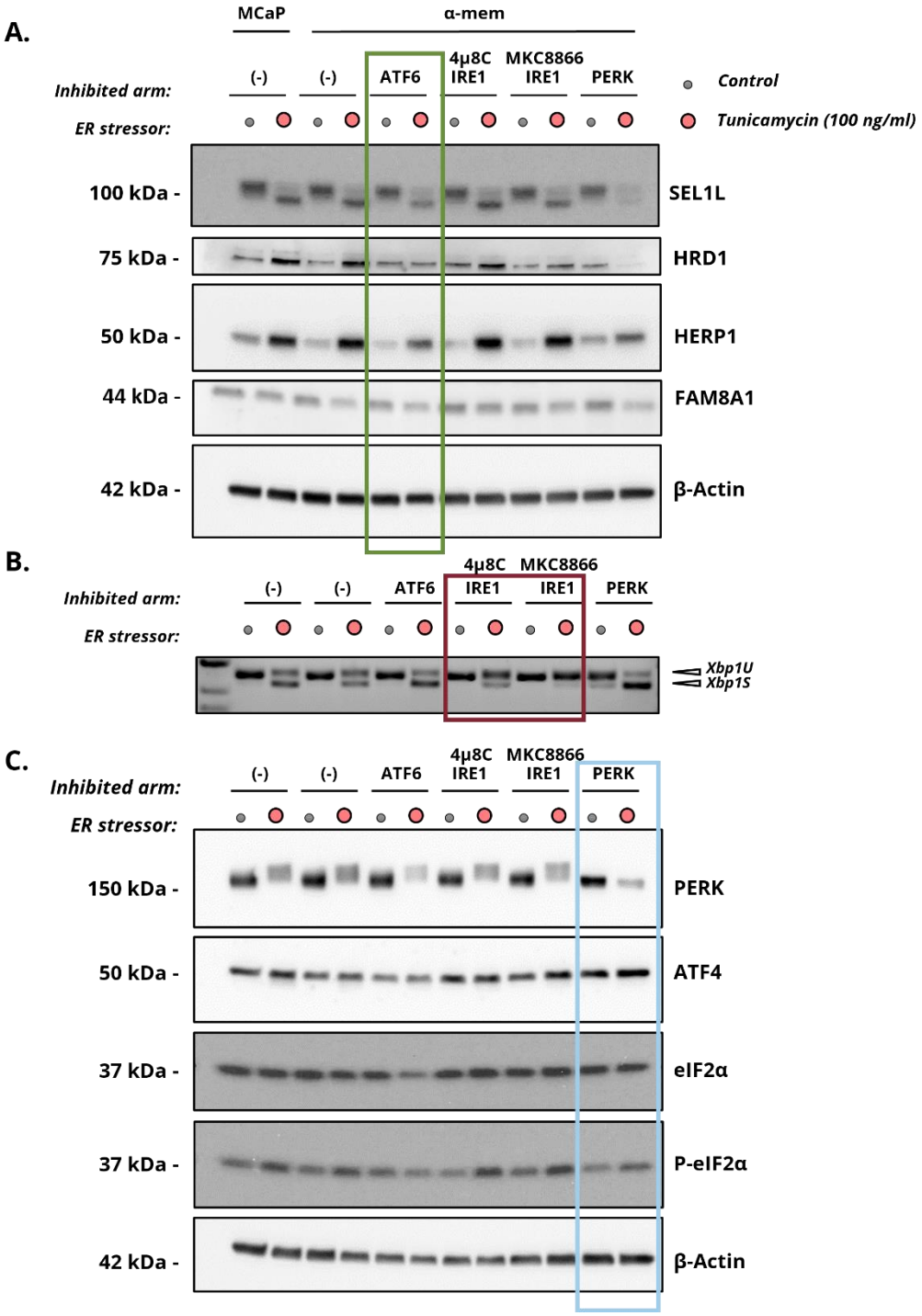



Figure 5.7 Effect of tunicamycin and the UPR inhibitors on the UPR components

ARCaPM cells were treated with the UPR inhibitors (1 μM final concentration) in the presence or absence of tunicamycin (100 ng/ml) after 24 h. ARCaPM cells grown in MCaP medium is used as control for basal levels of the components. Cell lysates were analysed by immunoblotting using anti-PERK, anti-ATF4, anti-eIF2α, anti-Phospho-eIF2α, anti-SEL1L, anti-HRD1, anti-HERP1 and anti-β-Actin antibodies. β-Actin was used as loading control.

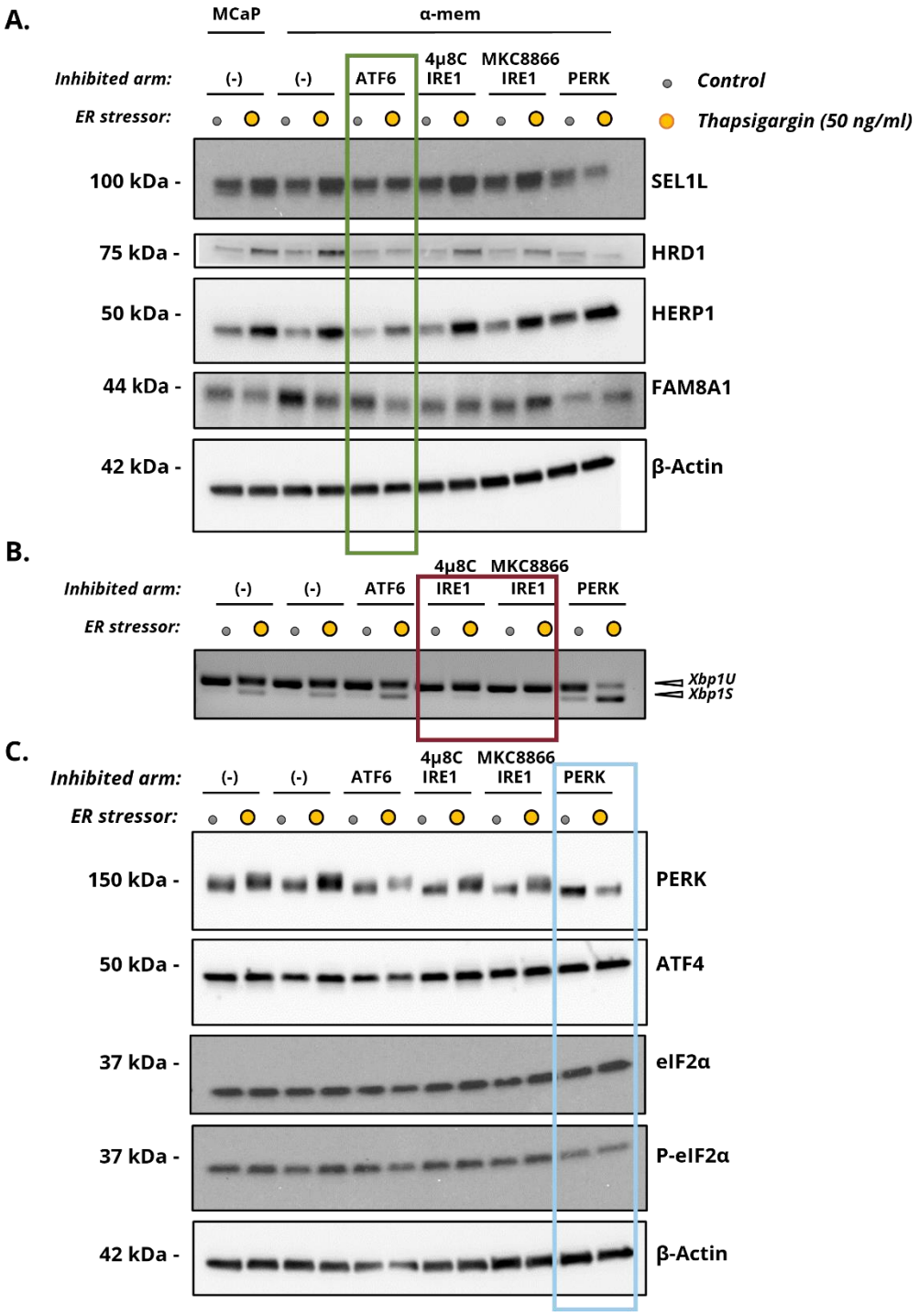



Figure 5.8 Effect of thapsigargin and the UPR inhibitors on the UPR components

ARCaPM cells were treated with the UPR inhibitors (1 μM final concentration) in the presence or absence of thapsigargin (50 ng/ml) after 24 h. ARCaPM cells grown in MCaP medium is used as control for basal levels of the components. Cell lysates were analysed by immunoblotting using anti-PERK, anti-ATF4, anti-eIF2α, anti-Phospho-eIF2α, anti-SEL1L, anti-HRD1, anti-HERP1 and anti-β-Actin antibodies. β-Actin was used as loading control.

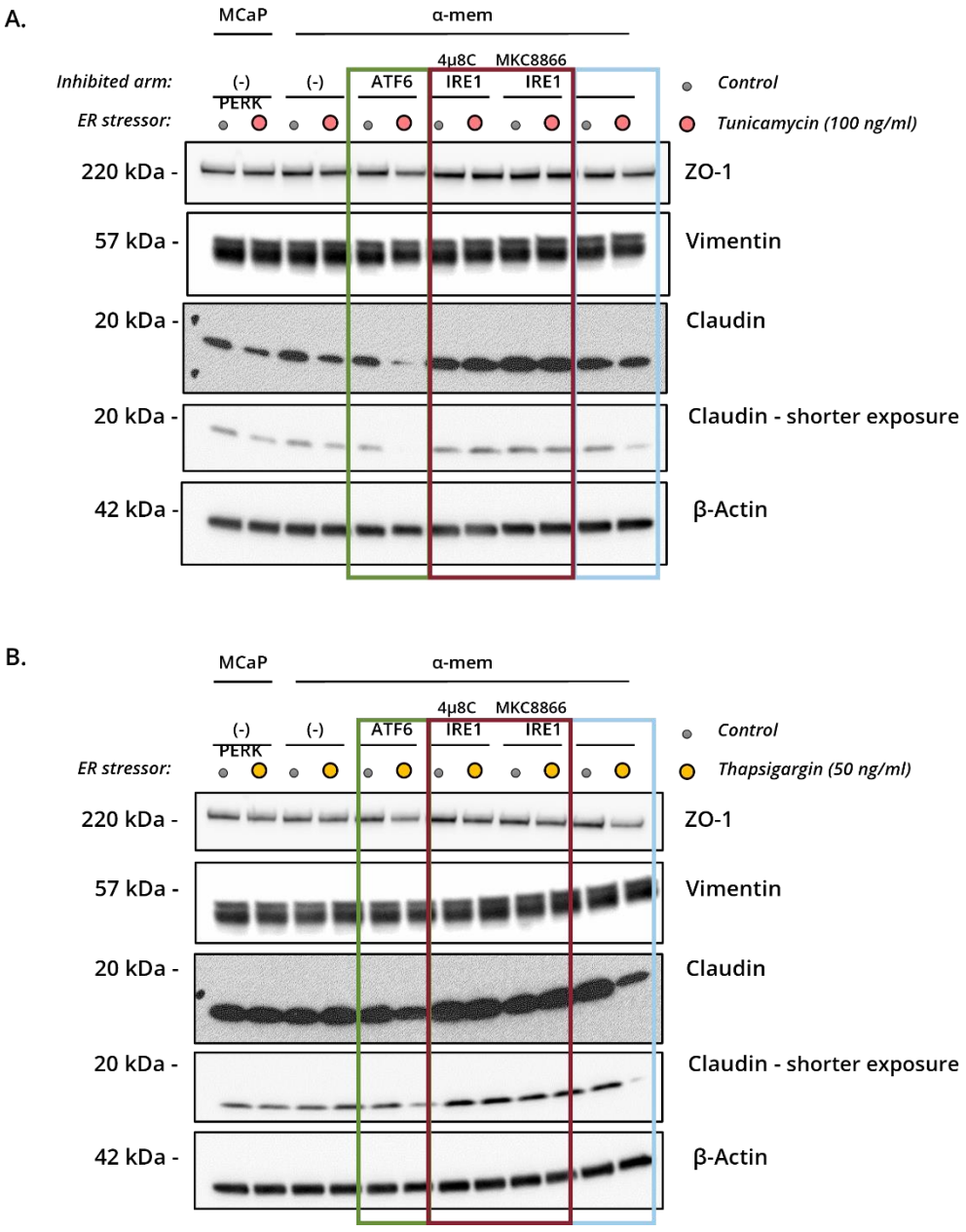
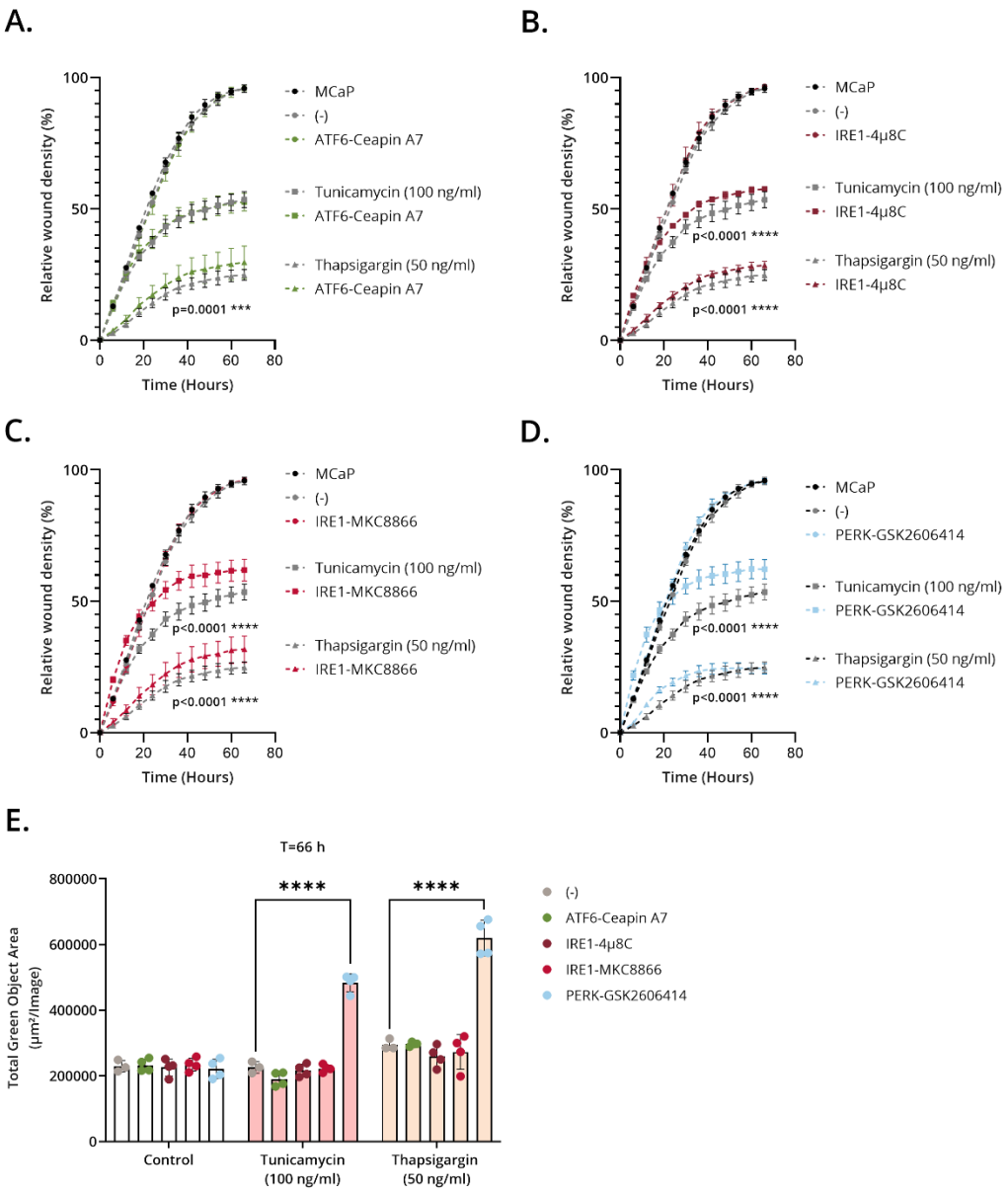



Figure 5.9 Effect of tunicamycin & thapsigargin on EMT markers

Immunoblotting of lysates from ARCaPM cells that were treated with the UPR inhibitors (1 μM final concentration) in the presence or absence of (A) tunicamycin (100 ng/ml) (B) thapsigargin (50 ng/ml) after 24 h. ARCaPM cells grown in MCaP medium is used as control for basal levels of the components. After 24 h of exposure, the protein levels of zonula occludens (ZO)-1, vimentin and claudin-1 were determined by western blotting. Membranes were probed with anti-ZO1, anti-Vimentin, anti-Claudin and anti-β-Actin was used as loading control.

ZO-1 is a junctional adaptor protein that has been reported to positively regulate cell migration [440]. Immunoblotting showed that levels of epithelial markers such as tight junction protein ZO-1 and Claudin levels were decreased by ER stressors tunicamycin or thapsigargin (Figure 5.9). ATF6 inhibition enhanced, the effect of tunicamycin and thapsigargin on ZO-1 and Claudin levels. However, IRE1 inhibition by 4μ8C or MKC8866 restored the effect of tunicamycin and thapsigargin on ZO-1 and Claudin levels, suggesting IRE1 dependent regulation of proteins of tight junctions in response to ER stress. These findings suggests that Tm or Tg-induced decrease in ZO-1 and Claudin is linked to the increase in the UPR not to any toxic effects of the stressors.

Next, to determine whether the effects of tunicamycin on the migratory capacity of ARCaPM cells were due to reduced survival of the cells, and to eliminate the effect of serum deprivation during the transwell assay, I performed scratch assays and monitored wound healing in a time course, simultaneously measuring cell death by SYTOX green. No significant effect of tunicamycin or thapsigargin on cell death was found in the timeframe in which the assays were performed except for with PERK inhibition. As observed in the transwell assay, tunicamycin and thapsigargin delayed wound healing in ARCaPM cells. The delay in wound healing in response to tunicamycin or thapsigargin was partially restored when the PERK or IRE1 pathways were inhibited (Figure 5.10).




## Figure 5.10 Effect of the UPR inhibitors on ARCaPM migration

ARCaPM cells were seeded into 96-well plates and were incubated at 37 °C to let cells grow to confluency. The wells are washed twice following to the application of the scratches, and the inhibitors (1 μM final concentration) ± tunicamycin (100 ng/ml) or thapsigargin (50 ng/ml) solution were added. The plates were placed in the IncuCyte® System. The software was set up to monitor the cells every six hours until the scratches closed in control wells (MCaP and α-mem medium). ATF6 pathway inhibition, with Ceapin-A7 (A), IRE1 pathway inhibition with 4μ8C (B) and MKC8866 (C), PERK pathway inhibition with GSK2606414 (D). Cell death was measured by the Sytox green (E). Data shows mean ± S. D.

*(A-D) Two-way ANOVA with Tukey's multiple comparison, column factor p-value shown. (E) Two-way ANOVA with Dunnett's multiple comparisons test, Alpha 0.05; ns P > 0.05, * P ≤ 0.05, ** P ≤ 0.01, *** P ≤ 0.001, **** P ≤ 0.0001)*

### 5.3.3 Effect of hypoxia on migration

The tumour microenvironment contains several physiological stress factors such as low levels of glucose, oxidative stress, and hypoxia that can induce a continuous ER stress and persistent UPR. Hypoxia is an important source of ER stress in solid tumours. The hypoxic environment of the bone can potentially promote tumour growth and metastasis. The levels of oxygen in untreated prostate tumours are reported to be as low as 0.3% and more than 12 times lower than the oxygen levels in the normal prostate [464, 465]. I therefore investigated ARCaPM cell migration in hypoxia as a physiological ER stressor, using similar approaches to those described for tunicamycin and thapsigargin. Culturing in 0.4% oxygen increased cell migration, despite the significant decrease in cell viability after 48 h assessed by Alamar Blue staining (Figure 5.11), suggesting that different ER stressors might play different roles in the prostate cancer cell migration.

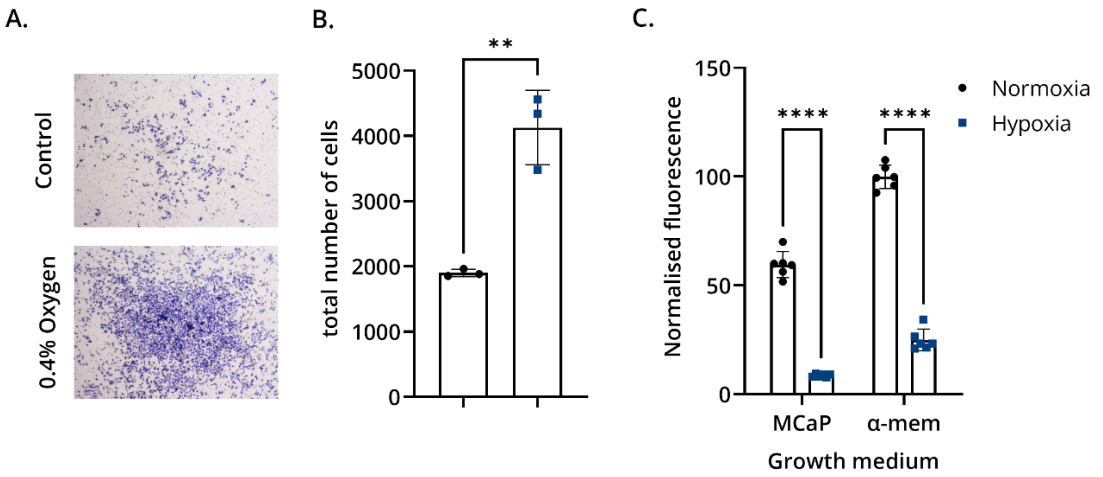



Figure 5.11 Effect of 0.4% hypoxia as stress inducer on the migration of ARCaPM cells

ARCaPM cells previously cultured MCaP medium to confluency and seeded in in the migration insert in 0.5% FBS containing α-mem as 3 inserts/condition. After 48 hours, cells that migrated through the 8 µm porous membrane were fixed, stained, and counted from five fields (top, centre, bottom, left and right) using a light microscope. Representative images of normoxia and hypoxia conditions are shown on the left (A). Data summarises 3 independent experiments and shows the mean ±S. D (B). Alamar Blue staining for cell viability based on metabolic activity (C).
*(B) Unpaired t-test, (C) Two-way ANOVA, Tukey's multiple comparison test; Alpha 0.05; ns P > 0.05, * P ≤ 0.05, ** P ≤ 0.01, *** P ≤ 0.001, **** P ≤ 0.0001)*

Next, the effect of inhibition of ATF6, IRE1 or PERK pathways on cell migration during hypoxia was studied using the transwell migration assay. First, I investigated the induction of different arms of the UPR in response to 0.4% hypoxia (Figure 5.12).

Hypoxia induces PERK activation and phosphorylation of eukaryotic initiation factor 2α (eIF2α), which suppresses mRNA translation, leading to reduced global translation [466]. Immunoblotting for components of the UPR shown a general decrease in the level of proteins in hypoxia. Both eIF2α and phosphorylated eIF2α increased in hypoxia as a result of PERK activation, and the increase in the levels were attenuated with PERK inhibitor. PERK protein levels followed the general trend, decreased in hypoxia due to decreased protein translation and the decrease in PERK protein levels were restored in PERK inhibited condition.

PERK inhibition in normal oxygen levels induced XBP1 splicing, indicating compensation by IRE1 pathway when PERK pathway cannot respond to basal levels of ER stress. Culturing in hypoxia decreased the XBP1 splicing induced by PERK inhibitor, as the hypoxia induces the PERK arm of the UPR.

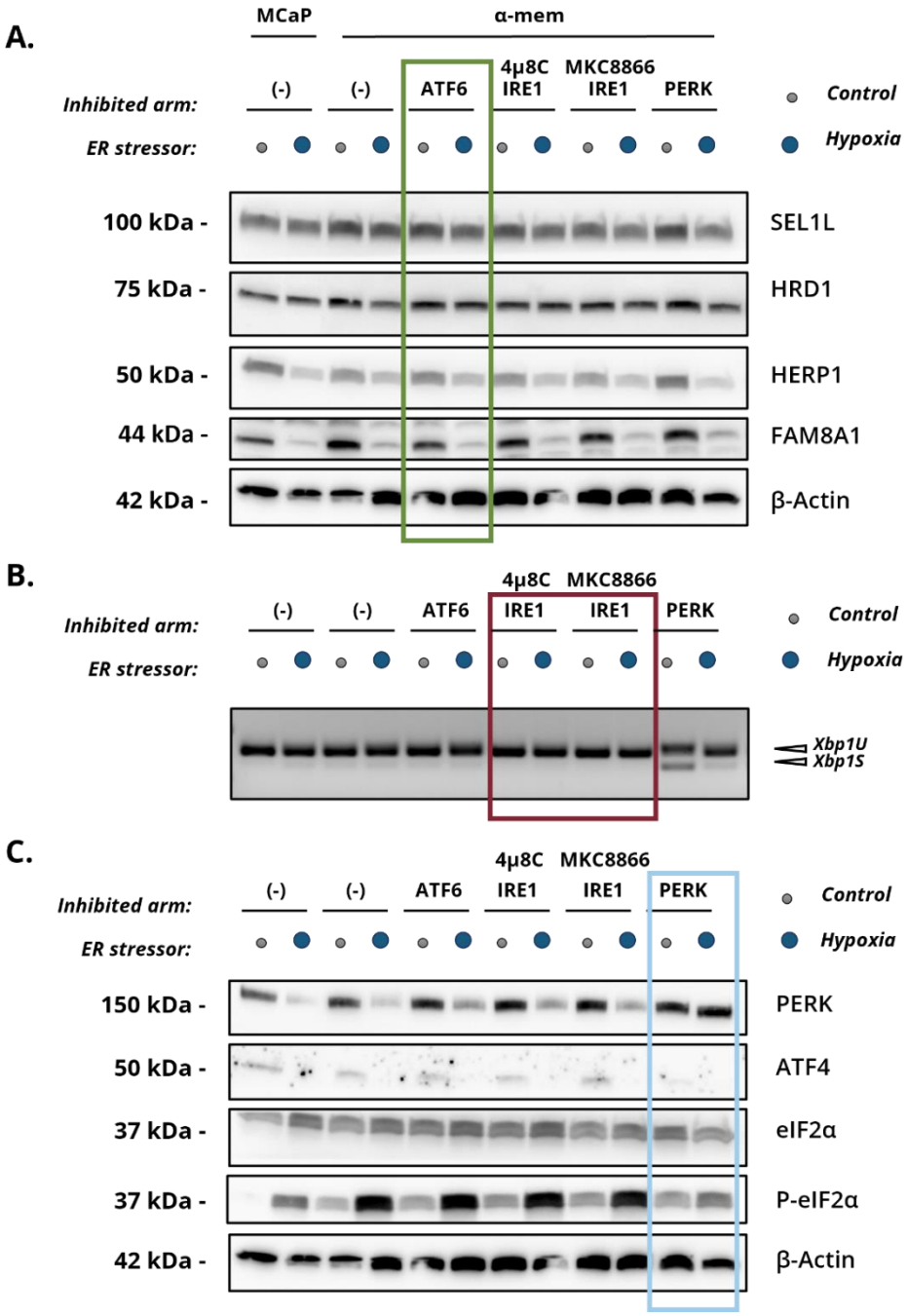



Figure 5.12 Effect of hypoxia and the UPR inhibitors on the UPR components

ARCaPM cells were cultured in normoxia or hypoxia (0.4% $O_2$) with the UPR inhibitors (1 μM final concentration) for 12 h. ARCaPM cells grown in MCaP medium is used as control for basal levels of the components. (A) and (C) Cell lysates were analysed by immunoblotting using anti-PERK, anti-ATF4, anti-eIF2α, anti-Phospho-eIF2α, anti-SEL1L, anti-HRD1, anti-HERP1 and anti-β-Actin antibodies. β-Actin was used as loading control. (B) The level of spliced XBP1 was assayed by PCR amplification of XBP1 with primers that can amplify both spliced and unspliced XBP1.

Immunoblotting for EMT-related proteins showed that the levels of epithelial marker ZO-1 was decreased whereas mesenchymal marker N-Cadherin was increased in hypoxia (Figure 5.13-A). The inhibitors of the different arms of the UPR did not enhance or attenuate the effect of hypoxia on ZO-1 or N-Cadherin, indicating an UPR independent increase.

Hypoxia inducible factor 1 (HIF1) is a transcription factor that controls how cells and tissues respond to hypoxia [467]. The heterodimeric protein HIF1 consists of two subunits: HIF1$\alpha$ and HIF1$\beta$. HIF1$\alpha$ is constitutively expressed in normoxic tissues and continually degraded by the enzyme prolyl hydroxylase. Low oxygen conditions, such as hypoxia, diminished blood flow (ischemia), or cancer growth, stabilise HIF1$\alpha$ [468]. When the HIF1$\alpha$ subunit is induced by hypoxia, it dimerises with HIF1$\beta$ to form an active transcription factor that triggers the expression of hypoxia-adaptation genes such those involved in angiogenesis, erythropoiesis, cell proliferation, and death [469, 470]. HIF1$\alpha$ and HIF1$\beta$ were used as markers for assessing the effect of hypoxia. The levels of both HIF1$\alpha$ and HIF1$\beta$ decreased in hypoxia due to general decrease in protein translation (Figure 5.13).

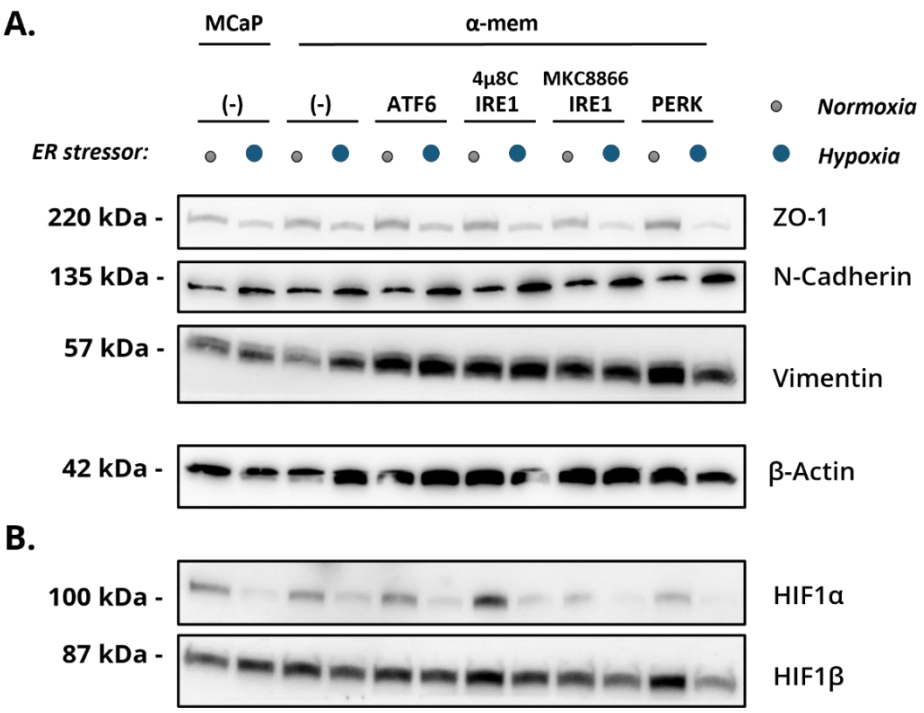



Figure 5.13 Effect of hypoxia and the UPR inhibitors on EMT markers

Immunoblotting of lysates from ARCaPM cells that were cultured in normoxia or hypoxia (0.4% $O_2$) with the UPR inhibitors (1 μM final concentration) for 12 h. ARCaPM cells grown in MCaP medium is used as control for basal levels of the components. After 24 h of exposure, the protein levels of zonula occludens (ZO)-1, N-Cadherin and vimentin were determined by western blotting. Membranes were probed with anti-ZO1, anti-N-Cadherin, anti-Vimentin, and anti-β-Actin antibodies. β-Actin was used as loading control.

Using transwell assays I investigated the effect of inhibiting the arms of the UPR on the hypoxia-induced increase in cell migration. Cell migration through transwell was studied at 0.4% oxygen levels, reported to be the median $O_2$ in prostate tumours [464]. Inhibiting the PERK pathway in hypoxia increased the number of cells migrated, however, the results were not statistically significant (Figure 5.14-A). Alkaline phosphatase activity slightly decreased in response to hypoxia; however, this was limited to only the MCaP medium (Figure 5.14-C).

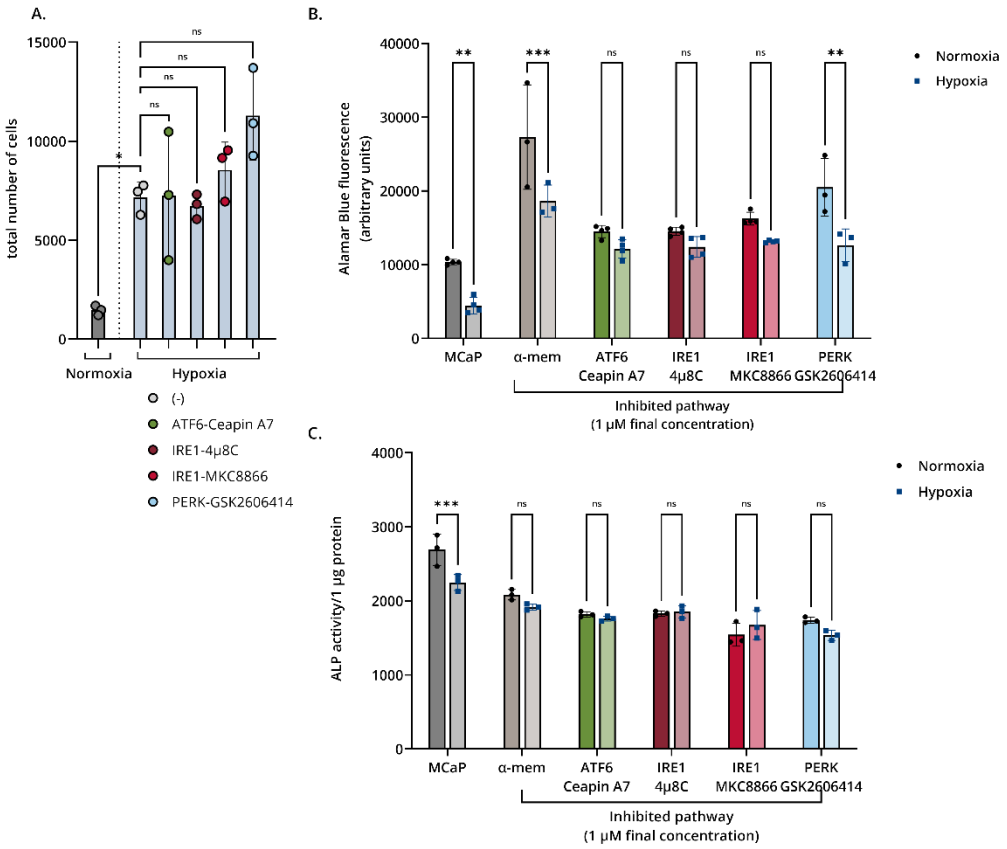



Figure 5.14 Effect of the UPR inhibitors on ARCaPM migration under hypoxia

The cells were treated with inhibitors of the UPR at 1 μM concentration and grown for 48 h under normal or low oxygen conditions (hypoxia). The migrated cells were counted from five fields of three replicates using a light microscope at 4X objectives. Number of migrated cells (A), Alamar Blue staining for cell viability based on metabolic activity (B). ALP activity was measured using a fluorogenic ALP substrate and normalised with 1 μg protein concentrations (C). Data summarises 3 independent experiments and shows the mean ±S. D.

*(A) One way ANOVA with Dunnett's multiple comparison, (B) and (C) Two-way ANOVA with Šidák's multiple comparison, Alpha 0.05; ns P > 0.05, * P ≤ 0.05, ** P ≤ 0.01, *** P ≤ 0.001, **** P ≤ 0.0001)*

Migration of ARCaPM cells across transwell membrane requires 48 h; however, the number of migrated cells is significantly lower after 24 h in hypoxia. Exposure to hypoxia slightly decreased cell viability after 36 h.

To monitor the effect of hypoxia on cell migration before hypoxia induces cell death, I performed scratch assays which allow tracking of wound closure after

shorter exposures to hypoxia. 12 h in hypoxia enhanced wound healing in ARCaPM cells, however, inhibiting different arms of the UPR by Ceapin-A7, 4μ8C, MKC8866 or GSK2606414 did not enhance or slow down the wound healing in hypoxia (Figure 5.15). After 12 h the cell death did not increase in hypoxia (Figure 5.16).

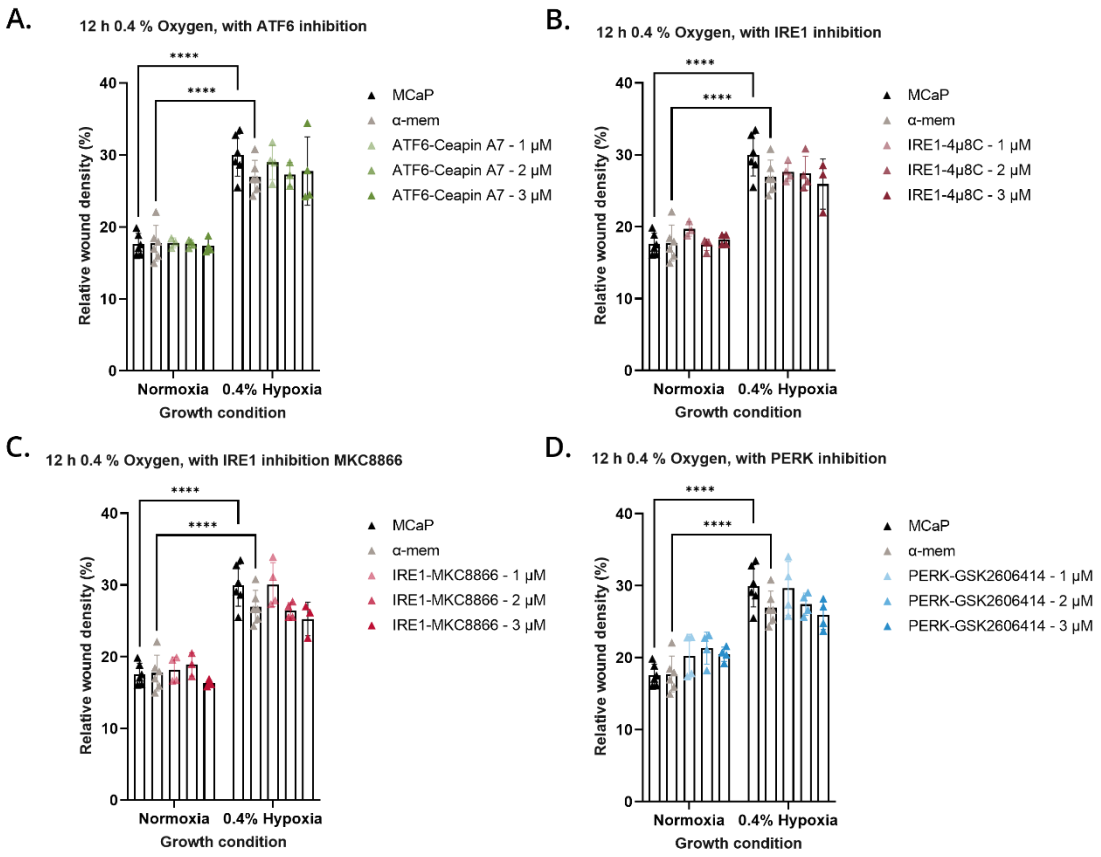



Figure 5.15 Early hypoxia induced wound healing in ARCaPM cells

Scratch-wound healing of ARCaPM cells in the presence of different inhibitors of the UPR. ARCaPM cells in a 96 well plate were scratch wounded with IncuCyte® WoundMaker and then incubated under hypoxia (0.4% $O_2$) or normoxia for 12 h. The images of the wounds in the wells were recorded and using IncuCyte S3. The wound width was measured immediately after scratch wounding and after 12 h of healing to determine the wound density. ATF6 pathway inhibition, with Ceapin-A7 (A), IRE1 pathway inhibition with 4μ8C (B) and MKC8866 (C), PERK pathway inhibition with GSK2606414 (D). Data shows mean ± S. D (n = 4).

*Two-way ANOVA, with Tukey's multiple comparisons test, with individual variances. Alpha 0.05; ns P > 0.05, * P ≤ 0.05, ** P ≤ 0.01, *** P ≤ 0.001, **** P ≤ 0.0001*

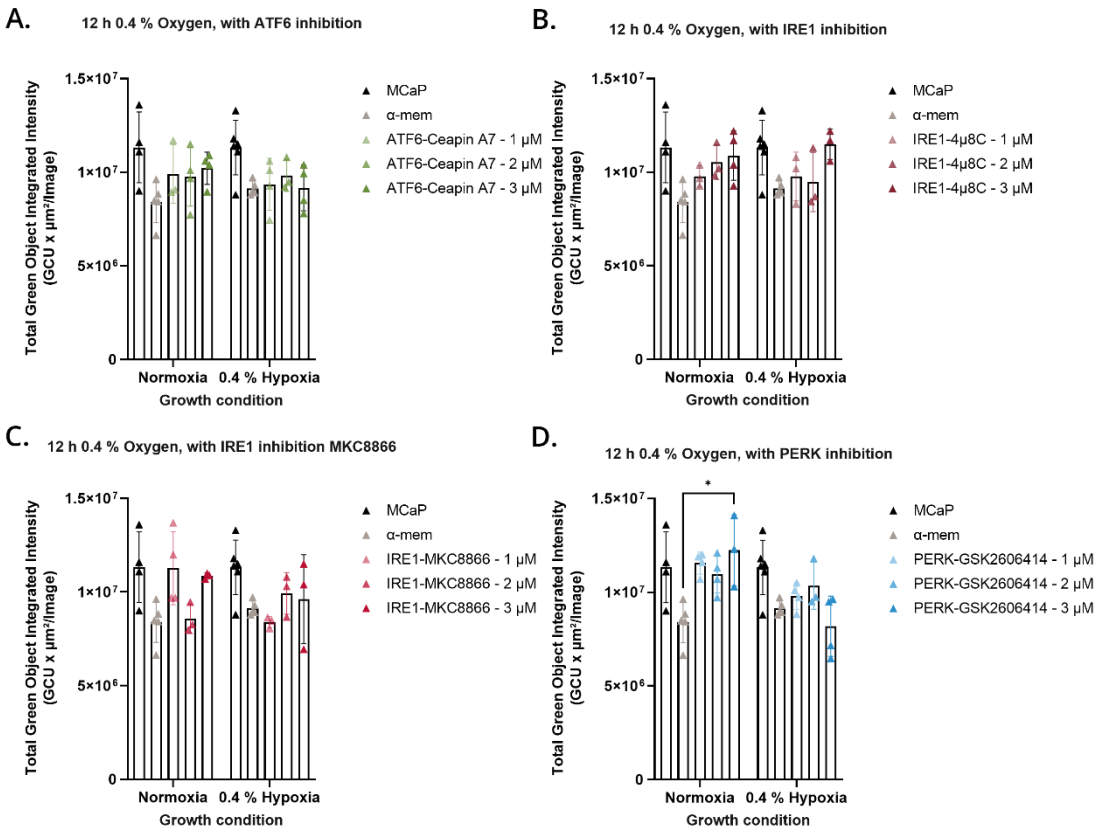



Figure 5.16 Cell death in ARCaPM after 12 h in hypoxia

Quantitative analysis toxicity was measured by the SYTOX green. ARCaPM cells seeded in a 96 well plate was treated with increasing concentrations of Ceapin-A7 for ATF6 pathway inhibition (A), 4µ8C and MKC8866 for IRE1 pathway inhibition (B) and (C), GSK2606414 for PERK pathway inhibition (D); under normoxia or hypoxia (0.4% $O_2$) for 12h. SYTOX green was added to the wells at 625 nM final concentration. Cell death is calculated based on the SYTOX green intake by dead cells and IncuCyte® S3 Software 2018C was used for data analysis. Data shows mean ± S.D. (n = 4).

*Two-way ANOVA, with Tukey's multiple comparisons test, with individual variances. Alpha 0.05; ns P > 0.05, * P ≤ 0.05, ** P ≤ 0.01, *** P ≤ 0.001, **** P ≤ 0.0001*

Next, I investigated the effect of hypoxia and the UPR inhibition on ARCaPM viability at later time points 12 h after the start of the incubation. The number of dead cells in normoxia and hypoxia were similar (Figure 5.17). Hypoxia increased cell death in ARCaPM cells after 24 h. Addition of the UPR inhibitors at different concentrations did not protect from hypoxia induced cell death.

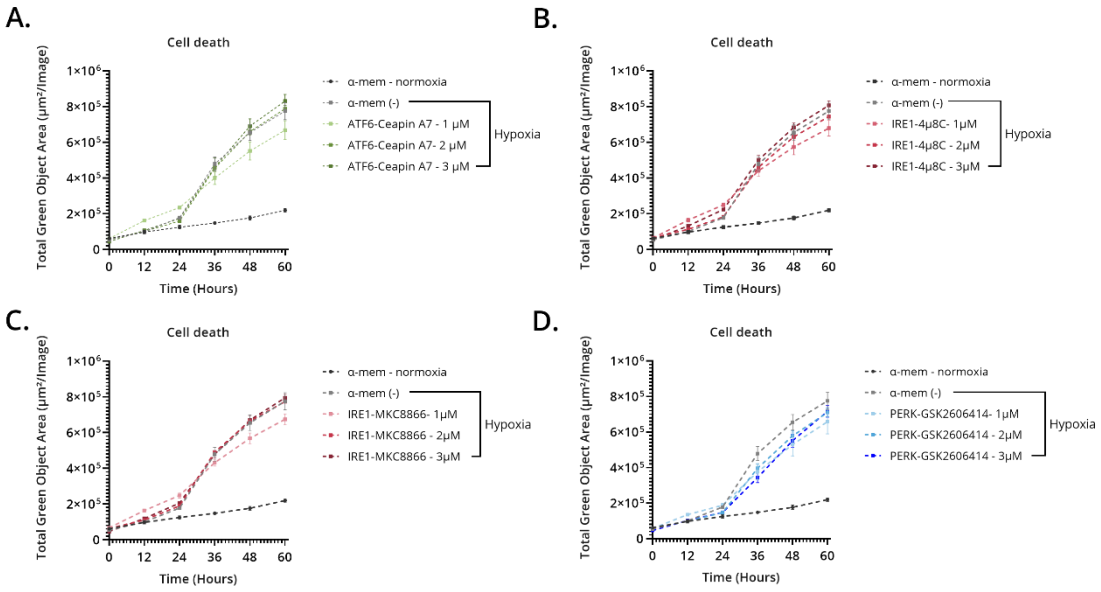



Figure 5.17 Prolonged hypoxia results in increased cell death in ARCaPM cells

Quantitative analysis of cell death induced by hypoxia in the presence of inhibitors targeting different arms of the UPR measured by the SYTOX green. ARCaPM cells seeded in a 96 well plate and incubated for 24 h to allow attachment. The cells were treated with increasing concentrations of Ceapin-A7 for ATF6 pathway inhibition (A), 4µ8C and MKC8866 for IRE1 pathway inhibition with (B) and (C), GSK2606414 for PERK pathway inhibition with (D); under normoxia or hypoxia (0.4% $O_2$). SYTOX green was added to the wells at 625 nM final concentration. Images were recorded for cell death with IncuCyte, measured as total green object area for cells stained green with SYTOX Green. Data shows mean ± S.D. (n = 4).

*Two-way ANOVA, with Tukey's multiple comparisons test, with individual variances. Alpha 0.05; ns P > 0.05, * P ≤ 0.05, ** P ≤ 0.01, *** P ≤ 0.001, **** P ≤ 0.0001*

I also measured wound healing under the same conditions and found that culturing ARCaPM cells in hypoxia for 12 h increased the wound healing, however, inhibitors of the UPR did not have an effect on this (Figure 5.18). Enhanced wound healing in hypoxia disappeared after culturing in hypoxia for a further 12 h following reoxygenation. At 24 h wound healing in normoxia and hypoxia was similar, and prolonged incubation under hypoxic conditions delayed wound healing compared to normal conditions. While early effect of hypoxia increased wound healing in ARCaPM cells up to 18 h, prolonged hypoxia after

24 h slowed down the healing (Figure 5.18). Hypoxia increases transwell migration however, hypoxia results in cell death in longer treatment. As hypoxia's effect on increasing migration is hindered by its effect on cell survival with longer exposure, the scope of low oxygen exposure is limited only to the duration where the cells are still alive.

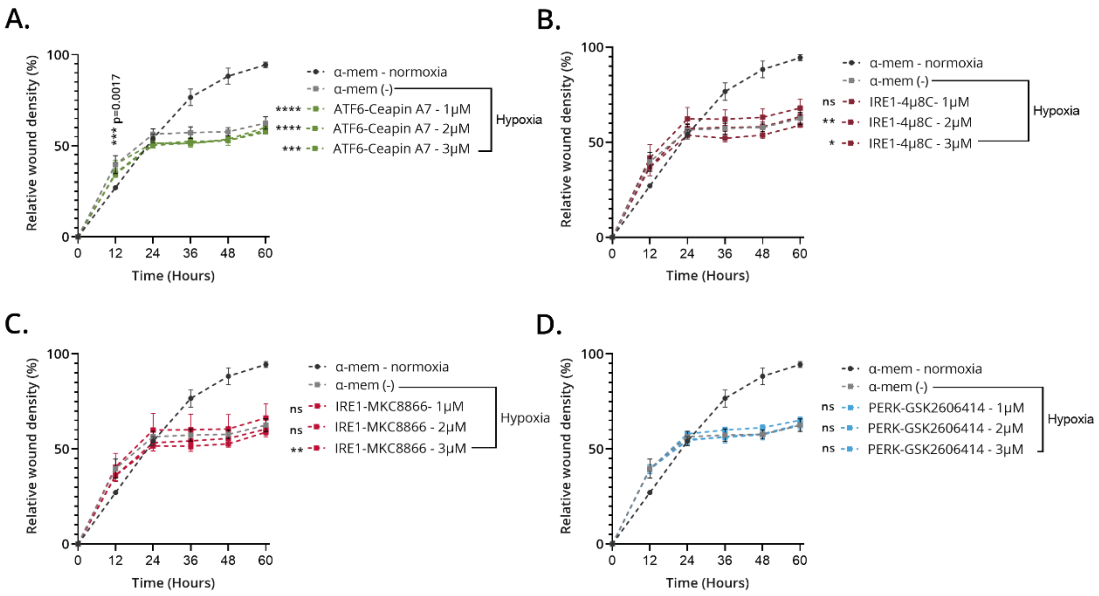



Figure 5.18 Prolonged hypoxia delayed wound healing in ARCaPM cells

Scratch-wound healing of ARCaPM cells in the presence of increasing concentration of different inhibitors of the UPR. ARCaPM cells in a 96 well plate were scratch wounded with IncuCyte® WoundMaker and then incubated under hypoxia (0.4% $O_2$) or normoxia. The wound width was measured immediately after scratch wounding and after every 12 h of healing to determine the wound density in a time course. The plate was reoxygenated every 12 h for the measurement of the wound width using IncuCyte. ATF6 pathway inhibition, with Ceapin-A7 (A), IRE1 pathway inhibition with 4μ8C (B) and MKC8866 (C), PERK pathway inhibition with GSK2606414 (D). Data shows mean ± S.D. (n = 4).

P value on ATF6 inhibition graph (vertical text) is a comparison between $\alpha$-mem in normoxia and $\alpha$-mem in hypoxia after 12 h. (*Two-way ANOVA with Šidák's multiple comparison.*) *Two-way ANOVA with Tukey's multiple comparison, statistical significance based on column factor p-value shown on the left side of each concentration indicate a comparison between that condition and α-mem in hypoxia. Alpha 0.05; ns P > 0.05, * P ≤ 0.05, ** P ≤ 0.01, *** P ≤ 0.001, **** P ≤ 0.0001*

## 5.4 Discussion

The work of this chapter has suggested a potential role for ER stress in migration although the effect of ER stress differed with different drivers of ER stress.

In the context of osteomimicry, prostate cancer cells have been shown to express markers associated with bone cells in the tumour-bone microenvironment, including RUNX2, RANKL, and ALPL. A previous study by Rao *et al.* found that tumour derived ALPL, a key component of prostate cancer bone metastasis plays a role in epithelial plasticity and PCa metastasis [438]. The UPR has the ability to control cytoskeleton remodelling and cell migration [471]. Hence, this chapter investigated the involvement of the UPR on EMT and migration in bone metastatic prostate cancer cells.

Baseline mRNA expression level of EMT related genes confirmed the reported phenotypical differences between ARCaPE and ARCaPM (Figure 3.8), and DVL3 and DVL3-SCM cells (Figure 5.1). Since tumour invasion and metastasis are dependent on EMT, I examined the role of the UPR in migratory capacity in ARCaP cells. The migratory capacity of ARCaPE and ARCaPM cells reflected their gene expression profile related to EMT (Figure 5.2).

The UPR may regulate cancer cell metastasis. Before metastasis, tumour cells commonly go through an EMT, which entails the adoption of a highly secretory phenotype and enhanced the UPR signalling. Tunicamycin impaired the migratory capacity of ARCaPM cells in a transwell migration assay (Figure 5.3). In a previous study, tunicamycin promoted metastasis in thyroid cancer cells by activation of MMP-13 expression by enhancing GRP78 expression [472]. Another study has shown that tunicamycin triggers cell invasion and migration in human colon adenocarcinoma cells, however, this effect was only observed after 6 hours

[473]. The optimised migration time for ARCaPM cells was 24 h. The duration of migration experiment allows tunicamycin to exert its cytotoxic effect, and thus, might compromise its effect on migration.

Inhibiting the arms of the UPR when the cells were not stressed did not alter the number of migrated cells (Figure 5.4). To investigate the role of the UPR arms in migration, and hence EMT, tunicamycin was used to increase ER stress in ARCaPM cells. Pre-treating ARCaPM cells did not protect ARCaPM cells from the cytotoxic effect of tunicamycin (Figure 5.6); thus, investigation of the role of the UPR on migration in transwell assay was limited due to the cytotoxic effect of the UPR inducers (Figure 5.5). *In vivo* experiments can overcome the requirement of ER stress inducer, as the cancer cells have elevated UPR due to the factors discussed in *Section 1.4.3*.

However, protein levels of EMT markers in response to tunicamycin revealed that levels of epithelial markers such as tight junction protein ZO-1 and Claudin were decreased by ER stressors tunicamycin or thapsigargin (Figure 5.9). ATF6 inhibition enhanced the effect of tunicamycin and thapsigargin on ZO-1 and Claudin levels. Inhibiting the ATF6 pathway in the presence of ER stress inducer forces the cells to activate the other arms of the UPR to compensate for the elevated stress. This indicates a role for the IRE1 and PERK signalling in EMT.

IRE1 inhibition by different inhibitors restored the effect of tunicamycin and thapsigargin on ZO-1 and Claudin levels (Figure 5.9), suggesting an IRE1-dependent regulation of proteins of tight junctions in response to ER stress. These findings suggests that Tm or Tg-induced decrease in ZO-1 and Claudin is linked to the increase in the UPR not to any toxic effects of the stressors. This study reveals involvement of the UPR in cell migration, where tight junction proteins operate as an interphase between the UPR and migration. This is supported by

another study where IRE1 has been shown to affect cytoskeleton dynamics and cell motility by directly binding filamin A, independent of its normal activity as a UPR signal transducer [471].

In glioma tumour cells, introducing a dominant negative mutant of IRE1 resulted in decreased proliferation and angiogenesis *in vivo*, but increased invasiveness [474]. IRE1 regulates glioma cell migration in this paradigm by RIDD-mediated degradation of the mRNA for *SPARC*, a protein necessary for glioma cell-extracellular matrix interactions. Inhibition of IRE1's RNase activity causes an increase in SPARC, which enhances tumour cell invasion [475]. As a result, while inhibiting IRE1 signalling may slow primary tumour growth, it may also promote a more invasive phenotype.

The levels of the UPR related proteins in response to tunicamycin/thapsigargin and inhibitors of the UPR reveals possible dynamics for ERAD regulation and the HRD1 complex. ER stress induces expression of ERAD components SEL1L, HRD1 and HERP1 (Figure 5.7 and Figure 5.8). Previous studies have suggested that HRD1 and its cofactor SEL1L form the core of a complex that aids in the degradation of misfolded proteins during the ubiquitin–proteasome-dependent ER-associated degradation pathway. HRD1 engages with cofactors to initiate the ERAD. HRD1's cytoplasmic region (designated the HAF-H domain) interacts with complementary areas in FAM8A1 and Herp cofactors. FAM8A1 modulates HERP's interaction with HRD1, which is necessary for ERAD [356]. In the cell, the bulk of HRD1 is in a complex with FAM8A1. When the shortened cytoplasmic versions of HRD1 were expressed, FAM8A1 was decreased (or missing). In the absence of HRD1, FAM8A1 was unstable and rapidly deteriorated.

Contrary to the elevated levels of SEL1L, HRD1 and HERP, the level of FAM8A1 decreased with ER stress and IRE1 inhibition restored the FAM8A1 levels (Figure

5.7 and Figure 5.8, green panel). FAM8A1 is stabilised in the cells if HAF-H domain of HRD1 is abundant. Decreased levels of FAM8A1 indicate disruption of the interaction between FAM8A1 and HRD1, as FAM8A1 is rapidly degraded in proteosome. Repeating the experiment in a similar setting, however in the presence of proteasome inhibitor MG132 could reveal if FAM8A1 is degraded in response to elevated ER stress. Alternatively, decreased level of FAM8A1 can be attributed to decreased mRNA expression if the half-life of FAM8A1 is low. To understand this, the response to tunicamycin needs to be investigated in a time course. As both FAM8A1 and HERP interact with HRD1, and as the levels of HERP is elevated in tunicamycin treated condition, it is possible that HRD1 complex is different under some circumstances. HERP-HRD1 dominated HRD1 complex formation might have been induced under the stress conditions. FAM8A1 interaction with HRD1 might tether HRD1 to a different site on ER membrane, perhaps away from proteosome.

Transwell migration assays require culturing for long enough time to allow migration across the membrane, and they require the termination of the experiment no later than the doubling time of the cells investigated. This is to ensure the differences on both sides of the membrane are due to migration, not to proliferation. As the cell division follows an exponential curve, transwell migration assays with a long incubation period may not be as accurate and be prone to misinterpretation. In addition, investigation of migration in transwell migration assay can also be misleading if the treatment is toxic or slows down the growth rate. Thus, I investigated the migration with scratch assays using the IncuCyte, which allows acquiring images with intervals.

Similar to the transwell assay, ER stress induction using tunicamycin or thapsigargin delayed wound healing in ARCaPM cells (Figure 5.10). The delay

in wound healing in response to tunicamycin or thapsigargin was partially restored when the PERK or IRE1 pathways were inhibited (Figure 5.10-B, C and D), indicating the involvement of the PERK and IRE1 arm in migration.

Invasion and metastasis require PERK activation in cells undergoing EMT, and among three arms of the UPR, EMT gene expression strongly correlate with PERK related genes in human tumour tissues [476]. After tail-vein injection into an immunocompromised animal, PERK inhibition reduced lung metastasis in breast carcinoma models [476].

As hypoxia is more relevant to physiological stress compared to tunicamycin or thapsigargin induced ER stress, next I investigated cell migration under hypoxia. The level of oxygen was adjusted to 0.4% as this was reported as the median oxygen levels in prostate tumours [464]. Inhibiting the different arms of the UPR by Ceapin-A7, 4μ8C, MKC8866 or GSK2606414 did not enhance or slow down the wound healing in hypoxia (Figure 5.15 and Figure 5.16), indicating that the effect of hypoxia induced increase in migration is not linked to the increase in the UPR. Longer exposure to hypoxia decreased proliferation of ARCaP cells, even if it was not cytotoxic (Figure 5.17). Thus, increased migration in response to hypoxia was limited to 18-20 h exposure to hypoxia (Figure 5.18). I also investigated cell migration in 2% oxygen as 2% oxygen is considered to be physiological hypoxia [464]. The effect of different oxygen on migration was similar to the 0.4% oxygen condition (data not shown).

Hypoxic stress is known to induce PERK pathway activation and PERK phosphorylation. As a result, hypoxia induces phosphorylation of eIF2$\alpha$ on Ser51, causing general translational repression [477]. Hypoxia activated the PERK arm of the UPR (Figure 5.12-C) and consequently increased the phosphorylated eIF2$\alpha$ levels. The effect of this was further observed in the decreased levels of several

other UPR related proteins (Figure 5.12-A). There is a bi-phasic response to phosphorylation of eIF2α under hypoxia [478]. Initially phosphorylation rises (after 8 hours), then falls after sustained exposure until it rises again after 48 hours, in a process controlled by the PERK-ATF4-CHOP-GADD34 axis. GADD34 causes eIF2α dephosphorylation that suppresses stress-induced gene expression in a negative feedback loop. This facilitates recovery from translational inhibition in the UPR.

Hypoxia causes HIF1α stabilisation due to suppression of proline hydroxylation, which results in decreased in HIF1α ubiquitination and degradation [479]. Surprisingly, immunoblotting for the markers of hypoxia HIF1α and HIF1β indicated that the HIF1α was stabilised in normoxia, and it decreased in hypoxia, which is completely opposite to what was expected. However, HIF1α stabilisation in normoxia is possible, although is very rare. Previous study by Jason Boyang Wu et al. has shown that HIF1α stabilisation by elevated monoamine oxidase A levels in metastatic prostate cancer cells, including ARCaPM cells [463]. This needs further investigation to verify the findings. For example, an alternative cell line, which is known to respond to hypoxia by increasing the HIF1α, should be treated in the same exact way and cultured in the same hypoxic incubator together with ARCaPM cells in the, and the response from these cells should be compared to ARCaPM cells. Yet, the response to hypoxic conditions can further be validated by HIF1α activity, for example, by investigating the mRNA levels of vascular endothelial growth factor A (*VEGFA*) or the glucose transporter protein type 1 (*GLUT1*), as these are transcriptional targets of HIF1α [480, 481].

By inhibiting the RNA binding protein YB-1 from engaging with the HIF1α mRNA 5' untranslated region, PERK activation decreases HIF1α protein synthesis [407]. Bortezomib induce cell death by activating PERK and also

represses the translation of HIF1α [388]. For better representation of hypoxia induction, earlier samples need to be collected after earlier time points (6 h and 12 h), as the levels of HIF1α first increase, then decrease due to bi-phasic response to eIF2α phosphorylation [482].

Overall, low doses of tunicamycin and thapsigargin allowed to study the effect of ER stress in ARCaPM cells without causing cytotoxicity. Scratch assays and protein levels of EMT markers indicated involvement of the IRE1/PERK arm in regulation of metastatic capacity in ARCaPM cells.

The results of this chapter have shown that inhibition of the arms of the UPR when the cells are not stressed did not decrease migratory capacity of ARCaPM cells, nor it did induce migration in ARCaPE cells. Investigation of the impact of UPR inhibitors required induction of stress, however, the use of ER stress inducers (tunicamycin, thapsigargin or hypoxia) were limited due to the cytotoxic effects. Both tunicamycin and thapsigargin slowed down the migration, but they decreased the protein levels of epithelial markers. This indicates the limitations of available ER stress inducers *in vitro*, but at the same time suggests evidence for the involvement of the UPR in promoting migration.

Transwell migration experiments were set up to allow migration of ARCaPM cells towards serum. To better dissect the bone metastatic potential of prostate cancer cells, the migratory capacity of ARCaP cells needs to be investigated using bone cells, conditioned media from osteoblasts/bone cells and/or TGF-β as chemoattractant. This will allow evaluation of the impact of the UPR on the seed and soil hypothesis *in vitro*.

Taken together, these studies provide evidence linking ER stress to migration, but also raise the intriguing notion that different drivers of ER stress may have

different effects on migratory behaviour. While this may reflect in part the impact of pharmacological inducers of ER stress on cell viability, it is intriguing to speculate that specific arms of the UPR may regulate prostate cancer migration, providing another mechanism by which the UPR may contribute to progression to prostate cancer bone metastasis.

# 6

# The effect of ALPL on the UPR

## 6.1 Introduction

Decreasing ALP activity increases epithelial characteristics in ARCaPM cells. The human prostate cancer ARCaPM cells can undergo mesenchymal to epithelial transition (MET) in response to ALPL knockdown by shRNA or siRNA [438]. Although, ALPL knockdown is known to induce MET, the involvement of the UPR in the mechanism of this induction in human prostate cancer cells is not studied. My studies have shown that the UPR decreases ALPL in prostate cancer cells, however it is unknown whether a feedback loop exists, with regulation of the UPR by ALPL.

## 6.2 Hypothesis and Objectives

In this chapter I hypothesised that knockdown of the alkaline phosphatase impacts the UPR components and potentially ERAD-associated genes in metastatic prostate cancer cell line ARCaPM. For this purpose, this chapter investigates:

- The changes in UPR components by western blotting and differential mRNA expression by RNA sequencing in ARCaPM cells after knockdown of ALPL gene by siRNA transfection or short hairpin RNA (lentiviral transduction)
- The interplay between ALPL, UPR and EMT

## 6.3 Results

While it is known that *ALPL* knockdown results in epithelial morphology, the interdependency of the UPR to this process has not been studied. To further evaluate the impact of *ALPL* in the UPR, five different lentiviral-based shRNA targeting the *ALPL* gene were used to stably reduce the levels of *ALPL* and ALP activity.

### 6.3.1 ALPL knockdown results in change in morphology of ARCaPM cells

Five different shRNAs were used to knockdown ALPL in ARCaPM cells. Knockdown of *ALPL* was confirmed by a significant decrease in ALP activity (Figure 6.1-B). Although all shALPL RNAs were able to decrease ALPL activity, the level of knockdown differed among the different shRNAs. *ALPL* knockdown resulted in a switch from spindle-shaped mesenchymal ARCaPM morphology to clustered, cobblestone-like cell shape, characteristic of ARCaPE cells (Figure 6.1-A). Different shRNAs had different level of impact on the morphology, with shALPL3 having the most significant morphological switch. This switch in morphology was supported by changes in the protein levels of EMT markers.

Loss of E-Cadherin expression causes cell adhesion to weaken during EMT. While the expression of mesenchymal-related markers, including as N-Cadherin, vimentin, and fibronectin, is elevated. Cells become more mobile and invasive as a result. Knockdown of *ALPL* with shALPL3 resulted in a clear switch from mesenchymal to epithelial markers, with an increase in ZO-1 and E-Cadherin; and a decrease in the level of N-Cadherin, Vimentin and Claudin compared to shSCR, giving ARCaPM cells ARCaPE-like expression of EMT markers (Figure 6.1-C).

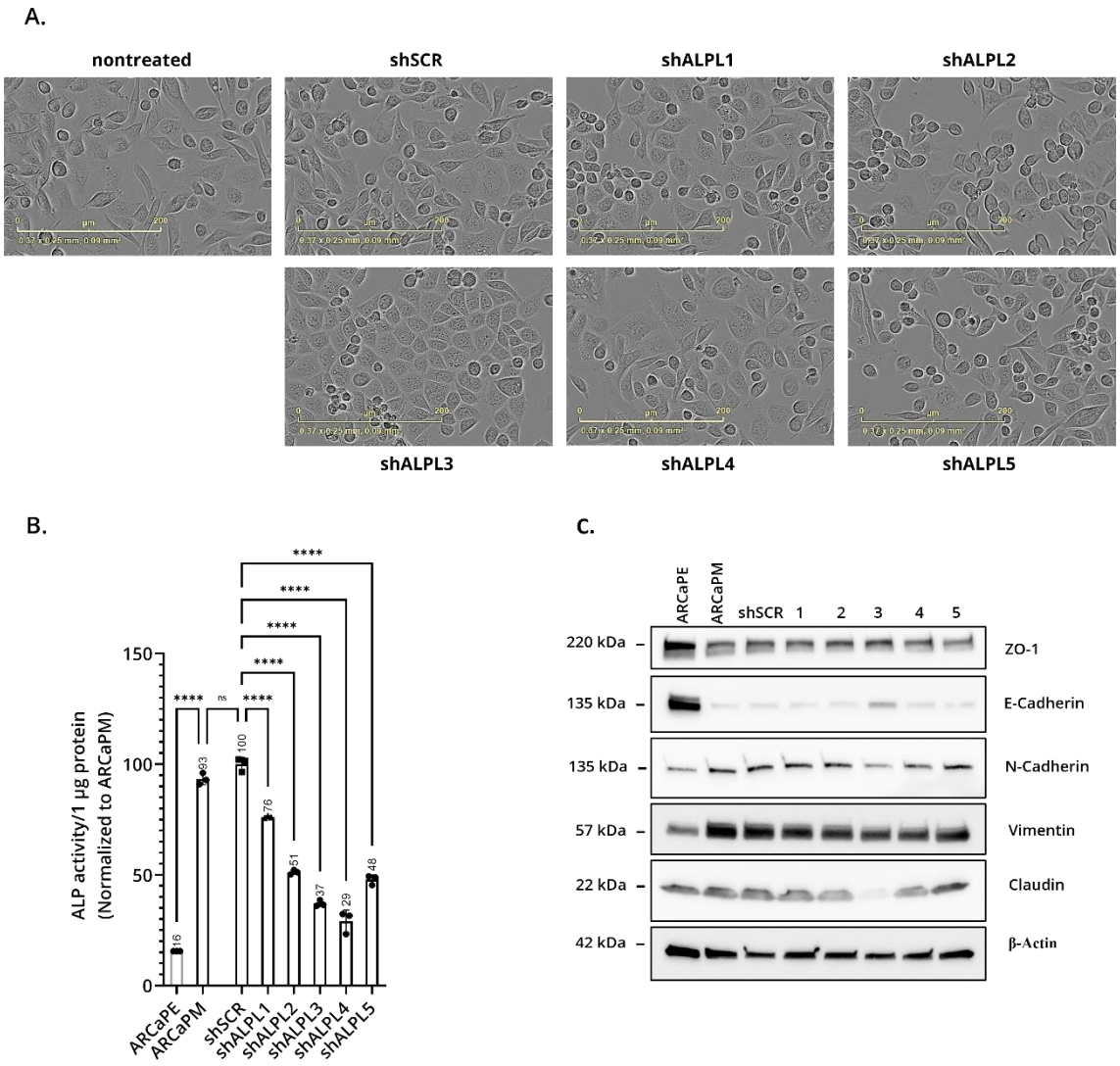



Figure 6.1 ALPL knockdown results in epithelial like morphology in ARCaPM cells

ARCaPM cells were transduced with lentiviral particles of control (shSCR) and ALPL-targeting shRNA(shALPL1-5). (A) 72 h after transduction cellular morphology was imaged using the IncuCyte (Essens Bioscience) at 20X objectives. (B) ALPL activity level was measured 72 h after transduction using a fluorogenic substrate. Data shows mean ± S. D. (C) Immunoblotting of lysates from ARCaPM cells for EMT markers. β-Actin was used as loading control.

*One-way ANOVA, with Tukey's multiple comparisons test. Alpha 0.05; ns P > 0.05, * P ≤ 0.05, ** P ≤ 0.01, *** P ≤ 0.001, **** P ≤ 0.0001*

### 6.3.2 Effect of ALPL knockdown on the UPR

Next, I investigated the effect of ALPL knockdown on the UPR markers. No significant effect was observed on cell death after 72 h (Figure 6.2-A). FAM8A1 level was elevated and HERP1 was decreased in response to *ALPL* knockdown with shALPL2 and shALPL3 (Figure 6.2-B), suggesting involvement of the ATF6 and IRE1 arms, and the ERAD pathway.

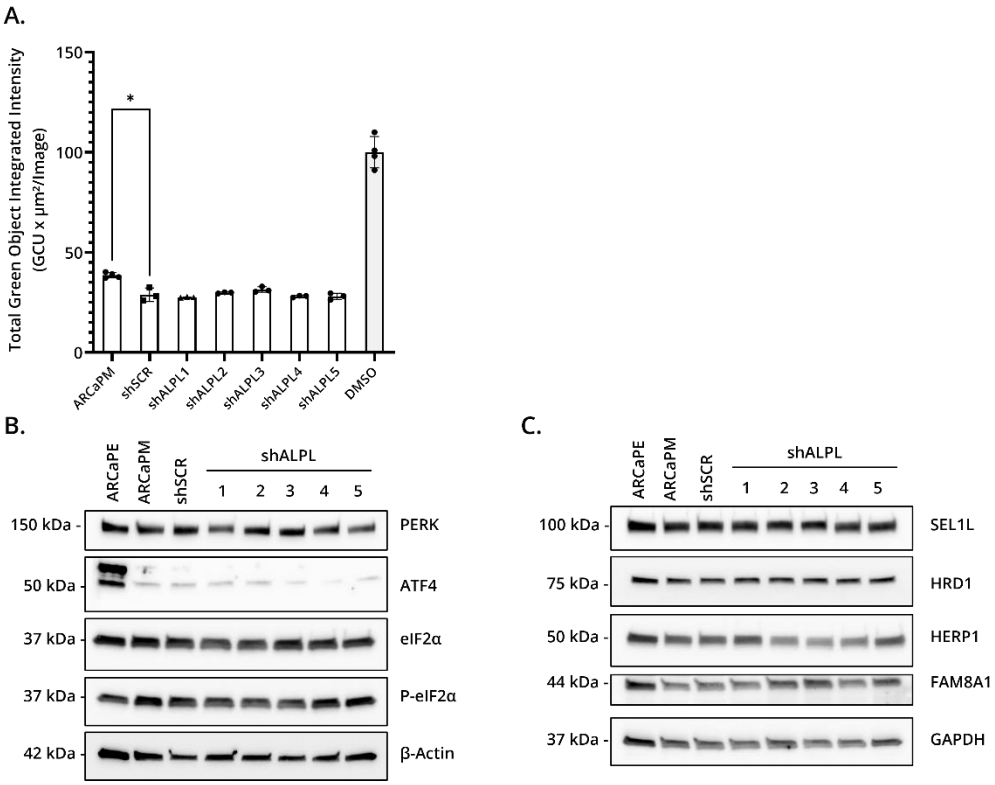



Figure 6.2 Markers of different arms of the UPR in response to ALPL knockdown in ARCaPM cells

(A) Cell death was measured in ARCaPM cells (72 h after lentiviral transduction for shRNA silencing) using SYTOX-green nucleic acid stain. Data shown as mean of triplicates ± standard deviation (SD) of fluorescence intensity of SYTOX, normalised to 10% DMSO treatment. (B) Immunoblotting of lysates from ARCaPM cells that were transduced with control shRNA and shRNAs targeting *ALPL* lentiviruses. ARCaPE cells grown to confluency was used as control for epithelial characteristics. Blots were analysed using anti-PERK, anti-ATF4, anti-eIF2α, anti-Phospho-eIF2α, anti-SEL1L, anti-HRD1, anti-HERP1, anti-FAM8A1 and anti-β-Actin antibodies. β-Actin and GAPDH were used as loading control.

*One-way ANOVA, with Tukey's multiple comparisons test. Alpha 0.05; ns $P > 0.05$, * $P \leq 0.05$, ** $P \leq 0.01$, *** $P \leq 0.001$, **** $P \leq 0.0001$*

### 6.3.3 RNA-Seq

Previous studies have found that, tumour-derived alkaline phosphatase controls epithelial plasticity in metastatic prostate cancer [438]. In previous chapters I have shown that inhibition of the IRE1 pathway with 4μ8C and PERK pathway with GSK2606414 increased ALP activity in ARCaPM cells whereas ER stress activation with tunicamycin, thapsigargin or growth in hypoxia decreased the levels of ALP activity.

In order to investigate the interplay between ALPL, EMT and the UPR, and the potential pathways affected by ALPL, I checked the transcriptomic profiling of ARCaPM cells after silencing of ALPL. As different shRNAs exhibited different levels of response, I validated the effect of ALPL knockdown by transient transfection of SMARTpool siALPL (a mixture of 4 siRNA). Similar to the shRNAs, transient transfection with siRNA targeting ALPL resulted in a tightly clustered, cobblestone-like appearance of ARCaPE like morphology in ARCaPM cells and a significant reduction in ALP activity (Figure 6.3). Similar to shRNA knockdown, immunoblotting after siRNA knockdown revealed a switch from mesenchymal to epithelial markers, with an increase in ZO-1 and E-Cadherin; and a decrease in the N-Cadherin, compared to siCTRL.

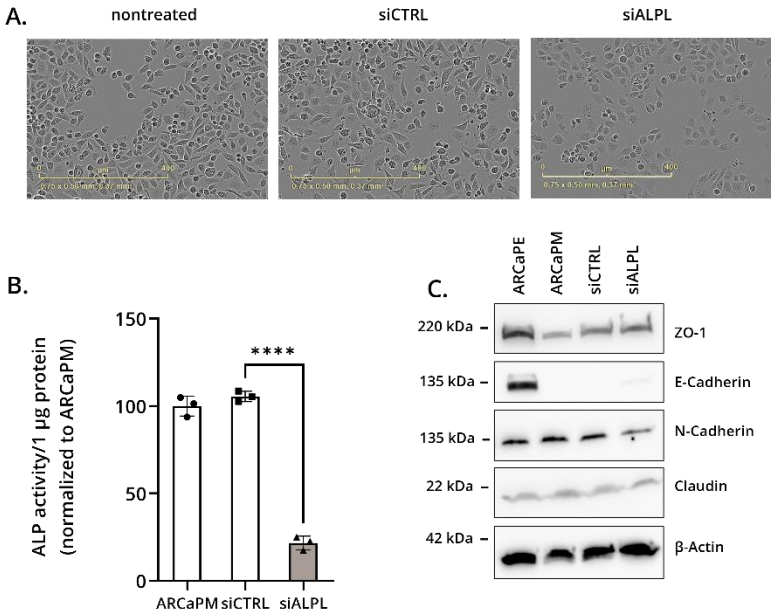



Figure 6.3 ALPL knockdown with siRNA results in epithelial like morphology in ARCaPM cells

(A) ARCaPM cells were transiently transfected with control siRNA or siRNA targeting ALPL. 72 h after transduction cellular morphology was imaged using the IncuCyte (Essens Bioscience) at 10X objectives. (B) ALPL activity level was measured 72 h after transduction using a fluorogenic substrate. Data shows mean ± S. D. (C) Immunoblotting of lysates from ARCaPM cells for EMT markers. β-Actin was used as loading control. siCTRL denote non-targeting control pool and siALPL denote ALPL-targeting siRNA pool.

*One-way ANOVA, with Tukey's multiple comparisons test. Alpha 0.05; ns P > 0.05, * P ≤ 0.05, ** P ≤ 0.01, *** P ≤ 0.001, **** P ≤ 0.0001*

Then, I prepared samples for RNA-Seq. A heat-map of top 50 significantly differed genes is shown in Figure 6.4. Hierarchical clustering of the samples show consistency between control group and siALPL treatment. This is further supported in distance matrix of the samples and Principal Component Analysis (PCA) in Supplementary Figure 8.3 and Figure 8.4. The volcano plot in Figure 6.5 represent the differential expression analysis with the significantly downregulated genes on the upper left, and significantly upregulated genes in the upper right of the plot. TPM3, TPM4, DDX3, EEF1A1, FAM120A and PMEPA1 are the most significantly downregulated genes in ALPL silenced samples. The transcription factor HMGA2, LMNB1, CDK6 are among the most significantly

upregulated genes in siALPL group. ALPL gene did not appear on the list of significantly changed genes; however, normalised counts for ALPL and UPR related genes are shown in Figure 6.6. ALPL was downregulated in siALPL samples, with a value of $p \leq 0.05$. Gene ontology enrichment analysis was done using an online software (ShinyGO v0.741, [483]). The remaining 13,551 genes that were not ranked among the significant genes were used as background. The pathways are sorted based on the number of genes annotated to a pathway, however, the generic pathways of cell biology are not described here. GO analysis showed enrichment of pathways involving mitochondrial genes including COX1 (mitochondrially encoded cytochrome c oxidase I), MT-ND4 (mitochondrially encoded NADH:ubiquinone oxidoreductase core subunit 4) and CYB (cytochrome b). The next pathway to follow the mitochondrial pathways was Oxydative phosphorylation. With 12 genes annotated, translation was also among the pathways that were enriched in RNA-Seq.

Two of the miRNA transport pathway genes, namely Y-box-binding protein 1 (YBX1) and heterogeneous nuclear ribonucleoproteins A2/B1 (HRNRPA2B1), were overrepresented in the GO analysis, bringing MiRNA transport pathway in significance.

The most significantly differed genes contained many ribosomal protein encoding genes (RPLs), which dominated most of the pathways in GO analysis. Repeating GO enrichment analysis after removing those genes from the significant gene list revealed muscle filament sliding, actin-myosin filament sliding and actin filament organization pathways among the most significantly represented pathways Table 8.23.

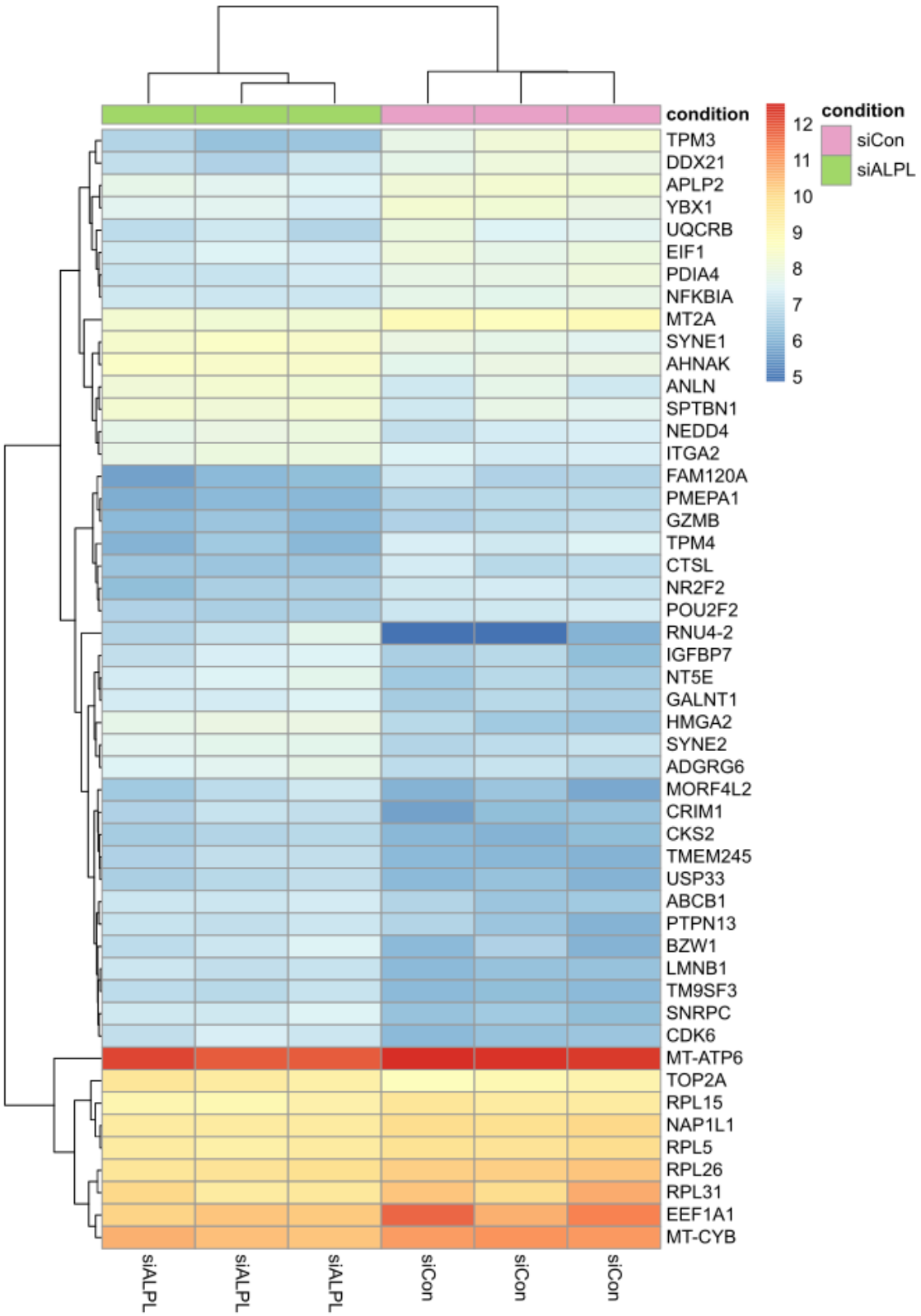



Figure 6.4 mRNA profiling of ALPL knockdown ARCaPM cells

The results of DESeq2 differential expression analysis in ascending order of adjusted p value (padj). The top 50 (i.e., most significant) genes are shown in this heatmap. Samples are clustered

hierarchically, and the legend shows the groups that were compared against each other for differential expression.

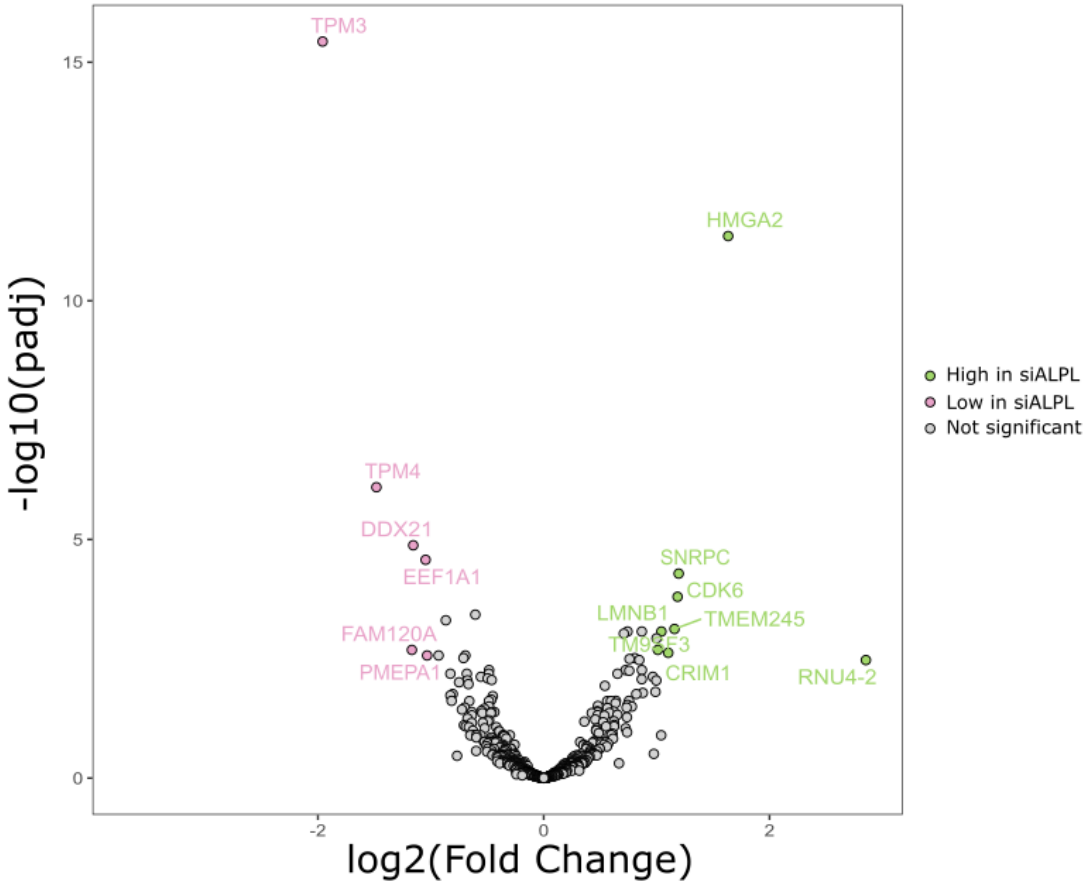



Figure 6.5 Volcano plot of the most differentially expressed genes

The volcano plot shows the results of the differential expression analysis as an intuitive visualisation. On the y axis is the negative logarithm (log10) of the adjusted p value and on the x axis is the log2 fold change. Hence, we are looking at significantly downregulated genes in the upper left quadrant and significantly upregulated genes at the upper right quadrant of this plot.

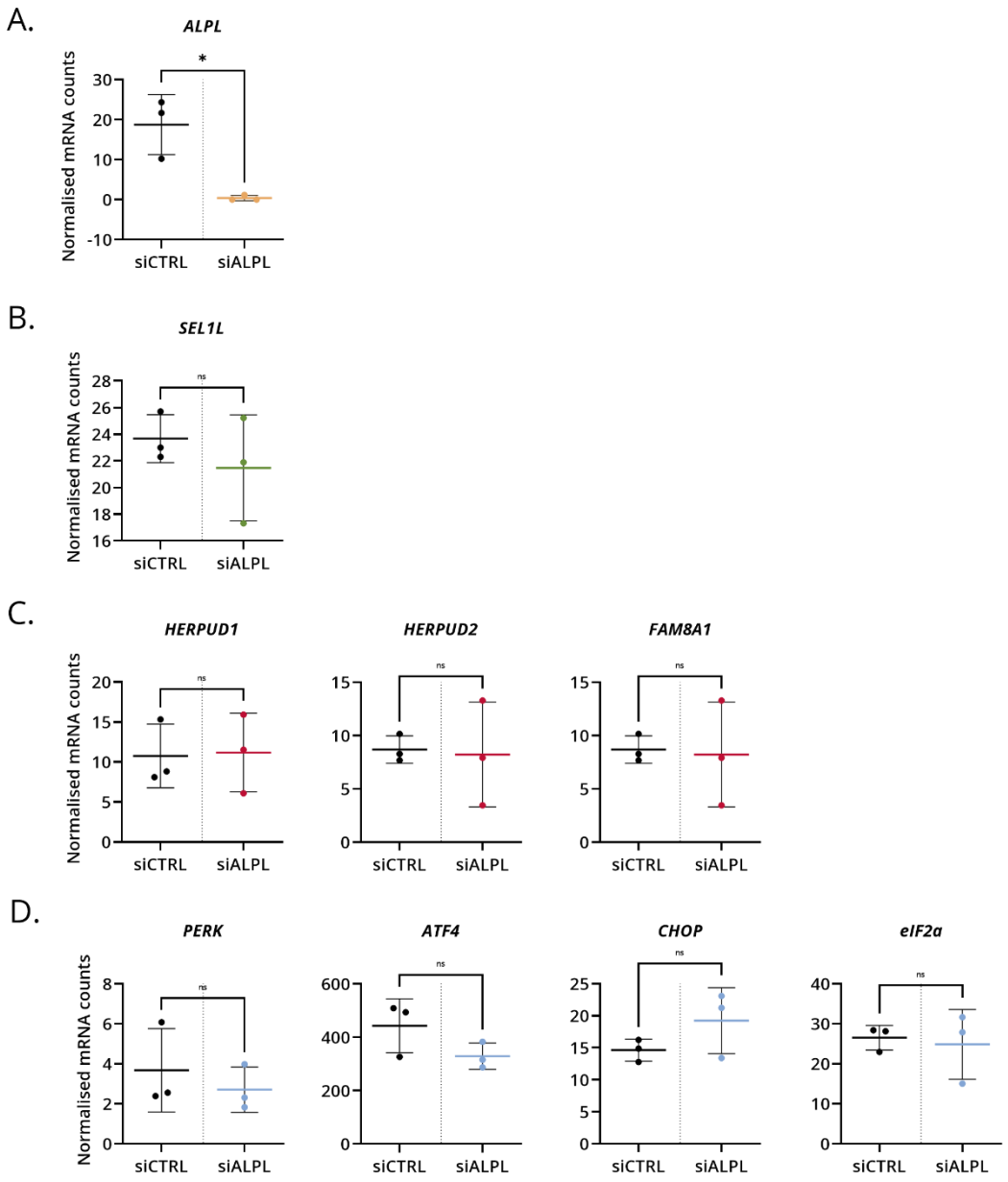



Figure 6.6 Normalised mRNA counts for ALPL and markers of the UPR

Normalised mRNA counts of (A) ALPL, (B) ATF6 pathway gene SEL1L, (C) ATF6 and IRE1 pathway genes, and (D) PERK pathway related genes and the genes.

*Unpaired t-test, Alpha 0.05; ns P > 0.05, * P ≤ 0.05, ** P ≤ 0.01, *** P ≤ 0.001, **** P ≤ 0.0001)*

## 6.4 Discussion

The work of this chapter has shown that knockdown of the alkaline phosphatase decreases the level of HERP1 and increases FAM8A1 levels; and induces changes in different pathways.

Besides maintaining homeostasis in response to ER stress, the UPR also functions to regulate cellular differentiation and maturation in the players of the skeletal system, namely osteoblasts, chondrocytes, and osteoclasts. ER stress functions as an internal regulator for cells in determining when to promote the expression of a particular set of genes during differentiation. A previous study by Rao *et al.* has identified a role for tumour derived ALPL in EMT [438]. Increased ALPL correlated with a mesenchymal phenotype and silencing of ALPL in mesenchymal cells resulted in epithelial transformation. The cells began to express epithelial markers, like CDH1, and the expression level of mesenchymal markers decreased. The changes in mRNA and protein EMT markers reflect the morphological changes. Decreased ALPL levels transformed the spindle-like phenotype of ARCaPM cells to cobblestone like morphology, similar to ARCaPE. In my work so far, inhibition of the IRE1 and PERK arms of the UPR resulted in increased alkaline phosphatase activity. Elevated ER stress promoted expression of mesenchymal markers, although the overall effect was decreased migration. The effect of ER stress inducers was reversed, or at least restored, when IRE1 or PERK arm was inhibited. Whether ALPL regulated the UPR was unclear, and no study has investigated if there was a feedback regulation between UPR and ALPL.

Silencing of ALPL in ARCaPM by lentiviral transduction transformed them to an ARCaPE-like phenotype (Figure 6.1-A), increased E-Cadherin levels and decreased N-Cadherin levels (Figure 6.1-B). Among the UPR related proteins,

HERP1 levels, an ER stress responsive protein, decreased with different ALPL shRNAs (Figure 6.2-C). Surprisingly, the level of FAM8A1 increased in the samples which HERP1 was decreased (Figure 6.2-C). Both HERP and FAM8A1 act as cofactors for the HRD1 complex, the key mediator of the ERAD. Previously FAM8A1 protein was proposed to facilitate the binding of Herp to Hrd1, an interaction that involves nucleation of Hrd1, SEL1L, and FAM8A1, essential for ERAD. My findings raise the possibility that these cofactors are in competition, or there is direct negative regulation between them.

Two different tropomyosin gene products TPM3 and TPM4 were ranked in the top three among the list of genes differentially expressed genes between siCTRL and siALPL groups (Figure 6.4). TPM3 was reduced by 3.9-fold and TPM4 was reduced by 2.8-fold in ALPL-depleted ARCaPM cells (calculated from *log2* fold change values in Table 8.21). Tropomyosins control the access and recruitment of other actin-binding proteins to the actin filaments, hence regulating their function, and enhancing the stiffness of actin filaments [484]. Different studies reported elevated tropomyosin expression during epithelial-mesenchymal transition of different cancer types including oesophageal cancer and hepatocellular carcinoma [485, 486]. This is consistent with the higher E-Cadherin levels seen in ARCaPM cells in response to ALPL knockdown (Figure 6.2-C and Figure 6.3-C).

HMGA2 (High Mobility Group AT-Hook 2) was the other top-ranked gene in the most over-represented gene list. HMGA2 encodes for a DNA-binding domain containing protein that acts as a transcriptional regulator. It has been reported to bind to the SNAI1 promoter and together with TGF-beta/Smad pathway regulate its expression for the induction of EMT [487]. Considering its role in

inducing EMT, it can be hypothesised that, HMGA2 might act as a downstream transcription regulatory factor for alkaline phosphatase for inducing EMT in PCa.

ALPL was not listed among the significantly different genes as the gene is filtered out in the analysis workflow. This was due to relatively low expression levels of it compared to the other genes on the list. However, the normalised gene counts from the RNA-seq show a significant reduction in siALPL, confirming robust knockdown (Figure 6.6). The relatively low expression is also evidenced by qRT-PCR of ALPL with a mean CT value around 31.07 for ARCaPM while the mean CT of the housekeeping gene GAPDH is 18.64 (three replicates of ARCaPM, with standard deviation of 0.23).

Gene set enrichment analysis for RNA-sequencing data with regard to control and ALPL knockdown revealed differentially expressed genes over-represented in pathways that involve protein targeting and localisation to ER, translation, and cytoskeleton binding (Table 8.22 and Table 8.23).

GO analysis revealed the most significantly enriched pathways as those related to mitochondria and oxidative phosphorylation. A recent study by Zheng *et al.* identified the ALPL (tissue nonspecific alkaline phosphatase) protein as a regulator of mitochondrial respiration and ATP synthesis inside bone and muscle progenitor cells [488]. Elevated mitochondrial oxidative phosphorylation has been shown to promote osteogenic differentiation by promoting β-catenin acetylation in bone marrow stromal cells [489]. It is possible that alkaline phosphatase regulates osteomimicry in cancer cells that are not bone related.

MiRNA transport pathway proteins were also enriched in the GO analysis, out of three genes that are listed in this pathway two of them appeared on the significantly different genes list. Previous work by Rao *et al.* identified six

different miRNAs that were significantly differently expressed in metastatic samples *as well as* came up as hits in functional screens in PC3 cells [490]. In another study, miRNA-15b promoted osteoblast differentiation in rat osteoprogenitor cells [491]. Further studies are required to investigate if there was a feedback regulation between ALPL and miRNAs.

Three ribosomal binding proteins RPL37, RPL6 and RPL5 that are involved in translation, were elevated when ALPL was silenced. ALPL can serve as key switch for PERK activation.

Considering the function of alkaline phosphatase as an enzyme that hydrolyse organic pyrophosphate esters and release inorganic pyrophosphate, it is unclear how ALPL relates to UPR and changes in EMT related genes. Studies have reported changes in ALPL with EMT; however, how ALPL changes EMT is not clearly investigated. For example, ALP levels increase in response to somatic cell reprograming to induced pluripotent stem cells [492].

One possible mechanism through which ALPL can EMT is through adenosinergic signalling, which involves the internalisation of adenosine from the extracellular environment to act as signalling molecule [493]. The importance of adenosine signalling in tumour microenvironment and its potential in different therapy approaches has been shown in different cancers [494]. One study has shown that ecto-5′-nucleotidase (NT5E), which catalyses the conversion of ATP to adenosine, promotes EMT in gastric cancer by activating RICS/RhoA signalling and promoting β-Catenin pathway [495]. In addition to this, another study has reported that NT5E acts redundantly with ALPL, as well as PAP (prostatic acid phosphatase), other ectonucleotidase that hydrolyse AMP to adenosine [496]. As NT5E came up as a differentially expressed gene after ALPL knockdown (Figure

6.4), further investigation is needed to check if ALPL induces EMT through similar pathway.

Another mechanism by which ALPL is linked to transcriptional regulation of genes related to EMT or the UPR is through activation of AMP-activated protein kinase (AMPK). ALP is shown to mediate osteogenesis by activation of AMPK as a result of hydrolysis of inorganic pyrophosphate [497]. Consequently, AMPK phosphorylate RUNX2 on its DNA binding domain, and promote translation of osteoblast differentiation genes [498]. Similarly, ALP activity can possibly regulate DNA binding of transcription factors other than RUNX2, including HMG2 which was differentially expressed after ALPL knockdown. It is otherwise challenging to explain how ALP as an enzyme might be acting upon pyrophosphate and act on cellular behaviour.

All these potential mechanisms that potentially explain ALPL activity to mostly EMT need further validation in ARCaPM cells. Due to limited time and resources, the differential expression from RNA-Seq could not be further validated using other techniques such as qPCR and western blotting. Overall, this chapter has shown that alkaline phosphatase is involved in different pathways beyond those related to bone, including the UPR and EMT, providing further evidence for a key role for ALPL in prostate cancer bone metastasis.

# 7

# Overall Discussion and Limitations

Taken together, my thesis suggests that the UPR components are reduced in osteoblastic PCa cells, and that inhibition of the UPR increases ALPL activity. PERK and IRE-1 seem to be the most important pathways (Chapter 3). The UPR may modulate prostate cancer bone disease, with ER stress reducing osteolytic factors, mediated by the PERK pathway (Chapter 4). Inducing ER stress *in vitro* using tunicamycin, thapsigargin, or culturing in hypoxia decreased ARCaPM migration due to cytotoxic effects, however, elevated UPR correlated with increased mesenchymal protein expression, with IRE1 and PERK pathways most likely to be involved (Chapter 5). Finally, alkaline phosphatase might act as the key factor that is involved in osteogenic potential and mesenchymal

characteristics of PCa cells, and both the IRE1 and PERK arms of the UPR have the potential to control ALP activity (Chapter 6).

Therapeutic efforts in prostate cancer have focused on the tumour itself, although the majority of PCa fatalities occur as a result of metastasis, mainly to the skeleton. The studies that linked the UPR to PCa have been discussed throughout this thesis. Several studies have connected UPR to bone-related processes or to EMT; however, the interaction between UPR, prostate cancer, and bone metastases has never been investigated. Given the importance of the UPR in PCa and the fact that bone metastasis is lethal, my study aimed to establish the involvement of the UPR in PCa bone metastasis.

Overall, my thesis can explain the role of the UPR in prostate cancer bone metastasis in the following ways:

During the early stages of cancer development, cells multiply quickly to increase cell numbers before undergoing the differentiation phase. After the establishment of the primary tumour, cancer cells start expressing different markers that begin to allow their spread to diverse secondary sites under the influence of specific stimuli. In the case of prostate cancer bone metastasis, when cells acquire differentiation signals, they become committed and begin to cease proliferating while also expressing early markers of osteoblast differentiation, including *RUNX2* and *SPARC*. This is correlated with that ARCaPE express *RUNX2* and *SPARC* at a high level but are not metastatic (*Section 3.3.1*, Figure 3.1).

The commitment for differentiation into a different cell type (or displaying characteristics yet not complete differentiation), essentially requires increased demand for the production of proteins required to initiate the transcriptional cascade for different lineages. At this stage, cells need to increase their protein

folding capacity to ensure correct folding of the nascent proteins, which involves elevation of the UPR. The three sensors of the stress need to balance the two different responses from the UPR, and ensure that pro-survival UPR is activated, instead of pro-apoptotic cascades. The proteins needed for correct folding of the nascent proteins, including the chaperones and the proteins involved in posttranslational modifications increase, while ERAD may be compensated at the risk of elevated unfolded and/or misfolded proteins. Here, decreased HERP levels may help to keep the activity of Hrd1 complex at minimal levels to maintain the unfolded proteins inside the ER, and further stimulate pathways required for correct folding. This hypothesis may correlate with the findings from *Section 3.3.2*, Figure 3.6. This is followed by EMT of PCa cells, which can be explained with two alternative mechanisms according to the findings from this study and the previously established gene interactions:

After the commitment for the osteoblast differentiation process (or osteomimicry), PCa cells express markers such as collagen type I and ALP, as well as osterix, osteopontin, osteonectin, and osteocalcin. PCa cells become osteomimetic, capable of mineral depositing in the extracellular matrix as a result of this successive upregulation (supported in Figure 3.2, Figure 3.3, Figure 3.4 and Figure 3.5). Elevated ALP can induce EMT in ARCaPM cells [438]. One possible explanation for ALP to induce EMT might be through mediating the transcriptional regulator HMGA2, which was differentially expressed after ALPL silencing which is shown in Figure 6.4, and discussed in *Section 6.4*.

Alternatively, activation of the PERK pathway as a result of increased UPR may account for EMT. PERK pathway activation induces ATF4 expression, which then induces *RANKL* expression through binding to its promoter. RANKL secreted by secondary tumours in bone leads to increased bone resorption which

then triggers PCa bone metastasis and drives the vicious cycle of bone turnover. Secreted RANKL has been shown to induce EMT in ARCaPE cells [242]. My thesis links the UPR to RANKL in *Section 4.3.2*, Figure 4.5, and hence can help to explain the link between UPR and bone metastatic potential in prostate cancer cells. Moreover, the results from *Chapter 5* indicate a role for the PERK arm of the UPR in migration capacity of ARCaPM cells (Figure 5.10).

Although this scenario is proposed based on findings from ARCaP cells, which have androgen repressed phenotype, it is still relevant to prostate cancer progression, as metastasis to secondary organs occurs after the CRPC.

One potential pathway that can link EMT, osteomimicry, and UPR is Wnt pathway; as it promotes EMT, induces osteoblast development in the bone, and the pathway can be inhibited by PERK arm of the UPR [499–501].

Despite the importance of my findings, there were several limitations in this study. First, it is difficult to trigger ER stress as it would happen under the physiological conditions, but this limitation is not unique to this study, as *in vitro* conditions differ from physiological conditions. The effect of tunicamycin or thapsigargin is very broad, and the changes induced may not truly represent physiological UPR. Nevertheless, considering the limitations and setting up the experiments accordingly, helps interpretation of the outcomes. For example, investigating whether the effect observed after tunicamycin or thapsigargin treatment are due to ER stress, UPR inhibitors are used in a systematic way, and are expected to restore the effect of tunicamycin, at least partially. Second, although there are specific inhibitors for each arm of the UPR, the chemicals that can trigger each arm of UPR are not abundant. This is partly reflecting the complex biology of the system: UPR is mediated by three different signal transducers, that can act collaboratively, which allows compensation between

different arms. For example, hypoxia is known to activate the PERK arm of the UPR. However, inhibiting PERK under hypoxic conditions results in compensation by the IRE1 arm. Although this might seem a limitation, it can also be regarded as an advantage. Most molecular biology approaches involve perturbation of a pathway with a compound, silencing or knockout of a gene, or restricting growth conditions. Although this approach helps the study of a specific gene or protein, a disadvantage is that the approach used in a particular study also has an effect on many more pathways, which are often ignored. However, the UPR is a well investigated pathway, and the indirect effect of inhibiting one arm can often be observed. For example, in Figure 5.12 the effect of inhibiting PERK pathway when it would otherwise be activated is compensated for by the IRE1 arm, which can be seen by the levels of XBP1 splicing.

The UPR is a mechanism by which the cells can deal with the stress of large number of proteins being abnormally produced. Increased cell proliferation is followed by elevated demand for protein production within the cancer cells while several factors create external stress in the tumour microenvironment. Cancer cells might be producing lots of proteins that are potentially not folded properly or are unfolded as they fail to fold into a quaternary structure. The UPR is an adaptive mechanism that not only degrades proteins, but also increases the folding capacity of the cells. In cancer cells, there is often increased transcription and translation, but then these translated proteins further require post-translational modifications (PTM). However, the capacity of the cells to be able to cope with all the PTM of the new peptides might not be sufficient. If a normal cell fails to deal with the high levels of unfolded proteins, it might undergo autophagy or apoptosis to ensure that the cell does not continue with misfolded proteins. Whereas cancer cells are upregulating the genes related to the UPR so

that they increase their capacity to fold the proteins adequately so that the excessive amount of translated will be modified to be functional.

Overall, my thesis research focused on the interdependency of three pathways known to be involved in PCa progression and metastasis: the UPR, EMT and osteomimicry.

Several proteosome inhibitors that have been shown to induce the UPR are in clinical use for targeting cancer. For example, bortezomib induce apoptosis in multiple myeloma cells through activation of the PERK arm of the UPR [502]. Other proteosome inhibitors used in multiple myeloma are Carfilzomib (Amgen) and Ixazomib (Takeda) [503, 504]. As the UPR has been shown to be elevated in different cancer types, inhibitors of the UPR potentially have anti-tumoral activity. For example, the IRE1$\alpha$ inhibitor MKC8866 decreased the proliferation of triple-negative breast cancer (TNBC) cells [505]. One study has shown that the PERK pathway was activated in an advanced mouse PCa model, as well as in human prostate cancer cells, and inhibition of eIF2$\alpha$ phosphorylation with ISRIB induced cell death [409]. MKC8866 has previously been used in mouse models. The effect of MKC8866 on prostate cancer xenografts has been studied alone and together with Enzalutamide in the Mills lab, and this study was reported with the tumour promoting role for IRE1$\alpha$-XBP1s pathway through c-MYC signalling [384]. GSK2606414 is a commonly used PERK inhibitor both in the concept of ER stress and in cancer. However it was shown to inhibit RIPK1 at comparable potency with the actual RIPK1 inhibitor [405]. Although the use of GSK2606414 is limited due to its off-target effects, a recently discovered small-molecule inhibitor of PERK signalling selectively inhibited colorectal cancer viability [506]. The effect of chemotherapeutics on the UPR activation is followed

by EMT induction mediated by upregulation of SNAI1 and ZEB1 gene expression [507].

During the course of osteogenic differentiation, changes in the UPR occurred earlier, before the formation of mineral crystals. Inhibition of the arms of the UPR increased alkaline phosphatase activity. Alkaline phosphatase activity was not further increased in osteogenic differentiation medium, suggesting that the UPR is upstream of the factors controlling the differentiation. Whether the UPR is a cause, or a consequence of metastasis (or both) is not yet clear. In order to investigate whether the UPR is a consequence of metastasis, in a migration experiment setup, it might be possible to collect pre-invading and invaded cells and compare whether the UPR is different, but this will be technically challenging as it is difficult to provide a chronic UPR without causing cell death.

In addition to the degree of the stress put on the cells and the use of these drugs, the other important thing is the temporal dynamics of the stress. Patients do not develop metastasis overnight, with the kinetics and dynamics of metastasis relatively slow in comparison to *in vitro* experimental systems. So, it is a challenge to recapitulate all of this *in vitro*. Bone metastases are hypoxic compared to normal tissues. While there are elements of hypoxia in the normal prostate gland and in prostate cancer, the metastases will likely be more hypoxic. However, interestingly my studies found distinct UPR responses to hypoxia as compared to pharmacological ER stressors, indicating the involvement of multiple pathways and responses.

The UPR is elevated in epithelial ARCaPE cells at baseline and ER stress impaired metastatic behaviour in ARCaPM cells. Orthotopic, intratibial bone metastases in mouse models could be used to investigate the physiological relevance of the UPR to prostate cancer bone metastasis. Cancer cells can be

implanted in mice after genetically silencing individual arms of the UPR to investigate the contribution of each arm to metastatic ability of the prostate to bone site. The mice could be treated with UPR inhibitors after engraftment of cancer cells to investigate the impact of inhibitors on bone metastatic progression. *In vivo* experiments could help gain a better understanding as to whether altered UPR is a driver of invasion and metastasis in prostate cells or if this alteration is a consequence of increased stress when prostate cells are seeded in the bone niche.

Culturing conditions of DVL3-SCM cells were very restrictive. The medium contains several important components, that can interfere with the phenotype studied. For example, leukaemia inhibitory factor is an osteoblastic differentiation factor [508]. However, it is not clear if any of these components are dispensable, or otherwise sufficient for their differentiation from parental DVL3 cells. The parental DVL3 cells have lower ALPL compared to DVL3-SCM cells. Understanding the mechanism through which SCM cells acquire the characteristics that make them different from parental cell line DVL3 can help in understanding the essential factors underlying osteomimicry. To study this, a potential strategy would be to exclude some supplements from their media and to study the mesenchymal and osteoblastic characteristic of the cells. Alternatively, systematic addition of the individual components required for SCM cells to serum can help in understanding the differentiation of DVL3 cells to SCM characteristics to check whether DVL3 would gain the characteristics of SCM cells.

RUNX2 and SPARC are master transcription factors for osteoblast differentiation. They are elevated at the onset of the osteoblast lineage commitment, and then decrease in mature osteoblasts. *RUNX2* and *SPARC* mRNA levels were elevated in ARCaPE while their levels were not detectable in

ARCaPM. On the other hand, alkaline phosphatase has higher mRNA and activity levels in ARCaPM. Considering the expression profile of the key factors in osteoblast differentiation. ARCaPM may represent the terminal phase of osteoblast differentiation.

Overall, my studies have demonstrated that the UPR plays a functional role in bone metastatic prostate cancer cells, with involvement in EMT, migration and osteomimicry. While it was not possible to discern a specific mechanism, reflecting the complex signalling pathways of the UPR, and the crosstalk between EMT and osteomimicry, my studies open up a new avenue for future studies. The identification of key components of the UPR underlying the biology of prostate cancer bone metastasis will undoubtedly reveal new therapeutic targets or approaches for treatment of advanced prostate cancer.

# 8

# Appendix

Table 8.1 Compounds used to induce UPR

| *Compounds* | *Details* | *Stock Conc.* | *Dilution* | *Final Conc.* |
|---|---|---|---|---|
| *Tunicamycin* | Abcam, ab120296 | 10 mg/ml | 1:10000 to 1:100000 | 0.1-1 μg/ml |
| *Thapsigargin* | Christianson Lab | 1 mg/ml | 1:1000 to 1:20000 | 0.05-1 μg/ml |

Table 8.2 Inhibitors of the UPR

| *Inhibited pathway* | *Compound* | *Details* | *Stock Conc.* | *Dilution* | *Final Conc.* |
|---|---|---|---|---|---|
| *ATF6 pathway* | Ceapin-A7 | Merck, SML2330 | 10 mM | 1:10000 | 1 μM |
| *IRE1 pathway* | 4μ8C | Christianson Lab | 50 mM | 1:50000 | 1 μM |
| | MKC8866 | Mills Lab | 15.5 mM | 1:15500 | 1 μM |
| *PERK pathway* | GSK2606414 | Sigma-Aldrich, 516535 | 10 mM | 1:10000 | 1 μM |

# 8.1 Materials

## 8.1.1 Primers used for human cell line samples

Table 8.3 Primers of EMT markers in human cell line

| *Gene* | *Forward Primer (5' – 3')* | *Reverse Primer (5' – 3')* |
|---|---|---|
| *SNAI1* | CCCAATCGGAAGCCTAACTA | GGACAGAGTCCCAGATGAGC |
| *SNAI2* | CTGTAGGGACCGCCGTGT | CACAGTGATGGGGCTGTATG |
| *TWIST* | AGCTGAGCAAGATTCAGACCC | GCAGCTTGCCATCTTGGAGT |
| *CDH1* | AGGCCAAGCAGCAGTACATT | ATTCACATCCAGCACATCCA |
| *CDH2* | TGGGAATCCGAGGAATGG | TGCAGATCGGACCGGATACT |
| *ZEB1* | CCAGGGAGGAGCAGTGAAAG | CCCCAGGATTTCTTGCCCTT |
| *VIM* | CCTTGAACGCAAAGTGGAATC | GACATGCTGTTCCTGAATCTGAG |
| *KRT14* | GGCCTGCTGAGATCAAAGACT | TCTGCAGAAGGACATTGGCAT |

Table 8.4 Primers of the unfolded protein response in human cell lines

| *Gene* | *Forward Primer (5' – 3')* | *Reverse Primer (5' – 3')* |
|---|---|---|
| *sXBP1* | CTGAGTCCGAATCAGGTGCAG | ATCCATGGGGAGATGTTCTGG |
| *usXBP1* | CAGCACTCAGACTACGTGCA | ATCCATGGGGAGATGTTCTGG |
| *Total XBP1* | TGGCCGGGTCTGCTGAGTCCG | ATCCATGGGGAGATGTTCTGG |
| *ATF4* | GTTCTCCAGCGACAAGGCTA | ATCCTGCTTGCTGTTGTTGG |
| *BIP* | TGTTCAACCAATTATCAGCAAACTC | TTCTGCTGTATCCTCTTCACCAGT |
| *GRP4* | GAAACGGATGCCTGGTGG | GCCCCTTCTTCCTGGGTC |
| *HERP1* | TAGAGAAAAGGCGTCGGGAT | GTGTGCGTCAAAGTAGCCTT |
| *HERP1* | TGGATTGGACCTATTCAGCAGC | GCAGGTACATAACAACGGTGGC |
| *HERP2* | TTCCACAAGCACAAACTGACCA | CTGGGTTGGGTTGACATTTGAT |
| *SEL1L* | CAGGGCTATGAAGTGGCACAAA | TCGGTGCCAAACCCATAGAAAT |
| *FAM8A1* | AAAATGATGGTTGTGGCACTTA | TGTATCACATGTCACAACTCGAA |
| *HRD1* | TCTTCCTCAAA TGTTTCCACTG | TCGTCATCAGGATGGCATAA |
| *XBP1* | TTACGAGAGAAAACTCATGGC | GGGTCCAAGTTGTCCAGAATGC |
| *PGK* | AAGAACAACCAGATAACAAACAAC | GTGGCTCATAAGGACTACCG |

Table 8.5 Primers of osteogenic differentiation markers in human cell lines

| *Gene* | *Forward Primer (5' – 3')* | *Reverse Primer (5' – 3')* |
|---|---|---|
| *COL1A1* | GAACATCACCTACCACTGCA | GTTGGGATGGAGGGAGTTTA |
| *ALPL* | ACGTGGCTAAGAATGTCATC | CTGGTAGGCGATGTCCTT |
| *RANK* | TGCAGCTCAACAAGGACACA | AGGAAGGTACAGTTGGTCCAG |
| *RANKL* | CCAGGTTGTCTGCAGCGT | TGCAGTGAGTGCCATCTT |
| *RANKL* | TCGTTGGATCACAGCACATCA | TATGGGAACCAGATGGGATGTC |
| *OPG* | CAGTGTCTTTGGTCTCCTGCT | ACACAGGGTAACATCTATTCCACA |
| *OPG* | GAACCCCAGAGCGAAATACA | TATTCGCCACAAACTGAGCA |
| *PTHRP_TOTAL* | CGGTGTTCCTGCTGAGCTA | TGCGATCAGATGGTGAAGGA |
| *PTHRP_139* | CGGTGTTCCTGCTGAGCTA | CACAATCGATAGAGATAC |
| *PTHRP_141* | CGGTGTTCCTGCTGAGCTA | CAGAATCCTGCAATATGTCC |
| *PTHRP_173* | CGGTGTTCCTGCTGAGCTA | GAGATCATTAGTTGCATATG |
| *PTH1R* | CTCCGGGAACAAAAAGTGGAT | CTGAGACCTCGGTGTATGGTG |
| *PTHLH* | TCGAGGTTCAAAGGTTTGCCT | CAGGTTGGAGGCGAGTTGAA |
| *RUNX2* | CCCCACGACAACCGCACCAT | CAGTCCGGCCCACAAATC |
| *DKK1* | GGTATTCCAGAAGAACCACC | GAGAGCCTTTTCTCCTATGC |
| *CTNNB1* | CCCACTGGCCTCTGATAAAGG | ACGCAAAGGTGCATGATTTG |
| *SPARC* | GTGCAGAGGAAACCGAAGAG | TCATTGCTGCCACCTTCTC |

Table 8.6 Primers of housekeeping genes in human cell lines

| *Gene* | *Forward Primer (5' – 3')* | *Reverse Primer (5' – 3')* |
|---|---|---|
| *GAPDH* | AGCCACATCGCTCAGACAC | GCCCAATACGACCAAATCC |

Table 8.7 Primers for XBP1 splicing assay in human cell lines

| *Gene* | *Forward Primer (5' – 3')* | *Reverse Primer (5' – 3')* |
|---|---|---|
| *XBP1* | GAGTTAAGACAGCGCTTGGG | ACTGGGTCCAAGTTGTCCAG |
| *ACTB* | CTGAGCGTGGCTACTCCTTC | GGCATACAGGTCCTTCCTGA |

### 8.1.2 Primers used for mouse cell line samples

Table 8.8 Primers of EMT markers in mouse cell lines

| *Gene* | *Forward Primer (5' – 3')* | *Reverse Primer (5' – 3')* |
|---|---|---|
| *Snai1* | CTGCTTCGAGCCATAGAACTAAAG | GAGGGGAACTATTGCATAGTCTGT |
| *Snai2* | CACTCCACTCTCCTTTACC | CAGACTCCTCATGTTTATGC |
| *Twist1* | CTCGGACAAGCTGAGCAAGATT | ATTTTCTCCTTCTCTGGAAACA |
| *Twist2* | CAGTGACTTCTGTGCCCTCA | TGAGAGCCTTGGTCCAGTTT |
| *Zeb1* | TGGCAAGACAACGTGAAAGA | AACTGGGAAAATGCATCTGG |
| *Cdh1* | GTCTCCTCATGGCTTTGC | CTTTAGATGCCGCTTCAC |

Table 8.9 Primers of the unfolded protein response in mouse cell lines

| *Gene* | *Forward Primer (5' – 3')* | *Reverse Primer (5' – 3')* |
|---|---|---|
| *sXbp1* | CTGAGTCCGAATCAGGTGCAG | GTCCATGGGAAGATGTTCTGG |
| *usXbp1* | CAGCACTCAGACTATGTGCA | GTCCATGGGAAGATGTTCTGG |
| *Atf4* | GGGTTCTGTCTTCCACTCCA | AAGCAGCAGAGTCAGGCTTTC |
| *Chop* | CCACCACACCTGAAAGCAGAA | AGGTGAAAGGCAGGGACTCA |
| *Bip* | TTCAGCCAATTATCAGCAAACTCT | TTTTCTGATGTATCCTCTTCACCAGT |
| *Grp94* | AAGAATGAAGGAAAAACAGGACAAAA | CAAATGGAGAAGATTCCGCC |
| *Edem* | CTACCTGCGAAGAGGCCG | GTTCATGAGCTGCCCACTGA |

Table 8.10 Primers of osteogenic differentiation markers in mouse cell lines

| *Gene* | *Forward Primer (5' – 3')* | *Reverse Primer (5' – 3')* |
|---|---|---|
| *Runx2* | AAATGCCTCCGCTG TTATGAA | GCTCCGGCCCACAAATCT |
| *Col1A1* | CCTGAGTCAGCAGATTGAGAACA | CCAGTACTC TCCGCTCTTCCA |
| *Alp* | AACCCAGACACAAGCATTCC | GCCTTTGAGGTTTTTG GTCA |
| *Rankl* | GCAGAAGGAACTGCAACACA | GATGGTGAGGTGTGCAAATG |
| *Pth1r* | CAGGCGCAATGTGACAAGC | TTTCCCGGTGCCTTCTCTTTC |
| *Pthrp* | CAGTGGAGTGTCCTGGTATT | GATCTCCGCGATCAGATGGT |
| *Opg* | CTGCCTGGGAAGAAGATCAG | TTGTGAAGCTGTGCAGGAAC |

Table 8.11 Primers of housekeeping genes in mouse cell lines

| *Gene* | *Forward Primer (5' – 3')* | *Reverse Primer (5' – 3')* |
|---|---|---|
| *Gapdh* | GTTGTCTCCTGCGACTTCA | GGTGGTCCAGGGTTTCTTA |

Table 8.12 TaqMan primer list

| *Gene* | *Species* | *Reporter Dye* | *Assay ID* |
|---|---|---|---|
| *Dkk1* | Mouse | FAM | Mm00438422_m1 |
| *Gapdh* | Mouse | VIC | 4352339E |

Table 8.13 Primers for XBP1 splicing assay in mouse cell lines

| *Gene* | *Forward Primer (5' – 3')* | *Reverse Primer (5' – 3')* |
|---|---|---|
| *Xbp1* | GATCCTGACGAGGTTCCAGA | ACAGGGTCCAACTTGTCCAG |
| *Actb* | AGCCATGTACGTAGCCATCC | CTCTCAGCTGTGGTGGTGAA |

### 8.1.3 The antibodies used in this study

Table 8.14 Antibodies used for detection of the UPR

| *Antibody* | *Alternative name* | *Dilution* | *Source* | *Cat. No* | *Host* | *Antibody type* | *Reacts with mouse?* |
|---|---|---|---|---|---|---|---|
| *PERK (D11A8)* | | 1:1000 | Cell Signaling | 5683S | Rabbit | Monoclonal IgG | No |
| *ATF4* | CREB-2 | 1:1000 | Santa Cruz Biotechnology | sc-390063 | Rabbit | Polyclonal IgG | Yes |
| *CHOP* | | 1:1000 | Cell Signaling | 2895S | Mouse | Monoclonal IgG | Yes |
| *peIF2α* | Ser51 | 1:1000 | Abcam | ab4837 | Rabbit | Polyclonal IgG | Yes |
| *eIF2α* | | 1:1000 | Cell Signaling | 5324S | Rabbit | Monoclonal IgG | Yes |
| *Sel-1L* | | 1:2000 | Santa Cruz Biotechnology | sc-48081 | Goat | Polyclonal IgG | No |
| *HERP1* | Herpud1 | 1:10000 | Abcam | ab150424 | Rabbit | Monoclonal IgG | Yes |
| *ATF6* | | 1:500 | Abcam | ab122897 | Mouse | Monoclonal IgG | No |
| *FAM8A1* | | 1:10000 | Ron R. Kopito Lab | | Rabbit | - | |
| *HRD1* | Synoviolin | 1:2000 | Bethyl-Cambridge Bioscience | a302-946A-M | Rabbit | Polyclonal IgG | Yes |
| *β-Actin* | | 1:10000 | Sigma Aldrich | A5316 | Mouse | Monoclonal IgG | Yes |
| *IgG (mouse): HRP* | | 1:5000 | Cell Signaling | 7076s | Horse | ECL secondary | |
| *IgG (rabbit): HRP* | | 1:5000 | Cell Signaling | 7074s | Goat | ECL secondary | |
| *IgG (goat): HRP* | | 1:15000 | Santa Cruz Biotechnology | sc-2020 | Donkey | ECL secondary | |

Table 8.15 Antibodies for EMT markers

| *Antibody* | *Alternative name* | *Dilution* | *Source* | *Cat. No* | *Host* | *Antibody type* | *Reacts with mouse?* |
|---|---|---|---|---|---|---|---|
| *CDH1* | E-Cadherin | 1:1000 | Cell Signaling | 3195S | Rabbit | Monoclonal IgG | Yes |
| *CDH2* | N-Cadherin | 1:500 | BD | 610920 | Mouse | Monoclonal IgG | |
| *Vimentin* | | 1:1000 | Cell Signaling | 5741P | Rabbit | Monoclonal IgG | Yes |
| *ZO-1* | | 1:1000 | Cell Signaling | 8193P | Rabbit | Monoclonal IgG | No |
| *Claudin-1* | | 1:1000 | Cell Signaling | 4933P | Rabbit | Polyclonal | Yes |
| *GAPDH* | | 1:1000 | Abcam | 9484 | Mouse | Monoclonal IgG | Yes |
| *β-Actin* | | 1:10000 | Sigma Aldrich | A5316 | Mouse | Monoclonal IgG | Yes |
| *Hif-1α* | | 1:1000 | Abcam | ab243860 | Rabbit | Monoclonal IgG | No |
| *Hif-1β* | | 1:1000 | Abcam | ab239366 | Rabbit | Monoclonal IgG | Yes |

Table 8.16 Detection reagents

| *Detection Reagent* | *Company* | *Cat. No.* | *Signal Strength* |
|---|---|---|---|
| *Novex™ ECL Chemiluminescent Substrate Reagent Kit* | ThermoFisher | WP20005 | Moderate |
| *Clarity Western ECL Substrate* | Bio-rad | 1705060 | Strong |

### 8.1.4 Antibiotics

Table 8.17 Concentration of commonly used antibiotics in bacterial cultures

| *Antibiotics* | *Concentration* |
|---|---|
| *Ampicillin* | 100 µg/mL |
| *Kanamycin* | 50 µg/mL |

### 8.1.5 Target sequences for shRNAs and siRNAs

shRNAs were contained in pLKO.1 backbone system and were obtained from Sigma. The details of control shRNA and shRNA targeting ALPL are listed below:

Table 8.18 Vectors used for lentiviral packaging

| | *Details* | *Target sequence* |
|---|---|---|
| *shRNA Control Plasmid* | Sigma, Cat. SHC002 | no known mammalian genes |
| *shALPL1* | TRCN0000052003 | CCCACAATGTGGACTACCTAT |
| *shALPL2* | TRCN0000052004 | CGTGGCTAAGAATGTCATCAT |
| *shALPL3* | TRCN0000052005 | GCGCAAGAGACACTGAAATAT |
| *shALPL4* | TRCN0000359258 | ATGTCTCCATGGTGGACTATG |
| *shALPL5* | TRCN0000359332 | AGTATGAGAGTGACGAGAAAG |

Table 8.19 siRNAs used in this study

| | *Details* | *Target sequence* |
|---|---|---|
| *siCTRL* | non-targeting control | Dharmacon, D-001206-13-05 |
| *siALPL* | ON-TARGETplus siRNA | L-008658-00-0005 |

### 8.1.6 Sequences of the capture oligos, adaptor and the indexes used in RNA-seq

| *Capture oligonucleotide* | *Sequence* |
|---|---|
| ***poly-T20VN*** | CAGACGTGTCCTCTTCCGATCTNNNNNNNNNNTTTTTTTTTTTTTTTTTTTVN |

| *Illumina 5' adaptor* | *Sequence* |
|---|---|
| ***HZG885*** | /5phos/AGATCGGAAGAGCGTCGTGTAGGGAAAGAGTGTddC |

Table 8.20 RNA-Seq index list

| *NEB #* | *Index Number* | *Sequence* |
|---|---|---|
| *#E7607A* | NEBNext i5 Index05 | 5´-AATGATACGGCGACCACCGAGATCTACACAGGCGAAGACACTCTTTCCCTACACGACGCTCTTCCGATC*T-3´ |
| *#E7608A* | NEBNext i5 Index06 | 5´-AATGATACGGCGACCACCGAGATCTACACTAATCTTAACACTCTTTCCCTACACGACGCTCTTCCGATC*T-3´ |
| *#E7610A* | NEBNext i5 Index08 | 5´-AATGATACGGCGACCACCGAGATCTACACGTACTGACACACTCTTTCCCTACACGACGCTCTTCCGATC*T-3´ |
| *#E7617A* | NEBNext i7 Index07 | 5´-CAAGCAGAAGACGGCATACGAGATAGCTTCAGGTGACTGGAGTTCAGACGTGTGCTCTTCCGATC*T-3´ |
| *#E7618A* | NEBNext i7 Index08 | 5´-CAAGCAGAAGACGGCATACGAGATGCGCATTAGTGACTGGAGTTCAGACGTGTGCTCTTCCGATC*T-3´ |
| *#E7619A* | NEBNext i7 Index09 | 5´-CAAGCAGAAGACGGCATACGAGATCATAGCCGGTGACTGGAGTTCAGACGTGTGCTCTTCCGATC*T-3´ |
| *#E7620A* | NEBNext i7 Index10 | 5´-CAAGCAGAAGACGGCATACGAGATTTCGCGGAGTGACTGGAGTTCAGACGTGTGCTCTTCCGATC*T-3´ |
| *#E7621A* | NEBNext i7 Index11 | 5´-CAAGCAGAAGACGGCATACGAGATGCGCGAGAGTGACTGGAGTTCAGACGTGTGCTCTTCCGATC*T-3´ |
| *#E7622A* | NEBNext i7 Index12 | 5´-CAAGCAGAAGACGGCATACGAGATCTATCGCTGTGACTGGAGTTCAGACGTGTGCTCTTCCGATC*T-3´ |

## 8.2 Supplementary Data

### 8.2.1 Dkk1 amplification plot in DVL3 and DVL3-SCM cells

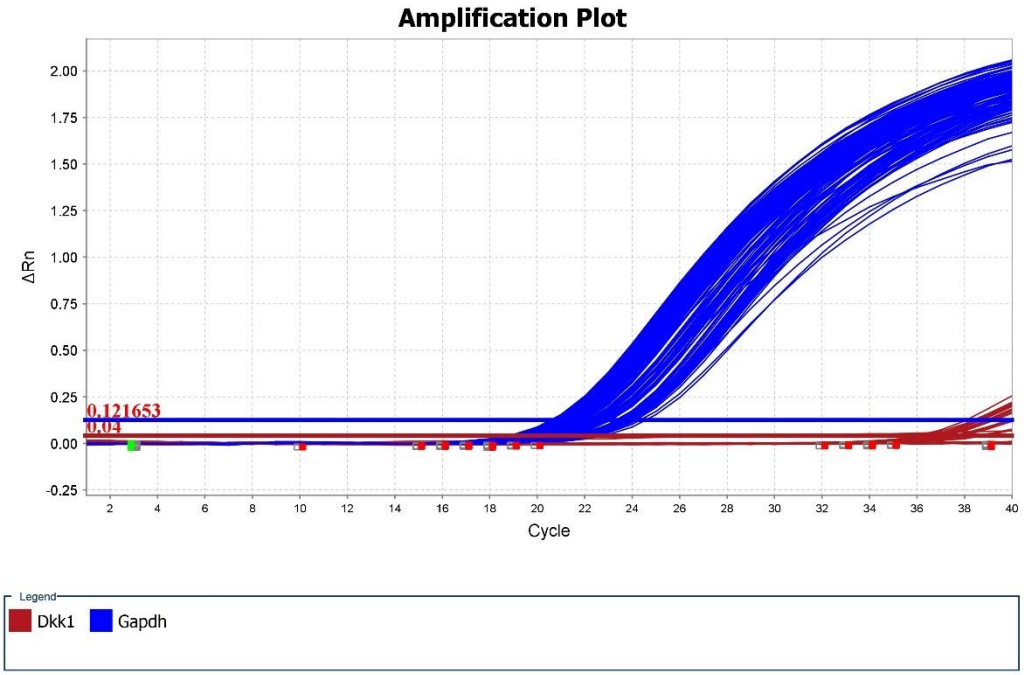



Figure 8.1 Amplification plot of Dkk1 and Gapdh in DVL3 and DVL3 SCM cells

Baseline-corrected normalised reporter (ΔRn) values of each sample plotted against cycle number on a continuous line.

- In the △Rn vs Cycle amplification plot, △Rn at each cycle is calculated with the following formula:
  ΔRn (cycle) = Rn (cycle) – Rn (baseline), where Rn = normalised reporter
- Normalised reporter (Rn) is calculated by Fluorescence signal from the reporter dye normalised to the fluorescence signal of the passive reference

### 8.2.2 Melt curves from qRT-PCR of SPARC in ARCaPM and ARCaPE

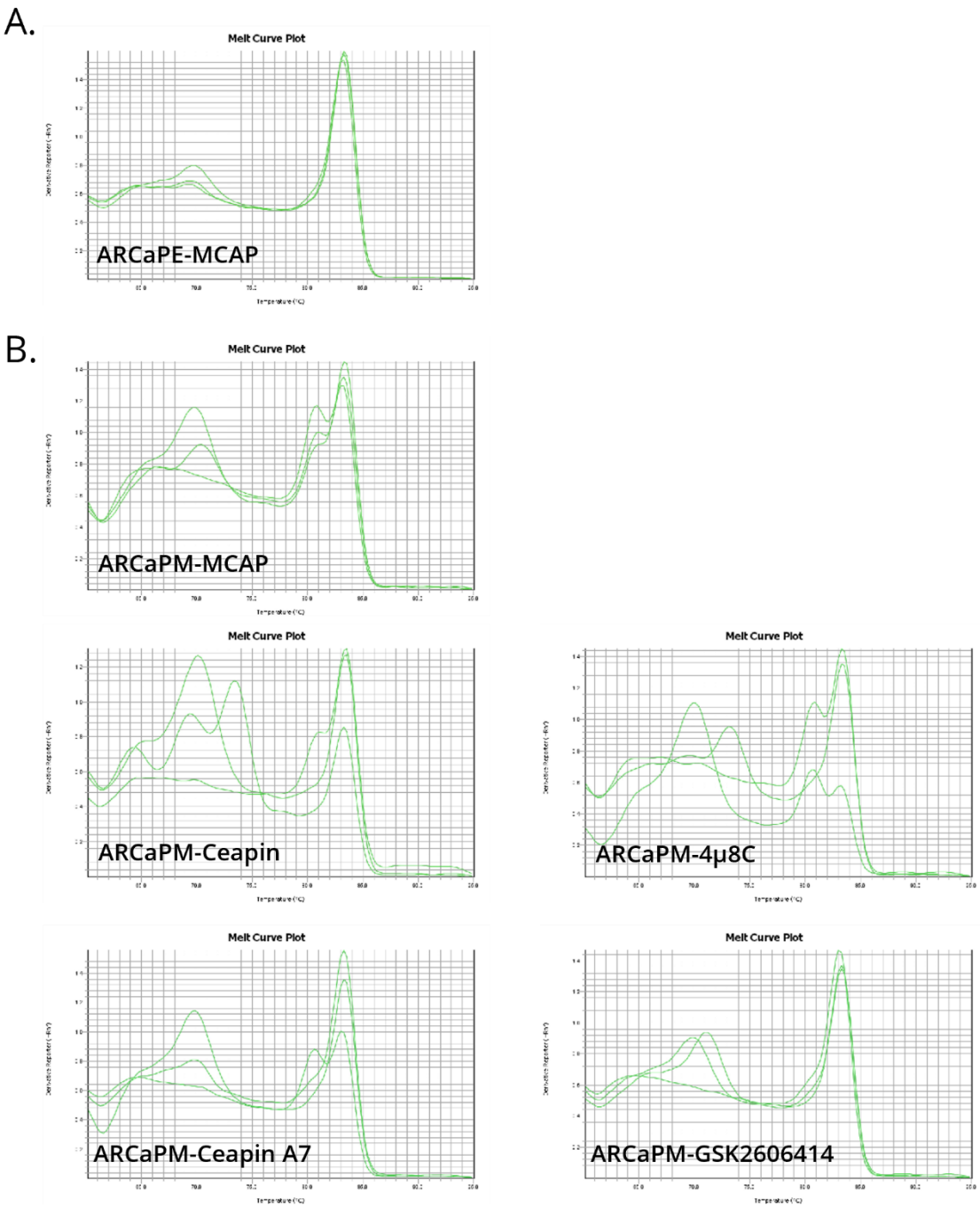



Figure 8.2 Melt curves from qRT-PCR of SPARC

(A) The amplicon from SPARC gene in ARCaPE cells produced a single peak in melt curve analysis while (B) the amplicon in ARCaPM cells revealed at least 2 peaks.

### 8.2.3 RNA-seq results

The following figures were generated by Dr. Srinivasa Rao.

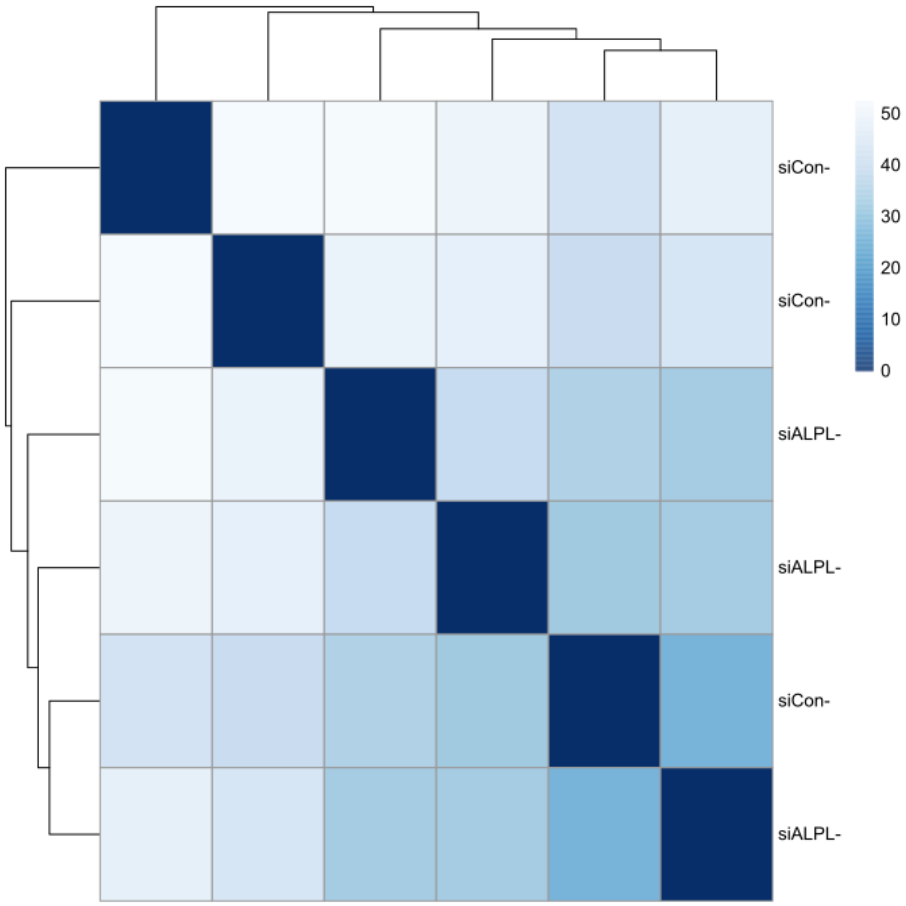



Figure 8.3 Distance matrix of samples

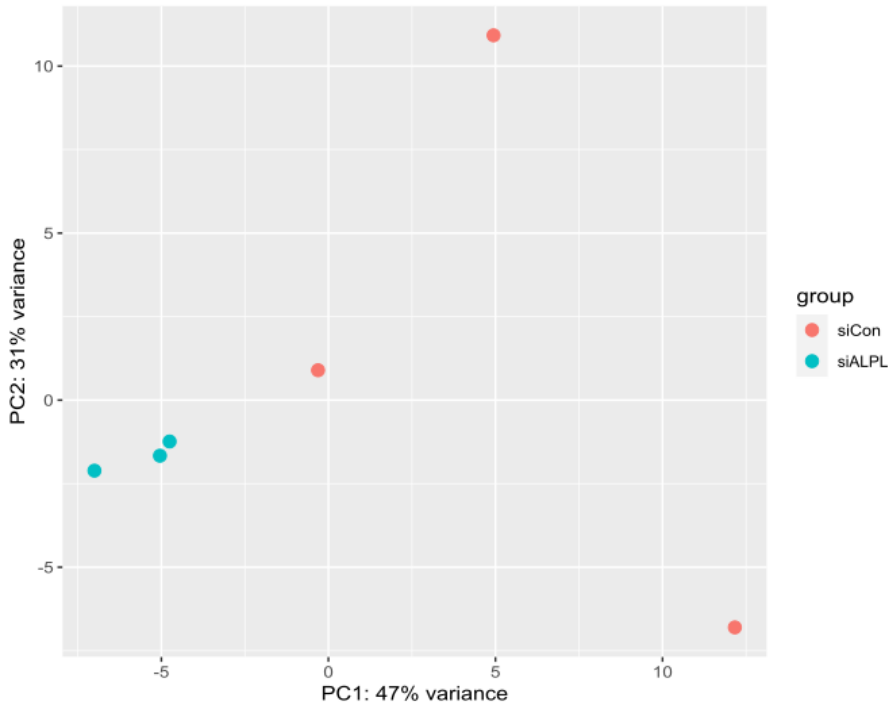



Figure 8.4 Principal component analysis of samples in RNA-seq

Table 8.21 List of most significantly differed genes with $P_{adjusted} \leq 0.05$

| *Gene* | *Log2 Fold Change* | *P value* | $P_{adjusted}$ |
|---|---|---|---|
| *TPM3* | -1.95822 | 5.42E-19 | 3.70E-16 |
| *HMGA2* | 1.633849 | 1.29E-14 | 4.40E-12 |
| *TPM4* | -1.48174 | 3.54E-09 | 8.05E-07 |
| *DDX21* | -1.15544 | 7.78E-08 | 1.33E-05 |
| *EEF1A1* | -1.04604 | 1.96E-07 | 2.67E-05 |
| *SNRPC* | 1.195665 | 4.57E-07 | 5.19E-05 |
| *CDK6* | 1.185896 | 1.63E-06 | 0.000158953 |
| *MT-CYB* | -0.60586 | 4.41E-06 | 0.000376039 |
| *PDIA4* | -0.86683 | 6.52E-06 | 0.000493922 |
| *TMEM245* | 1.158395 | 1.10E-05 | 0.000751452 |
| *SYNE1* | 0.742096 | 1.40E-05 | 0.000849539 |
| *SYNE2* | 0.868873 | 1.55E-05 | 0.000849539 |
| *LMNB1* | 1.042309 | 1.62E-05 | 0.000849539 |
| *AHNAK* | 0.709756 | 1.93E-05 | 0.000939998 |
| *NT5E* | 0.999583 | 2.60E-05 | 0.00118057 |
| *FAM120A* | -1.16763 | 4.95E-05 | 0.00206491 |
| *TM9SF3* | 1.011115 | 5.15E-05 | 0.00206491 |
| *CRIM1* | 1.103165 | 6.28E-05 | 0.002378325 |
| *PMEPA1* | -1.0329 | 8.31E-05 | 0.002699358 |
| *NR2F2* | -0.93106 | 7.62E-05 | 0.002699358 |
| *APLP2* | -0.69427 | 8.16E-05 | 0.002699358 |
| *YBX1* | -0.71038 | 9.96E-05 | 0.003059992 |
| *ANLN* | 0.805837 | 0.000103196 | 0.003059992 |
| *NEDD4* | 0.760489 | 0.000112467 | 0.003195937 |
| *GALNT1* | 0.846238 | 0.000126965 | 0.003372263 |
| *RNU4-2* | 2.853724 | 0.000128561 | 0.003372263 |
| *NAP1L1* | -0.48387 | 0.000229764 | 0.005454732 |
| *SPTBN1* | 0.725721 | 0.000231946 | 0.005454732 |
| *ABCB1* | 0.869455 | 0.00022659 | 0.005454732 |
| *ADGRG6* | 0.757533 | 0.000247955 | 0.005636837 |
| *RPL26* | -0.48595 | 0.000295464 | 0.006500213 |
| *UQCRB* | -0.82655 | 0.000315617 | 0.006512525 |
| *NFKBIA* | -0.68123 | 0.000307001 | 0.006512525 |
| *ITGA2* | 0.653846 | 0.000324671 | 0.006512525 |
| *MT2A* | -0.55672 | 0.000396641 | 0.007555389 |
| *CKS2* | 0.966938 | 0.000398818 | 0.007555389 |
| *RPL15* | -0.49619 | 0.000441999 | 0.00814712 |
| *PTPN13* | 0.868431 | 0.000472697 | 0.008483665 |
| *MT-ATP6* | -0.46065 | 0.000503773 | 0.008809564 |
| *RPL31* | -0.67563 | 0.000538453 | 0.009006352 |
| *BZW1* | 0.997213 | 0.000541438 | 0.009006352 |
| *POU2F2* | -0.74948 | 0.000605253 | 0.009828158 |
| *EIF1* | -0.66671 | 0.000678434 | 0.010760275 |
| *TOP2A* | 0.541976 | 0.000753184 | 0.011674346 |

| *Gene* | *Log2 Fold Change* | *P value* | $P_{adjusted}$ |
|---|---|---|---|
| *MORF4L2* | 0.990004 | 0.001030175 | 0.015612873 |
| *USP33* | 0.877817 | 0.001106283 | 0.016401844 |
| *CTSL* | -0.80571 | 0.001221347 | 0.01735331 |
| *IGFBP7* | 0.819825 | 0.001207119 | 0.01735331 |
| *GZMB* | -0.8264 | 0.001336147 | 0.01859698 |
| *RPL5* | -0.45123 | 0.001406275 | 0.019181588 |
| *MT-CO1* | -0.46307 | 0.00170492 | 0.022799122 |
| *UBE2C* | -0.81574 | 0.0018919 | 0.024075032 |
| *TPM1* | 0.639332 | 0.001906234 | 0.024075032 |
| *PHLDB2* | 0.755406 | 0.00189867 | 0.024075032 |
| *UACA* | -0.48534 | 0.001989866 | 0.024372793 |
| *SMC4* | 0.562465 | 0.002001285 | 0.024372793 |
| *TAX1BP1* | -0.65882 | 0.002048226 | 0.024377746 |
| *EIF4G2* | 0.595579 | 0.002073181 | 0.024377746 |
| *STXBP5* | 0.63613 | 0.002337774 | 0.027023082 |
| *OGFRL1* | 0.743217 | 0.002569688 | 0.029208787 |
| *HNRNPK* | 0.480202 | 0.002743279 | 0.03067076 |
| *RPL6* | -0.48387 | 0.002878325 | 0.031661576 |
| *LNPEP* | 0.780648 | 0.002935405 | 0.031776929 |
| *KPNB1* | -0.69984 | 0.00317366 | 0.033299021 |
| *MICAL2* | 0.734137 | 0.003144573 | 0.033299021 |
| *TFPI* | 0.564568 | 0.003287741 | 0.033973321 |
| *PHLDA1* | -0.52665 | 0.003454435 | 0.035163059 |
| *DNAJC21* | -0.72401 | 0.003653855 | 0.036646021 |
| *MT-CO2* | -0.54998 | 0.003924862 | 0.038793564 |
| *GNG11* | 0.474214 | 0.004076208 | 0.039713911 |
| *SLC38A2* | 0.620843 | 0.004200074 | 0.040344376 |
| *MYL10* | -0.63713 | 0.00438664 | 0.041328032 |
| *RPL37* | -0.43667 | 0.004484273 | 0.041328032 |
| *HNRNPA2B1* | 0.476712 | 0.004472124 | 0.041328032 |
| *HSP90B1* | -0.46205 | 0.004557004 | 0.04143836 |
| *HJURP* | 0.582191 | 0.004798838 | 0.043063256 |
| *S100A11* | -0.54382 | 0.004895154 | 0.043357082 |
| *MT-ND4* | -0.46796 | 0.005028613 | 0.04341157 |
| *CENPF* | 0.425725 | 0.005002979 | 0.04341157 |
| *MT-TP* | 0.65322 | 0.005521393 | 0.047069878 |
| *TM4SF1* | 0.478254 | 0.005695126 | 0.047951557 |
| *TMEM123* | -0.63604 | 0.00581044 | 0.048325856 |
| *DPYSL3* | 0.537552 | 0.005995441 | 0.049263743 |

### 8.2.4 Gene ontology enrichment analysis of most significantly overrepresented genes

Table 8.22 The top 30 of the most overrepresented pathways

| Pathway | N Genes | Pathway Genes | Ratio* | Enrichment FDR ⊀ |
|---|---|---|---|---|
| MiRNA transport | 2 | 3 | 0.667 | 4.38E-03 |
| Energy coupled proton transmembrane transport, against electrochemical gradient | 3 | 5 | 0.600 | 4.80E-04 |
| Electron transport coupled proton transport | 3 | 5 | 0.600 | 4.80E-04 |
| Negative regulation of cellular senescence | 3 | 21 | 0.143 | 5.32E-03 |
| SRP-dependent co-translational protein targeting to membrane | 6 | 112 | 0.054 | 1.32E-03 |
| Co-translational protein targeting to membrane | 6 | 118 | 0.051 | 1.49E-03 |
| Protein targeting to ER | 6 | 128 | 0.047 | 1.51E-03 |
| Establishment of protein localisation to endoplasmic reticulum | 6 | 132 | 0.045 | 1.55E-03 |
| Mitochondrial ATP synthesis coupled electron transport | 5 | 113 | 0.044 | 5.32E-03 |
| ATP synthesis coupled electron transport | 5 | 114 | 0.044 | 5.32E-03 |
| Nuclear-transcribed mRNA catabolic process, nonsense-mediated decay | 6 | 147 | 0.041 | 2.25E-03 |
| Respiratory electron transport chain | 5 | 131 | 0.038 | 8.98E-03 |
| Protein localisation to endoplasmic reticulum | 6 | 162 | 0.037 | 3.42E-03 |
| Oxidative phosphorylation | 6 | 168 | 0.036 | 3.86E-03 |
| Cytoplasmic translation | 6 | 169 | 0.036 | 3.86E-03 |
| Translational initiation | 8 | 229 | 0.035 | 1.17E-03 |
| Viral transcription | 7 | 217 | 0.032 | 2.25E-03 |
| Viral gene expression | 8 | 278 | 0.029 | 1.51E-03 |
| RRNA processing | 7 | 295 | 0.024 | 8.07E-03 |
| RRNA metabolic process | 7 | 307 | 0.023 | 8.98E-03 |
| Establishment of protein localisation to membrane | 8 | 421 | 0.019 | 9.26E-03 |
| Establishment of protein localisation to organelle | 10 | 588 | 0.017 | 4.89E-03 |
| Translation | 12 | 752 | 0.016 | 2.25E-03 |
| Peptide biosynthetic process | 12 | 783 | 0.015 | 2.96E-03 |
| Cell division | 10 | 659 | 0.015 | 8.98E-03 |
| Peptide metabolic process | 14 | 962 | 0.015 | 1.51E-03 |
| Viral process | 16 | 1158 | 0.014 | 1.32E-03 |
| Biological process involved in symbiotic interaction | 16 | 1241 | 0.013 | 1.51E-03 |
| Amide biosynthetic process | 12 | 950 | 0.013 | 9.26E-03 |
| Biological process involved in interspecies interaction between organisms | 22 | 2667 | 0.008 | 8.98E-03 |

* The pathways are sorted based on Ratio of N of genes annotated/Ngenes in pathway

⊀ False Discovery Rate

Table 8.23 The most overrepresented pathways excluding RPLs

| Pathway | N Genes | Pathway Genes | Ratio* | Enrichment FDR⊀ |
|---|---|---|---|---|
| MiRNA transport | 2 | 3 | 0.667 | 1.36E-02 |
| Energy coupled proton transmembrane transport, against electrochemical gradient | 3 | 5 | 0.600 | 3.72E-04 |
| Electron transport coupled proton transport | 3 | 5 | 0.600 | 3.72E-04 |
| Negative regulation of cellular senescence | 3 | 21 | 0.143 | 1.36E-02 |
| Negative regulation of cell aging | 3 | 28 | 0.107 | 2.31E-02 |
| Muscle filament sliding | 3 | 41 | 0.073 | 4.55E-02 |
| Actin-myosin filament sliding | 3 | 41 | 0.073 | 4.55E-02 |
| Mitochondrial ATP synthesis coupled electron transport | 5 | 113 | 0.044 | 1.36E-02 |
| Aerobic respiration | 4 | 91 | 0.044 | 3.91E-02 |
| ATP synthesis coupled electron transport | 5 | 114 | 0.044 | 1.36E-02 |
| Respiratory electron transport chain | 5 | 131 | 0.038 | 1.76E-02 |
| Oxidative phosphorylation | 6 | 168 | 0.036 | 1.36E-02 |
| Proton transmembrane transport | 5 | 174 | 0.029 | 4.28E-02 |
| Actin filament organization | 8 | 467 | 0.017 | 2.94E-02 |
| Cell division | 10 | 659 | 0.015 | 1.59E-02 |
| Response to abiotic stimulus | 13 | 1329 | 0.010 | 4.68E-02 |
| Regulation of cellular component organization | 20 | 2555 | 0.008 | 2.97E-02 |

* The pathways are sorted based on Ratio of N of genes annotated/Ngenes in pathway

⊀ False Discovery Rate

## 8.3 Permissions for use of third-party material in this thesis

Figure 1.1, Figure 1.2, Figure 1.3, Figure 1.4, Figure 1.5, Figure 1.6, Figure 1.7 and Figure 1.8 were created in Biorender.

Figure 1.3 was modified from [175], which was an "open access article distributed under the Creative Commons Attribution License which permits unrestricted use, distribution, and reproduction in any medium, provided the original work is properly cited.".

Permission for all figures and tables adapted or reproduced for use in this thesis (Figure 1.2, Figure 1.7, Figure 1.8 and Table 1.1) were obtained via Copyright Clearance Centre and the electronic copy of the licences were deposited in the Oxford University Research Archive (ORA) along with this thesis. The permissions from the licensors are acknowledged in corresponding figure legends.

# References


[1]. Cancer Research UK. https://www.cancerresearchuk.org/.

[2]. Wever, E. M., Draisma, G., Heijnsdijk, E. A. M. & De Koning, H. J. How does early detection by screening affect disease progression?: Modeling estimated benefits in prostate cancer screening. *Med. Decis. Mak.* 31, 550–558 (2011).

[3]. Scardino, P. T., Weaver, R. & Hudson, M. A. Early detection of prostate cancer. *Hum. Pathol.* 23, 211–222 (1992).

[4]. Scardino, P. T. The Gordon Wilson Lecture. Natural history and treatment of early stage prostate cancer. *Trans. Am. Clin. Climatol. Assoc.* 111, 201–241 (2000).

[5]. Rosenberg, M. T., Froehner, M., Albala, D. & Miner, M. M. Biology and natural history of prostate cancer and the role of chemoprevention. *Int. J. Clin. Pract.* 64, 1746–1753 (2010).

[6]. Cooperberg, M. R., Lubeck, D. P., Meng, M. V., Mehta, S. S. & Carroll, P. R. The changing face of low-risk prostate cancer: Trends in clinical presentation and primary management. *J. Clin. Oncol.* 22, 2141–2149 (2004).

[7]. Filson, C. P., Marks, L. S. & Litwin, M. S. Expectant management for men with early stage prostate cancer. *CA. Cancer J. Clin.* 65, 264–282 (2015).

[8]. Litwin, M. S. & Tan, H. J. The diagnosis and treatment of prostate cancer: A review. *JAMA - J. Am. Med. Assoc.* 317, 2532–2542 (2017).

[9]. BioRender. https://biorender.com/.

[10]. Hamdy, F. C., Donovan, J. L., Lane, J. A., Mason, M., Metcalfe, C., Holding, P., *et al.* 10-Year Outcomes after Monitoring, Surgery, or Radiotherapy for Localized Prostate Cancer. *N. Engl. J. Med.* 375, 1415–1424 (2016).

[11]. Chen, C. D., Welsbie, D. S., Tran, C., Baek, S. H., Chen, R., Vessella, R., Rosenfeld, M. G. & Sawyers, C. L. Molecular determinants of resistance to antiandrogen therapy. *Nat. Med.* 10, 33–39 (2004).

[12]. Buchanan, G., Irvine, R. A., Coetzee, G. A. & Tilley, W. D. Contribution of the androgen receptor to prostate cancer predisposition and progression. *Cancer and Metastasis Reviews* vol. 20 207–223 (2001).

[13]. Locke, J. A., Guns, E. S., Lubik, A. A., Adomat, H. H., Hendy, S. C., Wood, C.

A., Ettinger, S. L., Gleave, M. E. & Nelson, C. C. Androgen Levels increase by intratumoral de novo steroidogenesis during progression of castration-resistant prostate cancer. *Cancer Res.* 68, 6407–6415 (2008).

[14]. Gregory, C. W., He, B., Johnson, R. T., Ford, O. H., Mohler, J. L., French, F. S. & Wilson, E. M. A mechanism for androgen receptor-mediated prostate cancer recurrence after androgen deprivation therapy. *Cancer Res.* 61, 4315–9 (2001).

[15]. Heemers, H. V. & Tindall, D. J. Androgen receptor (AR) coregulators: A diversity of functions converging on and regulating the AR transcriptional complex. *Endocr. Rev.* 28, 778–808 (2007).

[16]. Xu, K., Wu, Z. J., Groner, A. C., He, H. H., Cai, C., Lis, R. T., *et al.* EZH2 Oncogenic Activity in Castration-Resistant Prostate Cancer Cells Is Polycomb-Independent. *Science (80-. ).* 338, 1465–1469 (2012).

[17]. Harris, W. P., Mostaghel, E. A., Nelson, P. S. & Montgomery, B. Androgen deprivation therapy: progress in understanding mechanisms of resistance and optimizing androgen depletion. *Nat. Clin. Pract. Urol. 2009 62* 6, 76–85 (2009).

[18]. Veldscholte, J., Ris-Stalpers, C., Kuiper, G. G. J. M., Jenster, G., Berrevoets, C., Claassen, E., van Rooij, H. C. J., Trapman, J., Brinkmann, A. O. & Mulder, E. A mutation in the ligand binding domain of the androgen receptor of human INCaP cells affects steroid binding characteristics and response to anti-androgens. *Biochem. Biophys. Res. Commun.* 173, 534–540 (1990).

[19]. Culig, Z., Stober, J., Gast, A., Peterziel, H., Hobisch, A., Radmayr, C., Hittmair, A., Bartsch, G., Cato, A. C. & Klocker, H. Activation of two mutant androgen receptors from human prostatic carcinoma by adrenal androgens and metabolic derivatives of testosterone. *Cancer Detect. Prev.* 20, 68–75 (1996).

[20]. Taplin, M. E., Rajeshkumar, B., Halabi, S., Werner, C. P., Woda, B. A., Picus, J., Stadler, W., Hayes, D. F., Kantoff, P. W., Vogelzang, N. J. & Small, E. J. Androgen receptor mutations in androgen-independent prostate cancer: Cancer and leukemia group B study 9663. *J. Clin. Oncol.* 21, 2673–2678 (2003).

[21]. Korpal, M., Korn, J. M., Gao, X., Rakiec, D. P., Ruddy, D. A., Doshi, S., *et al.* An F876l mutation in androgen receptor confers genetic and phenotypic resistance to MDV3100 (Enzalutamide). *Cancer Discov.* 3, 1030–1043 (2013).

[22]. Hu, R., Dunn, T. A., Wei, S., Isharwal, S., Veltri, R. W., Humphreys, E., *et al.* Ligand-independent androgen receptor variants derived from splicing of cryptic exons signify hormone-refractory prostate cancer. *Cancer Res.* 69, 16–22 (2009).

[23]. Cai, C. & Balk, S. P. Intratumoral androgen biosynthesis in prostate cancer pathogenesis and response to therapy. *Endocr. Relat. Cancer* 18, R175–R182

(2011).

[24]. Attar, R. M., Takimoto, C. H. & Gottardis, M. M. Castration-resistant prostate cancer: Locking up the molecular escape routes. *Clin. Cancer Res.* 15, 3251–3255 (2009).

[25]. Siegall, C. B., FitzGerald, D. J., Pastan, I., Schwab, G. & Nordan, R. P. Expression of the Interleukin 6 Receptor and Interleukin 6 in Prostate Carcinoma Cells. *Cancer Res.* 50, 7786–7788 (1990).

[26]. Siegsmund, M. J., Yamazaki, H. & Pastan, I. Interleukin 6 receptor mRNA in prostate carcinomas and benign prostate hyperplasia. *J. Urol.* 151, 1396–1399 (1994).

[27]. Hobisch, A., Rogatsch, H., Hittmair, A., Fuchs, D., Bartsch, G., Klocker, H., Bartsch, G. & Culig, Z. Immunohistochemical localization of interleukin-6 and its receptor in benign, premalignant and malignant prostate tissue. *J. Pathol.* 191, 239–244 (2000).

[28]. Soo, O. L., Pinder, E., Jae, Y. C., Lou, W., Sun, M. & Gao, A. C. Interleukin-4 stimulates androgen-independent growth in LNCaP human prostate cancer cells. *Prostate* 68, 85–91 (2008).

[29]. Ueda, T., Bruchovsky, N. & Sadar, M. D. Activation of the androgen receptor N-terminal domain by interleukin-6 via MAPK and STAT3 signal transduction pathways. *J. Biol. Chem.* 277, 7076–7085 (2002).

[30]. Hobisch, A., Eder, I. E., Putz, T., Horninger, W., Bartsch, G., Klocker, H. & Culig, Z. Interleukin-6 regulates prostate-specific protein expression in prostate carcinoma cells by activation of the androgen receptor. *Cancer Res.* 58, 4640–4645 (1998).

[31]. Chen, T., Wang, L. H. & Farrar, W. L. Interleukin 6 activates androgen receptor-mediated gene expression through a signal transducer and activator of transcription 3-dependent pathway in LNCaP prostate cancer cells. *Cancer Res.* 60, 2132–2135 (2000).

[32]. Drachenberg, D. E., Elgamal, A. A. A., Rowbotham, R., Peterson, M. & Murphy, G. P. Circulating levels of interleukin-6 in patients with hormone refractory prostate cancer. *Prostate* 41, 127–133 (1999).

[33]. Adler, H. L., McCurdy, M. A., Kattan, M. W., Timme, T. L., Scardino, P. T. & Thompson, T. C. Elevated levels of circulating interleukin-6 and transforming growth factor-β1 in patients with metastatic prostatic carcinoma. *J. Urol.* 161, 182–187 (1999).

[34]. Dutt, S. S. & Gao, A. C. Molecular mechanisms of castration-resistant prostate

cancer progression. *Futur. Oncol.* 5, 1403–1413 (2009).

[35]. Anassi, E. & Ndefo, U. A. Sipuleucel-T (Provenge) injection the first immunotherapy agent (Vaccine) for hormone-refractory prostate cancer. *P T* 36, 197–202 (2011).

[36]. Gunjur, A. Personalising the treatment of prostate cancer. *Lancet. Oncol.* 16, e592 (2015).

[37]. de Bono, J., Mateo, J., Fizazi, K., Saad, F., Shore, N., Sandhu, S., *et al.* Olaparib for Metastatic Castration-Resistant Prostate Cancer. *N. Engl. J. Med.* 382, 2091–2102 (2020).

[38]. Abida, W., Patnaik, A., Campbell, D., Shapiro, J., Bryce, A. H., McDermott, R., *et al.* Rucaparib in Men with Metastatic Castration-Resistant Prostate Cancer Harboring a BRCA1 or BRCA2 Gene Alteration. *J. Clin. Oncol.* 38, 3763–3772 (2020).

[39]. Mateo, J., Porta, N., Bianchini, D., McGovern, U., Elliott, T., Jones, R., *et al.* Olaparib in patients with metastatic castration-resistant prostate cancer with DNA repair gene aberrations (TOPARP-B): a multicentre, open-label, randomised, phase 2 trial. *Lancet Oncol.* 21, 162–174 (2020).

[40]. Mateo, J., Carreira, S., Sandhu, S., Miranda, S., Mossop, H., Perez-Lopez, R., *et al.* DNA-Repair Defects and Olaparib in Metastatic Prostate Cancer. *N. Engl. J. Med.* 373, 1697–1708 (2015).

[41]. Conteduca, V. & De Giorgi, U. Talazoparib: a new biomarker-directed therapy in advanced prostate cancer. *Lancet Oncol.* 22, 1203–1204 (2021).

[42]. Miranda, J., Viñal, D. & Pinto, Á. Radium 223 for the treatment of metastatic castration-resistant prostate cancer. *Arch. Esp. Urol.* 72, 500–507 (2019).

[43]. Hindié, E. & Morgat, C. Early use of abiraterone and radium-223 in metastatic prostate cancer. *Lancet Oncol.* 20, e229 (2019).

[44]. Weingärtner, K. Origin and development of carcinoma in the prostate. *Aktuelle Urol.* 34, 81–82 (2003).

[45]. McNeal, J. E. The zonal anatomy of the prostate. *Prostate* 2, 35–49 (1981).

[46]. Hoda, S. A. & Hoda, R. S. Histology for Pathologists. *Advances in Anatomic Pathology* vol. 15 124 (2008).

[47]. Timms, B. G. Prostate development: A historical perspective. *Differentiation* 76, 565–577 (2008).

[48]. Haffner, J., Potiron, E., Bouyé, S., Puech, P., Leroy, X., Lemaitre, L. & Villers, A. Peripheral zone prostate cancers: Location and intraprostatic patterns of spread at histopathology. *Prostate* 69, 276–282 (2009).

[49]. Shen, M. M. & Abate-Shen, C. Molecular genetics of prostate cancer: New prospects for old challenges. *Genes Dev.* 24, 1967–2000 (2010).

[50]. Hanahan, D. & Weinberg, R. A. The hallmarks of cancer. *Cell* 100, 57–70 (2000).

[51]. Hanahan, D. & Weinberg, R. A. Hallmarks of cancer: The next generation. *Cell* 144, 646–674 (2011).

[52]. De Marzo, A. M., Marchi, V. L., Epstein, J. I. & Nelson, W. G. Proliferative inflammatory atrophy of the prostate: Implications for prostatic carcinogenesis. *Am. J. Pathol.* 155, 1985–1992 (1999).

[53]. Bethel, C. R., Faith, D., Li, X., Guan, B., Hicks, J. L., Lan, F., Jenkins, R. B., Bieberich, C. J. & De Marzo, A. M. Decreased NKX3.1 protein expression in focal prostatic atrophy, prostatic intraepithelial neoplasia, and adenocarcinoma: Association with gleason score and chromosome 8p deletion. *Cancer Res.* 66, 10683–10690 (2006).

[54]. Sfanos, K. S. & de Marzo, A. M. Prostate cancer and inflammation: The evidence. *Histopathology* 60, 199–215 (2012).

[55]. Xia, Y. & Zweier, J. L. Superoxide and peroxynitrite generation from inducible nitric oxide synthase in macrophages. *Proc. Natl. Acad. Sci. U. S. A.* 94, 6954–6958 (1997).

[56]. Gunawardena, D., Raju, R. & Münch, G. Hydrogen peroxide mediates pro-inflammatory cell-to-cell signaling: A new therapeutic target for inflammation? *Neural Regen. Res.* 14, 1430–1437 (2019).

[57]. Weitzman, S. A. & Gordon, L. I. Inflammation and cancer: Role of phagocyte-generated oxidants in carcinogenesis. *Blood* 76, 655–663 (1990).

[58]. Tomlins, S. A., Mehra, R., Rhodes, D. R., Cao, X., Wang, L., Dhanasekaran, S. M., *et al.* Integrative molecular concept modeling of prostate cancer progression. *Nat. Genet.* 39, 41–51 (2007).

[59]. Nakayama, M., Gonzalgo, M. L., Yegnasubramanian, S., Lin, X., De Marzo, A. M. & Nelson, W. G. GSTP1 CpG island hypermethylation as a molecular biomarker for prostate cancer. *J. Cell. Biochem.* 91, 540–552 (2004).

[60]. Putzi, M. J. & De Marzo, A. M. Morphologic transitions between proliferative inflammatory atrophy and high-grade prostatic intraepithelial neoplasia. *Urology* 56, 828–832 (2000).

[61]. Bostwick, D. G. & Qian, J. High-grade prostatic intraepithelial neoplasia. *Mod. Pathol.* 17, 360–379 (2004).

[62]. Antonarakis, E. S., Keizman, D., Zhang, Z., Gurel, B., Lotan, T. L., Hicks, J. L., Fedor, H. L., Carducci, M. A., De Marzo, A. M. & Eisenberger, M. A. An immunohistochemical signature comprising PTEN, MYC, and Ki67 predicts progression in prostate cancer patients receiving adjuvant docetaxel after prostatectomy. *Cancer* 118, 6063–6071 (2012).

[63]. Bieberich, C. J., Fujita, K., He, W. W. & Jaj, G. Prostate-specific and androgen-dependent expression of a novel homeobox gene. *J. Biol. Chem.* 271, 31779–31782 (1996).

[64]. Bowen, C., Bubendorf, L., Voeller, H. J., Slack, R., Willi, N., Sauter, G., *et al.* Loss of NKX3.1 expression in human prostate cancers correlates with tumor progression. *Cancer Res.* 60, 6111–6115 (2000).

[65]. Brooks, J. D., Weinstein, M., Lin, X., Sun, Y., Pin, S. S., Bova, G. S., Epstein, J. I., Isaacs, W. B. & Nelson, W. G. CG island methylation changes near the GSTP1 gene in prostatic intraepithelial neoplasia. *Cancer Epidemiol. Biomarkers Prev.* 7, 531–536 (1998).

[66]. Mills, I. G. Maintaining and reprogramming genomic androgen receptor activity in prostate cancer. *Nat. Rev. Cancer* 14, 187–198 (2014).

[67]. Rebello, R. J., Oing, C., Knudsen, K. E., Loeb, S., Johnson, D. C., Reiter, R. E., Gillessen, S., Van der Kwast, T. & Bristow, R. G. Prostate cancer. *Nat. Rev. Dis. Prim.* 7, 1–27 (2021).

[68]. Vasioukhin, V. Hepsin paradox reveals unexpected complexity of metastatic process. *Cell Cycle* 3, 1394–1397 (2004).

[69]. Parsons, J. K., Gage, W. R., Nelson, W. G. & De Marzo, A. M. p63 protein expression is rare in prostate adenocarcinoma: Implications for cancer diagnosis and carcinogenesis. *Urology* 58, 619–624 (2001).

[70]. Signoretti, S., Waltregny, D., Dilks, J., Isaac, B., Lin, D., Garraway, L., Yang, A., Montironi, R., McKeon, F. & Loda, M. P63 Is a Prostate Basal Cell Marker and Is Required for Prostate Development. *Am. J. Pathol.* 157, 1769–1775 (2000).

[71]. Parsons, J. K. & Partin, A. W. Clinical interpretation of prostate biopsy reports. *Urology* 67, 452–457 (2006).

[72]. Montironi, R., Mazzucchelli, R., Algaba, F. & Lopez-Beltran, A. Morphological identification of the patterns of prostatic intraepithelial neoplasia and their importance. *J. Clin. Pathol.* 53, 655–665 (2000).

[73]. Hao, J., Jackson, L., Calaluce, R., McDaniel, K., Dalkin, B. L. & Nagle, R. B. Investigation into the mechanism of the loss of laminin 5 ($\alpha 3\beta 3\gamma 2$) expression in prostate cancer. *Am. J. Pathol.* 158, 1129–1135 (2001).

[74]. Narla, G., Heath, K. E., Reeves, H. L., Li, D., Giono, L. E., Kimmelman, A. C., *et al.* KLF6, a candidate tumor suppressor gene mutated in prostate cancer. *Science (80-. ).* 294, 2563–2566 (2001).

[75]. Yang, R. M., Naitoh, J., Murphy, M., Wang, H. J., Phillipson, J., DeKernion, J. B., Loda, M. & Reiter, R. E. Low p27 expression predicts poor disease-free survival in patients with prostate cancer. *J. Urol.* 159, 941–945 (1998).

[76]. Härkönen, P., Kyllönen, A. P., Nordling, S. & Vihko, P. Loss of heterozygosity in chromosomal region 16q24.3 associated with progression of prostate cancer. *Prostate* 62, 267–274 (2005).

[77]. Dutt, S. & Gao, A. C. The molecular basis of prostate carcinogenesis. in *The Molecular Basis of Human Cancer* (eds. Coleman, W. B. & Tsongalis, G. J.) 423–445 (Humana Press, 2016). doi:10.1007/978-1-59745-458-2_27.

[78]. Schaafsma, H. E., Bringuier, P. P., Oosterhof, G. O. N., Debruyne, F. M. J. & Schalken, J. A. Decreased E-Cadherin Expression Is Associated with Poor Prognosis in Patients with Prostate Cancer. *Cancer Res.* 54, 3929–3933 (1994).

[79]. Gao, A. C., Lou, W., Dong, J. T. & Isaacs, J. T. CD44 is a metastasis suppressor gene for prostatic cancer located on human chromosome 11p13. *Cancer Res.* 57, 846–849 (1997).

[80]. Nagle, R. B., Hao, J., Knox, J. D., Dalkin, B. L., Clark, V. & Cress, A. E. Expression of hemidesmosomal and extracellular matrix proteins by normal and malignant human prostate tissue. *Am. J. Pathol.* 146, 1498–1507 (1995).

[81]. Dong, J. T., Lamb, P. W., Rinker-Schaeffer, C. W., Vukanovic, J., Ichikawa, T., Isaacs, J. T. & Barrett, J. C. Kal1, a metastasis suppressor gene for prostate cancer on human chromosome 11p11.2. *Science (80-. ).* 268, 884–886 (1995).

[82]. Cairns, P., Okami, K., Halachmi, S., Halachmi, N., Esteller, M., Herman, J. G., Jen, J., Isaacs, W. B., Bova, G. S. & Sidransky, D. Frequent inactivation of PTEN/MMAC1 in primary prostate cancer. *Cancer Res.* 57, 4997–5000 (1997).

[83]. Duan, R., Du, W. & Guo, W. EZH2: A novel target for cancer treatment. *J. Hematol. Oncol.* 13, 1–12 (2020).

[84]. Xia, L., Zhu, X., Zhang, L., Xu, Y., Chen, G. & Luo, J. EZH2 enhances expression of CCL5 to promote recruitment of macrophages and invasion in lung cancer. *Biotechnol. Appl. Biochem.* 67, 1011–1019 (2020).

[85]. Jenkins, R. B., Qian, J., Lieber, M. M. & Bostwick, D. G. Detection of c-myc oncogene amplification and chromosomal anomalies in metastatic prostatic carcinoma by fluorescence in Situ hybridization. *Cancer Res.* 57, 524–531 (1997).

[86]. Dhanasekaran, S. M., Barrette, T. R., Ghosh, D., Shah, R., Varambally, S., Kurachi, K., Pienta, K. J., Rubin, M. A. & Chinnaiyan, A. M. Delineation of prognostic biomarkers in prostate cancer. *Nature* 412, 822–826 (2001).

[87]. Magee, J. A., Araki, T., Patil, S., Ehrig, T., Humphrey, P. A., Watson, M. A., Milbrandt, J., Catalona, W. J. & True, L. Expression profiling reveals hepsin overexpression in prostate cancer. *Cancer Res.* 61, 5692–5696 (2001).

[88]. Stamey, T. A., Warrington, J. A., Caldwell, M. C., Chen, Z., Fan, Z., Mahadevappa, M., McNEAL, J. E., Nolley, R. & Zhang, Z. Molecular genetic profiling of gleason grade 4/5 prostate cancers compared to benign prostatic hyperplasia. *J. Urol.* 166, 2171–2177 (2001).

[89]. Klezovitch, O., Chevillet, J., Mirosevich, J., Roberts, R. L., Matusik, R. J. & Vasioukhin, V. Hepsin promotes prostate cancer progression and metastasis. *Cancer Cell* 6, 185–195 (2004).

[90]. Tang, X., Mahajan, S. S., Nguyen, L. T., Béliveau, F., Leduc, R., Simon, J. A. & Vasioukhin, V. Targeted inhibition of cell-surface serine protease hepsin blocks prostate cancer bone metastasis. *Oncotarget* 5, 1352–1362 (2014).

[91]. Tannock, I. F., de Wit, R., Berry, W. R., Horti, J., Pluzanska, A., Chi, K. N., *et al.* Docetaxel plus Prednisone or Mitoxantrone plus Prednisone for Advanced Prostate Cancer. *N. Engl. J. Med.* 351, 1502–1512 (2004).

[92]. Petrylak, D. P., Tangen, C. M., Hussain, M. H. A., Lara, P. N., Jones, J. A., Taplin, M. E., *et al.* Docetaxel and Estramustine Compared with Mitoxantrone and Prednisone for Advanced Refractory Prostate Cancer. *N. Engl. J. Med.* 351, 1513–1520 (2004).

[93]. Bubendorf, L., Schöpfer, A., Wagner, U., Sauter, G., Moch, H., Willi, N., Gasser, T. C. & Mihatsch, M. J. Metastatic patterns of prostate cancer: An autopsy study of 1,589 patients. *Hum. Pathol.* 31, 578–583 (2000).

[94]. Lee, R. J., Saylor, P. J. & Smith, M. R. Treatment and prevention of bone complications from prostate cancer. *Bone* 48, 88–95 (2011).

[95]. Tiwari, R., Manzar, N. & Ateeq, B. Dynamics of Cellular Plasticity in Prostate Cancer Progression. *Front. Mol. Biosci.* 7, 130 (2020).

[96]. Blau, H. M., Pavlath, G. K., Hardeman, E. C., Chiu, C. P., Silberstein, L., Webster, S. G., Miller, S. C. & Webster, C. Plasticity of the differentiated state. *Science (80-. ).* 230, 758–766 (1985).

[97]. Yuan, S., Norgard, R. J. & Stanger, B. Z. Cellular plasticity in cancer. *Cancer Discov.* 9, 837–851 (2019).

[98]. Flavahan, W. A., Gaskell, E. & Bernstein, B. E. Epigenetic plasticity and the hallmarks of cancer. *Science (80-. ).* 357, (2017).

[99]. Onder, T. T., Gupta, P. B., Mani, S. A., Yang, J., Lander, E. S. & Weinberg, R. A. Loss of E-cadherin promotes metastasis via multiple downstream transcriptional pathways. *Cancer Res.* 68, 3645–3654 (2008).

[100]. Kalluri, R. & Weinberg, R. A. The basics of epithelial-mesenchymal transition. *J. Clin. Invest.* 119, 1420–1428 (2009).

[101]. Alumkal, J. J., Sun, D., Lu, E., Beer, T. M., Thomas, G. V., Latour, E., *et al.* Transcriptional profiling identifies an androgen receptor activity-low, stemness program associated with enzalutamide resistance. *Proc. Natl. Acad. Sci. U. S. A.* 117, 12315–12323 (2020).

[102]. Zou, M., Toivanen, R., Mitrofanova, A., Floch, N., Hayati, S., Sun, Y., *et al.* Transdifferentiation as a mechanism of treatment resistance in a mouse model of castration-resistant prostate cancer. *Cancer Discov.* 7, 736–749 (2017).

[103]. Nauseef, J. T. & Henry, M. D. Epithelial-to-mesenchymal transition in prostate cancer: Paradigm or puzzle? *Nat. Rev. Urol.* 8, 428–439 (2011).

[104]. Williams, E. D., Gao, D., Redfern, A. & Thompson, E. W. Controversies around epithelial–mesenchymal plasticity in cancer metastasis. *Nat. Rev. Cancer* 19, 716–732 (2019).

[105]. Huber, M. A., Kraut, N. & Beug, H. Molecular requirements for epithelial-mesenchymal transition during tumor progression. *Curr. Opin. Cell Biol.* 17, 548–558 (2005).

[106]. Battaglia, R. A., Delic, S., Herrmann, H. & Snider, N. T. Vimentin on the move: New developments in cell migration [version 1; referees: 2 approved]. *F1000Research* 7, (2018).

[107]. Their, J. P. Epithelial-mesenchymal transitions in tumor progression. *Nat. Rev. Cancer* 2, 442–454 (2002).

[108]. Angst, B. D., Marcozzi, C. & Magee, A. I. The cadherin superfamily: Diversity in form and function. *J. Cell Sci.* 114, 629–641 (2001).

[109]. Shapiro, L. & Weis, W. I. Structure and biochemistry of cadherins and catenins. *Cold Spring Harb. Perspect. Biol.* 1, a003053 (2009).

[110]. Halbleib, J. M. & Nelson, W. J. Cadherins in development: Cell adhesion, sorting,

and tissue morphogenesis. *Genes Dev.* 20, 3199–3214 (2006).

[111]. Yang, J., Mani, S. A., Donaher, J. L., Ramaswamy, S., Itzykson, R. A., Come, C., Savagner, P., Gitelman, I., Richardson, A. & Weinberg, R. A. Twist, a master regulator of morphogenesis, plays an essential role in tumor metastasis. *Cell* 117, 927–939 (2004).

[112]. Cano, A., Pérez-Moreno, M. A., Rodrigo, I., Locascio, A., Blanco, M. J., Del Barrio, M. G., Portillo, F. & Nieto, M. A. The transcription factor Snail controls epithelial-mesenchymal transitions by repressing E-cadherin expression. *Nat. Cell Biol.* 2, 76–83 (2000).

[113]. Hajra, K. M., Chen, D. Y. S. & Fearon, E. R. The SLUG zinc-finger protein represses E-cadherin in breast cancer. *Cancer Res.* 62, 1613–1618 (2002).

[114]. Isaacs, W. B., Carter, B. S., Debruyne, F. M. J. & Schalken, J. A. Expression of the Cellular Adhesion Molecule E-Cadherin Is Reduced or Absent in High-Grade Prostate Cancer. *Cancer Res.* 52, 5104–5109 (1992).

[115]. Nalla, A. K., Estes, N., Patel, J. & Rao, J. S. N-cadherin mediates angiogenesis by regulating monocyte chemoattractant protein-1 expression via PI3K/Akt signaling in prostate cancer cells. *Exp. Cell Res.* 317, 2512–2521 (2011).

[116]. Cao, Z. Q., Wang, Z. & Leng, P. Aberrant N-cadherin expression in cancer. *Biomed. Pharmacother.* 118, 109320 (2019).

[117]. Jaggi, M., Johansson, S. L., Baker, J. J., Smith, L. M., Galich, A. & Balaji, K. C. Aberrant expression of E-cadherin and beta-catenin in human prostate cancer. *Urol. Oncol. Semin. Orig. Investig.* 23, 402–406 (2005).

[118]. Guo, W. & Giancotti, F. G. Integrin signalling during tumour progression. *Nat. Rev. Mol. Cell Biol.* 5, 816–826 (2004).

[119]. Mol, A. J. M., Geldof, A. A., Meijer, G. A., Van Der Poel, H. G. & Van Moorselaar, R. J. A. New experimental markers for early detection of high-risk prostate cancer: Role of cell-cell adhesion and cell migration. *J. Cancer Res. Clin. Oncol.* 133, 687–695 (2007).

[120]. Slack-Davis, J. K. & Parsons, J. T. Emerging views of integrin signaling: Implications for prostate cancer. *J. Cell. Biochem.* 91, 41–46 (2004).

[121]. Schmelz, M., Cress, A. E., Scott, K. M., Burger, F., Cui, H., Sallam, K., McDaniel, K. M., Dalkin, B. L. & Nagle, R. B. Different Phenotypes in Human Prostate Cancer: $\alpha$6 or $\alpha$3 Integrin in Cell-extracellular Adhesion Sites. *Neoplasia* 4, 243–254 (2002).

[122]. Cress, A. E., Rabinovitz, I., Zhu, W. & Nagle, R. B. The $\alpha$6$\beta$1 and $\alpha$6$\beta$4 integrins

in human prostate cancer progression. *Cancer Metastasis Rev.* 14, 219–228 (1995).

[123]. Davis, T. L., Cress, A. E., Dalkin, B. L. & Nagle, R. B. Unique expression pattern of the α6β4 integrin and laminin-5 in human prostate carcinoma. *Prostate* 46, 240–248 (2001).

[124]. Mitra, S. K., Hanson, D. A. & Schlaepfer, D. D. Focal adhesion kinase: In command and control of cell motility. *Nat. Rev. Mol. Cell Biol.* 6, 56–68 (2005).

[125]. Jin, J. K., Dayyani, F. & Gallick, G. E. Steps in prostate cancer progression that lead to bone metastasis. *Int. J. Cancer* 128, 2545–2561 (2011).

[126]. Tremblay, L., Hauck, W., Aprikian, A. G., Begin, L. R., Chapdelaine, A. & Chevalier, S. Focal adhesion kinase (pp125(FAK)) expression, activation and association with paxillin and p50(CSK) in human metastatic prostate carcinoma. *Int. J. Cancer* 68, 164–171 (1996).

[127]. Rovin, J. D., Frierson, H. F., Ledinh, W., Parsons, J. T. & Adams, R. B. Expression of focal adhesion kinase in normal and pathologic human prostate tissues. *Prostate* 53, 124–132 (2002).

[128]. Winkler, J., Abisoye-Ogunniyan, A., Metcalf, K. J. & Werb, Z. Concepts of extracellular matrix remodelling in tumour progression and metastasis. *Nat. Commun.* 11, 1–19 (2020).

[129]. Morgia, G., Falsaperla, M., Malaponte, G., Madonia, M., Indelicato, M., Travali, S. & Mazzarino, M. C. Matrix metalloproteinases as diagnostic (MMP-13) and prognostic (MMP-2, MMP-9) markers of prostate cancer. *Urol. Res.* 33, 44–50 (2005).

[130]. Wood, M., Fudge, K., Mohler, J. L., Frost, A. R., Garcia, F., Wang, M. & Stearns, M. E. In situ hybridization studies of metalloproteinases 2 and 9 and TIMP-1 and TIMP-2 expression in human prostate cancer. *Clin. Exp. Metastasis* 15, 246–258 (1997).

[131]. Zhang, X. Y., Hong, B. F., Chen, G. F., Lu, Y. L. & Zhong, M. Significance of MMP2 and MMP9 expression in prostate cancer. *Zhonghua Nan Ke Xue* 11, (2005).

[132]. Pego, E. R., Fernández, I. & Núñez, M. J. Molecular basis of the effect of MMP-9 on the prostate bone metastasis: A review. *Urol. Oncol. Semin. Orig. Investig.* 36, 272–282 (2018).

[133]. Aalinkeel, R., Nair, B. B., Reynolds, J. L., Sykes, D. E., Mahajan, S. D., Chadha, K. C. & Schwartz, S. A. Overexpression of MMP-9 contributes to invasiveness of prostate cancer cell line LNCaP. *Immunol. Invest.* 40, 447–464 (2011).

[134]. Lichtinghagen, R., Musholt, P. B., Lein, M., Römer, A., Rudolph, B., Kristiansen, G., Hauptmann, S., Schnorr, D., Loening, S. A. & Jung, K. Different mRNA and protein expression of matrix metalloproteinases 2 and 9 and tissue inhibitor of metalloproteinases 1 in benign and malignant prostate tissue. *Eur. Urol.* 42, 398–406 (2002).

[135]. Overall, C. M. & López-Otín, C. Strategies for MMP inhibition in cancer: Innovations for the post-trial era. *Nat. Rev. Cancer* 2, 657–672 (2002).

[136]. Brehmer, B., Biesterfeld, S. & Jakse, G. Expression of matrix metalloproteinases (MMP-2 and -9) and their inhibitors (TIMP-1 and -2) in prostate cancer tissue. *Prostate Cancer Prostatic Dis.* 6, 217–222 (2003).

[137]. Schmitt, M., Wilhelm, O. G., Reuning, U., Krüger, A., Harbeck, N., Lengyel, E., *et al.* The urokinase plasminogen activator system as a novel target for tumour therapy. *Fibrinolysis and Proteolysis* 14, 114–132 (2000).

[138]. Morgan, H. & Hill, P. A. Human breast cancer cell-mediated bone collagen degradation requires plasminogen activation and matrix metalloproteinase activity. *Cancer Cell Int.* 5, 1–10 (2005).

[139]. Li, Y. & Cozzi, P. J. Targeting uPA/uPAR in prostate cancer. *Cancer Treat. Rev.* 33, 521–527 (2007).

[140]. Sheng, S. The urokinase-type plasminogen activator system in prostate cancer metastasis. *Cancer Metastasis Rev.* 20, 287–296 (2001).

[141]. Testa, J. E. & Quigley, J. P. The role of urokinase-type plasminogen activator in aggressive tumor cell behavior. *Cancer Metastasis Rev.* 9, 353–367 (1990).

[142]. Festuccia, C., Dolo, V., Guerra, F., Violini, S., Muzi, P., Pavan, A. & Bologna, M. Plasminogen activator system modulates invasive capacity and proliferation in prostatic tumor cells. *Clin. Exp. Metastasis* 16, 513–528 (1998).

[143]. Dong, Z., Saliganan, A. D., Meng, H., Nabha, S. M., Sabbota, A. L., Sheng, S., Bonfil, R. D. & Cher, M. L. Prostate cancer cell-derived urokinase-type plasminogen activator contributes to intraosseous tumor growth and bone turnover. *Neoplasia* 10, 439–449 (2008).

[144]. Kumano, M., Miyake, H., Muramaki, M., Furukawa, J., Takenaka, A. & Fujisawa, M. Expression of urokinase-type plasminogen activator system in prostate cancer: Correlation with clinicopathological outcomes in patients undergoing radical prostatectomy. *Urol. Oncol. Semin. Orig. Investig.* 27, 180–186 (2009).

[145]. Sloane, B. F. Cathepsin B and cystatins: Evidence for a role in cancer progression. *Semin. Cancer Biol.* 1, 137–152 (1990).

[146]. Fernández, P. L., Farré, X., Nadal, A., Fernández, E., Peiró, N., Sloane, B. F., Shi, G. P., Chapman, H. A., Campo, E. as & Cardesa, A. Expression of Cathepsins B and S in the progression of prostate carcinoma. *Int. J. Cancer* 95, 51–55 (2001).

[147]. Sinha, A. A., Quast, B. J., Wilson, M. J., Fernandes, E. T., Reddy, P. K., Ewing, S. L., Sloane, B. F. & Gleason, D. F. Ratio of cathepsin B to stefin A identifies heterogeneity within Gleason histologic scores for human prostate cancer. *Prostate* 48, 274–284 (2001).

[148]. Brubaker, K. D., Vessella, R. L., True, L. D., Thomas, R. & Corey, E. Cathepsin K mRNA and protein expression in prostate cancer progression. *J. Bone Miner. Res.* 18, 222–230 (2003).

[149]. Miyake, H., Hara, I. & Eto, H. Prediction of the extent of prostate cancer by the combined use of systematic biopsy and serum level of cathepsin D. *Int. J. Urol.* 10, 196–200 (2003).

[150]. Johnson, M. D., Torri, J. A., Lippman, M. E. & Dickson, R. B. The Role of Cathepsin D in the Invasiveness of Human Breast Cancer Cells. *Cancer Res.* 53, 873–877 (1993).

[151]. Hahnel, R., Harvey, J., Robbins, P. & Sterrett, G. Cathepsin-D in human breast cancer: Correlation with vascular invasion and other clinical and histopathological characteristics. *Anticancer Res.* 13, 2131–2135 (1993).

[152]. Hauschka, P. V., Mavrakos, A. E., Iafrati, M. D., Doleman, S. E. & Klagsbrun, M. Growth factors in bone matrix. Isolation of multiple types by affinity chromatography on heparin-Sepharose. *J. Biol. Chem.* 261, 12665–12674 (1986).

[153]. Casimiro, S., Guise, T. A. & Chirgwin, J. The critical role of the bone microenvironment in cancer metastases. *Mol. Cell. Endocrinol.* 310, 71–81 (2009).

[154]. Vessella, R. L., Corey, E., Guise, Clohisy, Rogers, Roodman, Weilbaecher, Smith & Suva. Targeting factors involved in bone remodeling as treatment strategies in prostate cancer bone metastasis. *Clin. Cancer Res.* 12, 6285s-6290s (2006).

[155]. Morrissey, C. & Vessella, R. L. The role of tumor microenvironment in prostate cancer bone metastasis. *J. Cell. Biochem.* 101, 873–886 (2007).

[156]. Kingsley, L. A., Fournier, P. G. J., Chirgwin, J. M. & Guise, T. A. Molecular biology of bone metastasis. *Mol. Cancer Ther.* 6, 2609–2617 (2007).

[157]. Doglioni, G., Parik, S. & Fendt, S. M. Interactions in the (pre)metastatic niche support metastasis formation. *Front. Oncol.* 9, 219 (2019).

[158]. Lehr, J. E. & Pienta, K. J. Preferential adhesion of prostate cancer cells to a human bone marrow endothelial cell line. *J. Natl. Cancer Inst.* 90, 118–123 (1998).

[159]. Cooper, C. R., McLean, L., Walsh, M., Taylor, J., Hayasaka, S., Bhatia, J. & Pienta, K. J. Preferential adhesion of prostate cancer cells to bone is mediated by binding to bone marrow endothelial cells as compared to extracellular matrix components in vitro. *Clin. Cancer Res.* 6, 4839–4847 (2000).

[160]. Mazo, I. B. & Von Andrian, U. H. Adhesion and homing of blood-borne cells in bone marrow microvessels. *J. Leukoc. Biol.* 66, 25–32 (1999).

[161]. Mårtensson, S., Bigler, S. A., Brown, M., Lange, P. H., Brawer, M. K. & Hakomori, S. itiroh. Sialyl-LewisX and related carbohydrate antigens in the prostate. *Hum. Pathol.* 26, 735–739 (1995).

[162]. Romanov, V. I. & Goligorsky, M. S. RGD-recognizing integrins mediate interactions of human prostate carcinoma cells with endothelial cells in vitro. *Prostate* 39, 108–118 (1999).

[163]. McCabe, N. P., De, S., Vasanji, A., Brainard, J. & Byzova, T. V. Prostate cancer specific integrin $\alpha v\beta 3$ modulates bone metastatic growth and tissue remodeling. *Oncogene* 26, 6238–6243 (2007).

[164]. Hall, C. L., Dai, J. L., Van Golen, K. L., Keller, E. T. & Long, M. W. Type I collagen receptor ($\alpha 2\beta 1$) signaling promotes the growth of human prostate cancer cells within the bone. *Cancer Res.* 66, 8648–8654 (2006).

[165]. Chu, K., Cheng, C. J., Ye, X., Lee, Y. C., Zurita, A. J., Chen, D. T., *et al.* Cadherin-11 promotes the metastasis of prostate cancer cells to bone. *Mol. Cancer Res.* 6, 1259–1267 (2008).

[166]. Turner, C. J. & Edwards, C. M. The Role of the Microenvironment in Prostate Cancer-Associated Bone Disease. *Curr. Osteoporos. Rep.* 14, 170–177 (2016).

[167]. Taichman, R. S., Cooper, C., Keller, E. T., Pienta, K. J., Taichman, N. S. & McCauley, L. K. Use of the stromal cell-derived factor-1/CXCR4 pathway in prostate cancer metastasis to bone. *Cancer Res.* 62, 1832–1837 (2002).

[168]. Sun, Y. X., Wang, J., Shelburne, C. E., Lopatin, D. E., Chinnaiyan, A. M., Rubin, M. A., Pienta, K. J. & Taichman, R. S. Expression of CXCR4 and CXCL12 (SDF-1) in human prostate cancers (PCa) in vivo. *J. Cell. Biochem.* 89, 462–473 (2003).

[169]. Sun, Y. X., Schneider, A., Jung, Y., Wang, J., Dai, J., Wang, J., *et al.* Skeletal localization and neutralization of the SDF-1(CXCL12)/CXCR4 axis blocks prostate cancer metastasis and growth in osseous sites in vivo. *J. Bone Miner. Res.* 20, 318–329 (2005).

[170]. Hart, C. A., Brown, M., Bagley, S., Sharrard, H. & Clarke, N. W. Invasive characteristics of human prostatic epithelial cells: Understanding the metastatic process. *Br. J. Cancer* 92, 503–512 (2005).

[171]. Clarke, N. W., Hart, C. A. & Brown, M. D. Molecular mechanisms of metastasis in prostate cancer. *Asian J. Androl.* 11, 57–67 (2009).

[172]. Kozlow, W. & Guise, T. A. Breast cancer metastasis to bone: Mechanisms of osteolysis and implications for therapy. *J. Mammary Gland Biol. Neoplasia* 10, 169–180 (2005).

[173]. Charhon, S. A., Chapuy, M. C., Delvin, E. E., Valentin-Opran, A., Edouard, C. M. & Meunier, P. J. Histomorphometric analysis of sclerotic bone metastases from prostatic carcinoma with special reference to osteomalacia. *Cancer* 51, 918–924 (1983).

[174]. Capulli, M., Paone, R. & Rucci, N. Osteoblast and osteocyte: Games without frontiers. *Arch. Biochem. Biophys.* 561, 3–12 (2014).

[175]. Amarasekara, D. S., Kim, S. & Rho, J. Regulation of osteoblast differentiation by cytokine networks. *Int. J. Mol. Sci.* 22, 1–16 (2021).

[176]. Pratap, J., Lian, J. B., Javed, A., Barnes, G. L., Van Wijnen, A. J., Stein, J. L. & Stein, G. S. Regulatory roles of Runx2 in metastatic tumor and cancer cell interactions with bone. *Cancer Metastasis Rev.* 25, 589–600 (2006).

[177]. Enomoto, H., Shiojiri, S., Hoshi, K., Furuichi, T., Fukuyama, R., Yoshida, C. A., *et al.* Induction of osteoclast differentiation by Runx2 through receptor activator of nuclear factor-κB ligand (RANKL) and osteoprotegerin regulation and partial rescue of osteoclastogenesis in Runx2-/- mice by RANKL transgene. *J. Biol. Chem.* 278, 23971–23977 (2003).

[178]. Yu, S., Zhu, K., Lai, Y., Zhao, Z., Fan, J., Im, H. J., Chen, D. & Xiao, G. ATF4 promotes β-catenin expression and osteoblastic differentiation of bone marrow mesenchymal stem cells. *Int. J. Biol. Sci.* 9, 256–266 (2013).

[179]. Sharma, U., Pal, D. & Prasad, R. Alkaline phosphatase: An overview. *Indian J. Clin. Biochem.* 29, 269–278 (2014).

[180]. Millán, J. L. *Mammalian Alkaline Phosphatases: From Biology to Applications in Medicine and Biotechnology*. *Mammalian Alkaline Phosphatases: From Biology to Applications in Medicine and Biotechnology* (2006). doi:10.1002/3527608060.

[181]. Magnusson, P., Degerblad, M., Sääf, M., Larsson, L. & Thorén, M. Different responses of bone alkaline phosphatase isoforms during recombinant insulin-like growth factor-I (IGF-I) and during growth hormone therapy in adults with growth hormone deficiency. *J. Bone Miner. Res.* 12, 210–220 (1997).

[182]. Magnusson, P., Löfman, O. & Larsson, L. Determination of alkaline phosphatase isoenzymes in serum by high-performance liquid chromatography with post-column reaction detection. *J. Chromatogr. B Biomed. Sci. Appl.* 576, 79–86

(1992).

[183]. Kuo, T. R. & Chen, C. H. Bone biomarker for the clinical assessment of osteoporosis: Recent developments and future perspectives. *Biomark. Res.* 5, 1–9 (2017).

[184]. Phan, T. C. A., Xu, J. & Zheng, M. H. Interaction between osteoblast and osteoclast: Impact in bone disease. *Histol. Histopathol.* 19, 1325–1344 (2004).

[185]. Crockett, J. C., Rogers, M. J., Coxon, F. P., Hocking, L. J. & Helfrich, M. H. Bone remodelling at a glance. *J. Cell Sci.* 124, 991–998 (2011).

[186]. Nelson, J. B., Hedican, S. P., George, D. J., Reddi, A. H., Piantadosi, S., Eisenberger, M. A. & Simons, J. W. Identification of endothelin-1 in the pathophysiology of metastatic adenocarcinoma of the prostate. *Nat. Med.* 1, 944–949 (1995).

[187]. Guise, T. A., Yin, J. J. & Mohammad, K. S. Role of endothelin-1 in osteoblastic bone metastases. *Cancer* 97, 779–784 (2003).

[188]. Chiao, J. W., Moonga, B. S., Yang, Y. M., Kancherla, R., Mittelman, A., Wu-Wong, J. R. & Ahmed, T. Endothelin-1 from prostate cancer cells is enhanced by bone contact which blocks osteoclastic bone resorption. *Br. J. Cancer* 83, 360–365 (2000).

[189]. Nelson, J. B., Chan-Tack, K., Hedican, S. P., Magnuson, S. R., Opgenorth, T. J., Bova, G. S. & Simons, J. W. Endothelin-1 production and decreased endothelin B receptor expression in advanced prostate cancer. *Cancer Res.* 56, 663–668 (1996).

[190]. Yin, J. J., Mohammad, K. S., Käkönen, S. M., Harris, S., Wu-Wong, J. R., Wessale, J. L., Padley, R. J., Garrett, I. R., Chirgwin, J. M. & Guise, T. A. A causal role for endothelin-1 in the pathogenesis of osteoblastic bone metastases. *Proc. Natl. Acad. Sci. U. S. A.* 100, 10954–10959 (2003).

[191]. Takuwa, Y., Masaki, T. & Yamashita, K. The effects of the endothelin family peptides on cultured osteoblastic cells from rat calvariae. *Biochem. Biophys. Res. Commun.* 170, 998–1005 (1990).

[192]. Tsukahara, H., Hori, C., Hiraoka, M., Yamamoto, K., Ishii, Y. & Mayumi, M. Endothelin subtype A receptor antagonist induces osteopenia in growing rats. *Metabolism.* 47, 1403–1407 (1998).

[193]. Nelson, J. B., Nguyen, S. H., Wu-Wong, J. R., Opgenorth, T. J., Dixon, D. B., Chung, L. W. K. & Inoue, N. New bone formation in an osteoblastic tumor model is increased by endothelin-1 overexpression and decreased by endothelin A receptor blockade. *Urology* 53, 1063–1069 (1999).

[194]. Nelson, J. B., Sellers, W. R., Nelson, J. B., Smith, M. R., Kantoff, P. W., Roach, M. & Oh, W. K. Endothelin inhibition: Novel therapy for prostate cancer. *J. Urol.* 170, (2003).

[195]. Kopetz, E. S., Nelson, J. B. & Carducci, M. A. Endothelin-1 as a target for therapeutic intervention in prostate cancer. *Invest. New Drugs* 20, 173–182 (2002).

[196]. Drake, J. M., Danke, J. R. & Henry, M. D. Bone-specific growth inhibition of prostate cancer metastasis by atrasentan. *Cancer Biol. Ther.* 9, 607–614 (2010).

[197]. Carducci, M. A., Padley, R. J., Breul, J., Vogelzang, N. J., Zonnenberg, B. A., Daliani, D. D., *et al.* Effect of endothelin-A receptor blockade with atrasentan on tumor progression in men with hormone-refractory prostate cancer: A randomized, phase II, placebo-controlled trial. *J. Clin. Oncol.* 21, 679–689 (2003).

[198]. Clines, G. A., Mohammad, K. S., Bao, Y., Stephens, O. W., Suva, L. J., Shaughnessy, J. D., Fox, J. W., Chirgwin, J. M. & Guise, T. A. Dickkopf homolog 1 mediates endothelin-1-stimulated new bone formation. *Mol. Endocrinol.* 21, 486–498 (2007).

[199]. Dijksterhuis, J. P., Petersen, J. & Schulte, G. WNT/Frizzled signalling: Receptor-ligand selectivity with focus on FZD-G protein signalling and its physiological relevance: IUPHAR Review 3. *Br. J. Pharmacol.* 171, 1195–1209 (2014).

[200]. Clevers, H. Wnt/β-Catenin Signaling in Development and Disease. *Cell* 127, 469–480 (2006).

[201]. Hay, E., Faucheu, C., Suc-Royer, I., Touitou, R., Stiot, V., Vayssière, B., Baron, R., Roman-Roman, S. & Rawadi, G. Interaction between LRP5 and Frat1 mediates the activation of the Wnt canonical pathway. *J. Biol. Chem.* 280, 13616–13623 (2005).

[202]. Kawano, Y. & Kypta, R. Secreted antagonists of the Wnt signalling pathway. *J. Cell Sci.* 116, 2627–2634 (2003).

[203]. Mani, S. A., Guo, W., Liao, M. J., Eaton, E. N., Ayyanan, A., Zhou, A. Y., *et al.* The Epithelial-Mesenchymal Transition Generates Cells with Properties of Stem Cells. *Cell* 133, 704–715 (2008).

[204]. Hall, C. L., Kang, S., MacDougald, O. A. & Keller, E. T. Role of Wnts in prostate cancer bone metastases. *J. Cell. Biochem.* 97, 661–672 (2006).

[205]. Yardy, G. W. & Brewster, S. F. Wnt signalling and prostate cancer. *Prostate Cancer Prostatic Dis.* 8, 119–126 (2005).

[206]. Gaur, T., Lengner, C. J., Hovhannisyan, H., Bhat, R. A., Bodine, P. V. N., Komm, B. S., Javed, A., Van Wijnen, A. J., Stein, J. L., Stein, G. S. & Lian, J. B.

Canonical WNT signaling promotes osteogenesis by directly stimulating Runx2 gene expression. *J. Biol. Chem.* 280, 33132–33140 (2005).

[207]. Cho, Y. D., Yoon, W. J., Kim, W. J., Woo, K. M., Baek, J. H., Lee, G., Ku, Y., Van Wijnen, A. J. & Ryoo, H. M. Epigenetic modifications and canonical wingless/int-1 class (WNT) signaling enable trans-differentiation of nonosteogenic cells into osteoblasts. *J. Biol. Chem.* 289, 20120–20128 (2014).

[208]. Boissan, M., De Wever, O., Lizarraga, F., Wendum, D., Poincloux, R., Chignard, N., *et al.* Implication of metastasis suppressor NM23-H1 in maintaining adherens junctions and limiting the invasive potential of human cancer cells. *Cancer Res.* 70, 7710–7722 (2010).

[209]. Chen, G., Shukeir, N., Potti, A., Sircar, K., Aprikian, A., Goltzman, D. & Rabbani, S. A. Up-regulation of Wnt-1 and β-catenin production in patients with advanced metastatic prostate carcinoma: Potential pathogenetic and prognostic implications. *Cancer* 101, 1345–1356 (2004).

[210]. Hall, C. L., Daignault, S. D., Shah, R. B., Pienta, K. J. & Keller, E. T. Dickkopf-1 expression increases early in prostate cancer development and decreases during progression from primary tumor to metastasis. *Prostate* 68, 1396–1404 (2008).

[211]. Hall, C. L., Bafico, A., Dai, J., Aaronson, S. A. & Keller, E. T. Prostate cancer cells promote osteoblastic bone metastases through Wnts. *Cancer Res.* 65, 7554–7560 (2005).

[212]. Ide, H., Yoshida, T., Matsumoto, N., Aoki, K., Osada, Y., Sugimura, T. & Terada, M. Growth regulation of human prostate cancer cells by bone morphogenetic protein-2. *Cancer Res.* 57, 5022–5027 (1997).

[213]. Abe, E., Yamamoto, M., Taguchi, Y., Lecka-Czernik, B., O'Brien, C. A., Economides, A. N., Stahl, N., Jilka, R. L. & Manolagas, S. C. Essential requirement of BMPs-2/4 for both osteoblast and osteoclast formation in murine bone marrow cultures from adult mice: Antagonism by noggin. *J. Bone Miner. Res.* 15, 663–673 (2000).

[214]. Gori, F., Thomas, T., Hicok, K. C., Spelsberg, T. C. & Riggs, B. L. Differentiation of human marrow stromal precursor cells: Bone morphogenetic protein-2 increases OSF2/CBFA1, enhances osteoblast commitment, and inhibits late adipocyte maturation. *J. Bone Miner. Res.* 14, 1522–1535 (1999).

[215]. Rentsch, C. A., Cecchini, M. G. & Thalmann, G. N. Loss of inhibition over master pathways of bone mass regulation results in osteosclerotic bone metastases in prostate cancer. *Swiss Med. Wkly.* 139, 220–225 (2009).

[216]. Masuda, H., Fukabori, Y., Nakano, K., Takezawa, Y., Suzuki, T. & Yamanaka,

H. Increased expression of bone morphogenetic protein-7 in bone metastatic prostate cancer. *Prostate* 54, 268–274 (2003).

[217]. Bentley, H., Seid, J. M., Russell, R. G. G., Hamdy, F. C., Williams, J. L., Hart, K. A. & Ohnstone, D. Expression of bone morphogenetic proteins in human prostatic adenocarcinoma and benign prostatic hyperplasia. *Br. J. Cancer* 66, 1159–1163 (1992).

[218]. Autzen, P., Robson, C. N., Bjartell, A., Malcolm, A. J., Johnson, M. I., Neal, D. E. & Hamdy, F. C. Bone morphogenetic protein 6 in skeletal metastases from prostate cancer and other common human malignancies. *Br. J. Cancer* 78, 1219–1223 (1998).

[219]. Thomas, B. G. & Hamdy, F. C. Bone morphogenetic protein-6: Potential mediator of osteoblastic metastases in prostate cancer. *Prostate Cancer Prostatic Dis.* 3, 283–285 (2000).

[220]. Dai, J., Keller, J., Zhang, J., Lu, Y., Yao, Z. & Keller, E. T. Bone morphogenetic protein-6 promotes osteoblastic prostate cancer bone metastases through a dual mechanism. *Cancer Res.* 65, 8274–8285 (2005).

[221]. Feeley, B. T., Gamradt, S. C., Hsu, W. K., Liu, N., Krenek, L., Robbins, P., Huard, J. & Lieberman, J. R. Influence of BMPs on the formation of osteoblastic lesions in metastatic prostate cancer. *J. Bone Miner. Res.* 20, 2189–2199 (2005).

[222]. Virk, M. S., Petrigliano, F. A., Liu, N. Q., Chatziioannou, A. F., Stout, D., Kang, C. O., Dougall, W. C. & Lieberman, J. R. Influence of simultaneous targeting of the bone morphogenetic protein pathway and RANK/RANKL axis in osteolytic prostate cancer lesion in bone. *Bone* 44, 160–167 (2009).

[223]. Lai, T. H., Fong, Y. C., Fu, W. M., Yang, R. Sen & Tang, C. H. Osteoblasts-derived BMP-2 enhances the motility of prostate cancer cells via activation of integrins. *Prostate* 68, 1341–1353 (2008).

[224]. Fürstenberger, G. & Senn, H. J. Insulin-like growth factors and cancer. *Lancet Oncol.* 3, 298–302 (2002).

[225]. Koch, H., Jadlowiec, J. A. & Campbell, P. G. Insulin-like growth factor-I induces early osteoblast gene expression in human mesenchymal stem cells. *Stem Cells Dev.* 14, 621–631 (2005).

[226]. Ganguly, S. S., Li, X. & Miranti, C. K. The host microenvironment influences prostate cancer invasion, systemic spread, bone colonization, and osteoblastic metastasis. *Front. Oncol.* 4, (2014).

[227]. Ryan, C. J., Haqq, C. M., Simko, J., Nonaka, D. F., Chan, J. M., Weinberg, V., Small, E. J. & Goldfine, I. D. Expression of insulin-like growth factor-1 receptor

in local and metastatic prostate cancer. *Urol. Oncol. Semin. Orig. Investig.* 25, 134–140 (2007).

[228]. Rubin, J., Chung, L. W. K., Fan, X., Zhu, L., Murphy, T. C., Nanes, M. S. & Rosen, C. J. Prostate Carcinoma Cells That Have Resided in Bone Have an Upregulated IGF-I Axis. *Prostate* 58, 41–49 (2004).

[229]. Ritchie, C. K., Andrews, L. R., Thomas, K. G., Tindall, D. J. & Fitzpatrick, L. A. The effects of growth factors associated with osteoblasts on prostate carcinoma proliferation and chemotaxis: Implications for the development of metastatic disease. *Endocrinology* 138, 1145–1150 (1997).

[230]. Grzmil, M., Hemmerlein, B., Thelen, P., Schweyer, S. & Burfiend, P. Blockade of the type I IGF receptor expression in human prostate cancer cells inhibits proliferation and invasion, up-regulates IGF binding protein-3 and suppresses MMP-2 expression. *J. Pathol.* 202, 50–59 (2004).

[231]. Kimura, T., Kuwata, T., Ashimine, S., Yamazaki, M., Yamauchi, C., Nagai, K., Ikehara, A., Feng, Y., Dimitrov, D. S., Saito, S. & Ochiai, A. Targeting of bone-derived insulin-like growth factor-II by a human neutralizing antibody suppresses the growth of prostate cancer cells in a human bone environment. *Clin. Cancer Res.* 16, 121–129 (2010).

[232]. Rubin, J., Fan, X., Rahnert, J., Sen, B., Hsieh, C. L., Murphy, T. C., Nanes, M. S., Horton, L. G., Beamer, W. G. & Rosen, C. J. IGF-I secretion by prostate carcinoma cells does not alter tumor-bone cell interactions in vitro or in vivo. *Prostate* 66, 789–800 (2006).

[233]. Hofbauer, L. C., Khosla, S., Dunstan, C. R., Lacey, D. L., Boyle, W. J. & Riggs, B. L. The roles of osteoprotegerin and osteoprotegerin ligand in the paracrine regulation of bone resorption. *J. Bone Miner. Res.* 15, 2–12 (2000).

[234]. Darnay, B. G., Besse, A., Poblenz, A. T., Lamothe, B. & Jacoby, J. J. TRAFs in RANK signaling. *Adv. Exp. Med. Biol.* 597, 152–159 (2007).

[235]. Boyle, W. J., Simonet, W. S. & Lacey, D. L. Osteoclast differentiation and activation. *Nature* 423, 337–342 (2003).

[236]. Schoppet, M., Preissner, K. T. & Hofbauer, L. C. RANK ligand and osteoprotegerin: Paracrine regulators of bone metabolism and vascular function. *Arterioscler. Thromb. Vasc. Biol.* 22, 549–553 (2002).

[237]. Ohtaka, M., Kawahara, T., Mochizuki, T., Takamoto, D., Hattori, Y., Teranishi, J. ichi, *et al.* RANK/RANKL expression in prostate cancer. *Int. J. Surg. Case Rep.* 30, 106–107 (2017).

[238]. Roodman, G. D. Mechanisms of Bone Metastasis. *N. Engl. J. Med.* 350, 1655–

1664 (2004).

[239]. Bartsch, R. & Steger, G. G. Role of denosumab in breast cancer. *Expert Opin. Biol. Ther.* 9, 1225–1233 (2009).

[240]. Stopeck, A. T., Lipton, A., Body, J. J., Steger, G. G., Tonkin, K., De Boer, R. H., *et al.* Denosumab compared with zoledronic acid for the treatment of bone metastases in patients with advanced breast cancer: A randomized, double-blind study. *J. Clin. Oncol.* 28, 5132–5139 (2010).

[241]. Hegemann, M., Bedke, J., Stenzl, A. & Todenhöfer, T. Denosumab treatment in the management of patients with advanced prostate cancer: Clinical evidence and experience. *Ther. Adv. Urol.* 9, 81–88 (2017).

[242]. Odero-Marah, V. A., Wang, R., Chu, G., Zayzafoon, M., Xu, J., Shi, C., Marshall, F. F., Zhau, H. E. & Chung, L. W. K. Receptor activator of NF-κB Ligand (RANKL) expression is associated with epithelial to mesenchymal transition in human prostate cancer cells. *Cell Res.* 18, 858–870 (2008).

[243]. Zhau, H. E., Odero-Marah, V., Lue, H. W., Nomura, T., Wang, R., Chu, G., Liu, Z. R., Zhou, B. P., Huang, W. C. & Chung, L. W. K. Epithelial to mesenchymal transition (EMT) in human prostate cancer: Lessons learned from ARCaP model. *Clin. Exp. Metastasis* 25, 601–610 (2008).

[244]. Liao, J., Li, X., Koh, A. J., Berry, J. E., Thudi, N., Rosol, T. J., Pienta, K. J. & McCauley, L. K. Tumor expressed PTHrP facilitates prostate cancer-induced osteoblastic lesions. *Int. J. Cancer* 123, 2267–2278 (2008).

[245]. Thomas, R. J., Guise, T. A., Yin, J. J., Elliott, J., Horwood, N. J., Martin, T. J. & Gillespie, M. T. Breast cancer cells interact with osteoblasts to support osteoclast formation. *Endocrinology* 140, 4451–4458 (1999).

[246]. Asadi, F., Farraj, M., Sharifi, R., Malakouti, S., Antar, S. & Kukreja, S. Enhanced expression of parathyroid hormone-related protein in prostate cancer as compared with benign prostatic hyperplasia. *Hum. Pathol.* 27, 1319–1323 (1996).

[247]. Bryden, A. A. G., Islam, S., Freemont, A. J., Shanks, J. H., George, N. J. R. & Clarke, N. W. Parathyroid hormone-related peptide: Expression in prostate cancer bone metastases. *Prostate Cancer Prostatic Dis.* 5, 59–62 (2002).

[248]. Hoey, R. P., Sanderson, C., Iddon, J., Brady, G., Bundred, N. J. & Anderson, N. G. The parathyroid hormone-related protein receptor is expressed in breast cancer bone metastases and promotes autocrine proliferation in breast carcinoma cells. *Br. J. Cancer* 88, 567–573 (2003).

[249]. Edwards, C. M. & Johnson, R. W. From Good to Bad: The Opposing Effects of PTHrP on Tumor Growth, Dormancy, and Metastasis Throughout Cancer

Progression. *Front. Oncol.* 11, 728 (2021).

[250]. Ongkeko, W. M., Burton, D., Kiang, A., Abhold, E., Kuo, S. Z., Rahimy, E., Yang, M., Hoffman, R. M., Wang-Rodriguez, J. & Deftos, L. J. Parathyroid hormone related-protein promotes epithelial-to-mesenchymal transition in prostate cancer. *PLoS One* 9, e85803 (2014).

[251]. Danielpour, D. Functions and regulation of transforming growth factor-beta (TGF-β) in the prostate. *Eur. J. Cancer* 41, 846–857 (2005).

[252]. Bello-DeOcampo, D. & Tindall, D. TGF-ß / Smad Signaling in Prostate Cancer. *Curr. Drug Targets* 4, 197–207 (2005).

[253]. Dallas, S. L., Zhao, S., Cramer, S. D., Chen, Z., Peehl, D. M. & Bonewald, L. F. Preferential production of latent transforming growth factor β-2 by primary prostatic epithelial cells and its activation by prostate-specific antigen. *J. Cell. Physiol.* 202, 361–370 (2005).

[254]. Josson, S., Matsuoka, Y., Chung, L. W. K., Zhau, H. E. & Wang, R. Tumor-stroma co-evolution in prostate cancer progression and metastasis. *Semin. Cell Dev. Biol.* 21, 26–32 (2010).

[255]. Yin, J. J., Selander, K., Chirgwin, J. M., Dallas, M., Grubbs, B. G., Wieser, R., Massagué, J., Mundy, G. R. & Guise, T. A. TGF-β signaling blockade inhibits PTHrP secretion by breast cancer cells and bone metastases development. *J. Clin. Invest.* 103, 197–206 (1999).

[256]. Kang, Y., Siegel, P. M., Shu, W., Drobnjak, M., Kakonen, S. M., Cordón-Cardo, C., Guise, T. A. & Massagué, J. A multigenic program mediating breast cancer metastasis to bone. *Cancer Cell* 3, 537–549 (2003).

[257]. Festuccia, C., Bologna, M., Gravina, G. L., Guerra, F., Angelucci, A., Villanova, I., Millimaggi, D. & Teti, A. Osteoblast conditioned media contain TGF-β1 and modulate the migration of prostate tumor cells and their interactions with extracellular matrix components. *Int. J. Cancer* 81, 395–403 (1999).

[258]. Gupta, G. P. & Massagué, J. Cancer Metastasis: Building a Framework. *Cell* 127, 679–695 (2006).

[259]. Parvani, J. G., Galliher-Beckley, A. J., Schiemann, B. J. & Schiemann, W. P. Targeted inactivation of β1 integrin induces β3 integrin switching, which drives breast cancer metastasis by TGF-β. *Mol. Biol. Cell* 24, 3449–3459 (2013).

[260]. Miyazono, K. Transforming growth factor-β signaling in epithelial-mesenchymal transition and progression of cancer. *Proc. Japan Acad. Ser. B Phys. Biol. Sci.* 85, 314–323 (2009).

[261]. Yang, H., Wang, L., Zhao, J., Chen, Y., Lei, Z., Liu, X., Xia, W., Guo, L. & Zhang, H. T. TGF-β-activated SMAD3/4 complex transcriptionally upregulates N-cadherin expression in non-small cell lung cancer. *Lung Cancer* 87, 249–257 (2015).

[262]. Xu, J., Lamouille, S. & Derynck, R. TGF-B-induced epithelial to mesenchymal transition. *Cell Res.* 19, 156–172 (2009).

[263]. biorender.com. Metastasis to Bone Disrupts Bone Homeostasis. https://app.biorender.com/biorender-templates (2021).

[264]. Liao, J. & McCauley, L. K. Skeletal metastasis: Established and emerging roles of parathyroid hormone related protein (PTHrP). *Cancer Metastasis Rev.* 25, 559–571 (2006).

[265]. Neville-Webbe, H. L. & Coleman, R. E. Bisphosphonates and RANK ligand inhibitors for the treatment and prevention of metastatic bone disease. *Eur. J. Cancer* 46, 1211–1222 (2010).

[266]. Lin, J. H. Bisphosphonates: A review of their pharmacokinetic properties. *Bone* 18, 75–85 (1996).

[267]. Smith, M. R., Saad, F., Coleman, R., Shore, N., Fizazi, K., Tombal, B., *et al.* Denosumab and bone-metastasis-free survival in men with castration-resistant prostate cancer: Results of a phase 3, randomised, placebo-controlled trial. *Lancet* 379, 39–46 (2012).

[268]. Robinson, R. G. Strontium-89–-precursor targeted therapy for pain relief of blastic metastatic disease. *Cancer* 72, 3433–3435 (1993).

[269]. Sartor, O., Reid, R. H., Hoskin, P. J., Quick, D. P., Ell, P. J., Coleman, R. E., Kotler, J. A., Freeman, L. M. & Olivier, P. Samarium-153-lexidronam complex for treatment of painful bone metastases in hormone-refractory prostate cancer. *Urology* 63, 940–945 (2004).

[270]. Goyal, J. & Antonarakis, E. S. Bone-targeting radiopharmaceuticals for the treatment of prostate cancer with bone metastases. *Cancer Lett.* 323, 135–146 (2012).

[271]. Brady, D., Parker, C. C. & O'Sullivan, J. M. Bone-targeting radiopharmaceuticals including radium-223. *Cancer Journal (United States)* vol. 19 71–78 (2013).

[272]. Nilsson, S. Radionuclide Therapies in Prostate Cancer: Integrating Radium-223 in the Treatment of Patients With Metastatic Castration-Resistant Prostate Cancer. *Curr. Oncol. Rep.* 18, 1–12 (2016).

[273]. Zaorsky, N. G., Shaikh, T., Murphy, C. T., Hallman, M. A., Hayes, S. B., Sobczak,

M. L. & Horwitz, E. M. Comparison of outcomes and toxicities among radiation therapy treatment options for prostate cancer. *Cancer Treatment Reviews* vol. 48 50–60 (2016).

[274]. Stylianou, N., Lehman, M. L., Wang, C., Fard, A. T., Rockstroh, A., Fazli, L., *et al.* A molecular portrait of epithelial–mesenchymal plasticity in prostate cancer associated with clinical outcome. *Oncogene* 38, 913–934 (2019).

[275]. Corey, E., Quinn, J. E., Buhler, K. R., Nelson, P. S., Macoska, J. A., True, L. D. & Vessella, R. L. LuCaP 35: A new model of prostate cancer progression to androgen independence. *Prostate* 55, 239–246 (2003).

[276]. Giaconia, J. M., Edgehouse, N. L., Pretlow, T. P., Pretlow, T. G. & Seftel, A. CWR22: Androgen-dependent Xenograft Model Derived from a Primary Human Prostatic Carcinoma. *Cancer Res.* 54, 6049–6052 (1994).

[277]. Nakouzi, N. Al, Bawa, O., le Pape, A., Lerondel, S., Gaudin, C., Opolon, P., Gonin, P., Fizazi, K. & Chauchereau, A. The IGR-CaP1 xenograft model recapitulates mixed osteolytic/ blastic bone lesions observed in metastatic prostate cancer. *Neoplasia (United States)* 14, 376–387 (2012).

[278]. Zhau, H. Y. E., Chang, S. M., Chen, B. Q., Wang, Y., Zhang, H., Kao, C., Sang, Q. A., Pathak, S. J. & Chung, L. W. K. Androgen-repressed phenotype in human prostate cancer. *Proc. Natl. Acad. Sci. U. S. A.* 93, 15152–15157 (1996).

[279]. Xu, J., Wang, R., Xie, Z. H., Odero-Marah, V., Pathak, S., Multani, A., Chung, L. W. K. & Zhau, H. E. Prostate cancer metastasis: Role of the host microenvironment in promoting epithelial to mesenchymal transition and increased bone and adrenal gland metastasis. *Prostate* 66, 1664–1673 (2006).

[280]. Haughey, C. M., Mukherjee, D., Steele, R. E., Popple, A., Dura-Perez, L., Pickard, A., *et al.* Development of a novel allograft model of prostate cancer: A new tool to inform clinical translation. *bioRxiv* (2020) doi:10.1101/2020.02.16.942789.

[281]. Cnop, M., Foufelle, F. & Velloso, L. A. Endoplasmic reticulum stress, obesity and diabetes. *Trends Mol. Med.* 18, 59–68 (2012).

[282]. Ron, D. Translational control in the endoplasmic reticulum stress response. *J. Clin. Invest.* 110, 1383–1388 (2002).

[283]. Ron, D. & Walter, P. Signal integration in the endoplasmic reticulum unfolded protein response. *Nat. Rev. Mol. Cell Biol.* 8, 519–529 (2007).

[284]. Bertolotti, A., Zhang, Y., Hendershot, L. M., Harding, H. P. & Ron, D. Dynamic interaction of BiP and ER stress transducers in the unfolded-protein response. *Nat. Cell Biol.* 2, 326–332 (2000).

[285]. Walter, P. & Ron, D. The unfolded protein response: From stress pathway to homeostatic regulation. *Science (80-. ).* 334, 1081–1086 (2011).

[286]. Credle, J. J., Finer-Moore, J. S., Papa, F. R., Stroud, R. M. & Walter, P. On the mechanism of sensing unfolded protein in the endoplasmic reticulum. *Proc. Natl. Acad. Sci. U. S. A.* 102, 18773–18784 (2005).

[287]. Haze, K., Yoshida, H., Yanagi, H., Yura, T. & Mori, K. Mammalian transcription factor ATF6 is synthesized as a transmembrane protein and activated by proteolysis in response to endoplasmic reticulum stress. *Mol. Biol. Cell* 10, 3787–3799 (1999).

[288]. Tsuru, A., Fujimoto, N., Takahashi, S., Saito, M., Nakamura, D., Iwano, M., Iwawaki, T., Kadokura, H., Ron, D. & Kohno, K. Negative feedback by IRE1β optimizes mucin production in goblet cells. *Proc. Natl. Acad. Sci. U. S. A.* 110, 2864–2869 (2013).

[289]. Martino, M. B., Jones, L., Brighton, B., Ehre, C., Abdulah, L., Davis, C. W., Ron, D., O'Neal, W. K. & Ribeiro, C. M. P. The ER stress transducer IRE1β is required for airway epithelial mucin production. *Mucosal Immunol.* 6, 639–654 (2013).

[290]. Imagawa, Y., Hosoda, A., Sasaka, S. ichi, Tsuru, A. & Kohno, K. RNase domains determine the functional difference between IRE1α and IRE1β. *FEBS Lett.* 582, 656–660 (2008).

[291]. Cox, J. S., Shamu, C. E. & Walter, P. Transcriptional induction of genes encoding endoplasmic reticulum resident proteins requires a transmembrane protein kinase. *Cell* 73, 1197–1206 (1993).

[292]. Morl, K., Ma, W., Gething, M. J. & Sambrook, J. A transmembrane protein with a cdc2+ CDC28-related kinase activity is required for signaling from the ER to the nucleus. *Cell* 74, 743–756 (1993).

[293]. Acosta-Alvear, D., Karagöz, G. E., Fröhlich, F., Li, H., Walther, T. C. & Walter, P. The unfolded protein response and endoplasmic reticulum protein targeting machineries converge on the stress sensor IRE1. *Elife* 7, (2018).

[294]. Yoshida, H., Matsui, T., Yamamoto, A., Okada, T. & Mori, K. XBP1 mRNA is induced by ATF6 and spliced by IRE1 in response to ER stress to produce a highly active transcription factor. *Cell* 107, 881–891 (2001).

[295]. Calfon, M., Zeng, H., Urano, F., Till, J. H., Hubbard, S. R., Harding, H. P., Clark, S. G. & Ron, D. IRE1 couples endoplasmic reticulum load to secretory capacity by processing the XBP-1 mRNA. *Nature* 415, 92–96 (2002).

[296]. Yoshida, H., Oku, M., Suzuki, M. & Mori, K. pXBP1(U) encoded in XBP1 pre-mRNA negatively regulates unfolded protein response activator pXBP1(S) in

mammalian ER stress response. *J. Cell Biol.* 172, 565–575 (2006).

[297]. Hollien, J. & Weissman, J. S. Decay of endoplasmic reticulum-localized mRNAs during the unfolded protein response. *Science (80-. ).* 313, 104–107 (2006).

[298]. Hollien, J., Lin, J. H., Li, H., Stevens, N., Walter, P. & Weissman, J. S. Regulated Ire1-dependent decay of messenger RNAs in mammalian cells. *J. Cell Biol.* 186, 323–331 (2009).

[299]. Nishitoh, H., Matsuzawa, A., Tobiume, K., Saegusa, K., Takeda, K., Inoue, K., Hori, S., Kakizuka, A. & Ichijo, H. ASK1 is essential for endoplasmic reticulum stress-induced neuronal cell death triggered by expanded polyglutamine repeats. *Genes Dev.* 16, 1345–1355 (2002).

[300]. Urano, F., Wang, X. Z., Bertolotti, A., Zhang, Y., Chung, P., Harding, H. P. & Ron, D. Coupling of stress in the ER to activation of JNK protein kinases by transmembrane protein kinase IRE1. *Science (80-. ).* 287, 664–666 (2000).

[301]. Mauro, C., Crescenzi, E., De Mattia, R., Pacifico, F., Mellone, S., Salzano, S., *et al.* Central role of the scaffold protein tumor necrosis factor receptor-associated factor 2 in regulating endoplasmic reticulum stress-induced apoptosis. *J. Biol. Chem.* 281, 2631–2638 (2006).

[302]. Ogata, M., Hino, S., Saito, A., Morikawa, K., Kondo, S., Kanemoto, S., *et al.* Autophagy Is Activated for Cell Survival after Endoplasmic ReticulumStress. *Mol. Cell. Biol.* 26, 9220–9231 (2006).

[303]. Harding, H. P., Zhang, Y. & Ron, D. Protein translation and folding are coupled by an endoplasmic- reticulum-resident kinase. *Nature* 397, 271–274 (1999).

[304]. Harding, H. P., Zhang, Y., Zeng, H., Novoa, I., Lu, P. D., Calfon, M., *et al.* An integrated stress response regulates amino acid metabolism and resistance to oxidative stress. *Mol. Cell* 11, 619–633 (2003).

[305]. Vattem, K. M. & Wek, R. C. Reinitiation involving upstream ORFs regulates ATF4 mRNA translation in mammalian cells. *Proc. Natl. Acad. Sci. U. S. A.* 101, 11269–11274 (2004).

[306]. Lu, P. D., Harding, H. P. & Ron, D. Translation reinitiation at alternative open reading frames regulates gene expression in an integrated stress response. *J. Cell Biol.* 167, 27–33 (2004).

[307]. Sanchez-Lopez, E., Zimmerman, T., Gomez Del Pulgar, T., Moyer, M. P., Lacal Sanjuan, J. C. & Cebrian, A. Choline kinase inhibition induces exacerbated endoplasmic reticulum stress and triggers apoptosis via CHOP in cancer cells. *Cell Death Dis.* 4, e933–e933 (2013).

[308]. Tsaytler, P., Harding, H. P., Ron, D. & Bertolotti, A. Selective inhibition of a regulatory subunit of protein phosphatase 1 restores proteostasis. *Science (80-. ).* 332, 91–94 (2011).

[309]. Puthalakath, H., O'Reilly, L. A., Gunn, P., Lee, L., Kelly, P. N., Huntington, N. D., *et al.* ER Stress Triggers Apoptosis by Activating BH3-Only Protein Bim. *Cell* 129, 1337–1349 (2007).

[310]. Wek, R. C., Jiang, H. Y. & Anthony, T. G. Coping with stress: EIF2 kinases and translational control. *Biochem. Soc. Trans.* 34, 7–11 (2006).

[311]. Yoshida, H., Uemura, A. & Mori, K. pXBP1(U), a negative regulator of the unfolded protein response activator pXBP1(S), targets ATF6 but not ATF4 in proteasome-mediated degradation. *Cell Struct. Funct.* 34, 1–10 (2009).

[312]. Yamamoto, K., Sato, T., Matsui, T., Sato, M., Okada, T., Yoshida, H., Harada, A. & Mori, K. Transcriptional Induction of Mammalian ER Quality Control Proteins Is Mediated by Single or Combined Action of ATF6$\alpha$ and XBP1. *Dev. Cell* 13, 365–376 (2007).

[313]. Teske, B. F., Wek, S. A., Bunpo, P., Cundiff, J. K., McClintick, J. N., Anthony, T. G. & Wek, R. C. The eIF2 kinase PERK and the integrated stress response facilitate activation of ATF6 during endoplasmic reticulum stress. *Mol. Biol. Cell* 22, 4390–4405 (2011).

[314]. Lin, J. H., Li, H., Yasumura, D., Cohen, H. R., Zhang, C., Panning, B., Shokat, K. M., LaVail, M. M. & Walter, P. IRE1 signaling affects cell fate during the unfolded protein response. *Science (80-. ).* 318, 944–949 (2007).

[315]. Lin, J. H., Li, H., Zhang, Y., Ron, D. & Walter, P. Divergent effects of PERK and IRE1 signaling on cell viability. *PLoS One* 4, e4170 (2009).

[316]. Braakman, I. & Hebert, D. N. Protein folding in the endoplasmic reticulum. *Cold Spring Harb. Perspect. Biol.* 5, a013201 (2013).

[317]. Christianson, J. C. & Ye, Y. Cleaning up in the endoplasmic reticulum: Ubiquitin in charge. *Nat. Struct. Mol. Biol.* 21, 325–335 (2014).

[318]. Christianson, J. C., Olzmann, J. A., Shaler, T. A., Sowa, M. E., Bennett, E. J., Richter, C. M., Tyler, R. E., Greenblatt, E. J., Wade Harper, J. & Kopito, R. R. Defining human ERAD networks through an integrative mapping strategy. *Nat. Cell Biol.* 14, 93–105 (2012).

[319]. Zhang, T., Xu, Y., Liu, Y. & Ye, Y. Gp78 functions downstream of Hrd1 to promote degradation of misfolded proteins of the endoplasmic reticulum. *Mol. Biol. Cell* 26, 4438–4450 (2015).

[320]. Olzmann, J. A., Kopito, R. R. & Christianson, J. C. The mammalian endoplasmic reticulum-associated degradation system. *Cold Spring Harb. Perspect. Biol.* 5, (2013).

[321]. Gonzalez, D. S., Karaveg, K., Vandersall-Nairn, A. S., Lal, A. & Moremen, K. W. Identification, expression, and characterization of a cDNA encoding human endoplasmic reticulum mannosidase I, the enzyme that catalyzes the first mannose trimming step in mammalian Asn-linked oligosaccharide biosynthesis. *J. Biol. Chem.* 274, 21375–21386 (1999).

[322]. Tremblay, L. O. & Herscovics, A. Cloning and expression of a specific human α1,2-mannosidase that trims Man9GlcNAc2 to Man8GlcNAc2 isomer B during N-glycan biosynthesis. *Glycobiology* 9, 1073–1078 (1999).

[323]. Olivari, S., Cali, T., Salo, K. E. H., Paganetti, P., Ruddock, L. W. & Molinari, M. EDEM1 regulates ER-associated degradation by accelerating de-mannosylation of folding-defective polypeptides and by inhibiting their covalent aggregation. *Biochem. Biophys. Res. Commun.* 349, 1278–1284 (2006).

[324]. Hosokawa, N., Tremblay, L. O., Sleno, B., Kamiya, Y., Wada, I., Nagata, K., Kato, K. & Herscovics, A. EDEM1 accelerates the trimming of α1,2-linked mannose on the C branch of N-glycans. *Glycobiology* 20, 567–575 (2010).

[325]. Hirao, K., Natsuka, Y., Tamura, T., Wada, I., Morito, D., Natsuka, S., *et al.* EDEM3, a soluble EDEM homolog, enhances glycoprotein endoplasmic reticulum-associated degradation and mannose trimming. *J. Biol. Chem.* 281, 9650–9658 (2006).

[326]. Hosokawa, N., Kamiya, Y., Kamiya, D., Kato, K. & Nagata, K. Human OS-9, a lectin required for glycoprotein endoplasmic reticulum-associated degradation, recognizes mannose-trimmed N-glycans. *J. Biol. Chem.* 284, 17061–17068 (2009).

[327]. Bernasconi, R., Pertel, T., Luban, J. & Molinari, M. A dual task for the Xbp1-responsive OS-9 variants in the mammalian endoplasmic reticulum: Inhibiting secretion of misfolded protein conformers and enhancing their disposal. *J. Biol. Chem.* 283, 16446–16454 (2008).

[328]. Christianson, J. C., Shaler, T. A., Tyler, R. E. & Kopito, R. R. OS-9 and GRP94 deliver mutant α1-antitrypsin to the Hrd1?SEL1L ubiquitin ligase complex for ERAD. *Nat. Cell Biol.* 10, 272–282 (2008).

[329]. Hosokawa, N., Wada, I., Nagasawa, K., Moriyama, T., Okawa, K. & Nagata, K. Human XTP3-B forms an endoplasmic reticulum quality control scaffold with the HRD1-SEL1L ubiquitin ligase complex and BiP. *J. Biol. Chem.* 283, 20914–20924 (2008).

[330]. Bernasconi, R., Galli, C., Calanca, V., Nakajima, T. & Molinari, M. Stringent requirement for HRD1, SEL1L, and OS-9/XTP3-B for disposal of ERAD-LS substrates. *J. Cell Biol.* 188, 223–235 (2010).

[331]. Sato, T., Sako, Y., Sho, M., Momohara, M., Suico, M. A., Shuto, T., *et al.* STT3B-Dependent Posttranslational N-Glycosylation as a Surveillance System for Secretory Protein. *Mol. Cell* 47, 99–110 (2012).

[332]. Carvalho, P., Stanley, A. M. & Rapoport, T. A. Retrotranslocation of a misfolded luminal ER protein by the ubiquitin-ligase hrd1p. *Cell* 143, 579–591 (2010).

[333]. Cormier, J. H., Tamura, T., Sunryd, J. C. & Hebert, D. N. EDEM1 Recognition and Delivery of Misfolded Proteins to the SEL1L-Containing ERAD Complex. *Mol. Cell* 34, 627–633 (2009).

[334]. Saeed, M., Suzuki, R., Watanabe, N., Masaki, T., Tomonaga, M., Muhammad, A., Kato, T., Matsuura, Y., Watanabe, H., Wakita, T. & Suzuki, T. Role of the Endoplasmic Reticulum-associated Degradation (ERAD) pathway in degradation of hepatitis C virus envelope proteins and production of virus particles. *J. Biol. Chem.* 286, 37264–37273 (2011).

[335]. Riemer, J., Appenzeller-Herzog, C., Johansson, L., Bodenmiller, B., Hartmann-Petersen, R. & Ellgaard, L. A luminal flavoprotein in endoplasmic reticulum-associated degradation. *Proc. Natl. Acad. Sci. U. S. A.* 106, 14831–14836 (2009).

[336]. Riemer, J., Hansen, H. G., Appenzeller-Herzog, C., Johansson, L. & Ellgaard, L. Identification of the PDI-family member ERp90 as an interaction partner of ERFAD. *PLoS One* 6, (2011).

[337]. Mueller, B., Lilley, B. N. & Ploegh, H. L. SEL1L, the homologue of yeast Hrd3p, is involved in protein dislocation from the mammalian ER. *J. Cell Biol.* 175, 261–270 (2006).

[338]. Mueller, B., Klemm, E. J., Spooner, E., Claessen, J. H. & Ploegh, H. L. SEL1L nucleates a protein complex required for dislocation of misfolded glycoproteins. *Proc. Natl. Acad. Sci. U. S. A.* 105, 12325–12330 (2008).

[339]. Iida, Y., Fujimori, T., Okawa, K., Nagata, K., Wada, I. & Hosokawa, N. SEL1L protein critically determines the stability of the HRD1-SEL1L Endoplasmic Reticulum-associated Degradation (ERAD) complex to optimize the degradation kinetics of ERAD substrates. *J. Biol. Chem.* 286, 16929–16939 (2011).

[340]. Klemm, E. J., Spooner, E. & Ploegh, H. L. Dual role of Ancient Ubiquitous Protein 1 (AUP1) in lipid droplet accumulation and Endoplasmic Reticulum (ER) protein quality control. *J. Biol. Chem.* 286, 37602–37614 (2011).

[341]. Okuda-Shimizu, Y. & Hendershot, L. M. Characterization of an ERAD Pathway

for Nonglycosylated BiP Substrates, which Require Herp. *Mol. Cell* 28, 544–554 (2007).

[342]. Schulze, A., Standera, S., Buerger, E., Kikkert, M., Van Voorden, S., Wiertz, E., Koning, F., Kloetzel, P. M. & Seeger, M. The ubiquitin-domain protein HERP forms a complex with components of the endoplasmic reticulum associated degradation pathway. *J. Mol. Biol.* 354, 1021–1027 (2005).

[343]. Brodsky, J. L. & Skach, W. R. Protein folding and quality control in the endoplasmic reticulum: Recent lessons from yeast and mammalian cell systems. *Curr. Opin. Cell Biol.* 23, 464–475 (2011).

[344]. Greenblatt, E. J., Olzmann, J. A. & Kopito, R. R. Derlin-1 is a rhomboid pseudoprotease required for the dislocation of mutant $\alpha$-1 antitrypsin from the endoplasmic reticulum. *Nat. Struct. Mol. Biol.* 18, 1147–1152 (2010).

[345]. Lilley, B. N. & Ploegh, H. L. A membrane protein required for dislocation of misfolded proteins from the ER. *Nature* 429, 834–840 (2004).

[346]. Ye, Y., Shibata, Y., Yun, C., Ron, D. & Rapoport, T. A. A membrane protein complex mediates retro-translocation from the ER lumen into the cytosol. *Nature* 429, 841–847 (2004).

[347]. Schulman, B. A. & Wade Harper, J. Ubiquitin-like protein activation by E1 enzymes: The apex for downstream signalling pathways. *Nat. Rev. Mol. Cell Biol.* 10, 319–331 (2009).

[348]. Ye, Y. & Rape, M. Building ubiquitin chains: E2 enzymes at work. *Nat. Rev. Mol. Cell Biol.* 10, 755–764 (2009).

[349]. Deshaies, R. J. & Joazeiro, C. A. P. RING domain E3 ubiquitin ligases. *Annu. Rev. Biochem.* 78, 399–434 (2009).

[350]. Smith, M. H., Ploegh, H. L. & Weissman, J. S. Road to ruin: Targeting proteins for degradation in the endoplasmic reticulum. *Science (80-. ).* 334, 1086–1090 (2011).

[351]. Nadav, E., Shmueli, A., Barr, H., Gonen, H., Ciechanover, A. & Reiss, Y. A novel mammalian endoplasmic reticulum ubiquitin ligase homologous to the yeast Hrd1. *Biochem. Biophys. Res. Commun.* 303, 91–97 (2003).

[352]. Kikkert, M., Doolman, R., Dai, M., Avner, R., Hassink, G., Van Voorden, S., Thanedar, S., Roitelman, J., Chau, V. & Wiertz, E. Human HRD1 Is an E3 Ubiquitin Ligase Involved in Degradation of Proteins from the Endoplasmic Reticulum. *J. Biol. Chem.* 279, 3525–3534 (2004).

[353]. Ye, Y., Meyer, H. H. & Rapoport, T. A. The AAA ATPase Cdc48/p97 and its

partners transport proteins from the ER into the cytosol. *Nature* 414, 652–656 (2001).

[354]. Liu, Y. & Ye, Y. Roles of p97-Associated Deubiquitinases in Protein Quality Control at the Endoplasmic Reticulum. *Curr. Protein Pept. Sci.* 13, 436–446 (2012).

[355]. Ye, Y. Diverse functions with a common regulator: Ubiquitin takes command of an AAA ATPase. *J. Struct. Biol.* 156, 29–40 (2006).

[356]. Schulz, J., Avci, D., Queisser, M. A., Gutschmidt, A., Dreher, L. S., Fenech, E. J., Volkmar, N., Hayashi, Y., Hoppe, T. & Christianson, J. C. Conserved cytoplasmic domains promote Hrd1 ubiquitin ligase complex formation for ER-associated degradation (ERAD). *J. Cell Sci.* 130, 3322–3335 (2017).

[357]. Schoebel, S., Mi, W., Stein, A., Ovchinnikov, S., Pavlovicz, R., DImaio, F., *et al.* Cryo-EM structure of the protein-conducting ERAD channel Hrd1 in complex with Hrd3. *Nature* 548, 352–355 (2017).

[358]. Wu, X., Siggel, M., Ovchinnikov, S., Mi, W., Svetlov, V., Nudler, E., Liao, M., Hummer, G. & Rapoport, T. A. Structural basis of ER-associated protein degradation mediated by the Hrd1 ubiquitin ligase complex. *Science* 368, (2020).

[359]. van den Boom, J. & Meyer, H. VCP/p97-Mediated Unfolding as a Principle in Protein Homeostasis and Signaling. *Mol. Cell* 69, 182–194 (2018).

[360]. Hänzelmann, P. & Schindelin, H. Characterization of an Additional Binding Surface on the p97 N-Terminal Domain Involved in Bipartite Cofactor Interactions. *Structure* 24, 140–147 (2016).

[361]. Bodnar, N. O., Kim, K. H., Ji, Z., Wales, T. E., Svetlov, V., Nudler, E., Engen, J. R., Walz, T. & Rapoport, T. A. Structure of the cdc48 atpase with its ubiquitin-binding cofactor ufd1–npl4. *Nat. Struct. Mol. Biol.* 25, 616–622 (2018).

[362]. Xu, Y., Liu, Y., Lee, J. G. & Ye, Y. A Ubiquitin-like domain recruits an oligomeric chaperone to a retrotranslocation complex in endoplasmic reticulum-associated degradation. *J. Biol. Chem.* 288, 18068–18076 (2013).

[363]. Xu, Y., Cai, M., Yang, Y., Huang, L. & Ye, Y. SGTA Recognizes a Noncanonical Ubiquitin-like Domain in the Bag6-Ubl4A-Trc35 Complex to Promote Endoplasmic Reticulum-Associated Degradation. *Cell Rep.* 2, 1633–1644 (2012).

[364]. Amano, T., Yamasaki, S., Yagishita, N., Tsuchimochi, K., Shin, H., Kawahara, K. I., *et al.* Synoviolin/Hrd1, an E3 ubiquitin ligase, as a novel pathogenic factor for arthropathy. *Genes Dev.* 17, 2436–2449 (2003).

[365]. Chen, Q., Zhong, Y., Wu, Y., Liu, L., Wang, P., Liu, R., Cui, F., Li, Q., Yang,

X., Fang, S. & Xie, Q. HRD1-mediated ERAD tuning of ER-bound E2 is conserved between plants and mammals. *Nat. Plants* 2, 1–7 (2016).

[366]. Gardner, R. G., Swarbrick, G. M., Bays, N. W., Cronin, S. R., Wilhovsky, S., Seelig, L., Kim, C. & Hampton, R. Y. Endoplasmic reticulum degradation requires lumen to cytosol signaling: Transmembrane control of Hrd1p by Hrd3p. *J. Cell Biol.* 151, 69–82 (2000).

[367]. Sun, S., Shi, G., Han, X., Francisco, A. B., Ji, Y., Mendonça, N., *et al.* Sel1L is indispensable for mammalian endoplasmic reticulum-associated degradation, endoplasmic reticulum homeostasis, and survival. *Proc. Natl. Acad. Sci. U. S. A.* 111, E582–E591 (2014).

[368]. Kamhi-Nesher, S., Shenkman, M., Tolchinsky, S., Fromm, S. V., Ehrlich, R. & Lederkremer, G. Z. A novel quality control compartment derived from the endoplasmic reticulum. *Mol. Biol. Cell* 12, 1711–1723 (2001).

[369]. Leitman, J., Shenkman, M., Gofmanb, Y., Shtern, N. O., Ben-Tal, N., Hendershot, L. M. & Lederkremer, G. Z. Herp coordinates compartmentalization and recruitment of HRD1 and misfolded proteins for ERAD. *Mol. Biol. Cell* 25, 1050–1060 (2014).

[370]. Kny, M., Standera, S., Hartmann-Petersen, R., Kloetzel, P. M. & Seeger, M. Herp regulates Hrd1-mediated ubiquitylation in a ubiquitin-like domain-dependent manner. *J. Biol. Chem.* 286, 5151–5156 (2011).

[371]. Hwang, J., Walczak, C. P., Shaler, T. A., Olzmann, J. A., Zhang, L., Elias, J. E. & Kopito, R. R. Characterization of protein complexes of the endoplasmicreticulum-associated degradation E3 ubiquitin ligase Hrd1. *J. Biol. Chem.* 292, 9104–9116 (2017).

[372]. Moenner, M., Pluquet, O., Bouchecareilh, M. & Chevet, E. Integrated endoplasmic reticulum stress responses in cancer. *Cancer Res.* 67, 10631–10634 (2007).

[373]. Dejeans, N., Manié, S., Hetz, C., Bard, F., Hupp, T., Agostinis, P., Samali, A. & Chevet, E. Addicted to secrete - novel concepts and targets in cancer therapy. *Trends Mol. Med.* 20, 242–250 (2014).

[374]. Oakes, S. A. Endoplasmic Reticulum Stress Signaling in Cancer Cells. *Am. J. Pathol.* 190, 934–946 (2020).

[375]. Oakes, S. A. Endoplasmic reticulum proteostasis: A key checkpoint in cancer. *Am. J. Physiol. - Cell Physiol.* 312, C93–C102 (2017).

[376]. Osorio, F., Tavernier, S. J., Hoffmann, E., Saeys, Y., Martens, L., Vetters, J., *et al.* The unfolded-protein-response sensor IRE-1α regulates the function of CD8α+ dendritic cells. *Nat. Immunol. 2014 153* 15, 248–257 (2014).

[377]. Greenman, C., Stephens, P., Smith, R., Dalgliesh, G. L., Hunter, C., Bignell, G., *et al.* Patterns of somatic mutation in human cancer genomes. *Nature* 446, 153–158 (2007).

[378]. Guichard, C., Amaddeo, G., Imbeaud, S., Ladeiro, Y., Pelletier, L., Maad, I. Ben, *et al.* Integrated analysis of somatic mutations and focal copy-number changes identifies key genes and pathways in hepatocellular carcinoma. *Nat. Genet.* 44, 694–698 (2012).

[379]. Parsons, D. W., Jones, S., Zhang, X., Lin, J. C. H., Leary, R. J., Angenendt, P., *et al.* An integrated genomic analysis of human glioblastoma multiforme. *Science (80-. ).* 321, 1807–1812 (2008).

[380]. Liu, J., Xiao, M., Li, J., Wang, D., He, Y., He, J., *et al.* Activation of UPR Signaling Pathway is Associated With the Malignant Progression and Poor Prognosis in Prostate Cancer. *Prostate* 77, 274–281 (2017).

[381]. Huggins, C. & Hodges, C. V. Studies on prostatic cancer i. the effect of castration, of estrogen and of androgen injection on serum phosphatases in metastatic carcinoma of the prostate. *Cancer Res.* 1, 293–297 (1941).

[382]. Segawa, T., Nau, M. E., Xu, L. L., Chilukuri, R. N., Makarem, M., Zhang, W., *et al.* Androgen-induced expression of endoplasmic reticulum (ER) stress response genes in prostate cancer cells. *Oncogene* 21, 8749–8758 (2002).

[383]. Sheng, X., Arnoldussen, Y. J., Storm, M., Tesikova, M., Nenseth, H. Z., Zhao, S., *et al.* Divergent androgen regulation of unfolded protein response pathways drives prostate cancer. *EMBO Mol. Med.* 7, 788–801 (2015).

[384]. Sheng, X., Nenseth, H. Z., Qu, S., Kuzu, O. F., Frahnow, T., Simon, L., *et al.* IRE1$\alpha$-XBP1s pathway promotes prostate cancer by activating c-MYC signaling. *Nat. Commun.* 10, 1–12 (2019).

[385]. Bai, S., Cao, S., Jin, L., Kobelski, M., Schouest, B., Wang, X., *et al.* A positive role of c-Myc in regulating androgen receptor and its splice variants in prostate cancer. *Oncogene* 38, 4977–4989 (2019).

[386]. Overcash, R. F., Chappell, V. A., Green, T., Geyer, C. B., Asch, A. S. & Ruiz-Echevarría, M. J. Androgen Signaling Promotes Translation of TMEFF2 in Prostate Cancer Cells via Phosphorylation of the $\alpha$ Subunit of the Translation Initiation Factor 2. *PLoS One* 8, e55257 (2013).

[387]. Pällmann, N., Livgård, M., Tesikova, M., Zeynep Nenseth, H., Akkus, E., Sikkeland, J., *et al.* Regulation of the unfolded protein response through ATF4 and FAM129A in prostate cancer. *Oncogene* 38, 6301–6318 (2019).

[388]. Zhu, K., Chan, W. K., Heymach, J., Wilkinson, M. & McConkey, D. J. Control

of HIF-Iα expression by eIF2α phosphrlation-mediated translational repression. *Cancer Res.* 69, 1836–1843 (2009).

[389]. Hsieh, C. L., Huang, H. S., Chen, K. C., Saka, T., Chiang, C. Y., Chung, L. W. K. & Sung, S. Y. A novel salicylanilide derivative induces autophagy cell death in castration-resistant prostate cancer via ER stress-activated PERK signaling pathway. *Mol. Cancer Ther.* 19, 101–111 (2020).

[390]. Wang, W. B., Feng, L. X., Yue, Q. X., Wu, W. Y., Guan, S. H., Jiang, B. H., Yang, M., Liu, X. & Guo, D. A. Paraptosis accompanied by autophagy and apoptosis was induced by celastrol, a natural compound with influence on proteasome, ER stress and Hsp90. *J. Cell. Physiol.* 227, 2196–2206 (2012).

[391]. Zhao, F., Huang, W., Zhang, Z., Mao, L., Han, Y., Yan, J. & Lei, M. Triptolide induces protective autophagy through activation of the CaMKKβ-AMPK signaling pathway in prostate cancer cells. *Oncotarget* 7, 5366–5382 (2016).

[392]. Yang, J., Wei, J., Wu, Y., Wang, Z., Guo, Y., Lee, P. & Li, X. Metformin induces ER stress-dependent apoptosis through miR-708-5p/NNAT pathway in prostate cancer. *Oncogenesis* 4, (2015).

[393]. Huang, Y. L., Chang, C. L., Tang, C. H., Lin, Y. C., Ju, T. K., Huang, W. P. & Lee, H. Extrinsic sphingosine 1-phosphate activates S1P5 and induces autophagy through generating endoplasmic reticulum stress in human prostate cancer PC-3 cells. *Cell. Signal.* 26, 611–618 (2014).

[394]. Gallagher, C. M., Garri, C., Cain, E. L., Ang, K. K. H., Wilson, C. G., Chen, S., *et al.* Ceapins are a new class of unfolded protein response inhibitors, selectively targeting the ATF6α branch. *Elife* 5, (2016).

[395]. Gallagher, C. M. & Walter, P. Ceapins inhibit ATF6α signaling by selectively preventing transport of ATF6α to the Golgi apparatus during ER stress. *Elife* 5, (2016).

[396]. Torres, S. E., Gallagher, C. M., Plate, L., Gupta, M., Liem, C. R., Guo, X., Tian, R., Stroud, R. M., Kampmann, M., Weissman, J. S. & Walter, P. Ceapins block the unfolded protein response sensor atf6α by inducing a neomorphic inter-organelle tether. *Elife* 8, (2019).

[397]. Coleman, O. I., Lobner, E. M., Bierwirth, S., Sorbie, A., Waldschmitt, N., Rath, E., *et al.* Activated ATF6 Induces Intestinal Dysbiosis and Innate Immune Response to Promote Colorectal Tumorigenesis. *Gastroenterology* 155, 1539-1552.e12 (2018).

[398]. Chang, K. C., Chen, P. C. H., Chen, Y. P., Chang, Y. & Su, I. J. Dominant expression of survival signals of endoplasmic reticulum stress response in Hodgkin

lymphoma. *Cancer Sci.* 102, 275–281 (2011).

[399]. Yarapureddy, S., Abril, J., Foote, J., Kumar, S., Asad, O., Sharath, V., *et al.* ATF6α Activation Enhances Survival against Chemotherapy and Serves as a Prognostic Indicator in Osteosarcoma. *Neoplasia (United States)* 21, 516–532 (2019).

[400]. Ri, M., Tashiro, E., Oikawa, D., Shinjo, S., Tokuda, M., Yokouchi, Y., *et al.* Identification of Toyocamycin, an agent cytotoxic for multiple myeloma cells, as a potent inhibitor of ER stress-induced XBP1 mRNA splicing. *Blood Cancer J.* 2, (2012).

[401]. Park, S. G., Kim, S. H., Kim, K. Y., Yu, S. N., Choi, H. D., Kim, Y. W., Nam, H. W., Seo, Y. K. & Ahn, S. C. Toyocamycin induces apoptosis via the crosstalk between reactive oxygen species and p38/ERK MAPKs signaling pathway in human prostate cancer PC-3 cells. *Pharmacol. Reports* 69, 90–96 (2017).

[402]. Thorpe, J. A. & Schwarze, S. R. IRE1α controls cyclin A1 expression and promotes cell proliferation through XBP-1. *Cell Stress Chaperones* 15, 497–508 (2010).

[403]. Axten, J. M., Medina, J. R., Feng, Y., Shu, A., Romeril, S. P., Grant, S. W., *et al.* Discovery of 7-methyl-5-(1-{[3-(trifluoromethyl)phenyl]acetyl}-2,3-dihydro-1H-indol-5-yl)-7H-pyrrolo[2,3-d]pyrimidin-4-amine (GSK2606414), a potent and selective first-in-class inhibitor of protein kinase R (PKR)-like endoplasmic reticulum kinase (PERK). *J. Med. Chem.* 55, 7193–7207 (2012).

[404]. Atkins, C., Liu, Q., Minthorn, E., Zhang, S. Y., Figueroa, D. J., Moss, K., *et al.* Characterization of a novel PERK kinase inhibitor with antitumor and antiangiogenic activity. *Cancer Res.* 73, 1993–2002 (2013).

[405]. Rojas-Rivera, D., Delvaeye, T., Roelandt, R., Nerinckx, W., Augustyns, K., Vandenabeele, P. & Bertrand, M. J. M. When PERK inhibitors turn out to be new potent RIPK1 inhibitors: Critical issues on the specificity and use of GSK2606414 and GSK2656157. *Cell Death Differ.* 24, 1100–1110 (2017).

[406]. Krishnamoorthy, J., Rajesh, K., Mirzajani, F., Kesoglidou, P., Papadakis, A. I. & Koromilas, A. E. Evidence for eIF2α phosphorylation-independent effects of GSK2656157, a novel catalytic inhibitor of PERK with clinical implications. *Cell Cycle* 13, 801–806 (2014).

[407]. Ivanova, I. G., Park, C. V., Yemm, A. I. & Kenneth, N. S. PERK/eIF2α signaling inhibits HIF-induced gene expression during the unfolded protein response via YB1-dependent regulation of HIF1α translation. *Nucleic Acids Res.* 46, 3878–3890 (2018).

[408]. Sidrauski, C., Acosta-Alvear, D., Khoutorsky, A., Vedantham, P., Hearn, B. R.,

Li, H., *et al.* Pharmacological brake-release of mRNA translation enhances cognitive memory. *Elife* 2013, (2013).

[409]. Nguyen, H. G., Conn, C. S., Kye, Y., Xue, L., Forester, C. M., Cowan, J. E., *et al.* Development of a stress response therapy targeting aggressive prostate cancer. *Sci. Transl. Med.* 10, 2036 (2018).

[410]. Wei, J., Sheng, X., Feng, D., McGrath, B. & Cavener, D. R. PERK is essential for neonatal skeletal development to regulate osteoblast proliferation and differentiation. *J. Cell. Physiol.* 217, 693–707 (2008).

[411]. Murakami, T., Saito, A., Hino, S. I., Kondo, S., Kanemoto, S., Chihara, K., *et al.* Signalling mediated by the endoplasmic reticulum stress transducer OASIS is involved in bone formation. *Nat. Cell Biol.* 11, 1205–1211 (2009).

[412]. Tohmonda, T., Miyauchi, Y., Ghosh, R., Yoda, M., Uchikawa, S., Takito, J., *et al.* The IRE1α-XBP1 pathway is essential for osteoblast differentiation through promoting transcription of Osterix. *EMBO Rep.* 12, 451–457 (2011).

[413]. Tohmonda, T., Yoda, M., Iwawaki, T., Matsumoto, M., Nakamura, M., Mikoshiba, K., Toyama, Y. & Horiuchi, K. IRE1α/XBP1-mediated branch of the unfolded protein response regulates osteoclastogenesis. *J. Clin. Invest.* 125, 3269–3279 (2015).

[414]. Nakashima, K., Zhou, X., Kunkel, G., Zhang, Z., Deng, J. M., Behringer, R. R. & De Crombrugghe, B. The novel zinc finger-containing transcription factor Osterix is required for osteoblast differentiation and bone formation. *Cell* 108, 17–29 (2002).

[415]. Horiuchi, K., Tohmonda, T. & Morioka, H. The unfolded protein response in skeletal development and homeostasis. *Cell. Mol. Life Sci.* 73, 2851–2869 (2016).

[416]. Yu, S., Franceschi, R. T., Luo, M., Fan, J., Jiang, D., Cao, H., *et al.* Critical role of activating transcription factor 4 in the anabolic actions of parathyroid hormone in bone. *PLoS One* 4, (2009).

[417]. Yang, X., Matsuda, K., Bialek, P., Jacquot, S., Masuoka, H. C., Schinke, T., *et al.* ATF4 is a substrate of RSK2 and an essential regulator of osteoblast biology: Implication for Coffin-Lowry syndrome. *Cell* 117, 387–398 (2004).

[418]. Xiao, G., Jiang, D., Ge, C., Zhao, Z., Lai, Y., Boules, H., Phimphilai, M., Yang, X., Karsenty, G. & Franceschi, R. T. Cooperative interactions between activating transcription factor 4 and Runx2/Cbfa1 stimulate osteoblast-specific osteocalcin gene expression. *J. Biol. Chem.* 280, 30689–30696 (2005).

[419]. Tominaga, H., Maeda, S., Hayashi, M., Takeda, S., Akira, S., Komiya, S., Nakamura, T., Akiyama, H. & Imamura, T. CCAAT/enhancer-binding protein β

promotes osteoblast differentiation by enhancing Runx2 activity with ATF4. *Mol. Biol. Cell* 19, 5373–5386 (2008).

[420]. Elefteriou, F., Benson, M. D., Sowa, H., Starbuck, M., Liu, X., Ron, D., Parada, L. F. F. & Karsenty, G. ATF4 mediation of NF1 functions in osteoblast reveals a nutritional basis for congenital skeletal dysplasiae. *Cell Metab.* 4, 441–451 (2006).

[421]. Yang, X. & Karsenty, G. ATF4, the osteoblast accumulation of which is determined post-translationally, can induce osteoblast-specific gene expression in non-osteoblastic cells. *J. Biol. Chem.* 279, 47109–47114 (2004).

[422]. Xu, F. & Teitelbaum, S. L. Osteoclasts: New Insights. *Bone Res.* 1, 11–26 (2013).

[423]. Xu, G., Liu, K., Anderson, J., Patrene, K., Lentzsch, S., Roodman, G. D. & Ouyang, H. Expression of XBP1s in bone marrow stromal cells is critical for myeloma cell growth and osteoclast formation. *Blood* 119, 4205–4214 (2012).

[424]. Cao, H., Yu, S., Yao, Z., Galson, D. L., Jiang, Y., Zhang, X., *et al.* Activating transcription factor 4 regulates osteoclast differentiation in mice. *J. Clin. Invest.* 120, 2755–2766 (2010).

[425]. Yokota, H., Hamamura, K., Chen, A., Dodge, T. R., Tanjung, N., Abedinpoor, A. & Zhang, P. Effects of salubrinal on development of osteoclasts and osteoblasts from bone marrow-derived cells. *BMC Musculoskelet. Disord.* 14, (2013).

[426]. Hamamura, K., Tanjung, N. & Yokota, H. Suppression of osteoclastogenesis through phosphorylation of eukaryotic translation initiation factor 2 alpha. *J. Bone Miner. Metab.* 31, 618–628 (2013).

[427]. Tohmonda, T., Yoda, M., Mizuochi, H., Morioka, H., Matsumoto, M., Urano, F., Toyama, Y. & Horiuchi, K. The IRE1$\alpha$-XBP1 pathway positively regulates parathyroid hormone (PTH)/PTH-related peptide receptor expression and is involved in PTH-induced osteoclastogenesis. *J. Biol. Chem.* 288, 1691–1695 (2013).

[428]. Livak, K. J. & Schmittgen, T. D. Analysis of relative gene expression data using real-time quantitative PCR and the 2-$\Delta\Delta\mathrm{CT}$ $\mathrm{method}$. *Methods* 25, 402–408 (2001).

[429]. Hou, Z., Jiang, P., Swanson, S. A., Elwell, A. L., Nguyen, B. K. S., Bolin, J. M., Stewart, R. & Thomson, J. A. A cost-effective RNA sequencing protocol for large-scale gene expression studies. *Sci. Rep.* 5, 1–5 (2015).

[430]. Miseq, V. & Systems, H. X. bcl2fastq2 Conversion Software Guide. (2015).

[431]. Grigoriev, I., Nordberg, H., Shabalov, I., Aerts, A., Cantor, M., Goodstein, D., *et al.* BBDuk. (2021).

[432]. Grigoriev, I. V., Nordberg, H., Shabalov, I., Aerts, A., Cantor, M., Goodstein, D., *et al.* The Genome Portal of the Department of Energy Joint Genome Institute. *Nucleic Acids Res.* 40, D26–D32 (2012).

[433]. Dobin, A., Davis, C. A., Schlesinger, F., Drenkow, J., Zaleski, C., Jha, S., Batut, P., Chaisson, M. & Gingeras, T. R. STAR: Ultrafast universal RNA-seq aligner. *Bioinformatics* 29, 15–21 (2013).

[434]. Love, M. I., Huber, W. & Anders, S. Moderated estimation of fold change and dispersion for RNA-seq data with DESeq2. *Genome Biol.* 15, 1–21 (2014).

[435]. Lin, D. L., Tarnowski, C. P., Zhang, J., Dai, J., Rohn, E., Patel, A. H., Morris, M. D. & Keller, E. T. Bone metastatic LNCaP-derivative C4-2B prostate cancer cell line mineralizes in vitro. *Prostate* 47, 212–221 (2001).

[436]. Bitting, R. L. & Armstrong, A. J. Potential predictive biomarkers for individualizing treatment for men with castration-resistant prostate cancer. *Cancer J. (United States)* 19, 25–33 (2013).

[437]. Logothetis, C. J. & Lin, S. H. Osteoblasts in prostate cancer metastasis to bone. *Nat. Rev. Cancer* 5, 21–28 (2005).

[438]. Rao, S. R., Snaith, A. E., Marino, D., Cheng, X., Lwin, S. T., Orriss, I. R., Hamdy, F. C. & Edwards, C. M. Tumour-derived alkaline phosphatase regulates tumour growth, epithelial plasticity and disease-free survival in metastatic prostate cancer. *Br. J. Cancer* 116, 227–236 (2017).

[439]. Langenbach, F. & Handschel, J. Effects of dexamethasone, ascorbic acid and β-glycerophosphate on the osteogenic differentiation of stem cells in vitro. *Stem Cell Res. Ther.* 4, 1–7 (2013).

[440]. Tornavaca, O., Chia, M., Dufton, N., Almagro, L. O., Conway, D. E., Randi, A. M., Schwartz, M. A., Matter, K. & Balda, M. S. ZO-1 controls endothelial adherens junctions, cell-cell tension, angiogenesis, and barrier formation. *J. Cell Biol.* 208, 821–838 (2015).

[441]. Takatsuki, A., Arima, K. & Tamura, G. Tunicamycin, a new antibiotic. I. Isolation and characterization of tunicamycin. *J. Antibiot. (Tokyo).* 24, 215–223 (1971).

[442]. Kaufman, R. J. Orchestrating the unfolded protein response in health and disease. *J. Clin. Invest.* 110, 1389–1398 (2002).

[443]. Cross, B. C. S., Bond, P. J., Sadowski, P. G., Jha, B. K., Zak, J., Goodman, J. M., Silverman, R. H., Neubert, T. A., Baxendale, I. R., Ron, D. & Harding, H. P. The molecular basis for selective inhibition of unconventional mRNA splicing by an IRE1-binding small molecule. *Proc. Natl. Acad. Sci. U. S. A.* 109, (2012).

[444]. Akech, J., Wixted, J. J., Bedard, K., Van Der Deen, M., Hussain, S., Guise, T. A., *et al.* Runx2 association with progression of prostate cancer in patients: Mechanisms mediating bone osteolysis and osteoblastic metastatic lesions. *Oncogene* 29, 811–821 (2010).

[445]. Klingler, A., Regensburger, D., Tenkerian, C., Britzen-Laurent, N., Hartmann, A., Stürzl, M. & Naschberger, E. Species-, organ- And cell-type-dependent expression of SPARCL1 in human and mouse tissues. *PLoS One* 15, e0233422 (2020).

[446]. Xiang, Y., Qiu, Q., Jiang, M., Jin, R., Lehmann, B. D., Strand, D. W., *et al.* SPARCL1 suppresses metastasis in prostate cancer. *Mol. Oncol.* 7, 1019–1030 (2013).

[447]. Gao, B., Lee, S. M., Chen, A., Zhang, J., Zhang, D. D., Kannan, K., Ortmann, R. A. & Fang, D. Synoviolin promotes IRE1 ubiquitination and degradation in synovial fibroblasts from mice with collagen-induced arthritis. *EMBO Rep.* 9, 480–485 (2008).

[448]. Iyer, S., Melendez-Suchi, C., Han, L., Baldini, G., Almeida, M. & Jilka, R. L. Elevation of the unfolded protein response increases RANKL expression. *FASEB BioAdvances* 2, 207–218 (2020).

[449]. Way, S. W. & Popko, B. Harnessing the integrated stress response for the treatment of multiple sclerosis. *Lancet Neurol.* 15, 434–443 (2016).

[450]. Han, J., Murthy, R., Wood, B., Song, B., Wang, S., Sun, B., Malhi, H. & Kaufman, R. J. ER stress signalling through eIF2$\alpha$ and CHOP, but not IRE1$\alpha$, attenuates adipogenesis in mice. *Diabetologia* 56, 911–924 (2013).

[451]. Solchaga, L. A., Penick, K. J. & Welter, J. F. Chondrogenic differentiation of bone marrow-derived mesenchymal stem cells: tips and tricks. *Methods Mol. Biol.* 698, 253–278 (2011).

[452]. Hamada, J., Onuma, H., Ochi, F., Hirai, H., Takemoto, K., Miyoshi, A., *et al.* Endoplasmic reticulum stress induced by tunicamycin increases resistin messenger ribonucleic acid through the pancreatic endoplasmic reticulum eukaryotic initiation factor 2$\alpha$ kinase-activating transcription factor 4-CAAT/enhancer binding protein-$\alpha$ homolog. *J. Diabetes Investig.* 7, 312–323 (2016).

[453]. Nosjean, O., Koyama, I., Goseki, M., Roux, B. & Komoda, T. Human tissue non-specific alkaline phosphatases: Sugar-moiety-induced enzymic and antigenic modulations and genetic aspects. *Biochem. J.* 321, 297–303 (1997).

[454]. Di, M., Wang, L., Li, M., Zhang, Y., Liu, X., Zeng, R., Wang, H., Chen, Y., Chen, W., Zhang, Y. & Zhang, M. Dickkopf1 destabilizes atherosclerotic plaques and promotes plaque formation by inducing apoptosis of endothelial cells through

activation of er stress. *Cell Death Dis.* 8, e2917–e2917 (2017).

[455]. Harding, H. P., Zyryanova, A. F. & Ron, D. Uncoupling proteostasis and development in vitro with a small molecule inhibitor of the pancreatic endoplasmic reticulum kinase, PERK. *J. Biol. Chem.* 287, 44338–44344 (2012).

[456]. Stockwell, S. R., Platt, G., Barrie, S. E., Zoumpoulidou, G., te Poele, R. H., Aherne, G. W., *et al.* Mechanism-based screen for G1/S checkpoint activators identifies a selective activator of EIF2AK3/PERK signalling. *PLoS One* 7, (2012).

[457]. Ganz, J., Shacham, T., Kramer, M., Shenkman, M., Eiger, H., Weinberg, N., *et al.* A novel specific PERK activator reduces toxicity and extends survival in Huntington's disease models. *Sci. Rep.* 10, (2020).

[458]. Moslehi, M., Cheki, M., Salehi-Marzijarani, M., Amuchastegui, T. & Gholamrezanezhad, A. Predictors of bone metastasis in pre-treatment staging of asymptomatic treatment-naïve patients with prostate cancer. *Rev. Esp. Med. Nucl. Imagen Mol.* 32, 286–289 (2013).

[459]. Yang, J. & Weinberg, R. A. Epithelial-Mesenchymal Transition: At the Crossroads of Development and Tumor Metastasis. *Dev. Cell* 14, 818–829 (2008).

[460]. Hance, M. W., Dole, K., Gopal, U., Bohonowych, J. E., Jezierska-Drutel, A., Neumann, C. A., Liu, H., Garraway, I. P. & Isaacs, J. S. Secreted Hsp90 is a novel regulator of the epithelial to mesenchymal transition (EMT) in prostate cancer. *J. Biol. Chem.* 287, 37732–37744 (2012).

[461]. Bacolod, M. D., Das, S. K., Sokhi, U. K., Bradley, S., Fenstermacher, D. A., Pellecchia, M., Emdad, L., Sarkar, D. & Fisher, P. B. Examination of Epigenetic and other Molecular Factors Associated with mda-9/Syntenin Dysregulation in Cancer Through Integrated Analyses of Public Genomic Datasets. *Adv. Cancer Res.* 127, 49–121 (2015).

[462]. Das, S. K., Pradhan, A. K., Bhoopathi, P., Talukdar, S., Shen, X. N., Sarkar, D., Emdad, L. & Fisher, P. B. The MDA-9/syntenin/IGF1R/STAT3 axis directs prostate cancer invasion. *Cancer Res.* 78, 2852–2863 (2018).

[463]. Wu, J. B., Shao, C., Li, X., Li, Q., Hu, P., Shi, C., *et al.* Monoamine oxidase A mediates prostate tumorigenesis and cancer metastasis. *J. Clin. Invest.* 124, 2891–2908 (2014).

[464]. McKeown, S. R. Defining normoxia, physoxia and hypoxia in tumours - Implications for treatment response. *Br. J. Radiol.* 87, (2014).

[465]. Vaupel, P., Höckel, M. & Mayer, A. Detection and characterization of tumor hypoxia using pO2 histography. *Antioxidants Redox Signal.* 9, 1221–1235 (2007).

[466]. Fels, D. R. & Koumenis, C. The PERK/eIF2α/ATF4 module of the UPR in hypoxia resistance and tumor growth. *Cancer Biol. Ther.* 5, 723–728 (2006).

[467]. Wang, G. L. & Semenza, G. L. Purification and characterization of hypoxia-inducible factor. *J. Biol. Chem.* 270, 1230–1237 (1995).

[468]. Semenza, G. L. Regulation of mammalian O2 homeostasis by hypoxia-inducible factor 1. *Annu. Rev. Cell Dev. Biol.* 15, 551–578 (1999).

[469]. Semenza, G. L. Targeting HIF-1 for cancer therapy. *Nat. Rev. Cancer* 3, 721–732 (2003).

[470]. Tanimoto, K., Yoshiga, K., Eguchi, H., Kaneyasu, M., Ukon, K., Kumazaki, T., *et al.* Hypoxia-inducible factor-1α polymorphisms associated with enhanced transactivation capacity, implying clinical significance. *Carcinogenesis* 24, 1779–1783 (2003).

[471]. Urra, H., Henriquez, D. R., Cánovas, J., Villarroel-Campos, D., Carreras-Sureda, A., Pulgar, E., *et al.* IRE1α governs cytoskeleton remodelling and cell migration through a direct interaction with filamin A. *Nat. Cell Biol.* 20, 942–953 (2018).

[472]. Zhao, G., Kang, J., Xu, G., Wei, J., Wang, X., Jing, X., *et al.* Tunicamycin promotes metastasis through upregulating endoplasmic reticulum stress induced GRP78 expression in thyroid carcinoma. *Cell Biosci.* 10, 1–10 (2020).

[473]. Gundamaraju, R., Vemuri, R., Ambati, R. R., Rangaswamy, L., Lu, W. & Eri D, R. Tunicamycin via ER stress mediated 6th hour time point aggravates cell migration, cell invasion and cell proliferation in colonic epithelial cells. *Adv. Cancer Biol. - Metastasis* 2, 100007 (2021).

[474]. Jabouille, A., Delugin, M., Pineau, R., Dubrac, A., Soulet, F., Lhomond, S., *et al.* Glioblastoma invasion and cooption depend on IRE1α endoribonuclease activity. *Oncotarget* 6, 24922–24934 (2015).

[475]. Dejeans, N., Pluquet, O., Lhomond, S., Grise, F., Bouchecareilh, M., Juin, A. lie, *et al.* Autocrine control of glioma cells adhesion and migration through IRE1a-mediated cleavage of SPARC mRNA. *J. Cell Sci.* 125, 4278–4287 (2012).

[476]. Feng, Y. X., Sokol, E. S., Del Vecchio, C. A., Sanduja, S., Claessen, J. H. L., Proia, T. A., Jin, D. X., Reinhardt, F., Ploegh, H. L., Wang, Q. & Gupta, P. B. Epithelial-to-mesenchymal transition activates PERK-eIF2α and sensitizes cells to endoplasmic reticulum stress. *Cancer Discov.* 4, 702–715 (2014).

[477]. Koumenis, C., Naczki, C., Koritzinsky, M., Rastani, S., Diehl, A., Sonenberg, N., Koromilas, A. & Wouters, B. G. Regulation of Protein Synthesis by Hypoxia via Activation of the Endoplasmic Reticulum Kinase PERK and Phosphorylation of the Translation Initiation Factor eIF2α. *Mol. Cell. Biol.* 22, 7405–7416 (2002).

[478]. Feldman, D. E., Chauhan, V. & Koong, A. C. The unfolded protein response: A novel component of the hypoxic stress response in tumors. *Mol. Cancer Res.* 3, 597–605 (2005).

[479]. Huang, L. E., Gu, J., Schau, M. & Bunn, H. F. Regulation of hypoxia-inducible factor 1$\alpha$ is mediated by an O2-dependent degradation domain via the ubiquitin-proteasome pathway. *Proc. Natl. Acad. Sci. U. S. A.* 95, 7987–7992 (1998).

[480]. Forsythe, J. A., Jiang, B. H., Iyer, N. V, Agani, F., Leung, S. W., Koos, R. D. & Semenza, G. L. Activation of vascular endothelial growth factor gene transcription by hypoxia-inducible factor 1. *Mol. Cell. Biol.* 16, 4604–4613 (1996).

[481]. Hayashi, M., Sakata, M., Takeda, T., Yamamoto, T., Okamoto, Y., Sawada, K., Kimura, A., Minekawa, R., Tahara, M., Tasaka, K. & Murata, Y. Induction of glucose transporter 1 expression through hypoxia-inducible factor 1$\alpha$ under hypoxic conditions in trophoblast-derived cells. *J. Endocrinol.* 183, 145–154 (2004).

[482]. Moszyńska, A., Collawn, J. F. & Bartoszewski, R. IRE1 endoribonuclease activity modulates hypoxic hif-1$\alpha$ signaling in human endothelial cells. *Biomolecules* 10, 1–14 (2020).

[483]. Ge, S. X., Jung, D., Jung, D. & Yao, R. ShinyGO: A graphical gene-set enrichment tool for animals and plants. *Bioinformatics* 36, 2628–2629 (2020).

[484]. Guven, K., Gunning, P. & Fath, T. TPM3 and TPM4 gene products segregate to the postsynaptic region of central nervous system synapses. *Bioarchitecture* 1, 284–289 (2011).

[485]. Chen, S., Shen, Z., Gao, L., Yu, S., Zhang, P., Han, Z. & Kang, M. TPM3 mediates epithelial-mesenchymal transition in esophageal cancer via MMP2/MMP9. *Ann. Transl. Med.* 9, 1338–1338 (2021).

[486]. Choi, H. S., Yim, S. H., Xu, H. D., Jung, S. H., Shin, S. H., Hu, H. J., Jung, C. K., Choi, J. Y. & Chung, Y. J. Tropomyosin3 overexpression and a potential link to epithelial-mesenchymal transition in human hepatocellular carcinoma. *BMC Cancer* 10, 1–11 (2010).

[487]. Thuault, S., Tan, E. J., Peinado, H., Cano, A., Heldin, C. H. & Moustakas, A. HMGA2 and Smads co-regulate SNAIL1 expression during induction of epithelial-to-mesenchymal transition. *J. Biol. Chem.* 283, 33437–33446 (2008).

[488]. Zhang, Z., Nam, H. K., Crouch, S. & Hatch, N. E. Tissue nonspecific alkaline phosphatase function in bone and muscle progenitor cells: Control of mitochondrial respiration and ATP production. *Int. J. Mol. Sci.* 22, 1–20 (2021).

[489]. Shares, B. H., Busch, M., White, N., Shum, L. & Eliseev, R. A. Active

mitochondria support osteogenic differentiation by stimulating-Catenin acetylation. *J. Biol. Chem.* 293, 16019–16027 (2018).

[490]. Rao, S. R., Howarth, A., Kratschmer, P., Snaith, A. E., Yapp, C., Ebner, D., Hamdy, F. C. & Edwards, C. M. Transcriptomic and Functional Screens Reveal MicroRNAs That Modulate Prostate Cancer Metastasis. *Front. Oncol.* 10, 292 (2020).

[491]. Vimalraj, S., Partridge, N. C. & Selvamurugan, N. A positive role of microRNA-15b on regulation of osteoblast differentiation. *J. Cell. Physiol.* 229, 1236–1244 (2014).

[492]. Takahashi, K., Tanabe, K., Ohnuki, M., Narita, M., Ichisaka, T., Tomoda, K. & Yamanaka, S. Induction of Pluripotent Stem Cells from Adult Human Fibroblasts by Defined Factors. *Cell* 131, 861–872 (2007).

[493]. Boison, D. & Yegutkin, G. G. Adenosine Metabolism: Emerging Concepts for Cancer Therapy. *Cancer Cell* vol. 36 582–596 (2019).

[494]. Burnstock, G. & Di Virgilio, F. Purinergic signalling and cancer. *Purinergic Signalling* vol. 9 491–540 (2013).

[495]. Xu, Z., Gu, C., Yao, X., Guo, W., Wang, H., Lin, T., *et al.* CD73 promotes tumor metastasis by modulating RICS/RhoA signaling and EMT in gastric cancer. *Cell Death Dis.* 11, 1–15 (2020).

[496]. Street, S. E., Kramer, N. J., Walsh, P. L., Taylor-Blake, B., Yadav, M. C., King, I. F., Vihko, P., Mark Wightman, R., Millán, J. L. & Zylka, M. J. Tissue-nonspecific alkaline phosphatase acts redundantly with PAP and NT5E to generate adenosine in the dorsal spinal cord. *J. Neurosci.* 33, 11314–11322 (2013).

[497]. Sato, M., Saitoh, I., Kiyokawa, Y., Iwase, Y., Kubota, N., Ibano, N., Noguchi, H., Yamasaki, Y. & Inada, E. Tissue-nonspecific Alkaline phosphatase, a possible mediator of cell maturation: Towards a new paradigm. *Cells* 10, (2021).

[498]. Chava, S., Chennakesavulu, S., Gayatri, M. B. & Reddy, A. B. M. A novel phosphorylation by AMP-activated kinase regulates RUNX2 from ubiquitination in osteogenesis over adipogenesis. *Cell Death Dis.* 9, 1–16 (2018).

[499]. Shan, S., Lv, Q., Zhao, Y., Liu, C., Sun, Y., Xi, K., Xiao, J. & Li, C. Wnt/β-catenin pathway is required for epithelial to mesenchymal transition in CXCL12 over expressed breast cancer cells. *Int. J. Clin. Exp. Pathol.* 8, 12357–12367 (2015).

[500]. Liu, X., Kim, J. H., Wang, J., Chen, X., Zhang, H., Kim, S. H., *et al.* Wnt signaling in bone formation and its therapeutic potential for bone diseases. *Ther. Adv. Musculoskelet. Dis.* 5, 13–31 (2013).

[501]. Liang, D., Khoonkari, M., Avril, T., Chevet, E. & Kruyt, F. A. E. The unfolded protein response as regulator of cancer stemness and differentiation: Mechanisms and implications for cancer therapy. *Biochem. Pharmacol.* 192, 114737 (2021).

[502]. Obeng, E. A., Carlson, L. M., Gutman, D. M., Harrington, W. J., Lee, K. P. & Boise, L. H. Proteasome inhibitors induce a terminal unfolded protein response in multiple myeloma cells. *Blood* 107, 4907–4916 (2006).

[503]. Khan, M. L. & Stewart, A. K. Carfilzomib: A novel second-generation proteasome inhibitor. *Futur. Oncol.* 7, 607–612 (2011).

[504]. Xie, J., Wan, N., Liang, Z., Zhang, T. & Jiang, J. Ixazomib–the first oral proteasome inhibitor. *Leukemia and Lymphoma* vol. 60 610–618 (2019).

[505]. Logue, S. E., McGrath, E. P., Cleary, P., Greene, S., Mnich, K., Almanza, A., *et al.* Inhibition of IRE1 RNase activity modulates the tumor cell secretome and enhances response to chemotherapy. *Nat. Commun.* 9, 1–14 (2018).

[506]. Rozpędek, W., Pytel, D., Wawrzynkiewicz, A., Siwecka, N., Dziki, A., Dziki, Ł., Diehl, J. A. & Majsterek, I. Use of Small-molecule Inhibitory Compound of PERK-dependent Signaling Pathway as a Promising Target-based Therapy for Colorectal Cancer. *Curr. Cancer Drug Targets* 20, 223–238 (2020).

[507]. Shah, P. P., Dupre, T. V., Siskind, L. J. & Beverly, L. J. Common cytotoxic chemotherapeutics induce epithelialmesenchymal transition (EMT) downstream of ER stress. *Oncotarget* 8, 22625–22639 (2017).

[508]. Cornish, J., Callon, K. E., Edgar, S. G. & Reid, I. R. Leukemia inhibitory factor is mitogenic to osteoblasts. *Bone* 21, 243–247 (1997).